ACTIVE VIBRATION CONTROL AND REAL-TIME SURFACE PROFILE MONITORING SYSTEM FOR A HIGH PERFORMANCE MACHINING PROCESS

by

Sedat Elmas

A Doctoral Thesis
Submitted in partial fulfilment of the requirement for the award of
Doctor of Philosophy of Loughborough University

April 2009

ABSTRACT

Rotary planing and moulding machining operations have been widely used within the woodworking industry for many years. As a result of these machining processes, the surface profile of machined timber consists of cuttermarks which determine the product quality. However, the presence of machine system variations does not guarantee the quality requirements. Most of the rotary machining improvement techniques applied to obtain an improved product quality focus on conventional methods such as tooling and spindle system design. The current state of the industry indicates that the design of rotary planing machines has probably reached its mechanical development limit, hence for an advanced machining process, mechatronics based improvement techniques are necessary. Therefore, the focus of this research work is directed towards the improvements on a mechatronics based small scale wood planer. Firstly, the effects of machining variations on the resultant surface form have been investigated. Especially, the effects of spindle vibrations and tooling inaccuracies on the surface finish have been analysed through simulation and further demonstrated through experimental work. With the introduced defect generation tool (DGT), the effect of a specific disturbance could be made to order, hence allowing generation of defects for quality investigations. This is not possible on existing machinery. Secondly, for an enhanced machining environment, surface profile information is desirable. Various surface profile measurement systems have been evaluated in terms of in-process deployment. Most of the evaluated measurement systems lack the measurement speed or exhibit other disadvantages which limit their implementation for real-time measurement purposes. Therefore, a novel in-process surface profile monitoring system (ISMS) has been introduced that is capable of extracting surface profile features in real-time. Thirdly, active vibration control has been implemented on the small scale planer. Unlike conventional design improvement methods, with the active vibration control approach the dynamic characteristics of the small scale planer were substantially improved, hence enabling a higher degree of freedom in terms of machining operation. This improvement allows machining operations beyond the limitations set by the mechanical properties of the planing system, thus enabling higher product quality where additional machining processes such as sanding could be obsolete.

ACKNOWLEDGEMENTS

This research work was carried out at the Mechatronics Research Centre, Department of Mechanical and Manufacturing Engineering, at Loughborough University during the period 2005-2008. This work was supported by the EPSRC Innovative Manufacturing and Construction Centre (IMCRC).

This research work has been completed under the supervision of Professor Mike Jackson to whom I wish to express my deep gratitude for his excellent guidance throughout the duration of this work. During our several meetings, his feedbacks and support have been invaluable.

I also wish to express my sincere thanks to my second supervisor Professor Rob Parkin for his support during the research period.

I also would like to thank Paolo Albertelli for our valuable collaboration.

Furthermore, I would like to thank Jo Mason for her kindness and help with the administration work.

I would like to thank all my colleagues at the Mechatronics Research Centre who made the research process enjoyable.

Dedicated to my parents Ekrem and Perihan Elmas

CONTENTS

NOMENCLATURE

A	piezoelectric actuator cross-sectional area	m^2
a_p	piezoelectric actuator prescribed displacement	m
C_p	piezoelectric actuator capacitance	F
D	cutterhead diameter	m
d	piezoelectric actuator layer thickness	m
D_3	electrical displacement	$C{\cdot}m^{-2}$
d_{33}	piezoelectric charge constant	m/V
d_t	cutterhead travel per cuttermark	m
E	Young's modulus	Pa
e_3	mechanical strain	-
E_3	electric field	V/m
E_h	relative error of surface waviness height	-
f	frequency	Hz
F_{max}	peak acceleration force	N
F_p	piezoelectric actuator load	N
F_{p0}	piezoelectric actuator blocked force	N
F_{po}	force generated by actuator	N
F_s	force from spindle support	N
h	waviness height	m
H_s	triangulation height	m
I, i	electrical current	A
k_p	piezoelectric actuator stiffness	N/m
k_s	spindle support stiffness	N/m
K^{σ}_3	relative dielectric constant at constant mechanical stress	-
L	length / actuator length	m
L_s	triangulation length	m

L_k	Kalman filter gain	-
m_c	cutterhead mass	kg
N	number of cutterhead knives	-
n	number of actuator layers	-
p	cuttermark length (pitch)	m
q	charge stored in piezoelectric actuator	C
R	cutterhead radius	m
R_a	driving amplifier impedance	Ω
S^E_{33}	mechanical compliance at constant electric field	Pa^{-1}
t	time	sec
V	voltage	V
v_c	cutting speed	m/sec
v_f	feed speed	m/sec
V_i	amplifier input voltage	V
V_o	amplifier output voltage	V
y	spindle displacement	m
y_0	piezoelectric actuator zero load displacement	m
y_v	vertical cutterhead pulse magnitude	m
γ	spindle support stiffness to actuator stiffness ratio	-
Δt	time to machine one cuttermark / vertical pulse width	sec
ε_0	vacuum permittivity	F/m
η	relative damping of vibration mode	-
μ	cutting speed to feed speed ratio	-
ρ	material density	$kg \cdot m^{-2}$
σ_3	mechanical stress	Pa
φ_i	incident angle	rad
ω	cutterhead speed	rpm

LIST OF FIGURES

LIST OF TABLES

Chapter 1 INTRODUCTION

1.1 Basic Principle of Woodworking Process

Rotary machining has been an essential part of the woodworking industry for many years. Especially, planing and moulding are considered to be the most effective machining processes within this domain. These processes are widely used for machining of wooden products such as window frames, door frames and many others with an acceptable surface quality. Many authors like Sims et al. (1985), Jackson (1986) and Brown et al. (2002), outlined the development of the woodworking machinery process. The basic principle of the rotary machining process is such that, a timber is being fed against a rotating cutterhead comprising of several cutting knives with the aim to remove material from the workpiece. This process is illustrated in Figure 1.1.

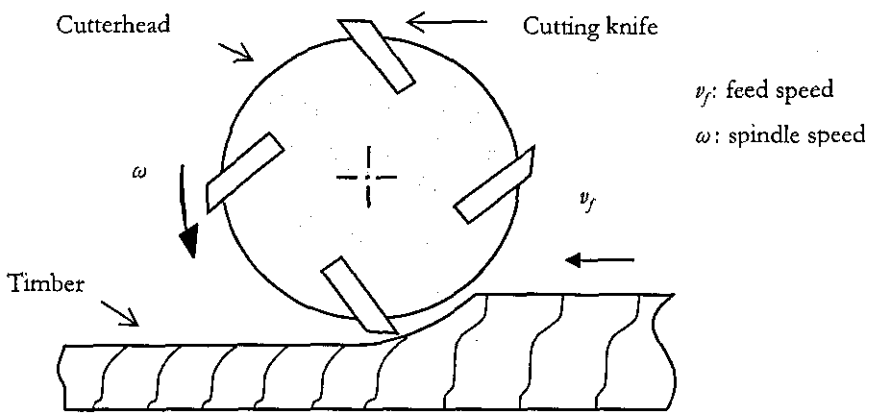

Figure 1.1 Wood machining process

1.2 Project Motivation

As a result of the rotary machining process, the machined timber surface has a series of waves, also called cuttermarks, which are generally accepted as unavoidable. According to the particular application, the surface profile of machined timber is subject to a given surface quality level, e.g. wood surface quality level for furniture applications are higher than the surfaces where they are coated or hidden by other materials. Although modern planing machines provide a good surface quality, the undesired variations within the machining process can reduce the surface quality remarkably. Moreover, for some applications where high surface quality is a requirement, additional machining processes such as sanding are required. Sanding is a costly operation and can reduce the geometric quality of profiled sections of timber. Furthermore, additional machining operations are not desirable from the economic point of view. Thus, it is desirable to improve the machining environment in order to avoid additional processes and ensure the surface finish that satisfies the quality requirements of a given application.

The current state of the industry indicates that the design of rotary planing machines has probably reached their mechanical development limit, hence for an enhanced machining environment, mechatronics based improvement approaches gain more importance. Therefore, a novel mechatronics based small scale planer designed within the Mechatronics Research Group, Department of Mechanical and Manufacturing Engineering, Loughborough University, will be improved by employing active vibration control. Unlike conventional design improvement methods, with the active vibration control approach, the dynamic characteristics of the small scale planer could be adapted for various machining environments, hence enabling a higher degree of freedom in terms of product quality.

1.3 Previous Work

A mechatronics based small scale planer was designed and built by Hynek (2004) as a part of his PhD project (Figure 1.2). The test rig and the previous work are described in more details in chapter 3.

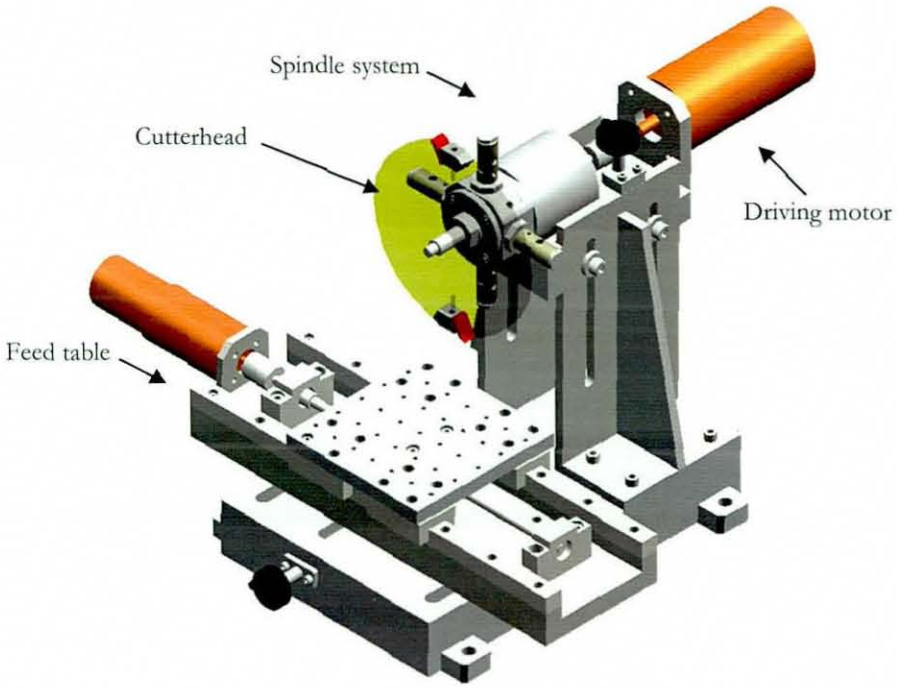

Figure 1.2 Previous work - test rig (Hynek 2004)

The objective of the previous work was focused on the surface profile improvement through modification of the machining process by vertical movement of the cutterhead. This machining method uses a real-time tool tip trajectory adjustment to improve the surface form. A whole cycle of the cutterhead movement and the effects of this process on the surface form are depicted in Figure 1.3. During the cutting process, the cutterhead starts moving upwards when the knife tip first touches the workpiece and then it starts moving downwards after its centre passes the cuttermark's midpoint.

The vertical cutterhead movement changes the knife tip path, thus the surface form. This method of machining improves the surface quality and provides shallow cuttermarks when compared to the conventional machining method (Figure 1.3).

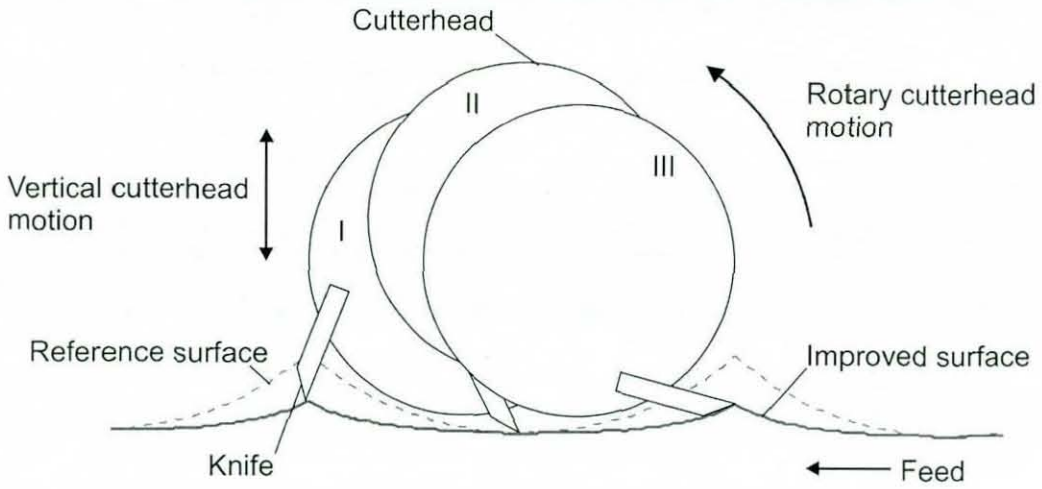

Figure 1.3 One cycle of the vertical cutterhead movement (Hynek 2004)

This approach can be perceived as wood shaping process which can be classified under the category of rotary machining process modification as described in the next chapter and depicted in Figure 2.4. However, this method requires high forces for the execution which are outside the performance range of the piezoelectric actuators. The limitations of this method are further described in more details in chapter 3.

Therefore, the focus of this research work for the improvement of the rotary machining process is directed towards a different route, namely towards the implementation of active vibration control.

1.4 Project Objectives

One of the main objectives of this research work is to improve the dynamic characteristics of the small scale planer for an enhanced machining environment. In order to achieve this goal, the characteristics of the test rig will be investigated and active vibration control is proposed to be implemented.

System variations present within the wood machining process can reduce the surface quality, thus the consistency of the product quality is not guaranteed. These variations and their effects on the resultant surface finish will be investigated. Especially the effects of spindle vibrations and tooling inaccuracies on the resultant surface form will be analysed through simulation and further demonstrated through experimental work.

Another contribution to an improved machining process is a surface profile monitoring system. Various surface profile measurement systems which could potentially be employed for in-process monitoring will be evaluated. Furthermore, development of a novel surface profile monitoring system is proposed which is capable of extracting surface profile information in real-time. Figure 1.4 shows an overview of the proposed advanced machining process.

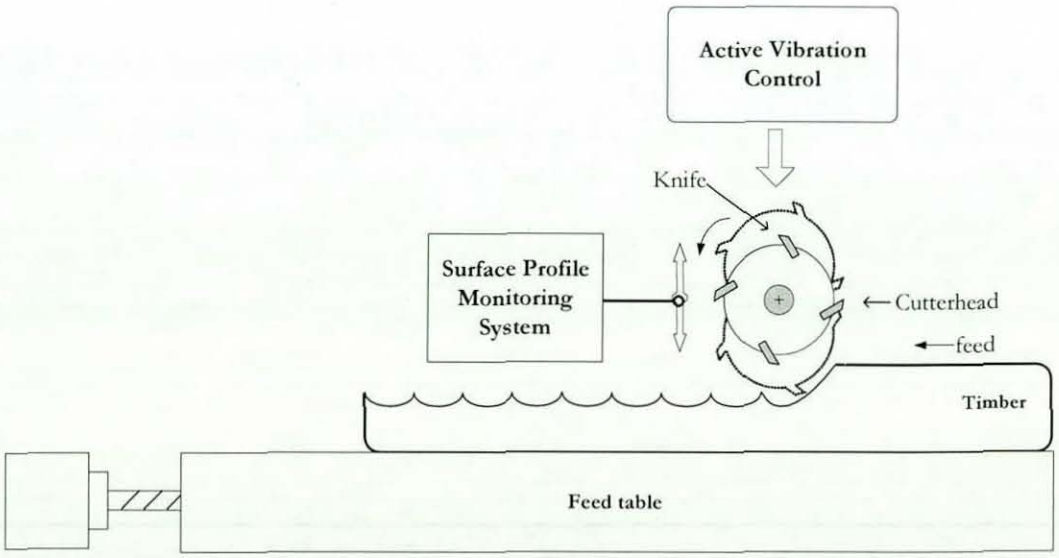

Figure 1.4 Overview of the proposed machining process

The three main project objectives can be summarized as follows:

- Analysis on surface waviness
- Surface profile inspection in real-time
- Implementation of active vibration control

1.5 Project Methodology

An overview of the research work is shown in Figure 1.5.

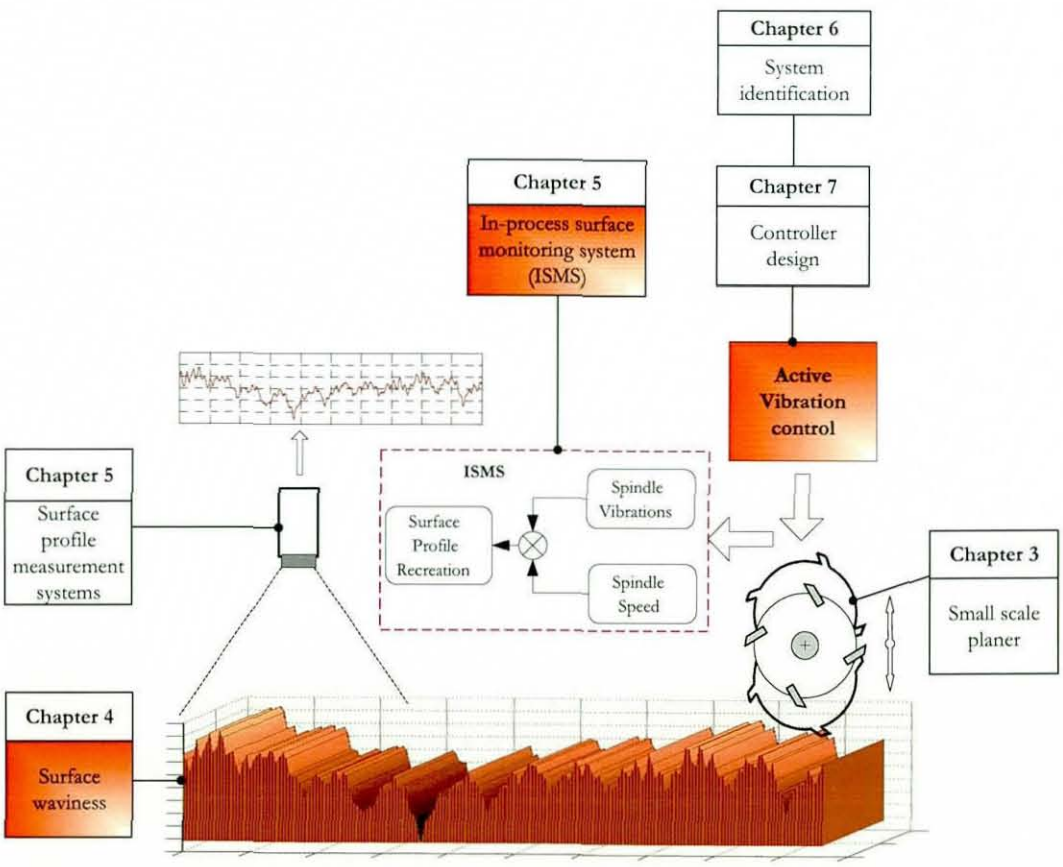

Figure 1.5 Overview of the research work

The three novelties achieved are presented in Chapter 4, Chapter 5 and Chapter 7. These are indicated in orange colour in Figure 1.5.

The research project is divided into five phases, namely:

- Literature review
- Previous work and test rig design
- Analysis on surface waviness and defects
- Surface profile measurement systems
- Active vibration control

The dissertation consists of nine chapters and organized as follows:

The literature review presented Chapter 2 provides improvement methods on woodworking machining as well as on active vibration control in rotary machining processes within both metalworking and woodworking domains. The amount of research in the woodworking domain for an enhanced machining environment is limited, therefore the improvement techniques used within the metalworking machining are investigated and their application for planing and moulding machining processes are outlined.

The previous work and the design of the test rig are described in Chapter 3. Furthermore, improvements and limitations of the previous work are outlined. Moreover, proposed improvement methods in contrast to the previous approach are highlighted.

Surface profile appearance forms are discussed in Chapter 4. Furthermore, the effects of machine system variations on the surface form are analysed. A novel defect generation tool (DGT) is introduced which is capable of analysing these effects through simulation as well as through experimental work. The DGT enables a broader understanding of the interaction between tool and workpiece and the resulting surface profile.

In order to analyse the quality of the machined surfaces, various surface profile measurement systems are described in Chapter 5. The advantages and disadvantages of the measurement techniques are discussed. Furthermore, a novel surface profile monitoring system for real-time application is introduced.

For the implementation of active vibration control, the system identification of the spindle unit is necessary. Therefore, actuator modelling and analysis on the dynamic characteristics of the spindle system are presented in Chapter 6.

Chapter 7 discusses the implementation of active vibration control. The focus is on the design of optimal control technique comprising of a Kalman filter. Results from the simulation and experimental work are presented and discussed.

The general discussion of the research work is presented in Chapter 8. The benefits of the improved machining process are outlined.

Chapter 9 provides the conclusions of the research work. Further improvement areas for future work are identified.

Chapter 2 LITERATURE SURVEY

The objective of this chapter is to discuss various aspects of wood machining process. Traditional methods as well as modern improvement strategies for an enhanced machining process are outlined. Furthermore, active and passive vibration control methods are briefly described and their practical application within the metal working as well as wood working machinery is investigated. The influence of vibrations has negative effects on the resultant surface quality of both metal and woodworking industry, thus vibration reductions methods implemented in both sectors are outlined. A technology roadmap which describes rotary machining process improvement techniques for an enhanced machining environment is presented.

2.1 Introduction to Woodworking Machining

Many applications within the woodworking industry make an extensive use of rotary machining process, especially moulding and planing machines are to be mentioned. The rotary machining of wood appears at first to be straight forward, however it is a very complex operation which has much in common with the milling of metals. The fundamental principle of the rotary machining lies in the material removal by cutting knives mounted on a rotating cutterhead. Woodworking machine tools have been used from the 14^{th} century starting from water wheels for saw mills (Sims, 1985). Nowadays, modern high speed moulders are constructed as modular flexible units which can be easily adopted for a particular machining operation. A modern high speed moulder is shown in Figure 2.1.

Rough sawn rectangular pieces of timber are used as raw material for the planing and moulding machines. The dimension of the raw material varies from *10* up to *100 mm* thickness with widths from *20* up to *300 mm*. The length of the workpiece is typically in the range of *250 mm* to *6 m*. Timber pieces are usually fed to the powered rollers

by hand and the feed system sends the material to the cutter blocks with feed speeds ranging from *5* to *120 m/min* (Jackson et al. 2002).

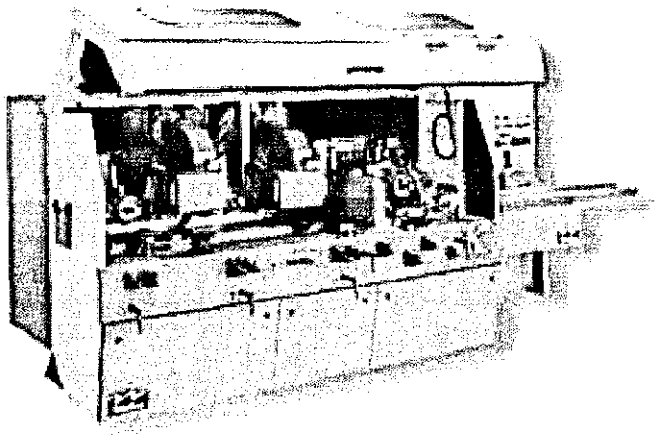

Figure 2.1 Modern six head moulder

A modern high speed moulder has usually more than one cutterhead in order to machine several faces of the workpiece. A typical moulder configuration consists of six spindles with the aim to machine all four sides of a workpiece in one operation (Figure 2.2)

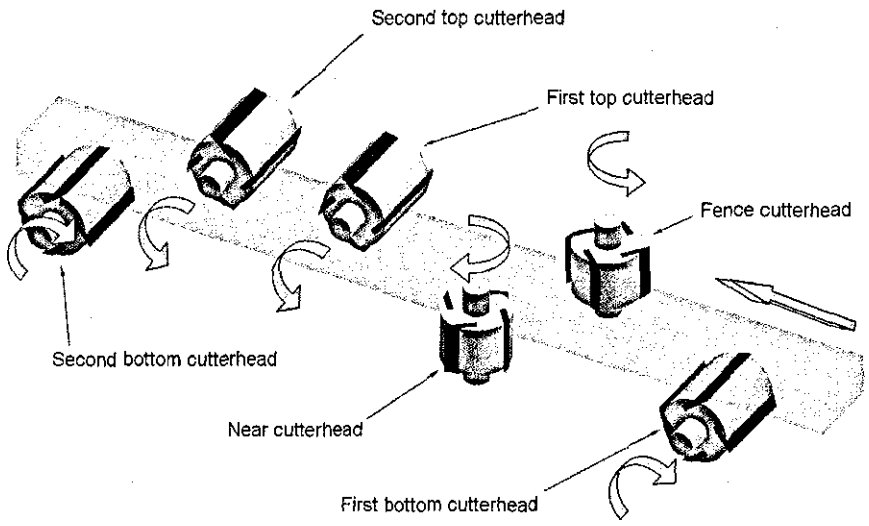

Figure 2.2 A typical modern moulder with six spindles (Hynek 2004)

However, this process is not entirely straight forward. It is being complicated by spindle run out, spindle vibrations, out of balance, shaft whirl, bearing play and other problems. These undesired variations are reflected to the surface finish which is perceived as poor quality product, thus needs further processing to meet the quality requirements.

Due to the kinematics of the rotary machining process, machined surface consists of wave forms. The wave forms, also called cuttermarks, can clearly be seen in Figure 2.3 (Hynek 2004).

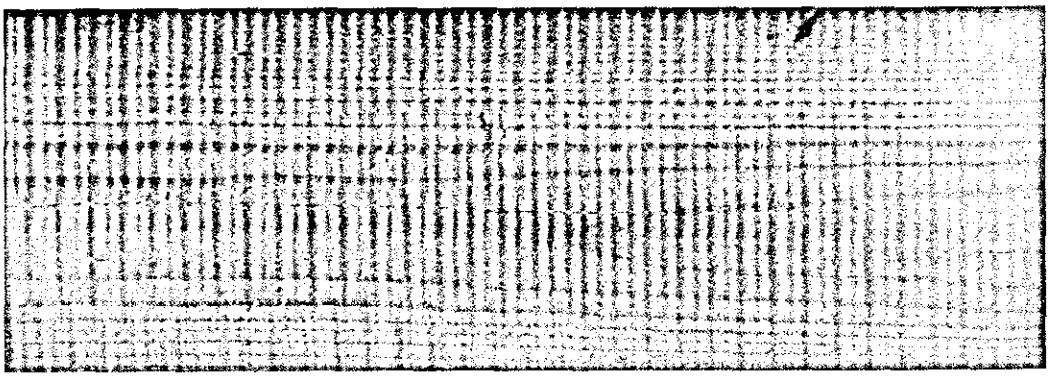

Figure 2.3 Surface waviness (Hynek 2004)

These cuttermarks may be acceptable for some application where the surface quality is not an issue. Cuttermarks shown in Figure 2.3 are, for example, not acceptable for some applications such as furniture or window frames. Therefore, to meet the surface quality requirements, further processing techniques such as sanding is performed to obtain a wave free surface (Taylor et al. 1999).

2.2 Overview on the Wood Surface Form Improvement Methods

Wood surface quality depends on many factors such as tool geometry and condition, vibrations as wells as on the rotary machining process (described in chapter 4 in more details). The surface quality of machined timber can be improved by suppressing the influence of these factors. Figure 2.4 shows an overview for improving the rotary machining process. Generally, the improvement techniques can be divided under three categories such as vibration suppression, tooling improvement and rotary machining modification.

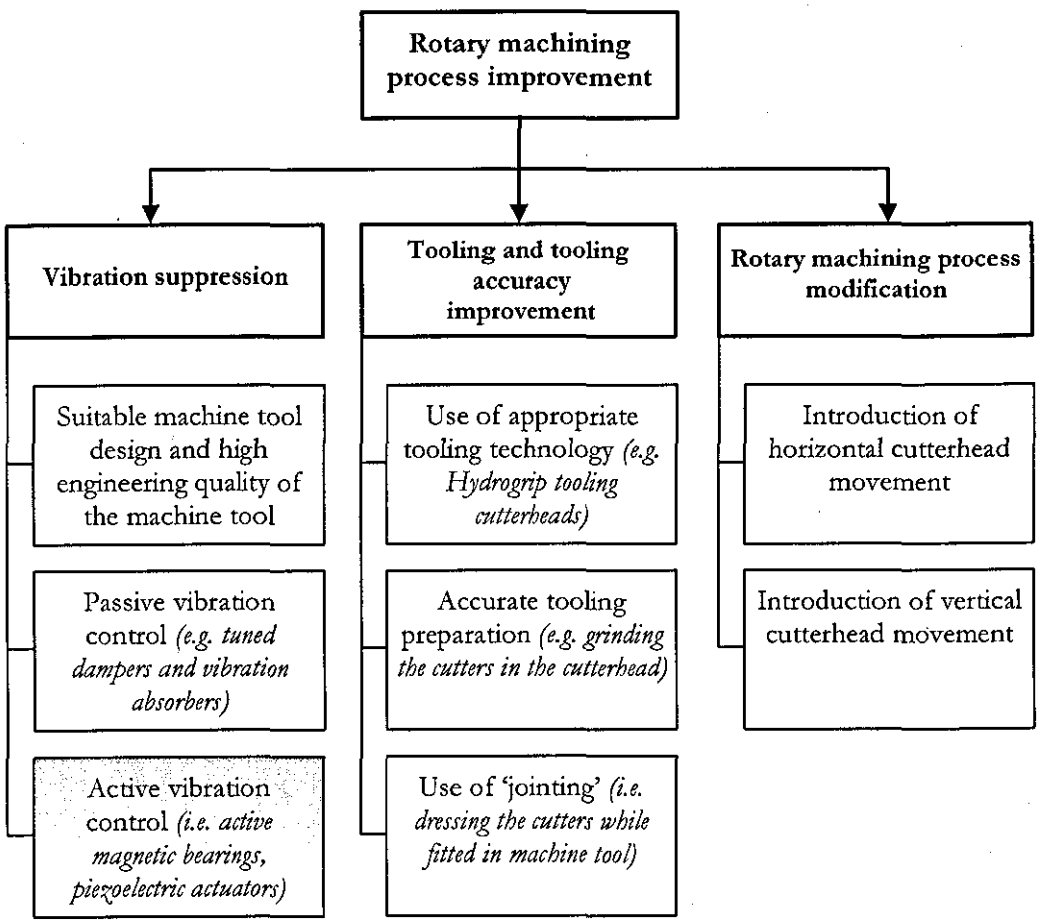

Figure 2.4 Rotary machining process improvement

The effects of vibration and tooling inaccuracies on the machined surface are shown through simulation as well as through experimental work which are discussed in chapter 4. Surface profile improvement through controlled modification of the vertical cutterhead movement is outlined in chapter 3. Figure 2.4 shows that the surface wave form can be improved by one of these approaches or by combination of them. The chosen method will depend on the particular application and the surface profile quality requirements, because each of these methods is capable of improving the surface quality from a different perspective.

To ensure a consistent product quality, undesired disturbances such as vibrations, tooling inaccuracies and machine tolerances need to be minimised. To achieve this goal, a considerable amount of research regarding tooling, design and process optimisation methods, has been carried out. These optimisation methods span over a wide range of application fields such as metal and woodworking industry where rotary machining methods are predominantly in use.

The advantages and disadvantages of these methods are described for vibration suppression techniques in section 2.3, for tooling accuracy improvement techniques in section 4.4 and for the vertical cutterhead movement in section 3.4. In order to achieve an advanced rotary machining process, active vibration control approach (indicated in Figure 2.4 in grey colour) has been proposed for the small scale planer, which is described in chapter 7 in more details.

2.3 Vibration Control – Background

Vibration is the repetitive, periodic response of a mechanical system. Any repetitive motion, even at higher frequencies with low amplitudes and irregular random behaviour is generally termed as vibration. Whereas repetitive regular motion at lower frequencies is called oscillation (De Silva 2007).

Vibrations are present in almost every dynamic system to a certain extent. Vibrations usually occur because of the dynamic effects of manufacturing tolerances, clearances, rolling and rubbing contact between machine components and unbalanced forces in rotating parts. The undesired vibration can coincide with the natural frequency of the system and cause excessive vibrations. Vibration analysis, observation and control are widely present within engineering systems which span from aeronautics, civil, manufacturing and mechatronic systems. Appropriate design and control are essential in maintaining high performance level and production efficiency as well as to avoid machine damage and structural fatigue. Therefore, it is essential from vibration control point of view, to understand the dynamic behaviour of the system in order to minimize the undesired vibrations, thus disturbances and its effects on the overall performance. This may be achieved by purely analytical means or with the help of simulation models through computer.

The system model and its vibration characteristics can be analysed either in the time domain or in the frequency domain. In the time domain, the independent variable of the vibration signal is time where the system itself is modelled as a set of differential equations. In the frequency domain, the independent variable of the vibrating system is the frequency where the system characteristics are modelled by input – output transfer functions. Transfer functions are often used to define the mechanical impedance, mobility, receptance and transmissibility of a system.

The relationship between the time and the frequency domain can then be analysed with the help of Fourier transformation. Frequency analysis enables to track the natural frequency and the mode shapes which are directly related to the fundamental movements of various parts of the dynamic system. Once the undesired mode shapes are determined they can be suppressed or minimized by appropriate means such as dampers or actuators to counteract the effects of vibration. This technique is the basis of vibration analysis and control which is used to either accomplish a passive or an active vibration control approach.

2.3.1 Passive Vibration Control

Passive vibration control method is based on the use of passive devices which do not require external power for their operation. Passive devices generally comprises of tuned dampers and dynamic absorbers. The sensing is implicit and the control is carried out through a force that is generated by the device as a result of its response to the vibration source.

2.3.1.1 Undamped Vibration Absorber

A dynamic absorber is a mass-spring-type mechanism with a very low damping, which can absorb the excitation force from the primary system and dissipate the energy slowly. Hence, it is also termed as an undamped vibration absorber. In Figure 2.5 the objective of the absorber is to reduce the vibratory response y_{pr} of the primary system caused by the vibration excitation F_{vib}. This goal is achieved, if the absorbers natural frequency is tuned so that it is equal to the excitation frequency, hence the primary system response y_{pr} will be zero and the primary system will not undergo any vibratory motion. This means that a tuned absorber applies a spring force to the primary system that is equal but opposite to the excitation force and thereby cancel each other.

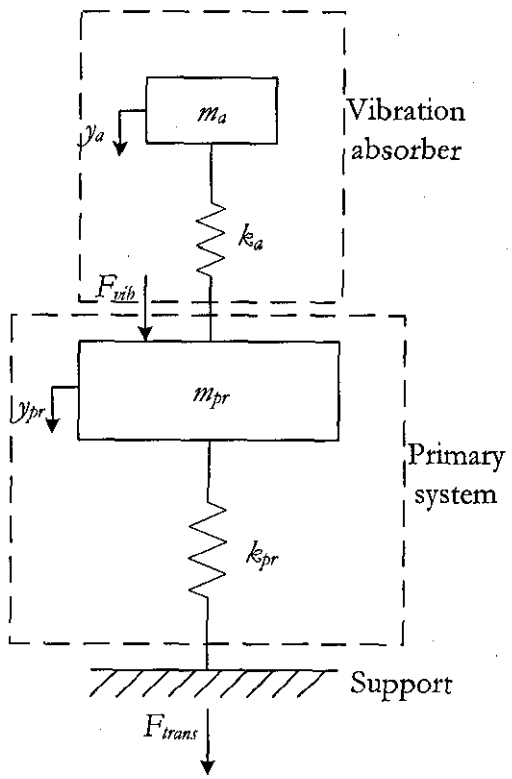

m_a absorber mass
k_a absorber stiffness
y_a absorber response
m_{pr} system mass
k_{pr} system stiffness
y_{pr} system response
F_{vib} vibration excitation
F_{trans} transmitted force

Figure 2.5 Undamped vibration absorber (De Silva 2007)

Further analysis need to be carried out in order to understand the overall characteristics of the whole system (primary system with the absorber). The transfer function (TF) of the system can be defined as $G = F_{trans}/F_{vib}$. Figure 2.6 shows that the TF of the primary system with the undamped absorber becomes zero at the natural frequency (ω_{n_sys}) of the primary system. However, the TF of the primary system with the undamped absorber introduces two more vibration modes in the system. The magnitude of the transfer function becomes infinite at either of these two vibration modes. These new vibration modes which are on either side of the suppressed natural frequency (ω_{n_sys}) reduce the effective bandwidth of the overall system. In order to suppress the introduced resonances, usually a damped vibration observer is used.

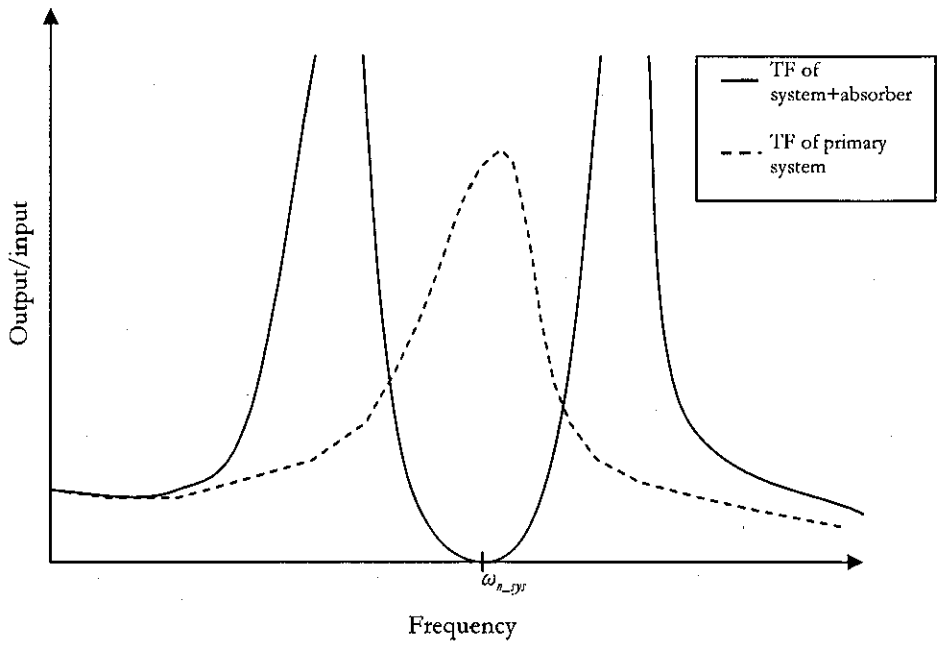

Figure 2.6 Transfer function of the primary system with and without an undamped absorber (De Silva 2007)

2.3.1.2 Damped Vibration Absorber

It should be noted that damping is not the primary mean by which the vibration control is achieved in a vibration absorber. Figure 2.7 demonstrates the primary system with a damped vibration absorber. Damping b_a mainly dissipates the energy which is being transferred to the absorber gradually. Furthermore, it reduces the excessive vibration magnitudes at the resonant frequencies which are created by adding the absorber to the primary system (Figure 2.8).

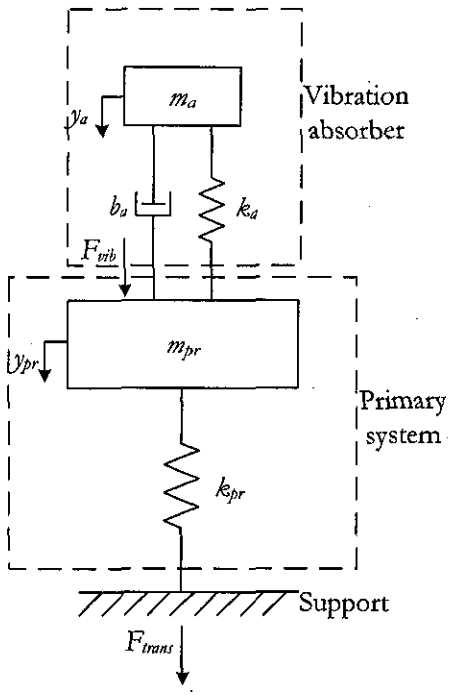

Figure 2.7 Damped vibration absorber (De Silva 2007)

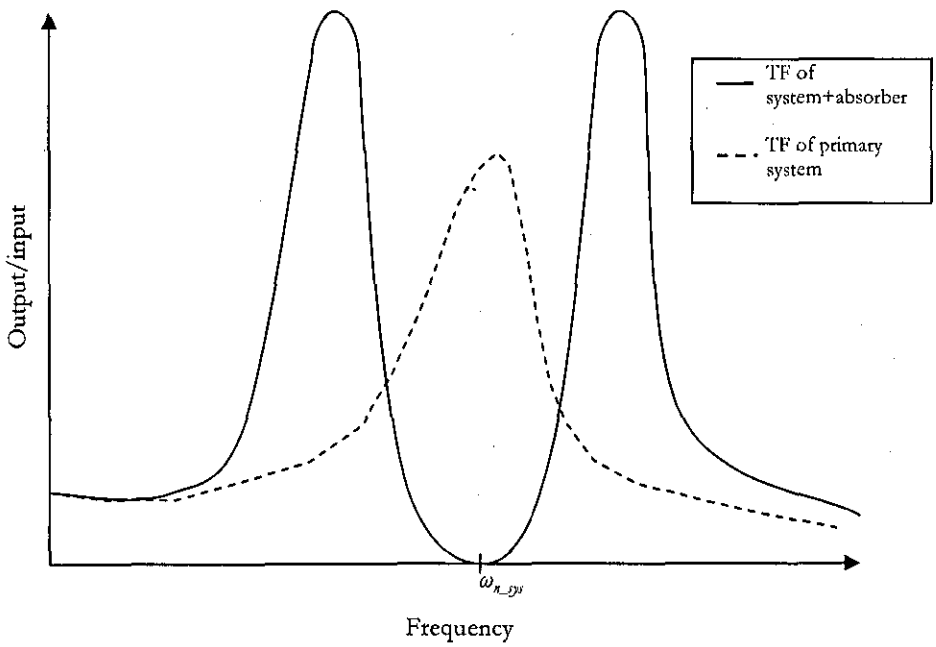

Figure 2.8 Overall system response with a damped vibration absorber (De Silva 2007)

The resonant frequencies of the overall system with the damped absorber are almost identical to the resonant frequencies with undamped system. However, the magnitudes at the resonant frequencies differ from the undamped system which is a desired characteristic. Figure 2.8 also reveals that for low damping ratios, the system response is very similar to the system response with an undamped absorber. When the damping ratio is large, the two masses (m_{pr} and m_a) seem to become a single mass and the primary system is only modified in its mass. The consequence of a large damping ratio is that it creates only one natural frequency which is in fact smaller than the natural frequency of the primary system without the damped absorber. Hence, the overall system bandwidth is further reduced and the effect of a vibration reduction is not fulfilled. A detailed analytical description of both damped and undamped absorbers is reported by De Silva, (2007).

These both common methods show the basic principal of vibration suppression with the help of passive devices such as vibration absorbers. However, passive control approach has some advantages and disadvantages.

Advantages of the passive vibration control method can be identified as follows

- Simple to design and implement
- They do not require any external power for their operation
- Cost effective method
- Robust and reliable

Disadvantages of the passive control method can be summarized as follows

- Effective only for a single excitation frequency
- In case of a different frequency (i.e. caused by an external disturbance), the absorber may create even more vibrations
- Creates more natural frequencies (depends on damping ratio value)
- Limits the system bandwidth

Both common passive vibration reduction methods revealed that the vibration reduction is mainly being achieved at the cost of system bandwidth. Therefore, active vibration control methods are desirable, because they can cope with different kinds of vibration frequencies without limiting the bandwidth of the system.

2.3.2 Basic Principle of Active Vibration Control

In the competitive global market sector, where high productivity and manufacturing flexibility become a requirement, more sophisticated and flexible control strategies are needed to suppress disturbances (i.e. undesired vibrations and machining variations). The limitations of the passive vibration control have been described in section 2.3.1 and it is noted that the control force which is generated in the passive device depends solely on the natural dynamics. In other words, once the passive vibration control system is designed (i.e. setting values for mass, damping constant, stiffness, location), it is not possible to adjust the control forces during the machine operation.

Since the passive device is designed for a particular excitation frequency, it is not always possible to directly target the control action at specific responses (i.e. undesired response of a system may contain various vibration frequencies). The passive control can be insufficient for complex and higher order systems. Therefore, it cannot always satisfy the vibration control performance needed for modular and complex machining systems (i.e. highly complex modern moulders and planers might show various excitation frequencies due to their dynamic behaviour). These drawbacks can be overcome by using an active vibration control method.

Figure 2.9 shows a general diagram of an active vibration control method. The vibrations of the mechanical plant are monitored with the appropriate sensors (i.e. accelerometer, eddy current probes) and the system response is used as feedback for the control system.

The controller compares the system response with the desired response and uses the error to generate appropriate control signals. This technique is termed as feedback control system, which is well-known and widely used for different kinds of applications.

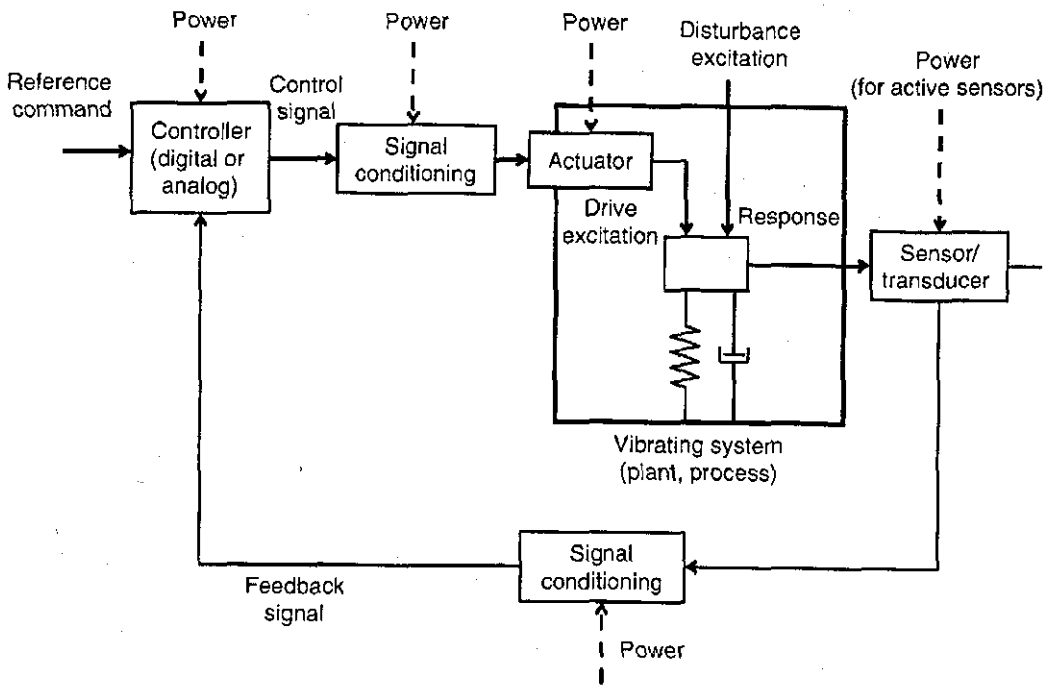

Figure 2.9 Active vibration control with feedback control method (De Silva 2007)

The actuators (i.e. piezoelectric or electromagnetic devices) convert the commands from the controller into mechanical excitation. The controller is generally a programming code based on mathematical operations (i.e. comparison between input and output) which make the use of existing simulation programs (i.e. Matlab/Simulink, LabView). Control signals generated by the controller are usually digital signals which need to be converted into analogue signals and they may be filtered and amplified with a signal conditioning unit into a form and forwarded to the actuator. Sensor signals are usually filtered and amplified with in the signal conditioning unit before they can be fed to the controller. Filtering the sensor signals with the appropriate filter methods is useful for removing the measurement noise.

There are different control strategies to implement the control law of an active vibration control system. Various control laws, both linear and nonlinear approaches have been developed for this purpose (i.e. linear quadratic regulator).

2.4 Application Fields of Active Vibration Control Techniques

Since the application of the rotary machinery has increased within the metal and woodworking industry, the problems with the undesired vibrations engaged researchers. The presence of vibrations in machining process reduces the machined surface quality immensely. These vibrations are considered as sources of structural fatigue and can cause tool and machine damage. They are also responsible for high noise levels (Hynek 2004).

The sources of vibrations within the machining process are machine tool, such as frame, slides, guide ways, bearings and, last but not least, the engineering quality of the spindle system. The spindle system generally comprises of the spindle itself including the discs mounted on it and the supporting parts such as bearings, squeeze film dampers, seals etc. Spindle systems are rotor systems, thus the analysis on rotor systems is applicable to spindle systems (Kramer et al. 1993).

The most common actuator type for active vibration control of rotor systems is active magnetic bearing (AMB) (Wang et al. 2001). Magnetic bearings are actively controlled to hold the rotor in a floating position. AMB apply magnetic force to the rotor to eliminate its undesirable motion without any contact. Figure 2.10 shows the principle of the AMB controlling a rotor (Schweitzer et al. 1994).

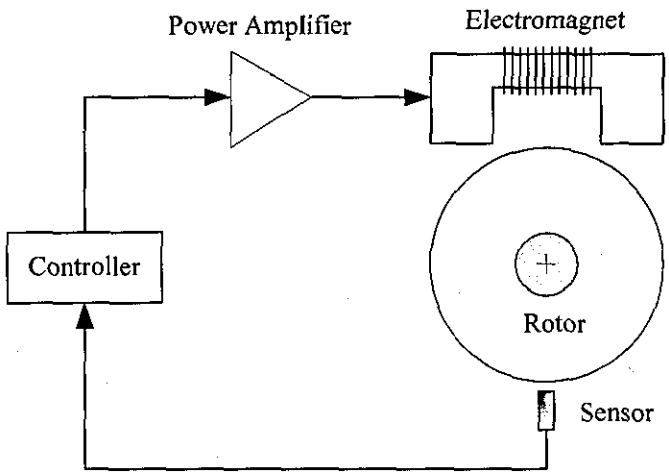

Figure 2.10 Basic principle of active magnetic bearings (Schweitzer et al. 1994)

A sensor measures the displacement of the rotor from its reference position and provides the controller with the information. The controller then produces a control signal and sends it to the power amplifier, which sends then appropriate control current to the electromagnet. A more detailed overview of the control scheme is presented in Figure 2.11.

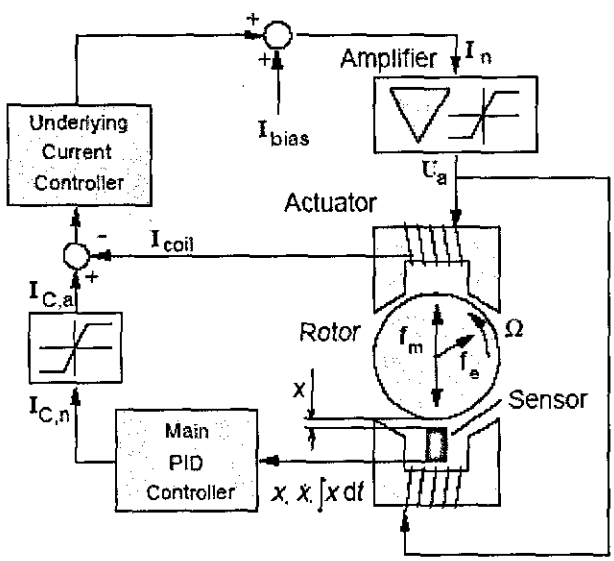

Figure 2.11 Basic control method of AMB (Steinschaden and Springer 1999)

The magnetic bearing consists of two pairs of actuators (electromagnets). Each pair is controlled independently, based on sensors measuring the rotor position and velocity in the x and y direction, respectively. These signals are the input signals for the main controller. An integral feedback gain eliminates steady state deviations from the centre position of the rotor. According to the output of the controller the amplifier supplies the voltage to produce the appropriate magnetic force within the actuator.

The main advantage of the AMBs is the contactless control of the rotor vibrations, thus it is lubrication free and exhibits no bearing wear, which is common to the contact type bearings. Furthermore, relatively high forces up to $40\ N/cm^2$ per bearing area can be produced to effectively deal with heavy rotor masses (Bleuler 1992). The gap in the bearing varies from micrometer range up to $20\ mm$. Larger gaps decrease the bearing forces immensely (Schweitzer et al. 1994).

Advantages of the AMB can be summarized as follows

- Contactless operation, thus no lubrication required
- The bearings are capable of providing high speeds
- At high speed operation, bearing losses are 5 to 20 times lower than the conventional bearings.
- Lower maintenance costs and higher lifetime expectations are one of the main reasons for their deployment
- High control forces can be achieved depending on the bearing size
- Depending on the control law, stiffness and damping of a rotor system can be modified. This characteristic allows passing critical rotor speeds with less vibration magnitudes.
- High precision in the control of the spindle displacement, control range reaches up to $1\ \mu m$.

Disadvantages of the AMBs can be defined as follows

- Relatively expensive due to complexity
- Bulky where high bearing forces are required
- Sophisticated high power amplifiers are needed for high control precision
- A high precision of the position of the rotor axis (in the range of *μm*) requires high resolution sensors and adequate signal processing to separate disturbance signals from the desired ones
- Eddy current losses will limit the rotation frequency of massive rotors (i.e. heating up, driving power)

The AMBs are generally used for high speed machining and turbo machinery (Nonami et al. 1996). The speed can reach up to *180 000 rpm* (Nordman 2006). Skricka et al. (2002) suggests that AMB systems can be improved with mechatronics approach by system integration. Beside the use of AMBs for different kinds of applications, they can also be used as an exciter and measurement instrument in order to identify the dynamic characteristics of a system. For example, system identification techniques have already been used in many applications for the identification of rotor dynamic coefficients such as stiffness, damping and inertia. One of the main problems to obtain the interested parameters is the excitation of the rotating structure during the operation. Especially, in the rotating machinery with built in mechatronic components, it is convenient to use the actuators as an exciter for system identification (Aenis et al. 2002). The knowledge about the system dynamics could be further used to increase the performance as well as to design new machines with the desired characteristics for particular applications (Nordmann 2006).

Vibration reduction methods within the rotary machining process mostly target to optimize the characteristics of the rotating components. Therefore, spindle system plays a more important role among vibration contributors. It is the essential part of a rotary machine and its dynamic properties directly affect the surface quality (Chen et al. 1994). Spindle vibrations caused by disturbances such as cutting forces, limit the machine tool performance significantly. Spindle dynamic properties are mainly determined by its design; therefore many researchers developed design strategies for optimal spindle design in order to avoid the structural vibrations. Lee et al. (2000) developed a diagram of modular optimisation procedure where machine design requirements and machine parameters such as critical speed, fatigue life, spindle deflections and rotor weight can be optimised (Figure 2.12).

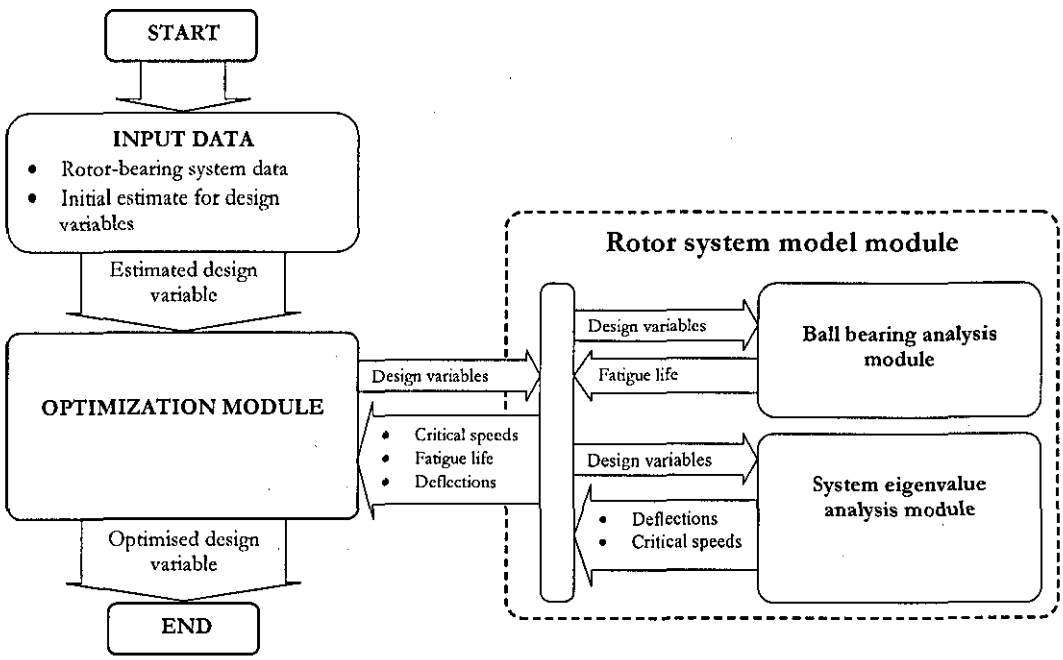

Figure 2.12 Modular optimisation procedure (Lee et al. 2000)

The reduction of the spindle nose deflection is an essential factor for chatter. Brandon et al. (1992) demonstrated a simple method for the reduction of the spindle nose deflection by optimal spacing of the bearings. The authors also report that the appropriate choice of bearings directly affect the chatter sensitivity.

The spindle system is critical for the woodworking as well as for the metalworking machine tools. The undesired spindle vibrations cause surface defects within the wood machining. Within the metalworking, the spindle stiffness is one of the key factors for chatter control and suppression. The onset of chatter directly affects the performance of the machine tool (Dohner et al. 1997). Chatter can generally be reduced by an active or passive approach or a combination of these two methods.

Firstly, passive vibration reduction is achieved by the use of passive devices, which change the frequency response of the system in such a way, so that the vibration level of chatter is reduced. As aforementioned, typical passive devices are tuned dampers, shock absorbers and squeeze film dampers. Secondly, active vibration control approach with the appropriate actuators (i.e. AMB, piezoelectric, electrostrictive actuators) can be used to control undesired excitation frequencies of a rotating system more efficiently (Abduljabbar et al. 1996). The following sections present vibration reduction methods applied to the metal and woodworking machinery.

2.4.1 Vibration reduction methods for metalworking machinery

The relative vibration between the workpiece and the cutting tool, also called chatter, occurs under some operating conditions. In the metal machining, chatter is a problem of instability that is characterized by violent vibrations, loud noise and poor quality of surface finish. This problem has affected the metalworking industry for a considerable time, therefore a lot of research has been carried out to minimize the chatter problem. Generally two factors are responsible for chatter: Firstly, the mode coupling, which means that the forces generated by the cutting process are coupled to the dynamic behaviour (i.e. stiffness, damping and inertia) of the machine structure. Secondly, the regeneration of surface waviness caused by interaction between tool and workpiece is regarded as a major chatter contributor. The latter is

by far the most common cause for chatter occurrence, thus this phenomenon has been studied by many researchers for decades (Ganguli et al. 2004).

Tobias et al. (1958) and some other researchers (i.e. Tlusty et al. 1963) were among the first to propose the phenomenon of regeneration to explain chatter instability within the turning process. During the machining process, the machine tool faces unbalanced cutting forces (depth of cut is varying after each knife rotation), thus vibrations are triggered. This tool vibration causes a wavy surface. After one full rotation, the tool faces the waves left during the previous pass. This causes fluctuation of the cutting forces and leaves more vibration marks on the workpiece surface. This process is called regeneration or regenerative chatter (Figure 2.13).

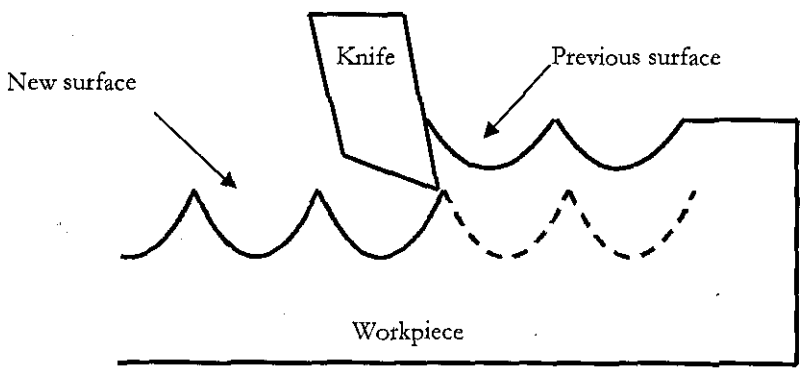

Figure 2.13 Regenerative chatter

The major step towards understanding the regenerative machine tool chatter was presented by Merritt (1965). This study, which focused on a stability theory for regenerative chatter in an orthogonal turning process with a feedback loop, was based on the theory of steady orthogonal cutting process. It has been found that the onset of machine chatter is a function of the spindle speed. Clearly, chatter can generally be described as a form of self-excited vibration which can be stabilized by increasing the damping of the vibration structure (Zhang et al. 2005). Chatter is not desirable, because it has an adverse effect on the machining accuracy, the surface finish and the tool life.

It also reduces the output performance by requiring a lower maximum metal removal rate (MMRR). MMRR is the quantitative measure of productive performance of a machine tool. From the cost aspect of view and because of the simplicity, a remarkable amount of research has been carried out to reduce the machine chatter and to increase the borderline of stability of the machine tool by using passive devices. Another method of chatter suppression is varying the spindle speed (Jemielniak et al. 1984, Al-Regib et al. 2003). This approach varies the spindle speed to avoid instabilities and seeks for regions (lobes) where a higher MMRR could be achieved (Takemura et al. 1974, Inamura and Sata 1974, Inamura et al. 1975, Sexton et al. 1977). However, many metalworking machines are not designed for a spindle speed variation during the cutting process. Figure 2.14 illustrates the relationship between the spindle speed, the depth of cut and the stability.

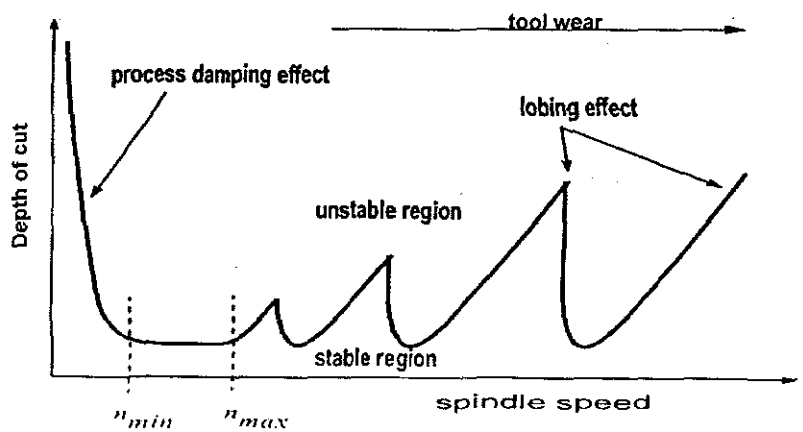

Figure 2.14 Stability limits of a typical machine tool (Dohner et al. 2004)

Metalworking machines are designed for a defined operation range between n_{min} and n_{max} (Figure 2.14), thus speed variation and its deployment could be very costly. Moreover, as shown in Figure 2.14, increasing the spindle speed to a stable operation region (for a better MMRR) would result in excessive tool wear (Dohner et al. 2004). It is impossible to completely eliminate vibrations exhibited by machine tools. A more efficient method of vibration suppression is the active vibration control technique (Benning et al. 1997). Herein the damper or the spindle is controlled

through sensors and actuators which produce controlled forces upon the structure to suppress measured machine vibrations.

2.4.1.1 Active Vibration Control within the Milling and Grinding

Liu et al. (1991) developed a dynamic absorber for chatter suppression in the milling process. A dynamic absorber mass is connected to the main system through passive elements (spring and damper). The authors determined then the optimum values of the spring and damping coefficients and could improve the stable operation range remarkably. Spindle vibration suppression via piezoelectric actuators has been investigated by Nagaya et al. (1997). Authors reported remarkable vibration suppression by using four piezoelectric actuators for X-Y positions of the spindle.

Zhang et al. (2005) developed a piezoelectric active control system to attenuate the workpiece vibrations during the milling of a flexible workpiece. The piezoelectric transducers were mounted on the surface of a flexible workpiece in order to actively damp the workpiece vibrations. Authors reported that for some applications involving a flexible workpiece, chatter can be avoided by choosing stable regions of the workpiece stability lobes rather than choosing the stability lobes of the machine tool. Authors implemented a positive feedback control method by using Matlab xPC target real-time software. Their experimental results with controller on and off showed that the chatter was reduced remarkably as it can be seen in Figure 2.15.

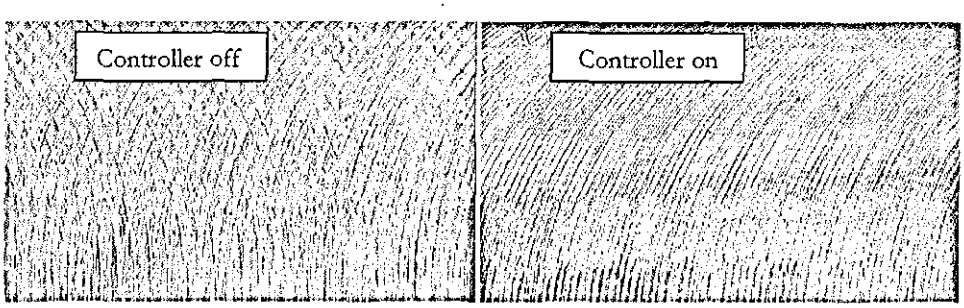

Figure 2.15 Comparison of surface profiles with controller on and off (Zhang et al. 2005)

However, this method is not suitable for practical applications, because the actuators were mounted on the workpiece which means that for each milling operation they have to be mounted and calibrated.

In the recent publication of the authors Sims et al. (2005) a very detailed mathematical approach for machine stability prediction has been investigated, where piezoelectric transducers were used to actively damp the chatter.

A similar design approach to the small scale planer (described in chapter 3) was introduced by Dohner et al. (2004) for vibration suppression of a milling machine (Figure 2.16).

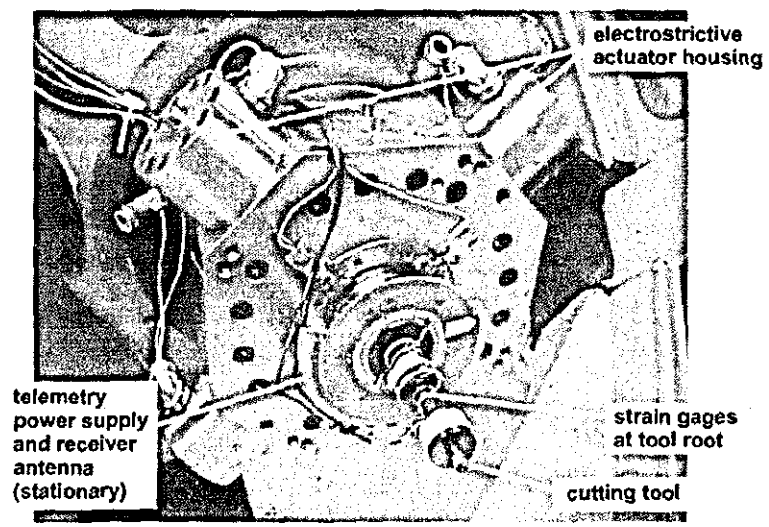

Figure 2.16 Spindle unit with four collocated electrostrictive actuators for a milling machine (Dohner et al. 2004)

Authors have implemented active vibration control using electrostrictive actuators surrounding the spindle unit (Figure 2.16). Strain gauges mounted on tool were used to sense vibration. This information was then sent to the control system where appropriate voltage signals for the electrostrictive actuators were defined. As a result of this process, actuators apply a force against the spindle unit. Optimal control technique, namely, linear quadratic gaussian regulator (LQG) was used to perform

the control action. Authors reported that LQG regulator produced high levels of robustness and performance. With the controlled forces produced by the electrostrictive actuators and exerted against the spindle, the authors reported a remarkable chatter reduction as shown in Figure 2.17.

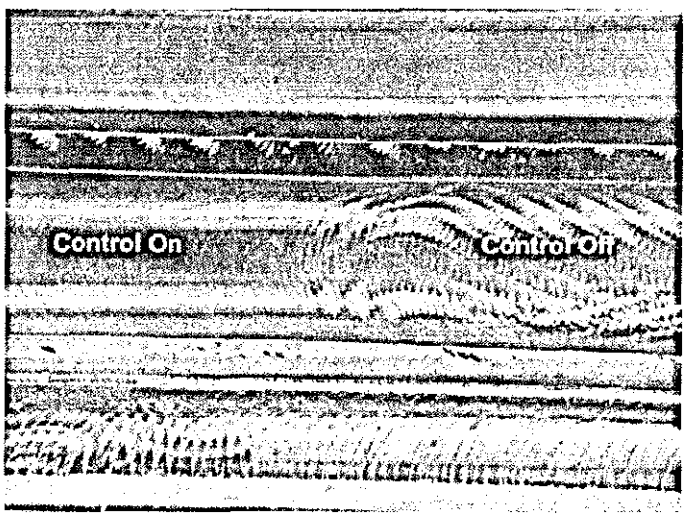

Figure 2.17 Surface finish improvement with LQG (Dohner et al. 2004)

Authors also reported that the maximum stable depth of cut could be increased by a factor of *4*. The main advantage of this approach is that the spindle speed is within the confined operation section of n_{min} and n_{max}, thus excessive tool wear would be avoided. However, the authors also outlined the complex set up of the experimental part. For example a telemetry system was built to transmit strain data from the rotating spindle to stationary receivers where further specific co-ordinate translation algorithm was necessary. Moreover, electrostrictive actuators are solid-state actuators similar to piezoelectric actuators. Electrostrictive material strains proportionally to the square of the applied voltage in contrast to piezoelectric element which expands proportionally to the applied voltage. Moreover, the capacitance of the electrostrictive actuator is four to five times higher than the capacitance of piezoelectric actuators, thus they require higher dynamic current for dynamic applications. Furthermore, as a result of high capacitance, the dynamic range of the electrostrictive actuators is limited.

Rashid et al. (2005) developed an active controlled workholding system for milling operation (Figure 2.18). Unlike the conventional control of the machine spindle, authors proposed to reduce machine chatter by controlling the workholding fixtures with piezoelectric actuators. Authors reported that the reduction of chatter is also possible by controlling the workholding fixture.

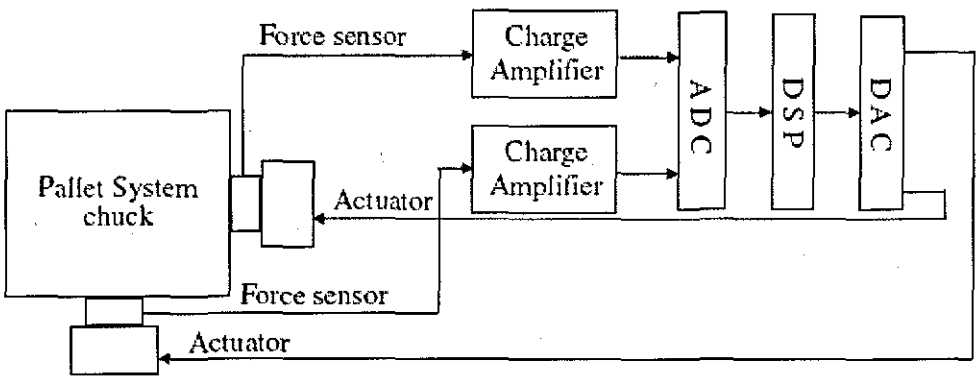

Figure 2.18 Active control system for the pallet system (Rashid et al. 2005)

Lauffer et al. (1998), Shankar et al. (1998) and Regelbrugge et al. (2002) developed a smart spindle unit for the chatter suppression of a milling machine. The goal of the research was to develop a chatter suppression system for horizontal octahedral hexapod milling machine in order to increase MMRR, which is generally limited by the onset of chatter. The spindle movement was controlled by four electrostrictive ceramic actuators. Their actuators consisted of five segments with *20 mm* of diameter which was glued together to form a *50 mm* long ceramic actuator with a stiffness of *300 N/μm*. The actuators were able to deliver *15 μm* stroke under a load of *6 kN* at maximum voltage of *150 V*. Their spindle unit was designed to operate at *6000 rpm* with a *30 HP* motor. Their experimental results showed that the stable depth of a full-immersion cut was increased by factor in the range of *2-20* and the depth of a partial-immersion cut was increased by *85-220 %*. The authors stated that the smart spindle unit could improve the productivity by factors ranging from *2 -20*.

2.4.1.2 Active Vibration Control within the Turning Process

A considerable amount of research on tool positioning within the turning process with piezoelectric actuators has been carried out by many researchers. Woronko et al. (2003) developed a single axis tool servo system for precision turning of local areas of the workpiece on a CNC machine. Force fluctuations during the turning process limit the precision of the machine. Capacitive displacement sensors were used as feedback for the control system which minimizes the tracking errors introduced by the non-linear behaviour of the piezoelectric actuators. In order to minimize the force variations, authors designed a solid flexure to transmit forces generated by the stack type piezoelectric actuator to the turning tool assembly. Authors reported that the piezoelectric actuators are capable of delivering the counter forces required for an accurate positioning of tool system within *20 nm* range.

For high precision diamond turning applications Paterson and Magreb (1985), Hara et al. (1990), Fawcett (1990), Okazaki (1990) and Shamoto et al. (1997) have also used piezoelectric actuators to improve tool positioning accuracy.

Andren et al. (2003) developed an active tool holder for a lathe. The holder was equipped with a piezoelectric stack type actuator and an integrated accelerometer. The actuator and the sensor were integrated into the tool holder simply by milling a space into the bottom part of the tool holder (Figure 2.19).

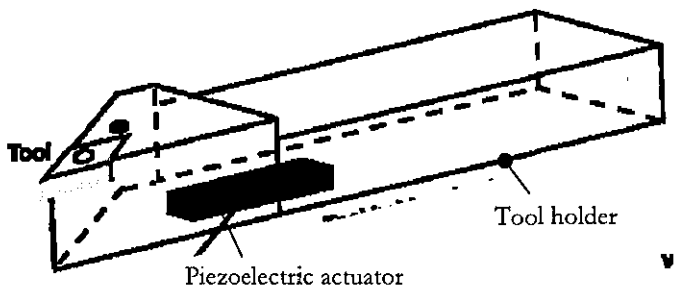

Figure 2.19 Active tool holder (Andren et al. 2003)

The authors reported a cutting tool vibration reduction level of *40 dB* at *3.3 kHz* for typical machining parameter settings (i.e. cutting speed = *80 m/min*, depth of cut = *0.9 mm* and feed rate = *0.25 mm/rev*). However, Hakansson et al. (1999) reported that the major drawback of this embedded actuator arrangement is the stiffness reduction of the tool holder by up to *20%*. This in turn set limitations on the actuator geometry in order to keep the tool holder stiffness at an acceptable level.

Ganguli et al. (2005) developed an active mass damper to suppress chatter present within the metal turning machine tool. Authors used a laser source to detect the vibrations and fed it in a closed loop opearion to the active mass damper, which set the damping coefficient so that a stable operation lobe was achieved.

An extensive numerical analysis on the chatter characteristics within the turning process was studied by Baker et al. (2002). In their studies, the authors used finite element method to model the structural machine parameters (machine design parameters) in order to identify the cross-coupling effects between tool and workpiece. However, the authors reported about the difficulty of predicting the cutting forces, which has limited their numerical method for chatter modelling.

Kim et al. (1997) developed an active control system for an ultra precision lathe. They used piezoelectric actuators to control the cutting tool. Authors reported a waviness reduction over *40%*.

2.4.1.3 Active Vibration Control within the Boring Process

Another typical example of a cutting tool used in the metal machining, which is susceptible to chatter, is the boring process. Wong et al. (1995) used active magnetic actuators to develop an active dynamic absorber for an overhung boring bar with *8:1* ratio. In this work, the electromagnetic force acting on the absorber were controlled to adapt the absorber frequency to the vibration frequency of the boring bar. The control method was based on the combination of the modal control and direct output feedback method. The modal control approach was basically used to determine the full state feedback of the system with the objective to define and control the critical modes of the system.

Tewani et al. (1991) simulated an active dynamic absorber with piezoelectric actuator to suppress chatter in a boring bar (Figure 2.20). Tewani et al. (1992) reported that piezoelectric actuators are capable of delivering the force and the bandwidth required to efficiently suppress the chatter by *30%*. The authors also used optimal control method for this application.

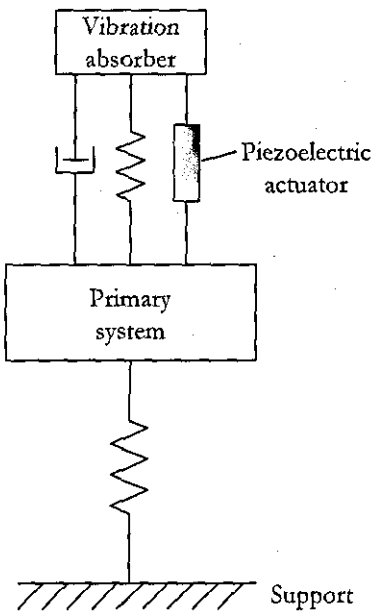

Figure 2.20 Active dynamic absorber with piezoelectric actuators (Tewani et al. 1991)

Min et al. (2002) developed a smart boring tool for line boring in the automotive industry. The boring bar is fixed to the rotating spindle at one end with a roughing cutter and a finishing cutter attached to the free end. A piezoelectric actuator controlled the finishing cutter. The position of the finishing cutter and the deflection of the boring bar relative to the spindle were measured by laser detectors. The design allowed the smart tool to be used with an automated tool changer. Thus, all the instrumentation including controller was built into the tool body, which rotated with the spindle. A non-contact power transformer provided power for the controller and the piezoelectric actuator. The non-contact power transformer was also used to transfer data between the smart tool and the machine tool itself. Their experiments showed that the tool tip position error could be reduced significantly.

Another application of the piezoelectric actuators for the boring operation is reported by Chiu et al. (2002). They developed an overhung boring bar servo system for on-line correction of roundness errors. The control of the cutting tip is realized via a lever structure with a piezoelectric actuator on one end and the cutting tip on the opposite end. Strain gauges are used to measure the position of the cutting tip. The boring bar was able to correct roundness errors as high as *20 μm*. The authors reported roundness error reduction as high as *40%*.

Tanaka et al. (1994) used piezoelectric actuators to develop an active damper to attenuate chatter of a slender boring bar. Authors detected the chatter frequency and produced a counter force with the help of piezoelectric actuators to suppress the targeted frequencies by increasing the damping. A similar approach has been reported by Matsabura et al. (1989), Pratt and Nayfeh (1998, 1999) who modelled the dynamic characteristics of a boring bar by using impulse forces generated by the piezoelectric actuator and measured the system response with an accelerometer in order to define the frequency response function (FRF). The relevant modes of the system were then defined with the aim to increase damping and reduce chatter at the desired frequencies.

2.4.2 Vibration reduction methods for woodworking machinery

It should be noted that in the metalworking machinery, chatter is one of the main factors which results in poor surface quality, whereas within the woodworking, the main factors responsible for surface quality are tool settings, tool inaccuracies and spindle vibrations.

To date, productivity improvement techniques within the furniture industry have paid little attention for further research and development of woodworking machines (Ratnasingam et al. 1996). The competitive market of the woodworking products is mainly driven by low raw material and labour costs. Although wood machining process is an essential part of the furniture manufacturing, it has not been considered as the main objective to enhance the productivity. Wood is a precious natural resource and the growing demand for woodworking products will further increase the raw material costs. In order to compensate for the increased raw material prices and further increase the throughput, manufacturing machines within the woodworking domain are required to finish the end products more efficiently (Ratnasingam et al. 1999). The manufacturing costs however reveal that ca. *23%* of the total production costs are related to the machining process. Thus, improvements within the woodworking machinery will inevitably lead to higher production throughput and reduce manufacturing costs (Hoff et al. 1997).

Research on wood machining process world wide is mainly focused on tool improvement, reduction of cutting edge wear and component design optimisation (Ratnasingam et al. 2005). Therefore, there is a very little amount of research reported on the woodworking machinery in terms of vibration control. The presence of the vibrations during the machining process results in surface waviness. Vibrations mainly occur between the relative movements of the cutterhead and the workpiece. These vibrations can be suppressed by a passive or active approach as aforementioned in the metalworking domain.

Active vibration control techniques implemented within the metalworking machinery are mainly focused on controlling the spindle vibrations. There is no significant record of research in the vibration control of woodworking machinery. Therefore, the technologies developed to actively control spindle vibrations for the metal working machinery are widely applicable to the woodworking machinery, because the needs of woodworking machinery are assumed to be similar to those of the metalworking sector which gained more attention in terms of research and funding.

Brown et al. (2002) developed a method to improve the surface waviness by reducing the cuttermarks height. This was achieved by additional cutterhead movement in horizontal direction. With this approach, the cutterhead moves horizontally when each knife contacts the timber surface. Before the subsequent knife touches the workpiece, the cutterhead retract to the standard position. This method changes the shape of the cuttermarks and they become shallower than the scallop-like cuttermarks produced by the conventional machining process, thus a smoother surface was achieved.

Circular saws are widely used in woodworking for many applications such as lumber manufacturing, furniture industry and home workshops. Wood is a precious natural resource and its availability has become more limited, hence its price is increasing. Active vibration suppression of sawmills has become an economic necessity in terms of material recovery, because *12 %* of the machined wood in sawmills is sawdust and further *7 %* is lost in planer shaving of uneven surfaces resulting from saw blade vibrations. It has been reported that dust is hazardous to human health and in particular cases it can lead to nasal cancer (Palmqvist et al. 1999). Therefore, the vibration suppression, hence dust reduction is not only an economic issue but also important in terms of healthy working environment. Most studies on circular saws have been focused on improving saw design with the aim to increase the stiffness which in turn would minimize the resonant vibrations.

Schajer et al. (2001) studied the effect of vibration in circular saws and outlined the interaction between workpiece and the saw blades. Ellis and Mote (1979) were among the pioneers to use active AMBs for circular saw blades to minimise the vibration. Authors reported an increase and damping values at about *400%*, hence saw blade vibrations were suppressed remarkably. Wang et al. (2001) investigated on the implementation of modal control method for a circular saw equipped with magnetic actuators. Chen et al. (2003) implemented optimal control technique for the same circular saw machine reported by Wand et al. (2001). Authors used two pairs of electromagnetic actuators mounted along the horizontal diameter of the saw blade in proximity of the blade surface to perform active control. The vibration of the saw blade is measured with the non-contact proximity sensors. This information is fed to the control system to determine the driving current for the magnetic actuators (Figure 2.21).

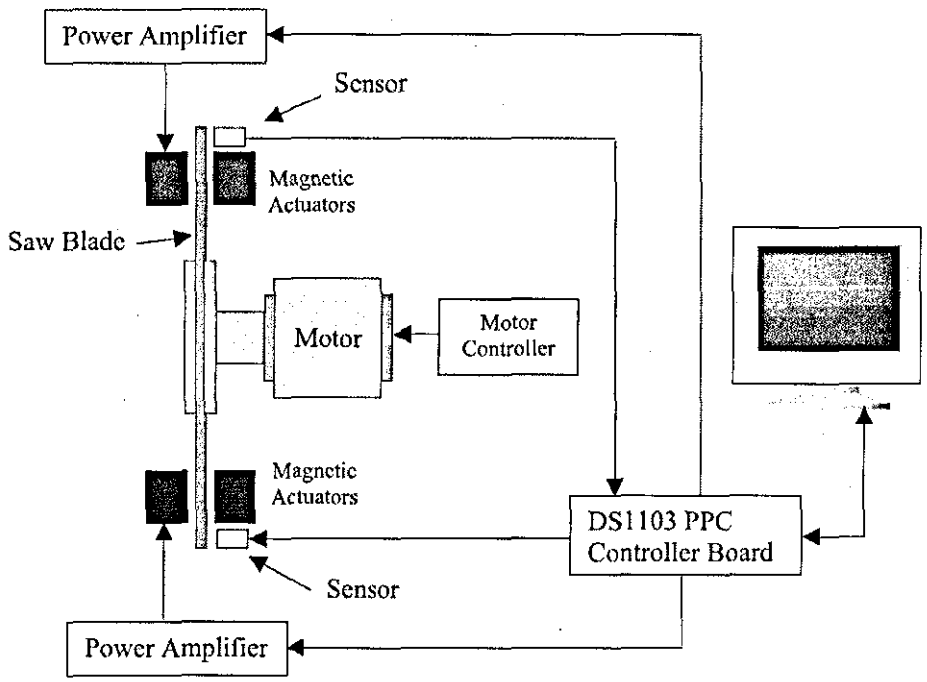

Figure 2.21 Schematic diagram for active vibration control of a saw blade (Chen et al. 2003)

The active vibration control law was realised with the LQG regulator (Figure 2.22).

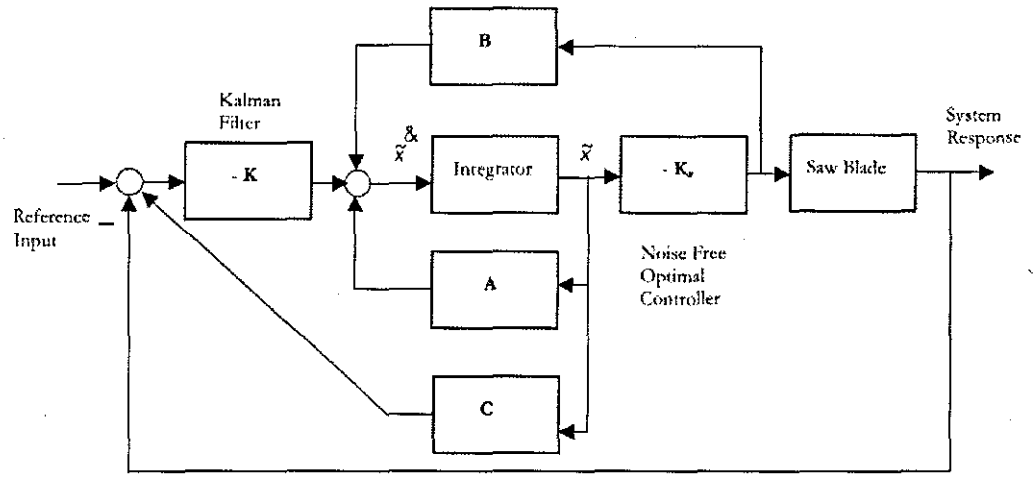

Figure 2.22 Active vibration control with LQG regulator

LQG regulator is an optimal control method which is a time integral of a quadratic function of the system states and inputs (Lewis 1992). The main objective of this approach is to minimize the state response with minimal control effort. LQG method is also known as cost minimisation method. In case of vibration control, the cost function contains vibration response (i.e. signal and disturbance) as the state variables and minimizes the control effort which is needed to suppress the disturbances. Disturbances were determined and the Kalman filter (optimal estimator) was used to estimate the feedback signal. Authors reported remarkable vibration reduction as high as 66%. The benefits of reduced vibrations are improved machine tool life, high product quality, noise reduction and significant economic wood recovery.

The LQG control approach is also proposed for the small scale planer (optimal control and Kalman filter are described in more details in chapter 7).

Chapter 3 PREVIOUS WORK – SMALL SCALE PLANER

The aim of this chapter is to introduce the previous work and to outline the improvements that are proposed as a part of this research work. Furthermore, the capabilities of the small scale planer as well as its limitations are discussed. A small scale planer was built by Hynek (2004) as part of his PhD project. It is capable of improving the surface form by vertical cutterhead movement. The small scale planer comprises of mechanical design, instrumentation and control which are introduced in the next sections.

3.1 Design of the Small Scale Planer

The small scale planer consists of a base frame on which the feed table and spindle system are mounted (Figure 3.1). The spindle system can be displaced vertically for controlled cutting conditions. The feed table consists of a ball screw, high precision linear guides and feed bed on which the workpiece can be mounted.

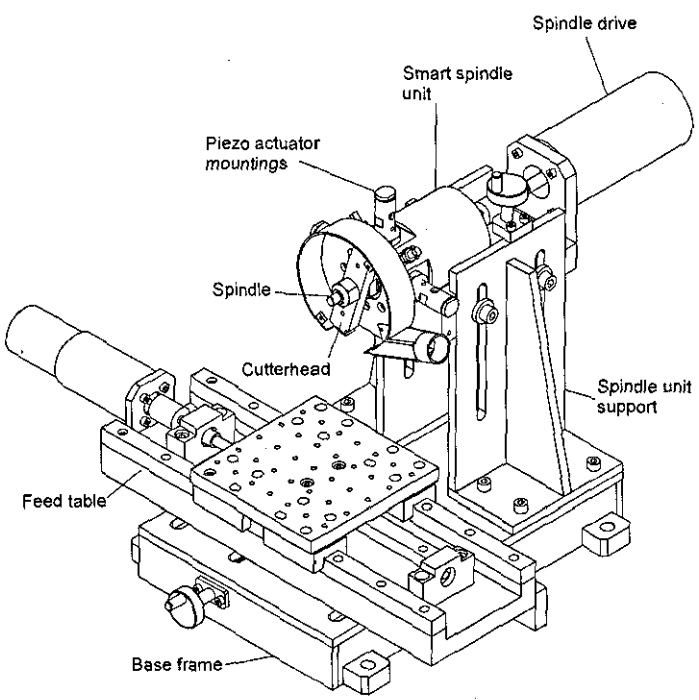

Figure 3.1 Small scale planer (Hynek 2004)

The cutterhead is located on the overhung end of the spindle. The spindle is supported by two precision angular contact ball bearings. The vertical cutterhead movement is accomplished by the displacement of the front bearing. It can also be described as a cantilever system. This arrangement introduces cutterhead and knife tilt. The maximum amount of the knife tilt is less than *8 %* so that its effect on the resultant surface can be neglected.

The front bearing is fitted in the front ring which is supported by four spacers (Figure 3.2). Four piezoelectric actuators are mounted on the front bearing. Applying appropriate voltage levels to the piezoelectric actuators controls the movement of the spindle in the plane perpendicular to the spindle's rotational axis.

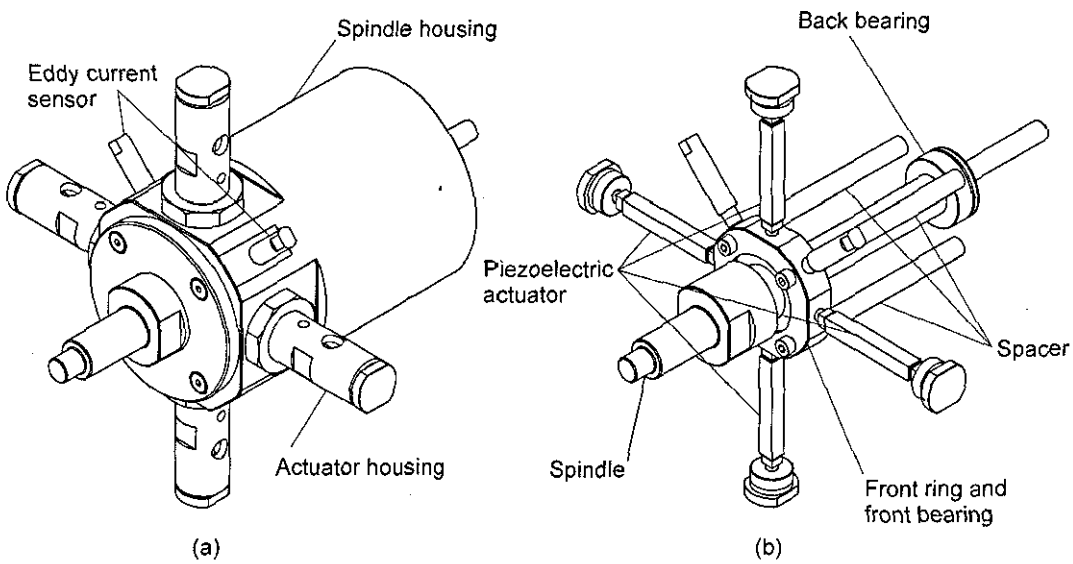

Figure 3.2 Spindle system with piezoelectric actuators and eddy current sensors (Hynek 2004)

The spindle displacement in the plane perpendicular to the spindle's rotational axes needs to be measured in order to control its movement. The movement of the spindle is measured via two eddy current sensors by measuring the movement of the front bearing.

3.2 Instrumentation of the Small Scale Planer

The small scale planer has been instrumented with an incremental encoder, two eddy current sensors, signal conditioning circuits, four driving amplifiers (one amplifier for each piezoelectric actuator) and a control computer in order to implement the controlled cutterhead displacement. Figure 3.3 shows the instrumentation with all key components along with the signal flow between the small scale planer and control computer presented by the multifunction I/O card.

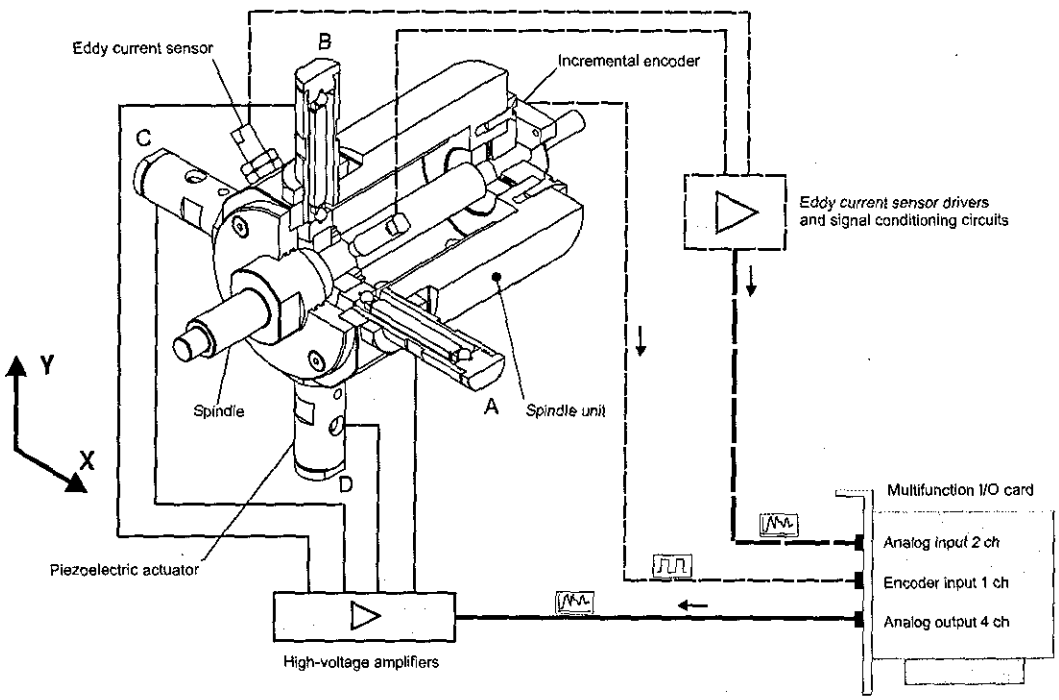

Figure 3.3 Instrumentation of small scale planer (Hynek 2004)

The spindle unit is equipped with two non-contact eddy current sensors to measure the XY displacement of the spindle. The eddy current signals are then amplified with the eddy current driver in order to increase the resolution and minimize the influence of the noise. These signals are then converted into digital signals with the multifunction I/O card. Instrumentation specifications can be found in the appendix A.

It is also equipped with an incremental encoder in order to measure the angular position of the spindle. These two measures (XY displacement and the angular position of the spindle) are then used to send appropriate signals to the high voltage driving amplifier. The amplifier send then a corresponding voltage level to the piezoelectric actuator, which apply a force against the spindle and cause a controlled displacement.

The small scale planer's instrumentation includes control computers, which are used to acquire the sensor readings (incremental encoder and eddy current sensor readings) in order to adjust the input voltage for the piezoelectric actuators in real time. Matlab xPC Target prototyping environment is used to carry out the real-time control applications. Matlab xPC-Target prototyping environment consists of a host computer and a target computer, which are connected via Ethernet link with capacity *10 Mb/sec* as depicted in Figure 3.4.

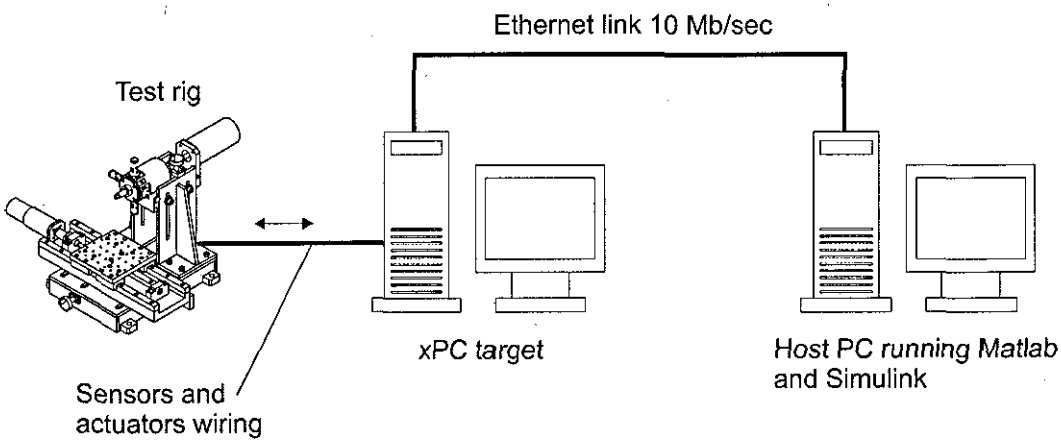

Figure 3.4 Matlab xPC-Target prototyping environment (Hynek 2004)

The xPC target computer is running under xPC-Target real-time kernel, and the host computer is running under Windows 2000 with Matlab/Simulink program. The xPC target computer is equipped with a multifunction I/O card which provides sensor readings. The real-time application is designed within Simulink on the host PC.

After compiling the Simulink diagram, the executable code is uploaded via Ethernet link to the xPC target PC which is capable of executing applications in real-time. The reason for using two control computers is that, the applications cannot be executed in real-time with a PC running under Windows.

3.3 Operation Principle of the Piezoelectric Actuators

The piezoelectric actuators are capable of controlling the vertical spindle movement by ca. $\pm 18\ \mu m$. Actuator specifications are stated in the Table 3.1. All four piezoelectric actuators are identical.

Table 3.1 Piezoelectric actuator specification

Max input voltage, V	150	V
Actuator stiffness, k_p	14	N/μm
Zero load displacement @ 150V, y_0	40	μm
Blocked force, F_{p0}	0.56	kN
Actuator capacitance, C_p	2.3	μF
Cross-sectional area, A	25	mm^2
Length, L	19.5	mm

The piezoelectric actuator expands when a voltage is applied to its electrodes. Their displacement is proportional to the applied voltage. Driving voltage is in the range from 0 to $150\ V$ for low voltage piezoelectric actuators. Maximum displacement under no load condition varies from 8 to $100\ \mu m$. The maximum exerted pushing force is in the range from 0.2 to $4\ kN$ for piezoelectric stack-type actuators. This type of actuator is able to act only in one direction, since they are susceptible to tensile stress. They are not able to pull the force. Therefore, two opposing actuators for each axis acting in "push-pull" operation shown in Figure 3.5. The actuator characteristics and operation are described in more details in Chapter 6.

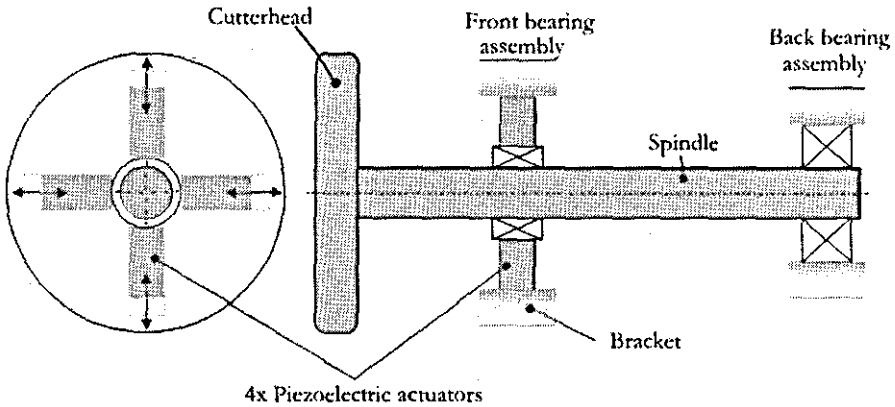

Figure 3.5 Actuator and spindle model

3.4 Surface Form Improvement by Vertical Cutterhead Movement

The principle behind the vertical cutterhead movement is that when a knife is at the start of the cutting path, the cutterhead moves upwards and reaches its point of maximum displacement when the line connecting the knife tip and cutterhead centre is perpendicular to the machined surface. After reaching its maximum point, the cutterhead moves downwards (Figure 3.6).

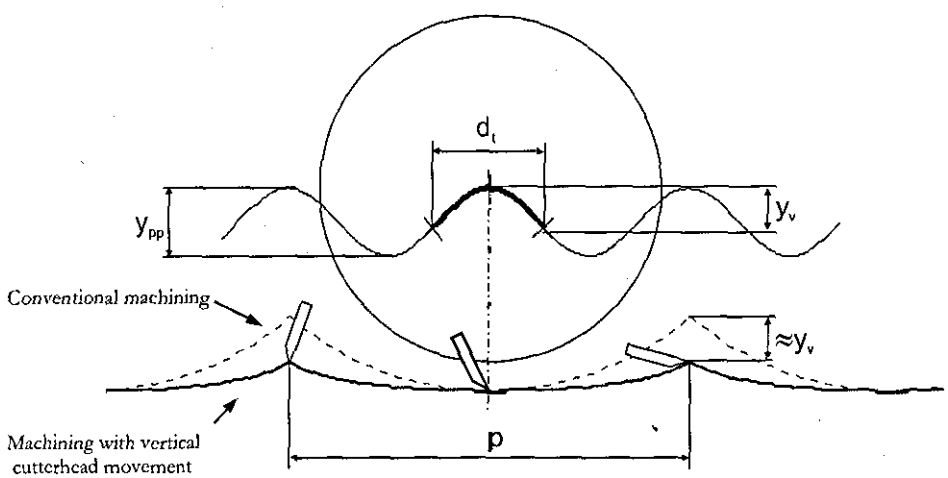

Figure 3.6 Principle of vertical cutterhead movement (Hynek 2004)

The cutterhead movement takes place in a very narrow time window Δt. It is defined by the machining parameters such as cutting speed v_c, feed speed v_f and length of cuttermark p. The time window can be expressed as follows:

$$\Delta t = \frac{p}{v_c + v_f}. \tag{3.1}$$

The time, Δt, can also be perceived as the time that the cutterhead needs to travel for one cuttermark length p (Figure 3.7).

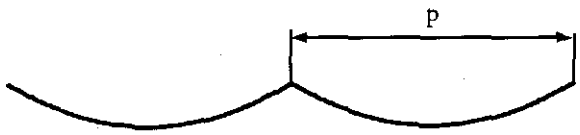

Figure 3.7 Cuttermark length, p

The resultant surface can only be influenced during this time window Δt. The vertical cutterhead movement influences the knife tip path and the resultant surface form. The shape of the cuttermarks becomes shallow in comparison to the surface produced by the conventional machining method. The waviness height is reduced approximately by the amount of the vertical movement y_v that takes place within the time window Δt (Figure 3.6). The vertical pulses are implemented in an open loop control. The position of the vertical pulse is synchronized with the cutterhead rotation so that, at the peak of the pulse, the knife tip is in the cuttermark's centre. The cutterhead angular position, measured by the encoder attached to the spindle, is used to trigger the pulses.

The small scale planer is capable of reducing waviness heights up to 65% compared to waviness heights machined by the conventional machining operation. Figure 3.8 shows the difference between the cuttermarks' heights of a conventional machined surface and the one machined with vertical cutterhead movement method.

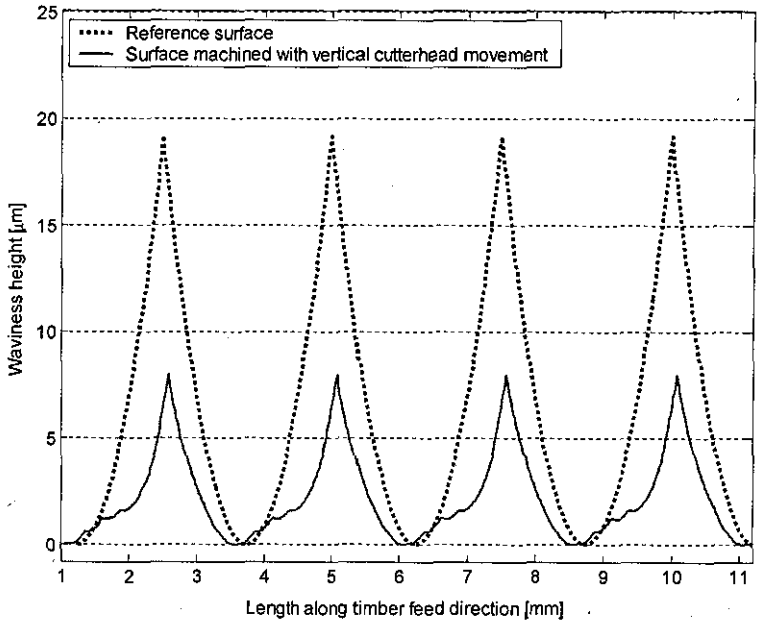

Figure 3.8 Surface form improvement by vertical cutterhead displacement (Hynek 2004)

3.5 Limitations of the Vertical Cutterhead Movement Method

The vertical cutterhead movement was implemented as a pulse train with the pulse width equal to the time window Δt and the pulse magnitude equal to the desired waviness reduction (i.e. *2-20 µm* considering typical waviness height). The conventional rotary machining of timber is characterized by a high cutting speed, typically within the range *20-100 m/s*. This machining speed would result in a very narrow time window. For example, a surface with cuttermark length of *1 mm*, machined with the cutting speed of *40 m/s*, according to equation (3.1) would require the pulse width *25 µs* to reduce the surface waviness (i.e. given the fact that the feed speed is negligibly small and typically in the range of $v_f \approx 1\ m/s$). Equation (3.2) further describes the dependency of the pulse width on the machining parameters as reported by Hynek (2004).

$$\Delta t = \frac{2\pi}{N\omega(\mu+1)} \tag{3.2}$$

Where ω is the rotational cutterhead speed, N number of cutting knives and $\mu=v_c/v_f$ is the cutting speed to feed speed ratio. The parameter μ is a suitable measure for describing the rotary machining process with typical values ranging from *40* up to *300*. Generally lower values of μ indicate machining operations with lower cutting speed and lower feed rates (i.e. $v_c=30\ m/s$, $v_f=0.1\ m/s$), whereas higher values of μ refer to higher cutting speed and higher feed rates (i.e. $v_c=80\ m/s$, $v_f=1.6\ m/s$). Figure 3.9 shows the values of $1/\Delta t$ for typical range of cutterhead speed and the ratio μ for a single knife cutterhead (i.e. $N=1$). The pulse width is in the range from *25* μs up to *1 ms* and it is even N times smaller for multi-knife cutterhead.

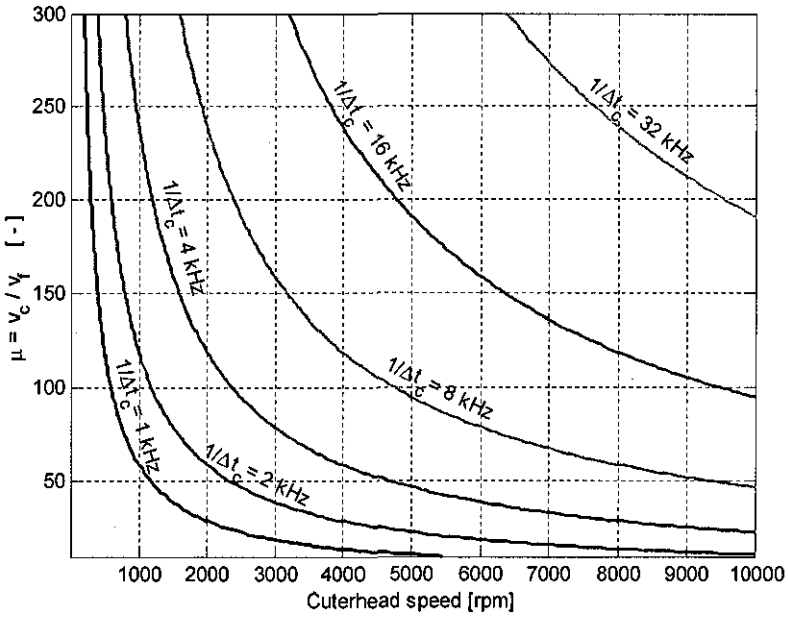

Figure 3.9 Pulse width dependencies on machining parameters (Hynek 2004)

Genereally, high values of μ results in very narrow pulse widths and low values of μ in wider pulse widths. However, the pulse width depends also on the rotational spindle speed. For example, for a single knife cutterhead with radius *50 mm* running at *10000 rpm* with *13 m/min* feed speed, results in *241* for the μ ratio and the pulse width is *25* μs. If the cutterhead speed is reduced to *4000 rpm*, the μ ratio corresponds to *97* and the pulse width is reduced to *155* μs.

This duration of the time window available for controlling the vertical cutterhead movement is still very narrow and set some limitations on this approach. The narrow pulse suggests that the force due to acceleration is very high. An estimation of the acceleration force can be obtained by assuming that the cutterhead follows a sine wave as defined by equation (3.3).

$$y = \frac{y_v}{2}\sin\left(2\pi\frac{1}{\Delta t}t\right) \tag{3.3}$$

Where y_v is the pulse magnitude and Δt is the pulse width. The peak acceleration force is then defined as follows

$$F_{max} = m_c y_v \frac{2\pi^2}{\Delta t^2} \tag{3.4}$$

where m_c is the cutterhead mass. The dependence of the peak acceleration force on the cutterhead mass and the pulse width for a pulse magnitude of *10 μm* is shown in Figure 3.10.

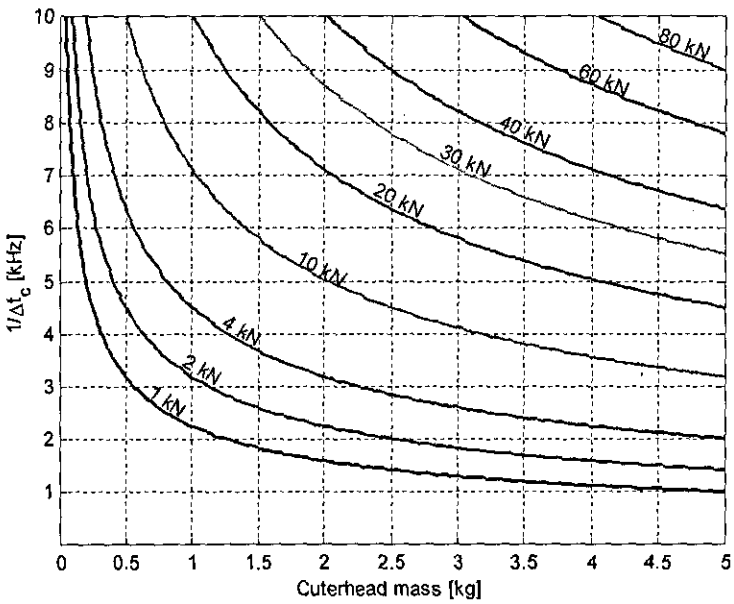

Figure 3.10 Peak acceleration force vs cutterhead mass (Hynek 2004)

For narrow time windows, the piezoelectric actuators are not capable of providing high forces within the available short time period to perform the vertical cutterhead movement. For example, the peak acceleration force for a *5 kg* cutterhead osciallting with peak to peak amplitude of *10 μm* at *8 kHz* is *63 kN*. These operating ranges are outside the performance envelope of the available piezoelectric actuator (i.e. when compared with Table 3.1). Therefore, the vertical cutterhead movement for reducing surface waviness is more suitable for lower cutting parameters (i.e. spindle speed=*600 rpm*, feed speed=*1.5m/min*) where the time window is wider.

3.6 Improvements Compared to Previous Work

The small scale planer has, beside cutting speed limitation, another restriction. The width and the magnitude of required pulse train (for vertical cutterhead movement) has to be set according to the desired waviness reduction level. Once the pulse characteristic has been defined, the vertical cutterhead movement follows the same pattern. Therefore, it is not adaptable to undesired vibrations and disturbances. Its application focuses more on wood shaping rather than suppressing vibrations which can cause severe surface defects on the machined surface profile. Although Hynek (2004) has shown through simulation as well as through experimental work that the controlled vertical cutterhead movement can reduce the surface waviness remarkably, this technique is not applicable within the real woodworking planer where higher throughputs rates are desired, thus higher control forces from the actuator are required.

Therefore the focus of this thesis is to develop a closed loop control system in order to suppress the undesired vibrations, hence achieving an enhanced machining environment. Unlike the previous approach which is mainly focused on rotary machining improvement through modification of the cutterhead displacement, the proposed improvement method targets a different improvement method, namely active vibration control.

This is achieved by implementing the optimal control method on the small scale planer (optimal control strategy is described in more details in chapter 7).

As a result of this control method, the dynamic characteristics of the spindle system will be further improved so that spindle speed can be increased regardless of the knife cutting frequency which may be beyond the first natural frequency of the spindle system. This capability would allow increasing the spindle speed at its maximum range irrespective of the natural frequency of the system, hence a higher operating range will be achieved. This in turn would yield higher surface quality and higher throughput rates. Furthermore, a surface profile monitoring system is proposed which is capable of providing surface profile information in real-time (described in chapter 5 in more details). These improvements are the main objectives of this research work.

Chapter 4 SURFACE WAVINESS ON MACHINED TIMBER

The objective of this section is to outline the occurrence of the waveforms on the machined timber as well as to point out the machining variations and their effects on the resultant surface quality. Machine system variations can often affect the consistency of the surface profile pattern. Especially, spindle vibrations and cutterhead inaccuracies have great impact on the resultant surface waviness quality. These effects are first described theoretically and further investigated through simulation as well as experimental work.

4.1 Wood Machining Principle

Rotary machining has been an essential part of the woodworking industry for over two centuries and is applied to good effect in planing and moulding machinery. The principle of the rotary machining process is such that a timber is fed towards a rotating cutterhead containing a certain number of cutting knives. This process is illustrated in Figure 4.1.

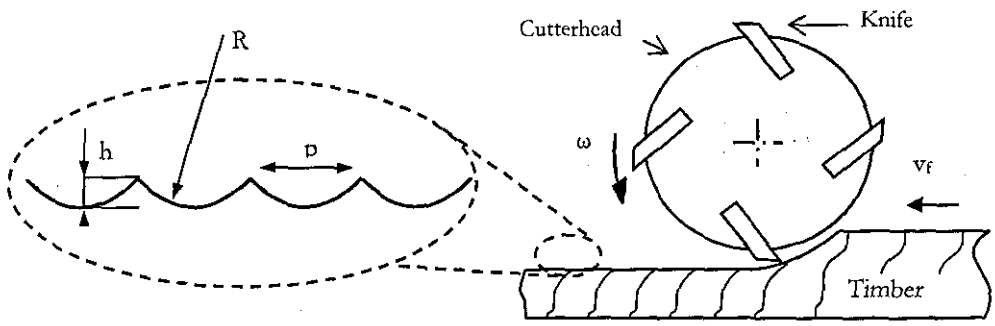

Figure 4.1 Principle of rotary machining process

This machining process is similar to milling metals in up-cutting mode. The main differences between these two cutting modes are the cutting speed and the feed speed.

Cutting speed for wood machining lies in the range *30 – 80 m/s* compared with *0.5 – 1.5 m/s* for the milling of metals. The feed speed within the woodworking machinery is correspondingly high, ranging from *0.08 m/s* up to *1.6 m/s* (Hynek 2004). Figure 4.1 shows the machined timber surface which is not ideally smooth and flat but consists of a series of waves due to the kinematics of the rotary machining process. The surface waves, also called cuttermarks, are generally accepted as unavoidable. The length of the cuttermark p, also called pitch, is usually taken as a measure of surface quality. Table 4.1 shows the different quality levels with the typical corresponding heights produced by a cutterhead with diameter D= *120 mm*.

Table 4.1 Surface quality classification

Surface quality	Cuttermark length (mm)	Cuttermark height (μm)
Average	2.0 - 2.5	8.3 - 13
Good	1.5 - 1.8	4.7 – 6.8
High	<1 .0	<2

A good surface quality is characterized by a cuttermark length between *1.5 – 1.8 mm* with *4.7 – 6.8 μm* height and surface waviness should follow a uniform pattern. The high quality surface finish should have cuttermarks of *1 mm* length in a regular manner. This profile is almost undetectable with human eyes and the regularity of the waves appears as "wave free" (Jackson et al. 2002).

The length of the cuttermarks p depends on the workpiece feed speed v_f, the cutterhead rotational speed ω and the number of finishing cutting knives N. This relationship can be expressed by equation (4.1).

$$p = \frac{v_f}{\omega \cdot N} \tag{4.1}$$

It is often assumed, for simplicity, that the shape of the cuttermarks is circular and that the surface can be considered as a series of intersecting circular arcs. The waviness height h of the simplified surface can then be expressed by the following equation

$$h = R - \sqrt{R^2 - \frac{p^2}{4}} \tag{4.2}$$

where as R is the cutterhead radius. These equations (4.1) and (4.2) are well established and widely used (Jackson et al. 2002).

4.2 Surface Profile Modelling

In planing and moulding machining processes, the rotating knives at the rotating speed ω, removes material (i.e. in form of wood chips) from the workpiece. The resultant surface wave shapes are cycloid due to kinematics of the rotary machining process (Luo et al. 2003, Palmqvist et al. 2003). However, the particular machining characteristics of these processes (i.e. cutting knives are straight in contrast to the helical cutting edges used within metalworking) allow a simplified 2D model of the surface form.

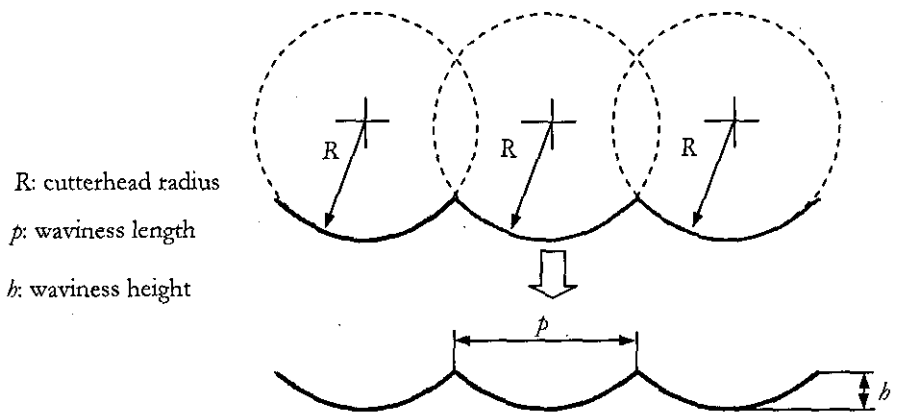

Figure 4.2 Circular arc theory to model surface waviness

The most simple surface form model is the circular arc theory which is based on the intersection of a series of circular arcs (Figure 4.2). It should be pointed out that the length of the cuttermark is independent of the cutterhead radius which is described by the equation (4.1). The length p is simply the distance that the timber travels between two consecutive knives. Due to the kinematics of the rotary machining process the cycloidal shape of the cuttermarks is slightly shallower than the approximation through the circular arcs theory which is compared in Figure 4.3.

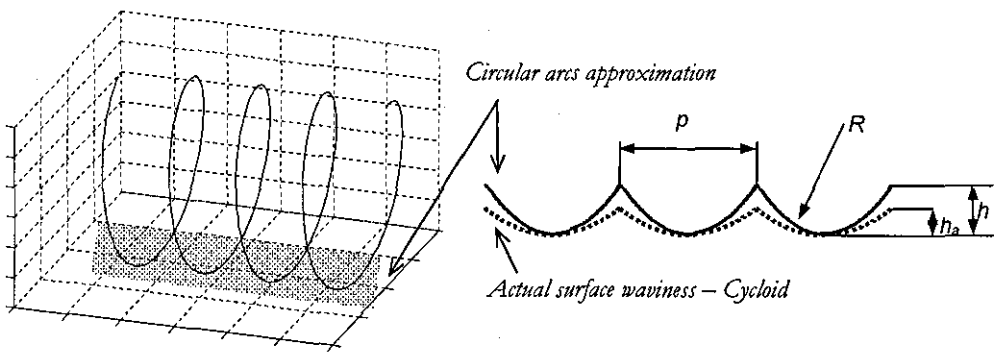

Figure 4.3 Shape of cuttermarks as a series of cycloidal path

The cycloid surface height is ca. 5% lower than the simplified circular height expressed by equation (4.2) (Hynek 2004).

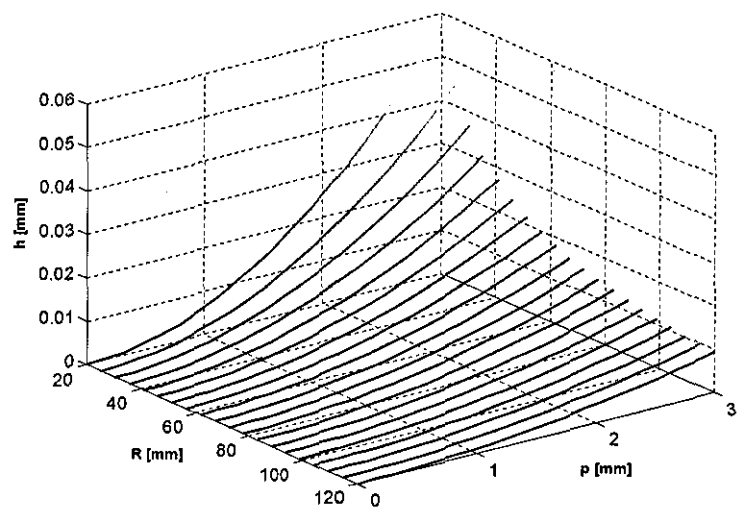

Figure 4.4 Dependencies among the parameters R, p and h

This low error ratio justifies the use of surface waviness approximation by the circular arcs for rotary machining process used within the woodworking domain. An exact calculation of the cycloidal path can be found in the appendix B. Figure 4.4 shows the dependency among the factors (cutterhead radius R, cuttermark length p and cuttermark height h) which form the resultant surface profile.

4.3 Surface Profile Characterisation

The surface quality of the machined workpiece is characterized by two features (Jackson et al. 2002):

- surface roughness
- surface waviness

Surface roughness is defined as the shorter-wavelength component of the surface waviness. Roughness appears together with the surface waviness. It could also be interpreted as the surface waviness distortion with higher frequencies. Figure 4.5 displays the difference between the surface roughness and an ideal surface waviness.

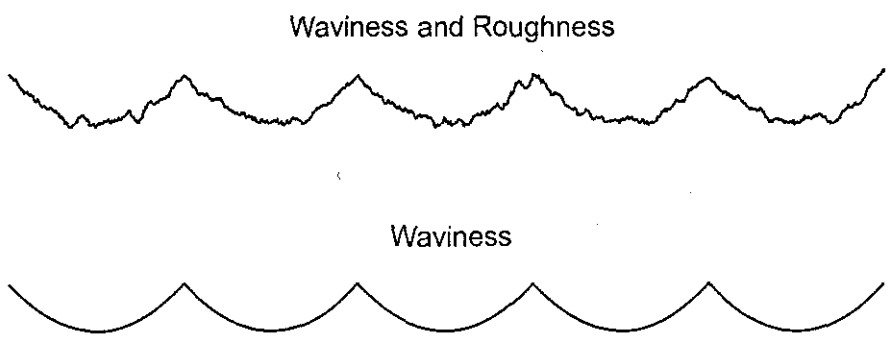

Figure 4.5 Wood surface profile with roughness and waviness

Surface roughness is predominantly affected by the following factors (Jackson et al. 2002):

- Workpiece properties (i.e. wood species, moisture content etc.)
- Cutting knife condition
- Velocity of the cutting knife relative to the workpiece
- Average chip thickness

Clearly, the end surface form of a machined timber consists of waviness plus a certain amount of roughness. For some application such as window frames or furniture, the surface waviness has a higher importance than the surface roughness. Ideal surface waviness is defined as the longer-wavelength component of the surface profile which is predominately determined by the feed speed, spindle speed and cutterhead radius. The real surface form of a machined timber however, is highly susceptible to machine system variations, which in turn can lead to inconsistent surface quality levels. The variations can be divided into three major groups. Firstly, workpiece properties such as wood species and moisture content affect the surface quality. Secondly, machining parameters such as cutterhead speed, feed speed and number of cutting knives primarily determine the waviness form. Thirdly, undesired vibrations and inaccuracies within the machining process can reduce the surface quality severely. Some of these variations especially the effects of tooling inaccuracies and the spindle vibrations on the surface form are outlined in section 4.4.

4.4 Surface Defects and their Appearance Forms on Machined Timber

In the previous sections 4.1 to 4.3, factors that affect the surface quality and surface form of machined timber are outlined. In this section, the effect of spindle vibrations and machine tools, particularly the effects of cutting tool inaccuracies are analysed and demonstrated through simulation as well as experimental work.

To date, it has not been possible to control the wood machining process so that the effect of specific disturbances such as tooling inaccuracies or cutterhead vibrations can be generated to confirm the theory presented. Although the systematic investigation reported by Jackson et al. (2007) provides unique insight into understanding some of the basic engineering influences on machine performance. The mechatronics control approach presented in this section is capable of producing surface defects to order. Whilst this may seem at odds with reducing defects, it is part of the wider understanding of how tool path inaccuracies cause surface waviness defects. The surface profile analysis is carried out as follows

- The effect of single-knife finish is simulated and experimentally demonstrated
- The effect of two-knife finish is simulated and experimentally shown
- The influence of tooling and relocation inaccuracies on the surface form are analysed
- The effect of cutterhead vibrations, especially the effects of vertical spindle vibrations on the resultant surface form are studied and experimentally demonstrated

4.4.1 Single - Knife Finish

The "single knife finish" exists where the surface wave form is determined by the cutter with the largest radius in the cutterhead. This results from the insufficient precision of the cutting knives due to the cutter sharpening machine tolerances and the relocation inaccuracies between the cutter sharpening machine and planing machine spindles. It is not possible to produce cutting tools of exactly the same size. However, there are tolerance levels which indicate the quality of cutting edges. The difference between the cutting knife with the largest radius and the cutting knife with the shortest radius is defined as the "total indicated run-out" (TIR).

The difference among the cutting tool radii can reach up to *50 μm* for knives set in a cutterhead using a setting gauge (Jackson et al. 2002). For example, considering a cutterhead with two cutting edges and a TIR of *50 μm* located on a spindle rotating at *6000 rpm* with a timber feed of *12 m/min*. The resultant surface would have a pitch of *2 mm* which is in the low quality range, whereas with zero TIR, the ideal surface pitch would be *1 mm* which is a high quality finish, because the number of finishing knives is now $N=2$ (Figure 4.6). According to equation (4.1), the pitch p is also defined by the number of knives N. The higher the number of knives N the shorter the waviness length, hence a better surface finish can be achieved.

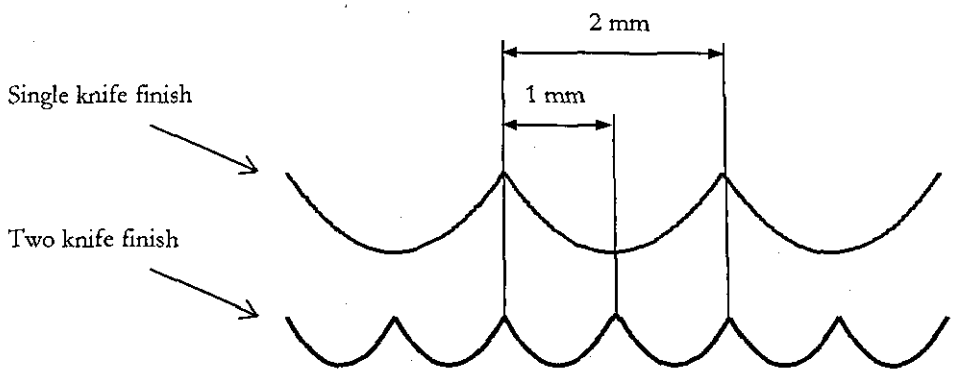

Figure 4.6 The effect of single knife finish and two knife finish on the ideal surface form

As aforementioned, high values of TIR cause that only the knife with the largest radius leave cuttermarks on the machined surface. This leads to lower surface quality and reduces the performance of the machining operation. A solution to minimize the effect of TIR is to grind the cutters in the cutterhead. Cutters ground in the cutterhead and then relocated on the planing machine spindle using hydrogrip tooling results in typically *5-10 μm* TIR but the inaccuracies cannot be completely removed. Despite the deployment of high precision knives and the grinding of the knives in the cutterhead, the uniformity of the surface waviness with an acceptable surface quality cannot be assured. Figure 4.7 shows the effect of a cutterhead consisting of two knives with different radii.

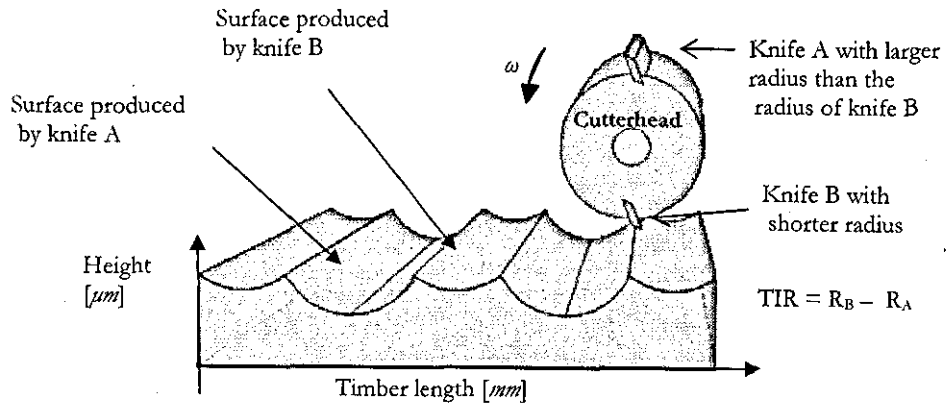

Figure 4.7 Effect of lower TIR values on the resultant surface

The resultant surface is somewhat variable and contains shorter cuttermarks (caused by the cutting knife with smaller radius) and longer cuttermarks (caused by the knife with the larger radius) with a certain level of surface roughness. The obtained surface form with different knife radii (different values of TIR) can lead to so called "surface defects". The process of dressing cutting knives in the cutterhead is also defined as "jointing" with the aim to true the cutting edges and to achieve a multi-knife finish.

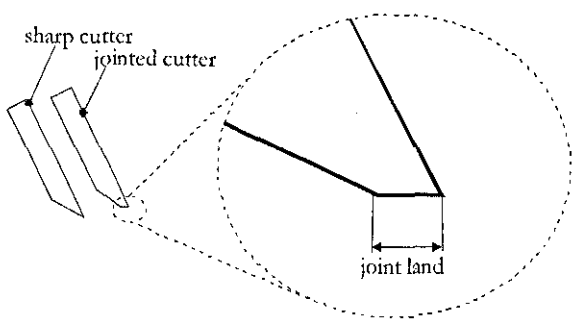

Figure 4.8 Jointed cutter with joint land

The process of jointing produces "joint land" on the cutting edge (Figure 4.8). The difference in radius of the individual cutters results in joint land width variation which causes significant cutting force variation and correspondingly poor surface

roughness and waviness quality (Jackson et al. 2002). Nevertheless for some applications this process can provide an acceptable surface quality.

4.4.1.1 Experiment and Simulation to Produce Single - Knife Finish

This section aims to show the differences between the expected and the machined surface for a single knife finish. Experimental tests involved simply generating a single knife finish to compare the simulation of a perfect surface and that produced by the test rig (described in chapter 3) with no radial displacement of the spindle centre.

A cutterhead with two cutting knives is chosen with a TIR value of *70 μm* to ensure that only one cutter produces a finishing wave. The machined surface profile was measured by a contact based stylus tracer (Figure 4.9).

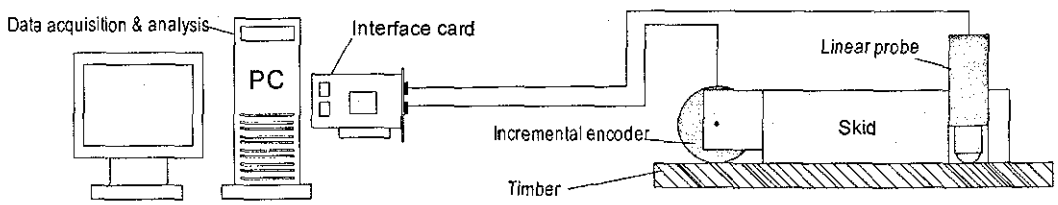

Figure 4.9 Surface measurement via stylus tracer

With this surface measurement technique, the stylus tip contacts the machined surface and it is moved along the timber. The surface height (i.e. y-axis) is measured by the vertical movement of the stylus tip whereas the waviness length (i.e. x-axis) is measured by the incremental encoder. The resultant surface profile is a combination of both measures. Figure 4.10 presents a reference simulated ideal surface produced by the knife with the larger cutting radius. Setting machining spindle speed to *400 rpm* with a feed speed of *30 mm/s* results according to equation (4.1) in wave length p of *4.5 mm* and equation (4.2) gives a corresponding waviness height of *42 μm*.

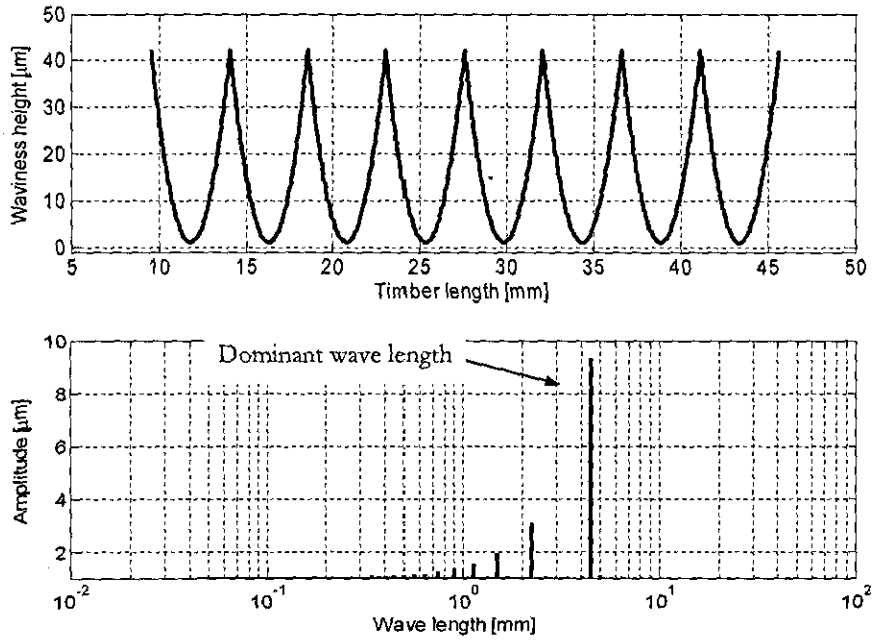

Figure 4.10 Simulation to create single-knife finish

The same machining parameters used for the simulation are set for the small scale planer to produce a single knife finish (Figure 4.11).

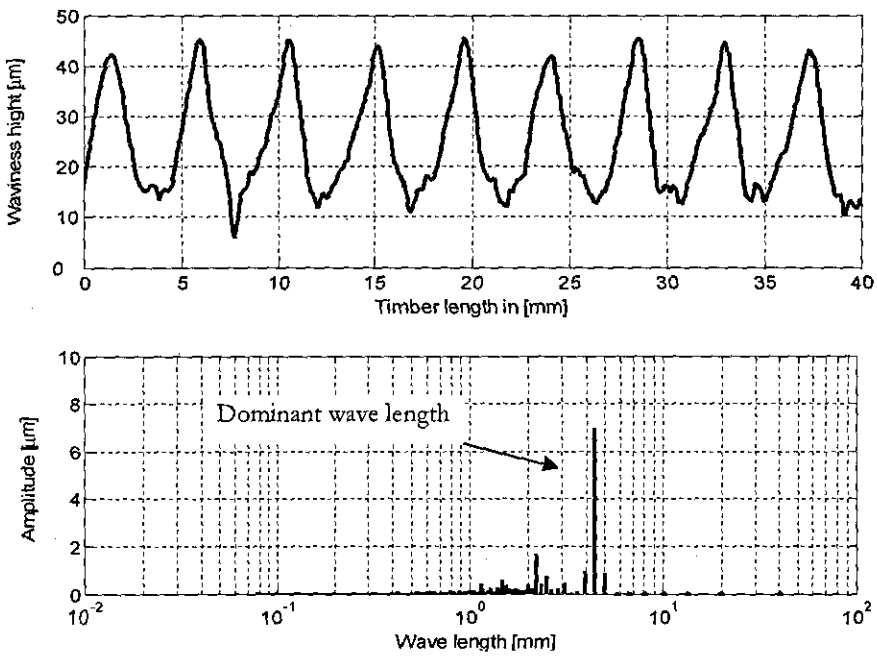

Figure 4.11 Experiment to produce single-knife finish

Analysis on the surface form with the Fast Fourier Transform (FFT) provides a better insight into the dominant wavelengths which form the resultant surface profile. Results from the FFT analysis show that both simulated (Figure 4.10) and machined (Figure 4.11) surfaces have the dominant wavelength at *4.5 mm* which is the pitch of the resultant surface. It should be pointed out that the unit for the frequency is determined as 1/(unit length) i.e. *1/mm*, which can be perceived as the number of cuttermarks per unit length.

The machined surface height is ca. *12 %* lower than the simulated ideal surface form. The deviation from the simulated surface form is due to the factors such as the cutting edge condition and geometry, cutterhead vibrations as well as the material properties (e.g. elasticity) which are not considered within the simulation. In the real machining process all these factors influence the resultant wave form.

4.4.1.2 Experiment to produce Two - Knife Finish

Two - Knife finish is a desired machining operation. According to equation (4.1) the higher the number of engaging cutting knives N, the smaller the pitch p. Figure 4.12 shows the difference between the surface profile of a single - knife and two - knife finish for the same machining parameter settings ($\omega = 450\ rpm$, $v_f = 30\ mm/s$). Both samples are machined with the small scale planer.

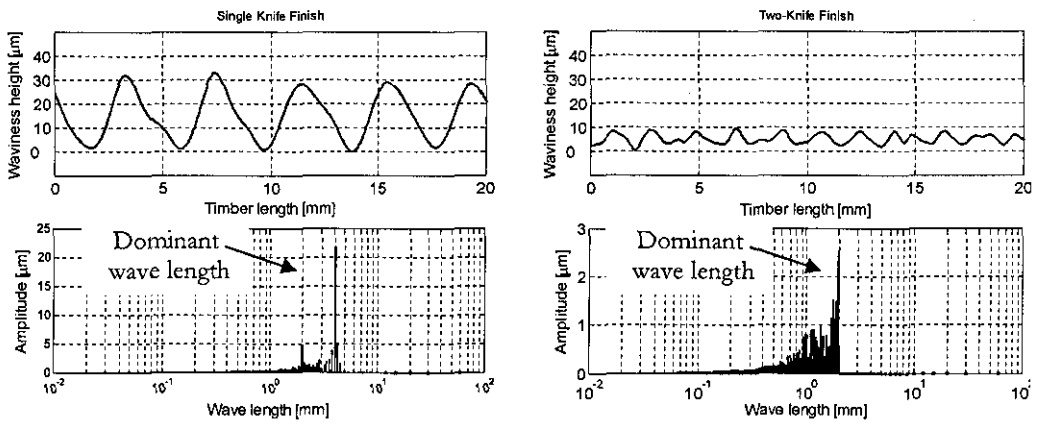

Figure 4.12 Comparison, Single-Knife finish vs. Two-Knife finish

Results from the FFT analysis show that single-knife finish has the double wave length when compared with the two - knife finish (Figure 4.12). The corresponding waviness height of the single – knife finish is almost four times higher than the two–knife finish operation. This difference in surface profile quality points out the importance of the run out (TIR) of the cutting knives involved within the real cutting process.

4.4.2 The Effects of a Proud Knife on the Surface Form

The involvement of the cutting knives needs to be assured prior to the machining operation in order to achieve a higher surface quality. As mentioned in section 4.4.1, it is not always technically possible and economical to achieve a high precision degree of circular cutting path through sophisticated relocation methods and cutting edge grinding operation. The effect of proud knife on the resultant surface is illustrated in Figure 4.13 where the knife 3 is larger than the other cutting knives thus removes more material and causes larger cuttermarks on the surface.

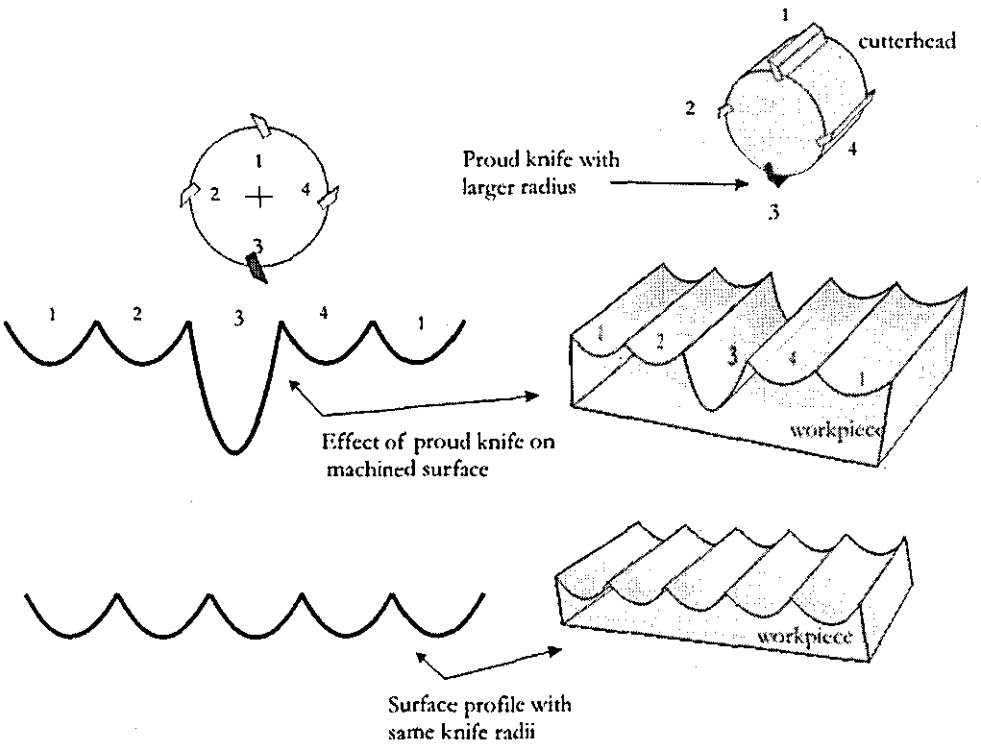

Figure 4.13 Effect of proud knife on the surface

The simulation in Figure 4.14 demonstrates the effect of so called proud knife on a cutterhead with four mounted knives where one of the knives radius is $10\mu m$ larger than the common radius.

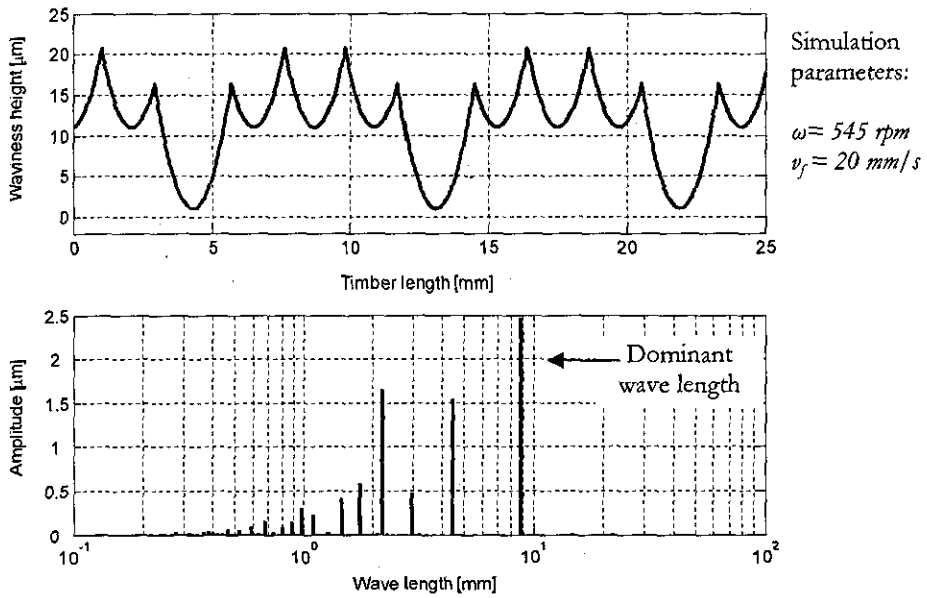

Figure 4.14 Simulated surface with proud knife

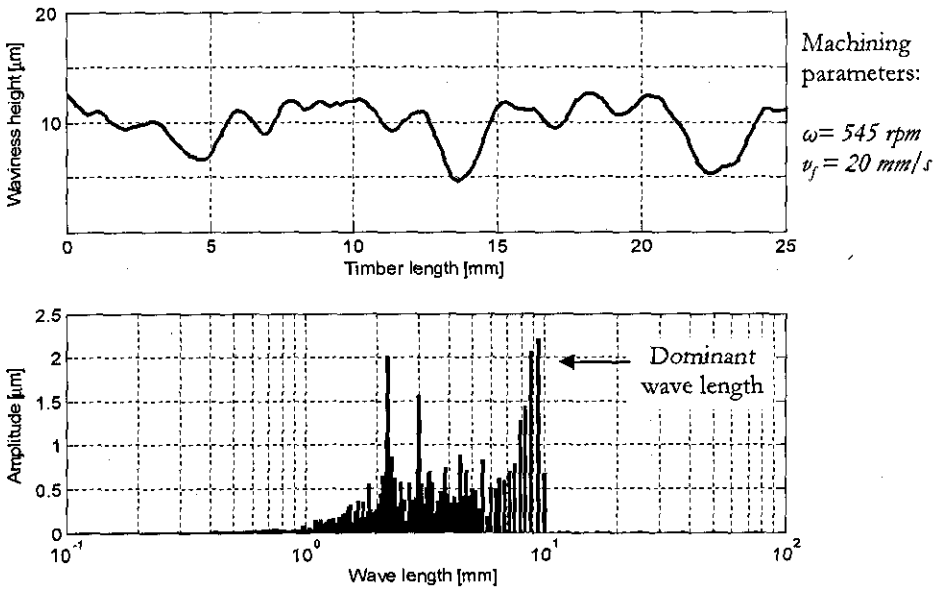

Figure 4.15 Machined surface with proud knife

The simulation in Figure 4.14 shows that the proud knife causes larger wave lengths on the surface which has negative effects on the surface quality. The simulated effect of proud knife (Figure 4.14) as well as the machined specimen with proud knife (Figure 4.15) show that the dominant wave length is four times higher than the expected wavelength of *2.2 mm*. This also indicates that the knife with the largest radius leaves more distinct cuttermarks on the surface, hence causes a surface of reduced quality.

4.4.3 The Effect of Cutterhead Vibrations on the Surface Form

In high speed woodworking a machinery cutterhead can have up to *20* cutting knives. As it can be seen from equation (4.1), the greater the number of cutting knives the higher the timber feed speed for a given good quality (*~1 mm*) of wave pitch. The requirement for multi-knife finish is that all the cutting edges have the same radius. To realise this goal the jointing process is applied at the rotating cutterhead with the aim to true all the cutting edges to the same radius. The consequence of this jointing process is a cutter with zero back clearance angle that rubs the timber surface. All of the aforementioned precision improvement techniques have elevated the jointing process to a high level in order to reduce the rubbing effect, but it is still present. In addition the joint land width, determined by cutter tracking errors and also machine spindle/structural vibration, causes variations in normal cutting force (radial push off force) which produces cutter spindle deflection and hence variation in the cutter path (Jackson et al. 2002).

One particular case is where a four-knife cutterhead with cutters ground to the same radii is subject to a *1/rev* displacement at the spindle rotational frequency. The cutterhead vibration depicted in Figure 4.16 depends on the type of defect modelling case. Five different defect types are specified by Jackson et al. (2002) and many others are possible depending on the TIR values and machine operation condition.

Figure 4.16 shows that the cutting knives B and D are not affected by *1/rev* vibration, whereas cutting knife A is pulled out of the workpiece and on the contrary cutting knife C is pushed into the workpiece by the vibration magnitude.

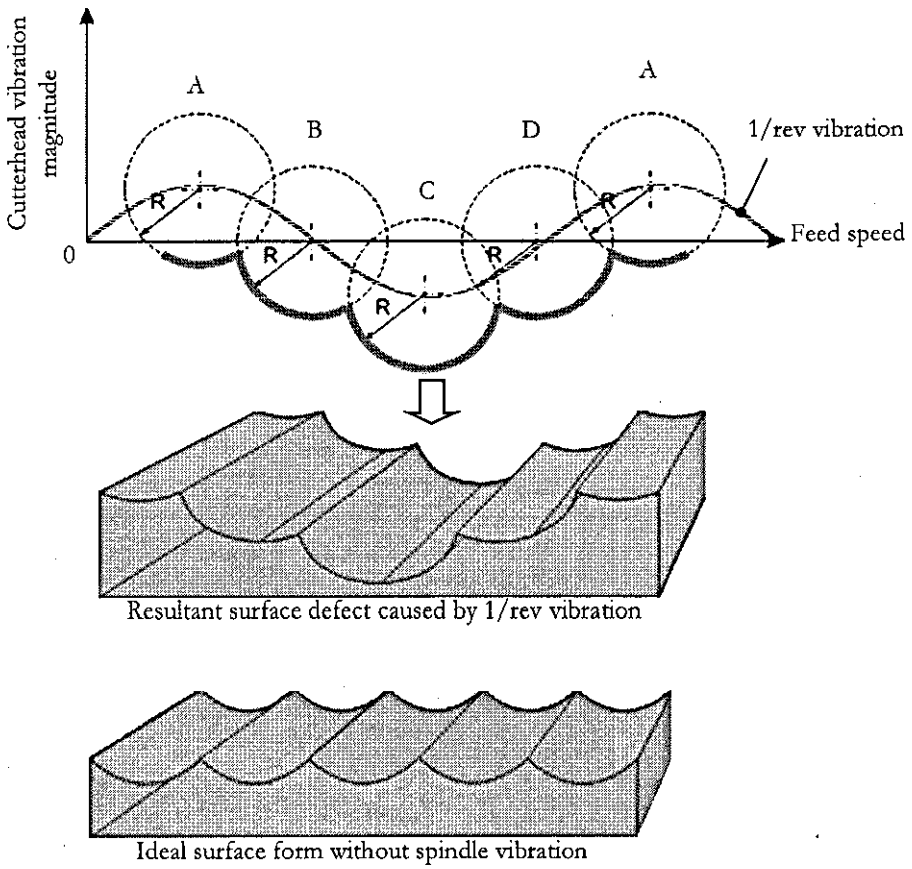

Figure 4.16 Effect of 1/rev spindle vibration on the surface form

This is shown for the case where the positive maximum of the vibration displacement aligns with cutter A. Variations in this particular case occur, depending on the phase relationship between the cutting knife rotational angle and the maximum or minimum point of the interfering with the *1/rev* vibration cycle. The resultant surface model in Figure 4.16 is based on the circular arcs theory and represents a surface defect. Each cutting knife removes material from the surface with respect to their vibration magnitude.

The resultant surface defect is superimposed by the adjacent circles in a plane representing the depth and length of the surface form. Figure 4.16 also demonstrates the greatest impact on the resultant surface, when the knife passing frequency coincides with the *1/rev* vibration crest. It should be pointed out that the angular position of the cutterhead is not controlled on planing and moulding machines and so the vibration effect is arbitrary each time a cutterhead is placed on the machine spindle. When this surface defect is compared with the ideal surface form, the difference between the surface qualities is unacceptable (Figure 4.16). Simulation of the machined timber surface profiles has been carried out to assist in analysis of produced surface defects and to investigate the effects of disturbances independent of workpiece properties.

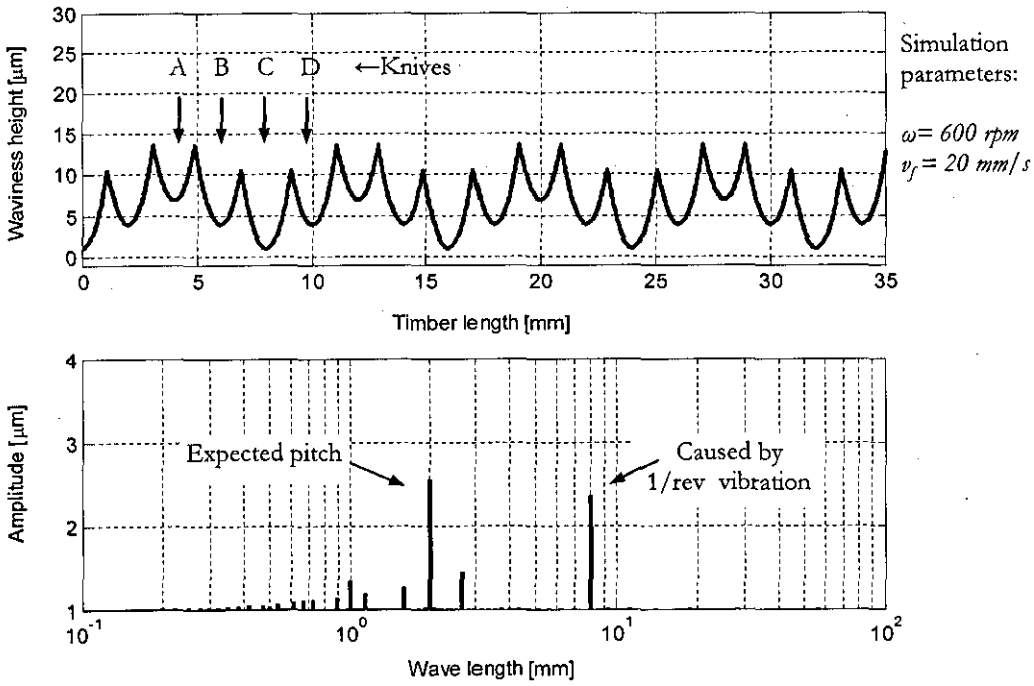

Figure 4.17 Simulation of the surface defect caused by 1/rev vibration

Figure 4.17 shows the simulation of the surface defect caused by the *1/rev* spindle vibration.

The *1/rev* spindle vibration frequency is set to the cutterhead speed with an amplitude of *6 μm* peak to peak. It can be observed that the surface profile does not consist of regular waves. For a normal machining operation (without spindle vibration) a wavelength of *2 mm* with *8.33 μm* of waviness height would be expected. For the additional spindle vibrations, the FFT analysis shows the dominant wavelength at *2 mm* and also at *8 mm* which is four times larger than the expected value of the wavelength under normal operating conditions (Figure 4.17). This is because knife C is pushed into the workpiece, hence cutting deeper while knife A is pushed upwards from the surface, thus removing less material from the workpiece.

Experimental work on surface defects caused by the spindle vibration has been performed with the small scale planer. These defects are machined by real time controlled displacement of the cutterhead during the machining operation. The *1/rev* case is reported here for a four knife cutterhead case. In order to generate this defect, a series of vertical displacements in a sequence is used (Figure 4.18).

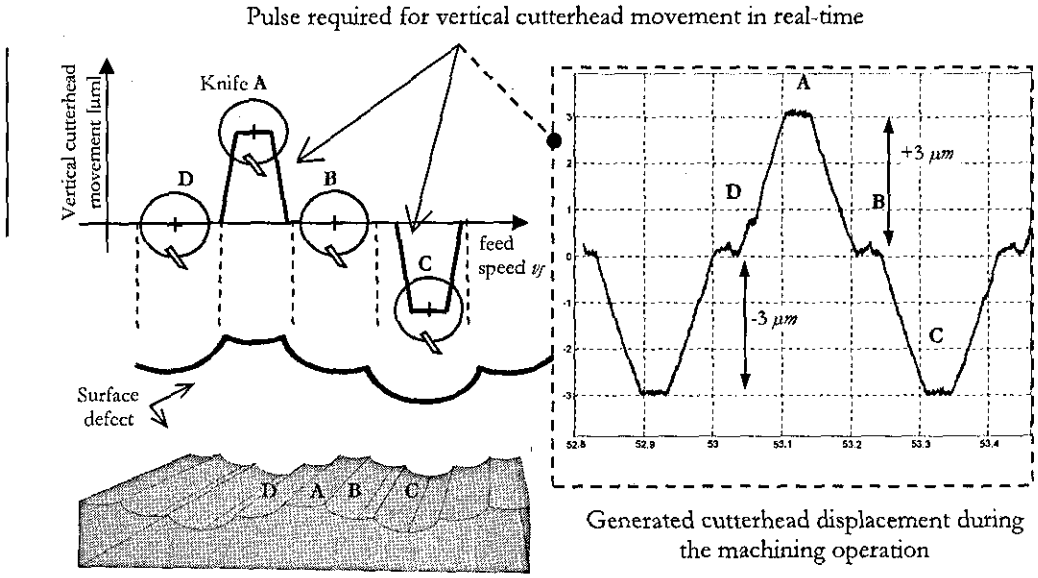

Figure 4.18 Vertical cutterhead displacement to produce surface defects

Before the cutting knife first touches the surface of the workpiece, it starts to move vertically upwards with a defined pulse generated by the piezoelectric actuators (Figure 4.18 point A). The height of the pulse correlates with the defined vibration amplitude. Figure 4.18 illustrates the vertical cutterhead movement, where the workpiece is stationary and the cutterhead travels along the workpiece. This modification is chosen for a better illustration of the cutterhead movement, since in the real machining operation, the cutterhead is fixed and the feed table moves towards the rotating cutterhead. For the experimental work, only one cutting knife is chosen to machine a specific surface defect. This allows generation of any type of interfering vibration and cutter inaccuracy profile via the software map generated on the host PC. The combination of the surface simulation and the controlled cutterhead displacement for surface defect generation is termed as "Defect Generation Tool" (DGT). The usefulness of the DGT cannot be overstated. It is impossible to generate defect conditions on real machines with this degree of control. Thus, separation of various factors that influence the surface waviness is problematic. With this introduced controlled cutterhead displacement, different types of defect scenarios can be generated and the effect of various factors can be separated which will contribute to broader understanding of machining variations.

Figure 4.19 shows the surface defect caused by a programmed *1/rev* spindle vibration on the test rig. Machining parameters are spindle speed ω at *600 rpm* and feed speed at *20 mm/s*. The *1/rev* spindle vibration frequency is set to the cutterhead speed with amplitude of *6 μm* peak to peak. It can be observed that the surface profile of the machined timber does not consist of regular waves. As previously mentioned for a normal machining operation (without spindle vibration) a wavelength of *2 mm* with *8.33 μm* of waviness height would be expected.

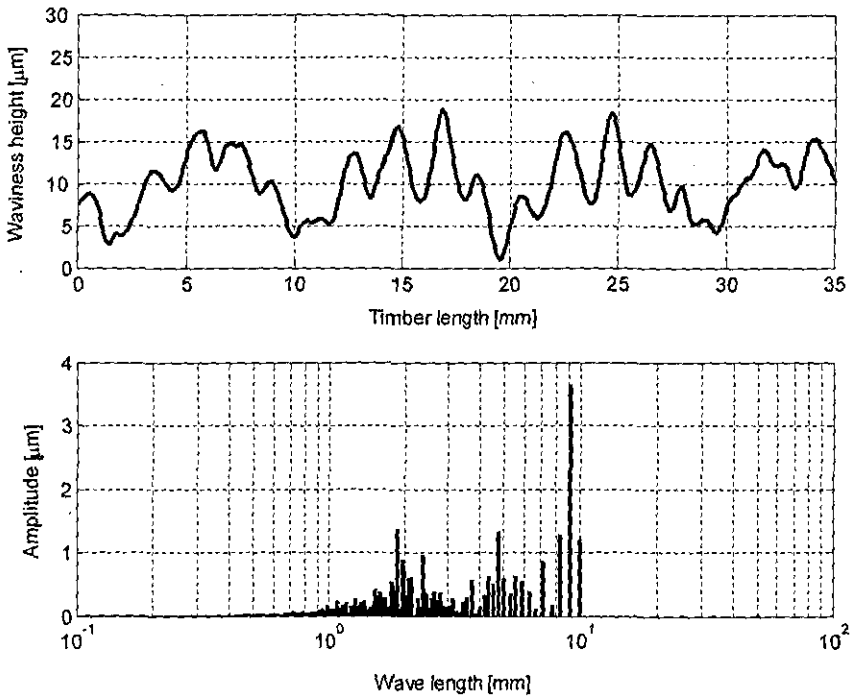

Figure 4.19 Machined surface defect caused by 1/rev vibration

The FFT analysis shows the dominant wavelength at *2 mm* and also at *8 mm* which is four times larger than the expected value of the wavelength under normal operating conditions (Figure 4.19). This is in good agreement with the simulation results depicted in Figure 4.17. The FFT analysis of the machined surface also shows that the surface waviness consists of more harmonic components than the simulated one this is due to the simulation which does not consider the inhomogeneous workpiece properties. Both simulated and machined surfaces show that the effect of the undesirable spindle vibration on the resultant surface is evident (Elmas et al. 2007). In the next chapter, various surface profile measurement systems are discussed and their application capabilities as well as their limitations are evaluated. Furthermore a novel surface profile monitoring system is introduced which can be used for in-process surface quality inspection of machined timber.

Chapter 5 SURFACE PROFILE MEASUREMENT SYSTEMS

The aim of this chapter is to introduce different surface profile measurement systems which can monitor and measure the surface profile of machined timber. The dynamic behaviour of wood machining process can reduce the surface quality of machined timber. The machining variations, hence their effects on the resultant surface finish have been investigated through simulation as well as experimental work in chapter 4. In order to monitor the surface quality, a surface profile measurement system is required for an enhanced machining environment. Various surface profile methods are studied and their advantages and disadvantages are highlighted. Furthermore, a surface profile re-recreation technique has been developed to assist the existing measurement techniques. Unlike other conventional measurement techniques, the developed monitoring strategy is capable of monitoring the surface profile in real-time.

5.1 Introduction to Surface Profile Measurement Methods

The effect of tooling inaccuracies and spindle vibrations on the surface quality are discussed in chapter 4 which have been shown through simulation as well as through experimental tests. These variations are reflected to the machined surface, which can lead to unacceptable quality levels. In order to meet the requirements for a consistent surface quality and increased production efficiency, surface quality information is desirable. Process control and monitoring have significant impact on the efficiency of machining operations in terms of productivity and quality (Gallina et al. 2005). Therefore, it is essential to obtain surface profile information during the machining process. Especially, the attention is to be given to the in-process monitoring systems. There are various surface profile measurement systems employed in the industry to assess the surface quality, however most of these systems are only suitable for off-line measurement purposes (i.e. laboratory work).

These measurement systems are briefly introduced and their advantages and disadvantages with respect to in-process operation as well as their capabilities for wood surface measurement are outlined.

Various surface profile measurement systems have been developed in the recent years for an automated environment. The measurement techniques can be classified into two main groups

- contact based method
- non-contact method

5.2 Contact-based Measurement Techniques

The contact based method generally consists of a stylus tracer in form of a mechanical profilometer (Kiran et al. 1998). In this most common method, the stylus tip contacts the machined surface and it is driven along the workpiece (Wong and Li 1999). The surface profile is recorded by the vertical movement of the stylus tip. The surface waviness measurements are usually within the micrometer range which is sufficient for most industrial applications. For special applications this range is further refined up to nanometre scale as reported by some researchers (Garrat and Nettleton 1992, Groeger et al. 2005, Dietzsch et al. 2007). According to Bennet (1992), Talysurf stylus measurement equipment manufactured by Taylor and Hobson is one of the most common contact measurement instruments within the industry.

This contact based method is also used to obtain the surface profile of machined specimens presented in chapter 4. The basic principle of the stylus instrument can also be found in section 4.4.1.1 (Figure 4.9). This technique is simple and accurate enough to measure the surface profile of the machined timber.

However, this technique has two main disadvantages which are reported by Faust (1987), Yoo et al. (1990), and Jackson et al. (2002). One of the main problems of this method is that it cannot be used for in-process surface quality measurement. It is not suitable for surface profile measurement of timber machined at high throughput rates (i.e. *40 m/min*), since the stylus tip tends to jump at high measuring speed. This effect called "bouncing" occurs when the stylus tip looses contact with the machined surface.

Another major disadvantage of this technique is the deformation of the measured timber surface through the metal stylus tip, due to the force applied on the surface of the machined workpiece. Furthermore, due to finite stylus tip radius, the surface texture is integrated to some extent, hence the measured surface profile is afflicted with inaccuracies. Some damages were also observed during the surface profile measurement of the specimens machined with the small scale planer. Due to these disadvantages, the application of the contact based stylus for on-line surface profile inspection is limited.

5.3 Non-contact Measurement Systems

In order to monitor the quality of machined surfaces, various non-contact measurement techniques have been investigated over the years. Most of the methods used for non-contact measurements are optical methods which include optical profilometers (mostly laser based), microscopes, image analyzers, imaging spectrographs, interferometers, fibre-optic transducers, white-light speckles, laser scattering, optical light sectioning systems (Sandak and Tanaka 2003, Sandak and Tanaka 2005, Shinozaki et al. 2004, Yang et al. 2005). Especially the light sectioning method and the two-image photometric stereo method (WSMS) are introduced. Both methods have been developed by Yang (2006) at the Mechatronics Research Centre at Loughborough University.

One of these above mentioned measurement systems could potentially be used to obtain surface profile information. The light sectioning method, optical profilometer (laser based) and the WSMS have been used in this research project in order to evaluate their capabilities for different surface profiles of machined specimens.

5.3.1 Optical Profilometer – Talysurf CLI

The optical profilometer is similar to the stylus profilometer in many aspects. The major difference is that the optical profilometer uses a non-contact 'optical stylus', while the stylus profilometer uses a contact stylus. This method has been used as reference because of its high resolution within the micrometer range. The Talysurf system shown in Figure 5.1 is calibrated with standardised artefacts and the calibrations can be traced back to the NPL (National Physical Laboratory) standards (UKAS certificate number 29248).

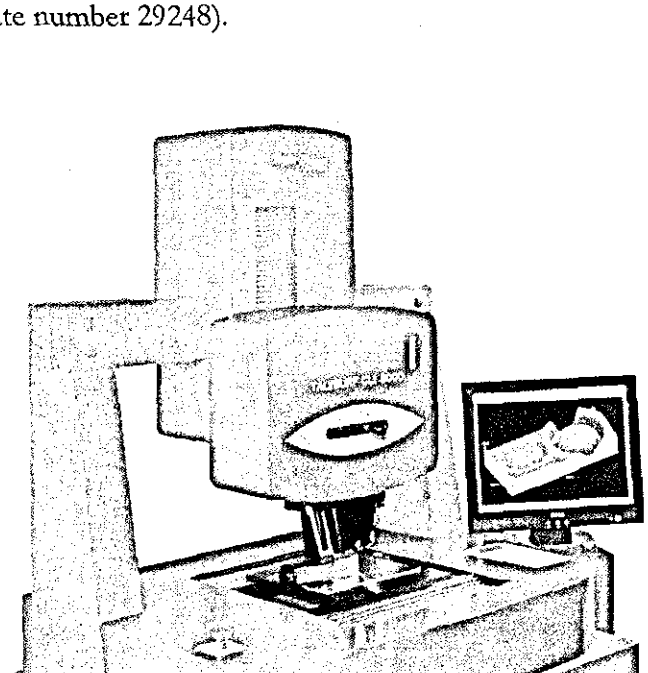

Figure 5.1 Talysurf optical profilometer (Taylor Hobson 2007)

The system consists of a precision X-Y translation table to hold the sample underneath the probes and provide the scanning motion. The stand-off distance (Z-direction) of the Talysurf can be adjusted to achieve focusing of the probe. The Talymap software from Taylor Hobson is used for data acquisition and processing. A typical generated surface from Talymap is shown in Figure 5.2.

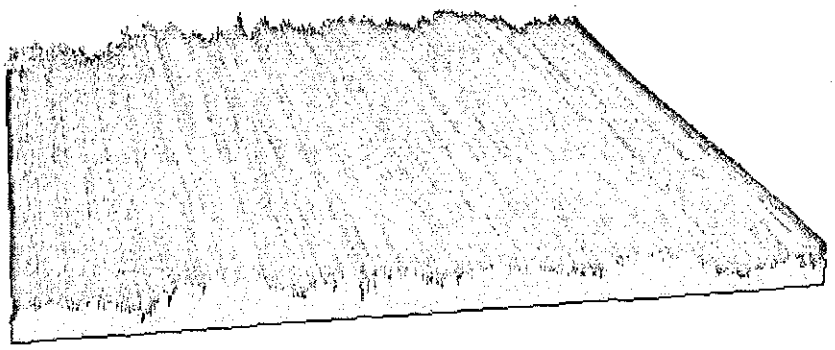

Figure 5.2 3D mapping of a measured surface generated by Talymap software

5.3.2 Light Sectioning Method

The principle of the light sectioning method is depicted in Figure 5.3. A laser stripe projected onto the machined surface from the side of the workpiece produces a light section. Due to the cuttermarks on the machined surface, the light section appears in the form of a wavy line on the overhead camera image (Yang et al. 2006). The light section is captured by the camera which is located perpendicular to the surface. The image is then processed off-line by Matlab image processing toolbox. A light-sectioned image taken by the camera is also shown in Figure 5.3. The principle of the image processing is based on the mathematical relationship between the angle of the laser stripe and the light section on the machined surface (Figure 5.4).

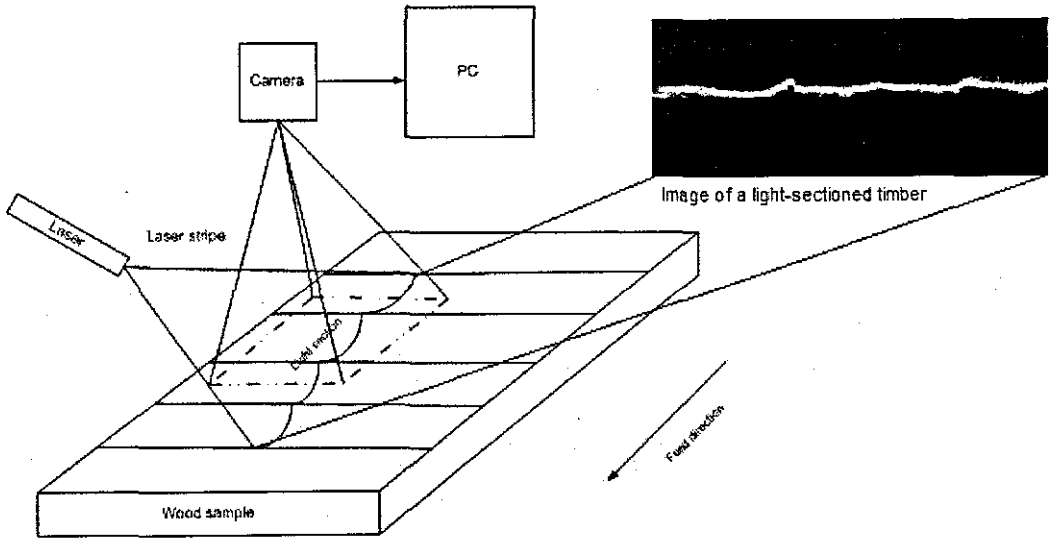

Figure 5.3 Light-sectioning method and the image obtained through the camera

Equation (5.1) shows the triangular relationship between the triangulation height H_s, the corresponding length L_s and the incidence angle φ_i.

$$H_s = L_s \cdot \tan \varphi_i \tag{5.1}$$

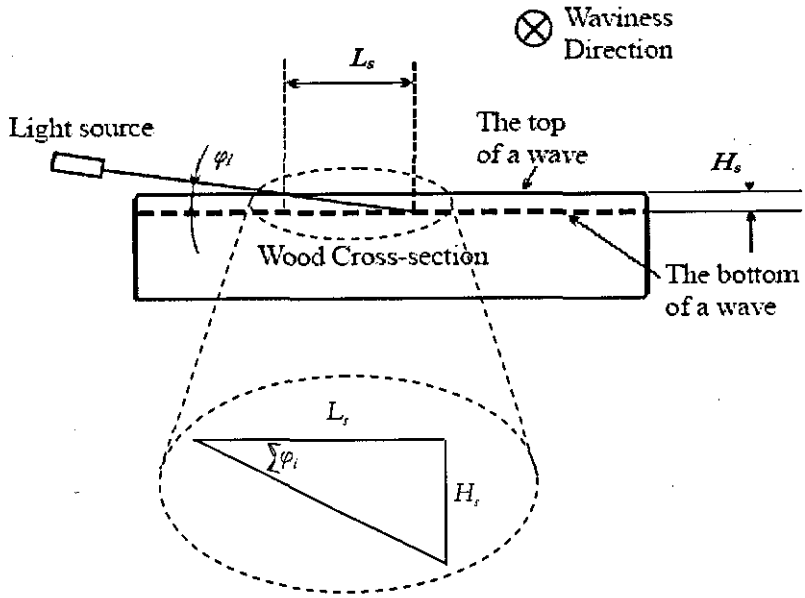

Figure 5.4 Basic principle of the light sectioning method (Yang et al. 2006)

5.3.3 Two-image Photometric Stereo Method - WSMS

This method was first proposed and demonstrated by Yang (2006) as part of the Wood Surface Measurement System (WSMS). The experimental setup is illustrated in Figure 5.5.

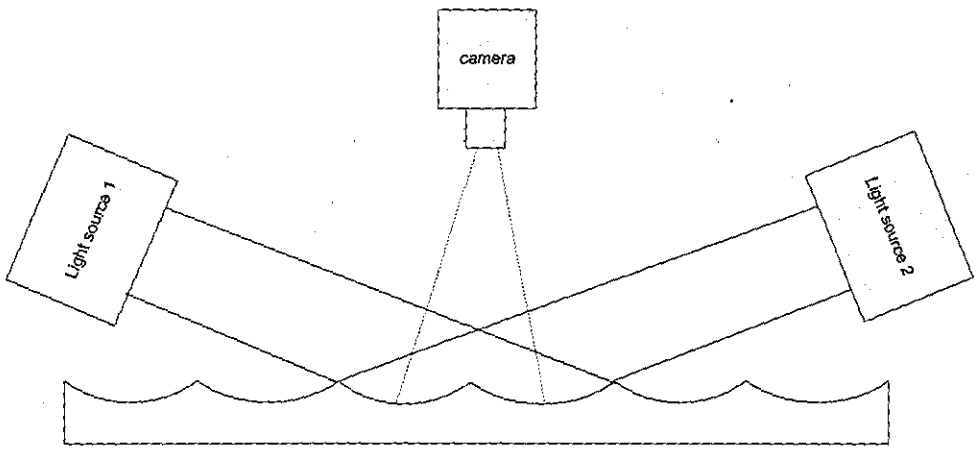

Figure 5.5 Experimental setup of the photometric stereo method (Yang 2006)

The light sources consist of a laser, a collimator and a beam expander. A camera takes image of the timber surface with light source 1 turned on. Then another image is taken by switching off the first light source and turning on light source 2. Surface profile of the machined timber is obtained by comparing and transforming the surface shape function to a 2-D profile. This two-image photometric stereo method will be referred to as WSMS. The actual test rig is shown in Figure 5.6.

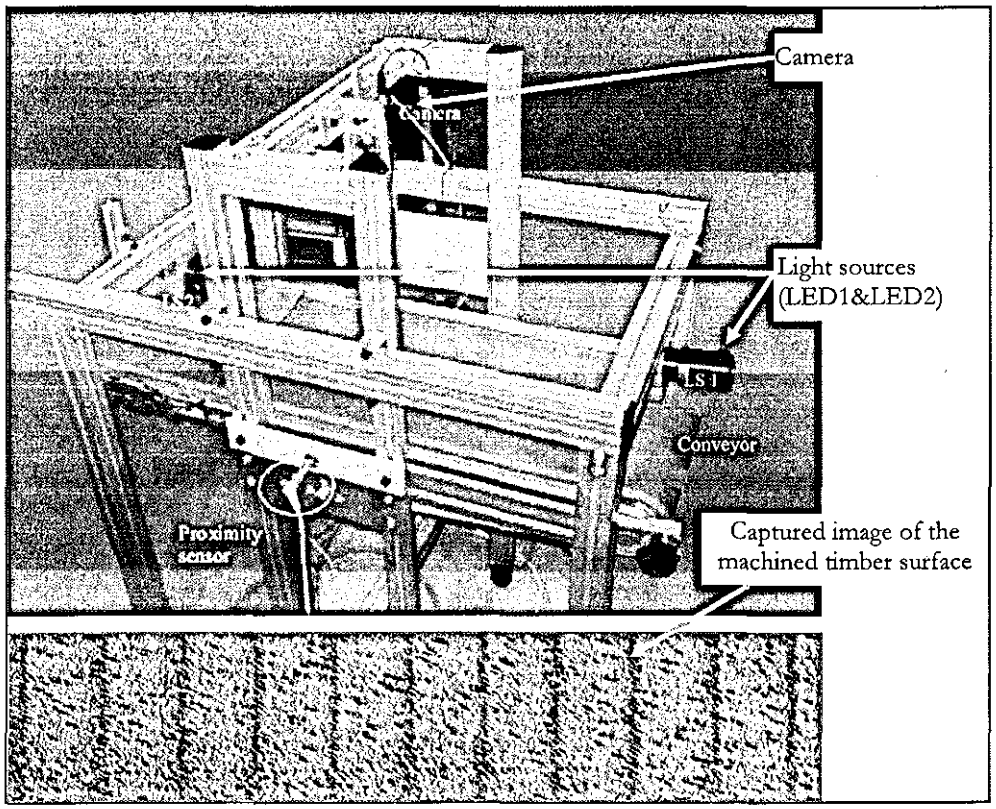

Figure 5.6 Test rig of the WSMS

5.3.4 Evaluation of Light Sectioning Method and WSMS

This section reports surface profile measurement results obtained by the three different optical measurement methods. Two samples are used to make a comparative study of the aforesaid methods. The first sample is a machined timber of *2 mm* pitch length, while the second one is a black nylon with surface defect caused by *1/rev* vibration which is also used in section 4.4.3. The *1/rev* defect is machined on the test rig (described in Chapter 3) with *6 μm* peak to peak vibration amplitude with the spindle speed of *600 rpm* and the feed speed of *20 mm/s*.

5.3.4.1 Wood Sample with 2 mm Pitch

Surface profile of the machined timber with *2 mm* pitch and the corresponding Fast Fourier Transform (FFT) results of the surface are shown in this sub-section. As discussed by Harris (1978), the FFT analysis is a reliable method to reveal the wavelength components that make up a given waveform. This is a very useful technique of determining the fundamental pitch present in the measurement data.

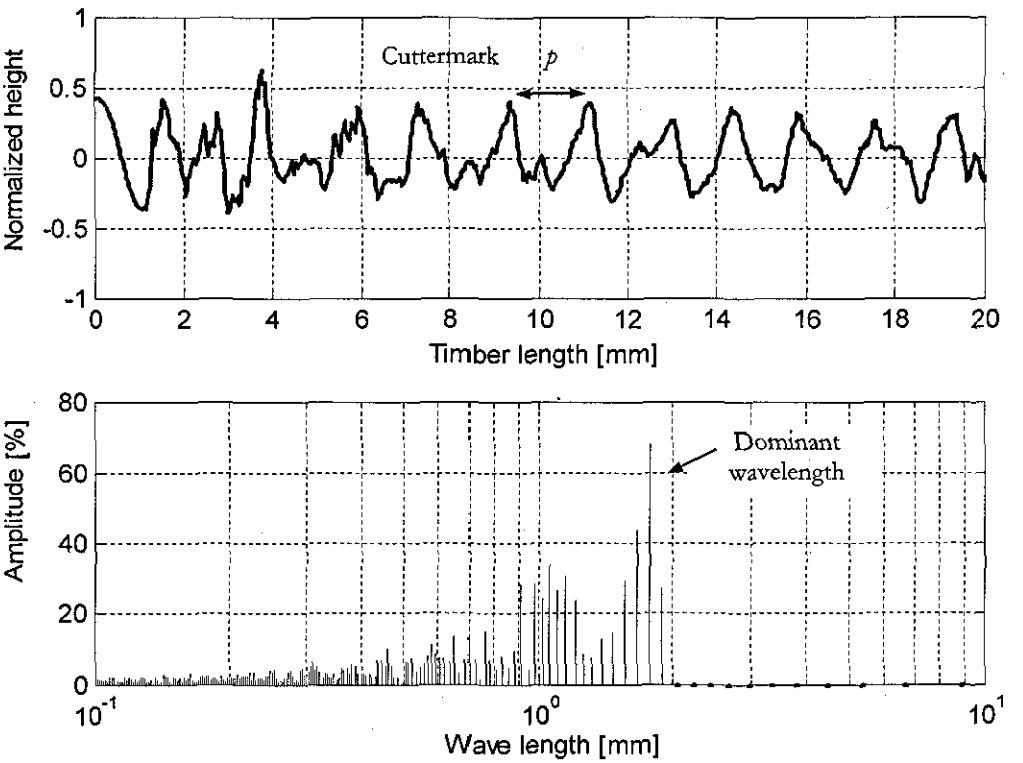

Figure 5.7 Surface profile and FFT analysis of machined timber obtained with light sectioning method

Figure 5.7 depicts the surface profile obtained with the use of light-sectioning method. From the normalized profile measurement data it is evident that there are periodic cutter-marks on the timber surface. When the FFT analysis of the surface profile is carried out, it can be seen that the main wavelength component is *1.8 mm*. This value is somewhat close to the fundamental wavelength of *2.0 mm* in this specimen.

Due to the scattering effects of the laser beams on the edges of the specimen, the measurement accuracy decreases which can also be observed in Figure 5.7 at the beginning of the measurement (i.e. from *0* to *5 mm*) where a more noisy behaviour of the waviness is apparent. Since the sample surface is not ideally flat, the laser scattering would be present to a certain degree depending on the tilting effect of the machined surface. This measurement technique also requires a precise setting of the laser beam by considering the incident angle for every measurement which also affects the overall scatter characteristics of the laser beam. For example if the incident angle is too low (i.e. <1°) then the scattering of the laser beam increases if it is >5° the measurement precision decreases (Yang 2006). Furthermore the inspection area is limited to the laser beam length of up to *50 mm*. This measurement technique also needs to be performed under exclusion of the ambient light which can affect the measurement quality.

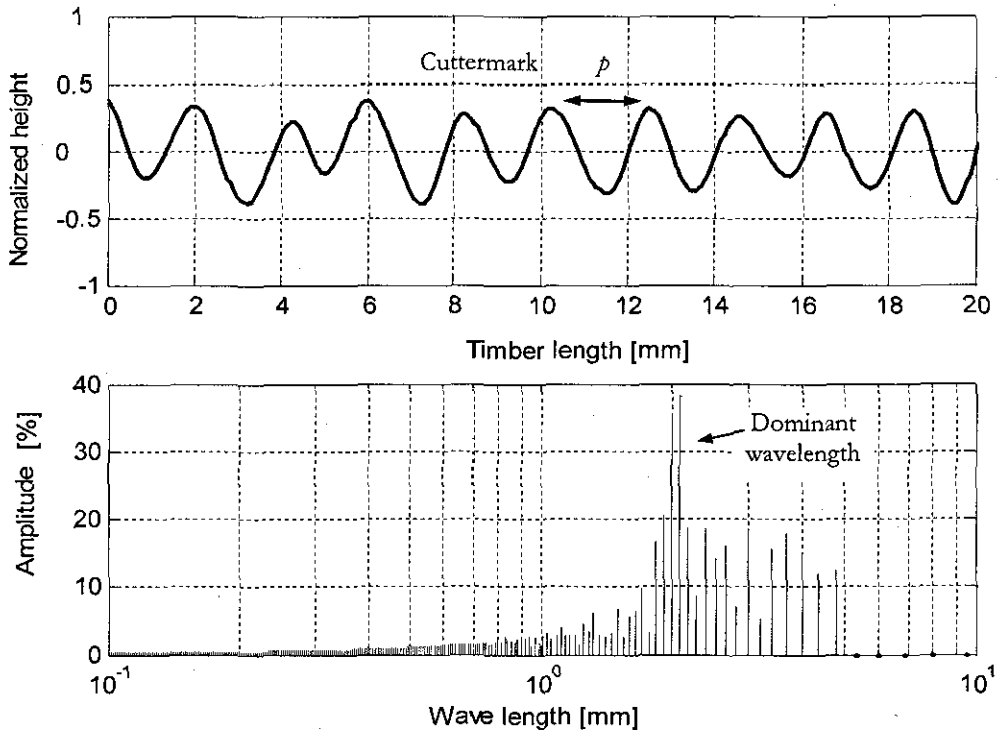

Figure 5.8 Surface profile and FFT analysis of machined timber obtained using WSMS

The surface profile of the same machined timber as obtained by the use of WSMS is shown in Figure 5.8. It can be seen that the system is able to detect the periodic nature of machined surface waviness. The FFT analysis reveals that the dominant wavelength present in the measured data is approximately *2 mm*. Thus, the measurement obtained from the WSMS for a machined timber with *2 mm* pitch agrees very closely to the actual surface finish. Surface profile measurement data of the sample using Talysurf is shown in Figure 5.9. This measurement serves as the benchmark for all the other systems as this measurement can be traced back to NPL standards.

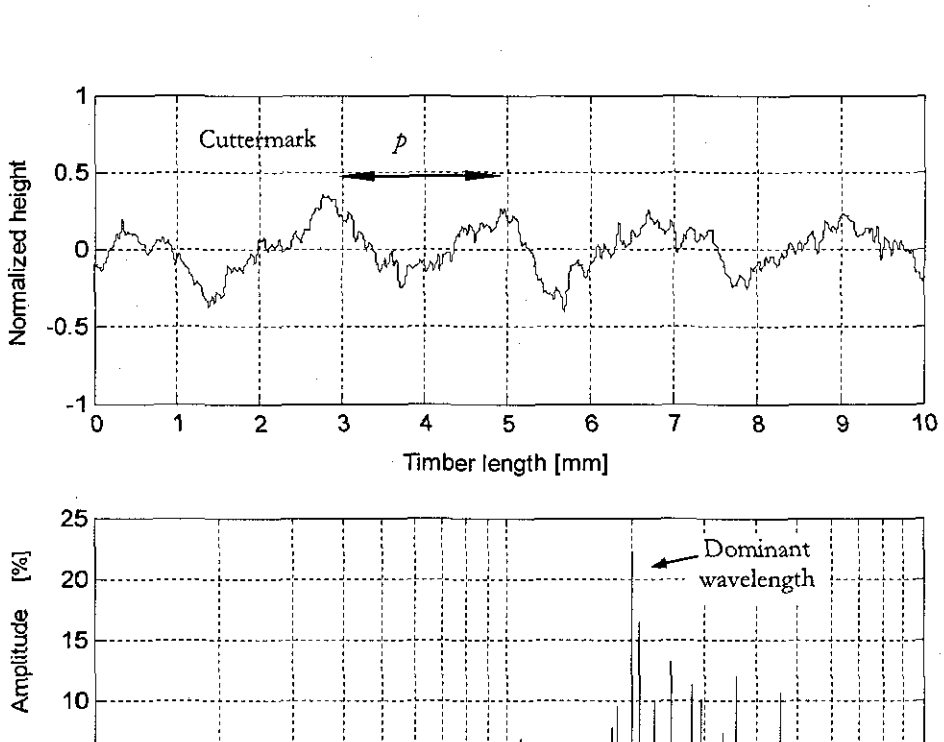

Figure 5.9 Surface profile and FFT analysis of timber measured using Talysurf

Figure 5.9 shows the measured surface profile of machined timber. In contrast to other both systems, the surface appears to have high frequency components added to the machined waviness pattern.

These high frequency components are more significant than the surface measured with other methods as the FFT plot indicates. Because the Talysurf has a very high resolution of measurement (*1 μm*), apart from the waviness pattern on wood, it also measures the constituent grains of the timber. Thus, the measurement appears more 'noisy' due to the additionally measured roughness of the surface. As all three optical measurements candidates show the capability of measuring the surface profile of the machined timber at *2 mm* pitch, the measurement difficulty level has been raised by the next specimen. A surface defect with *6 μm* peak to peak vibration amplitude is machined on a black plastic sample in order to minimize the effect of workpiece properties such as the inhomogeneous nature of timber. For the non contact measurement systems is this type of defect indeed difficult to detect, firstly due to the very low waviness heights variation and secondly due to the black colour of the sample which absorb the light thus adding uncertainty in the accuracy of profile detection. In other words this defect is to show the limitations of the surface profile measurement candidates.

5.3.4.2 1/rev Defect Surface Measurement

The surface profile of a black nylon sample with machined defect was measured with all three optical systems. The light sectioning method was unable to detect the surface profile of the defect sample. This was due to the fact that, the projected laser light was fully absorbed by the black-coloured sample. Thus, no light pattern formed on the surface and as a result, the camera wasn't able to capture any meaningful image. Therefore, in this sub-section only results obtained from the Talysurf and the WSMS have been reported. Figure 5.10 shows the surface defect measured by the Talysurf. The FFT analysis shows that the dominant wavelength is at approximately *8 mm*, which is four times the expected wavelength of *2 mm*. This is in good agreement with the defect analysis caused by *1/rev* vibration described in chapter 4.

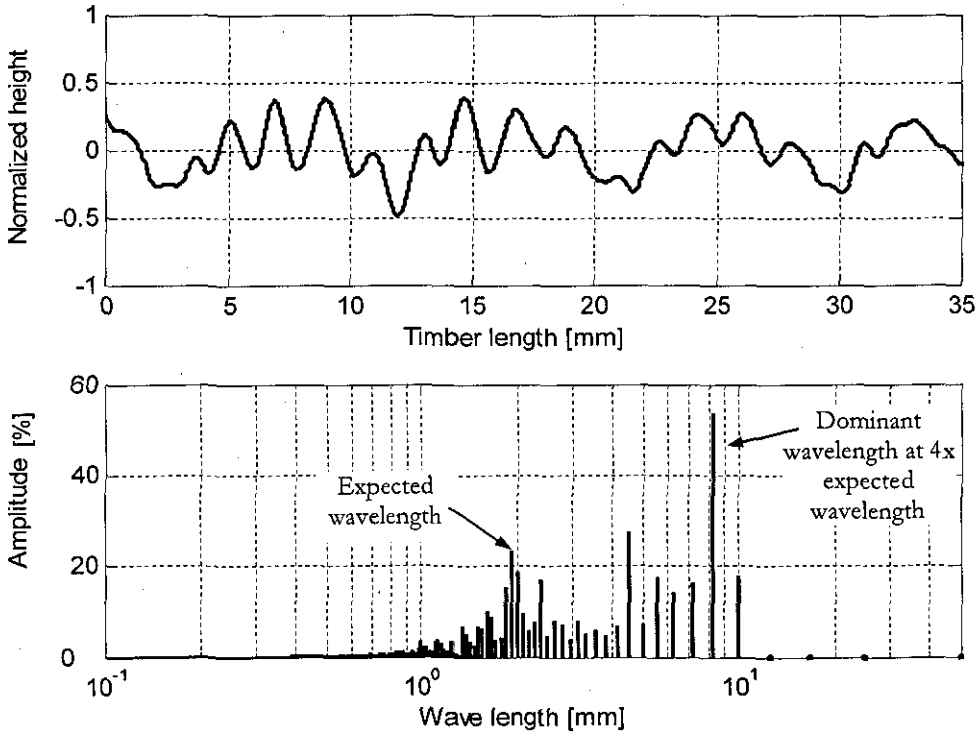

Figure 5.10 Surface profile and FFT analysis of defect using Talysurf

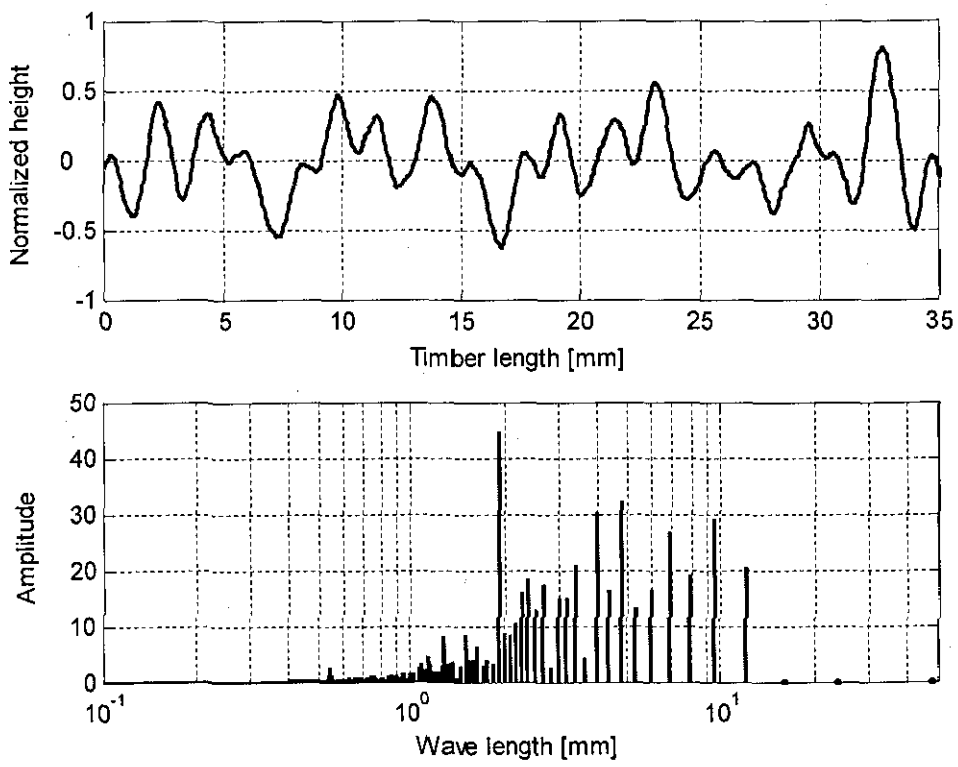

Figure 5.11 Surface profile and FFT analysis of defect using WSMS

Surface profile measurement results obtained from the WSMS system is shown in Figure 5.11. It can be noticed that the shape of the plot corresponds closely to the one obtained through Talysurf. The FFT analysis however is not conclusive in comparison to measurement through Talysurf. Nevertheless the WSMS is still capable of measuring the shape of the surface defect and it can distinguish between the normal surface profiles (no radial displacement of the spindle) and the surface defects.

The Talysurf has been used as the benchmark for the samples, as its measurements are traceable to UKAS (United Kingdom Accreditation Standards) standards. Measurements revealed that the Talysurf not only picked up the waviness but also the surface roughness. Thus, in order to extract the waviness pattern from the measurement data, some filtering is required. Around 20 minutes time was required to measure a sample of *50 mm* length. Thus, it is a very slow process and not suitable for online inspection of wood machining process where high throughput rates up to *40 m/min* are required.

The light sectioning method could not be used to measure the black nylon sample with defect. However, the *2 mm* regular pitch length could be satisfactorily measured using this method. The main drawback of this system has been the tedious setup of the incident angle and the extensive filtering for surface profile extraction from the images. Nevertheless this technique can potentially be employed for offline surface analysis. Moreover for higher pitch values (i.e. *>2 mm*) the precision of the measurement increases significantly. However this method is not suitable to measure high quality surfaces where the pitch is lower than *1.5 mm* (Yang, 2006). Apart from that, high signal processing requirements and the lack of measurement speed are the major drawbacks of this system, which restricts its implementation for in-process inspection.

The WSMS system is capable of measuring both the regular machined surface as well as the surface defect. Data acquisition with the system took only a few seconds and the analysis of the captured image to obtain the 2-D profile only about a minute. Thus, it was the fastest among the three methods of surface profile measurement. Also with the help of this system, a machined area of the sample was measured (10mmx35mm), thus providing an averaged profile of that area with a higher overall accuracy. The measured area can be expanded according to the camera lens magnification settings.

It should be pointed out that all the other measurement systems are only capable of measuring a line trace on the machined surface at a time. In case of the talysurf a 3 D image of the surface can be measured simply by measuring a number of line traces and extrapolating them (i.e. 3 D image shown in Figure 5.2 is obtained by extrapolating 10 line traces). However, with the number of traces the measurement time is correspondingly high. Despite higher measurement speed of the WSMS than the other measurement systems it's application is also limited for real-time inspection due to the data processing time. Therefore an additional surface profile monitoring system has been developed which can assist the existing surface profile measurement methods for in-process inspection.

5.4 Novel In-Process Surface Monitoring System (ISMS)

The optical measurement systems evaluated in section 5.3 showed that they are bulky to fit near cutterhead and lack the measurement speed due to the sophisticated image processing algorithms, thus they are not sufficient for applications where real-time surface monitoring is required. These drawbacks limit their application range for an automated process environment. Therefore, an additional surface profile extraction is desirable to assist the optical methods which would enable real-time inspection during the machining process.

This section introduces a novel surface profile re-recreation method by considering the spindle speed and spindle vibration during the machining operation. For any dynamic optimization of the machining process, characteristics of those dynamic components can be monitored for an enhanced machining environment. The proposed in-process surface profile monitoring system (ISMS) is mainly focused on extracting surface profile information from the cutterhead vibrations and the cutterhead speed.

Figure 5.12 shows the schematic principle of the ISMS in the machining environment. Spindle vibrations are measured with the eddy current probes and the spindle speed is monitored via an incremental encoder which are mounted on the spindle system (sensor arrangement is described in more details in section 3.2). From these sensor outputs, surface profile of the machined timber is re-created in real-time.

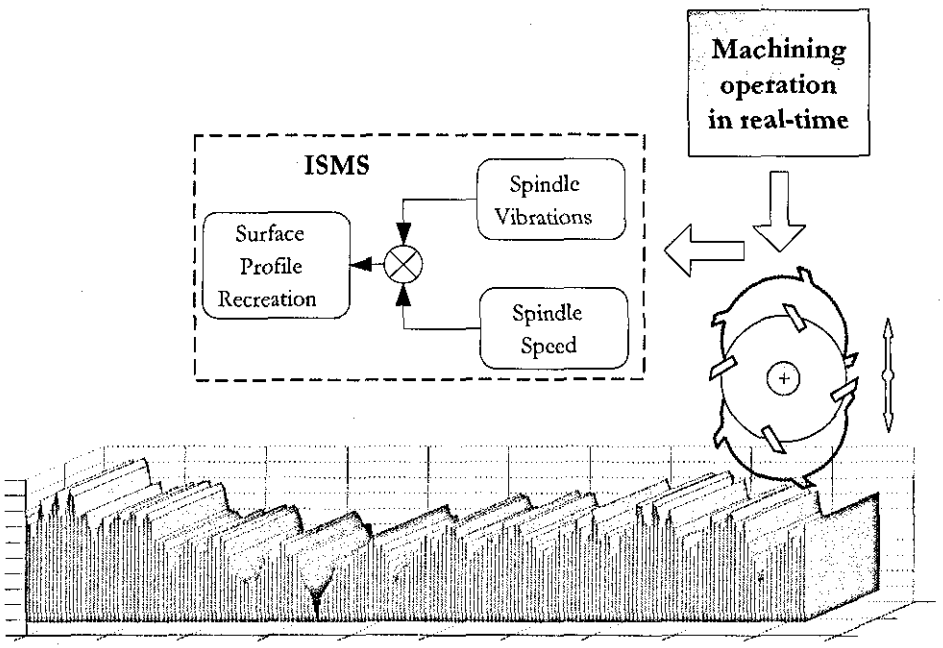

Figure 5.12 In-process surface profile monitoring system

5.4.1 Surface Profile Assessment by using Spindle Speed

A wood sample with *2 mm* pitch was machined and the corresponding spindle speed and the spindle vibrations were captured during the machining process. The ideal expected surface is simulated which is shown in (Figure 5.13) For example, if the spindle speed is set to *600 rpm* and the feed speed to *20 mm/s* then according to the equation (4.1) and (4.2) the pitch is *2 mm* with *8.33 μm* of waviness height (Figure 5.13). These values are taken as ideal expected values which are compared with the machined and the re-created surface pitch and height.

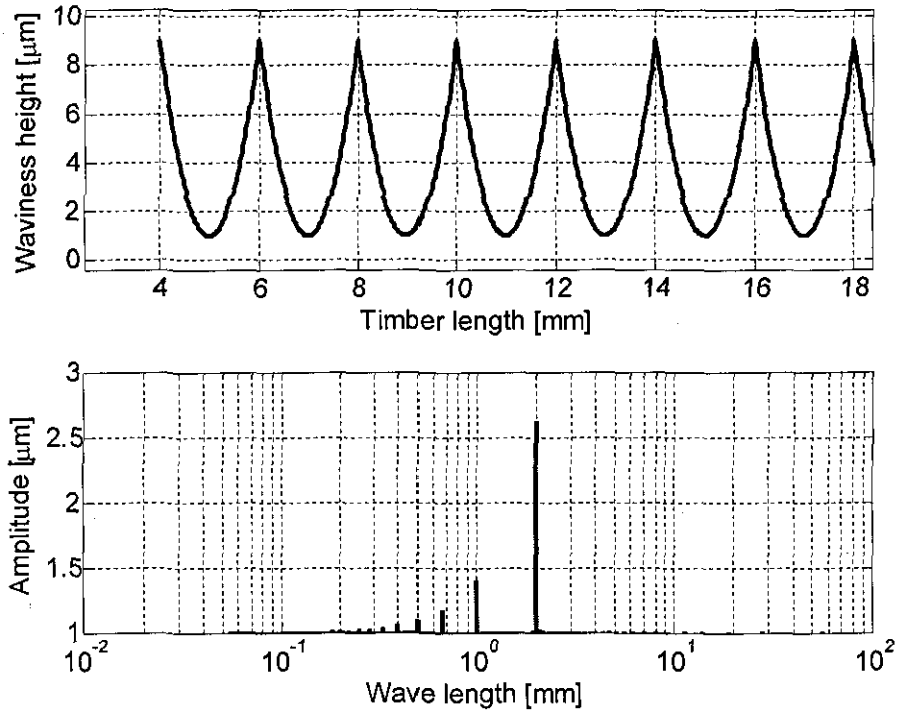

Figure 5.13 Simulation of 2 mm pitch surface

It should be noted that the surface profile is measured with the contact based stylus profilometer for verification and reference purposes only, since during the machining process the surface profile assessment should only be assessed through the spindle speed and the spindle vibration. With a programming code, the surface profile information such as pitch and corresponding height are extracted from the measured

surface profile by simply defining the maxima and minima of the traced surface profile (Figure 5.14).

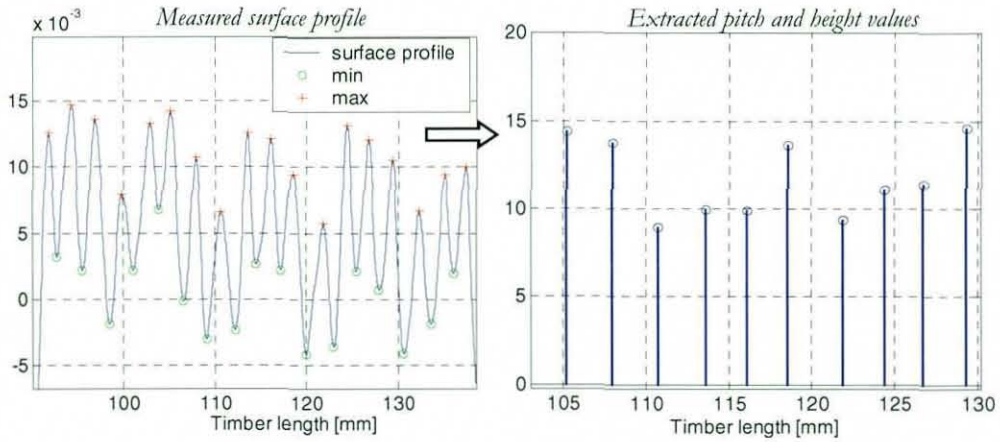

Figure 5.14 Machined surface profile with extracted waviness height and pitch

During the machining process, the spindle speed is monitored by an incremental encoder. The encoder is counting two thousand pulses for each revolution. The time that the cutterhead needs to perform one revolution is extracted from these readings. When the spindle speed is monitored over the whole machining cycle, from Figure 5.15 it can be seen that the spindle speed is varying during the machining process.

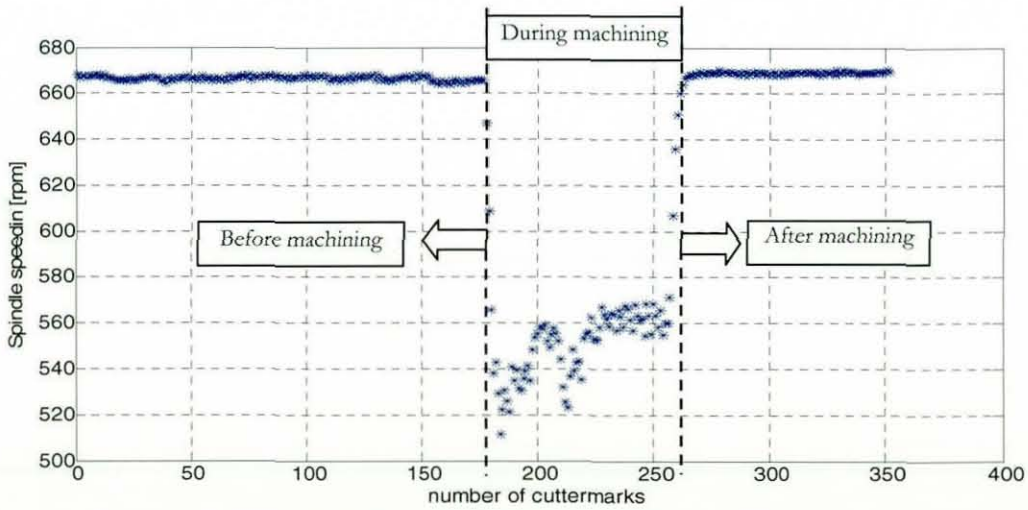

Figure 5.15 Spindle speed measurement during the machining process

Since the spindle speed is measured, the surface profile characteristics such as pitch and height can be calculated by the equations (4.1) and (4.2) respectively. The calculated pitch and corresponding heights are shown in Figure 5.16.

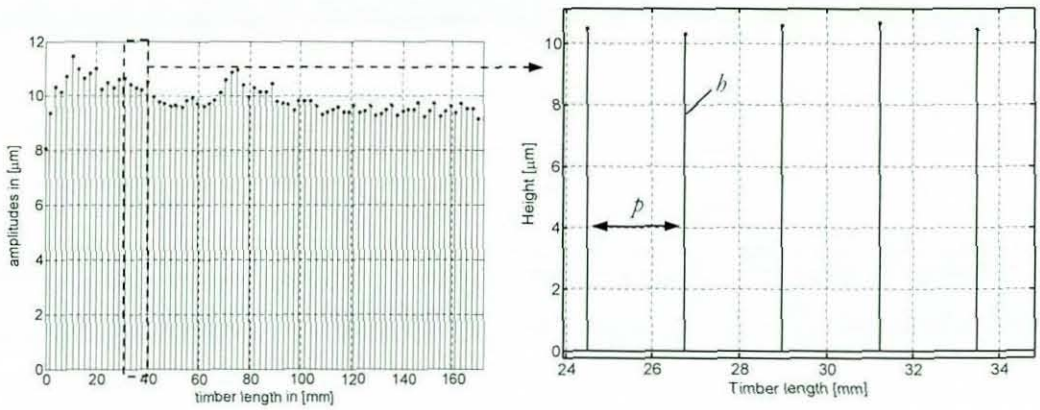

Figure 5.16 Re-created surface profile by using spindle speed

Beside the pitch value, surface quality can also be assessed by the uniformity of the surface waviness. Herein the wave width variation ratio R_w, is a useful indication which is already being used by the timber processing industry (Jackson et al. 2002). This ratio is defined as:

$$R_w = \frac{W_{\min}}{W_{\max}} \tag{5.2}$$

where W_{min} and W_{max} are defined as the minimum and maximum wave width respectively. The corresponding height variation ratio may be calculated as follows:

$$R_h = \frac{h_{\min}}{h_{\max}} \tag{5.3}$$

where h_{min} and h_{max} indicate the minimum and maximum wave height respectively. The closer the values of R_w and R_h to *1* the higher the consistency of the surface form. This is a desired quality characteristic.

As it is shown in Table 5.1, the difference between the mean pitch values and the recreated and measured surface profile is at about 3 % and the difference between the width variation ratio of measured and re-created surface profile is less than 10% which is in good agreement. However, the recreated surface profile through spindle speed does not take the work piece properties as well as the dynamic behaviour of the machining process (i.e. cutterhead vibrations) into account. Therefore spindle vibrations are analysed in the following section.

Table 5.1 Comparison among the simulated, measured and recreated surface profile

	simulated ideal surface	measured surface with stylus	re-created surface from spindle speed
p_{mean} [mm]	2.0	2.11	2.18
h_{mean} [μm]	8.33	11.66	9.89
R_w	1	0.72	0.79
R_h	1	0.63	0.70

5.4.2 Surface Profile Assessment by using Spindle Vibrations

At a first glance surface profile re-creation through spindle speed seems to be in a good agreement with the simulated and traced surface profiles (Table 5.1) however, this method does not consider the dynamic behaviour of the spindle system. As it is described in section 4.4.3 spindle vibrations can cause surface defects, thus reducing the surface quality. If there are any vibrations causing surface defects additional information about the spindle dynamic behaviour is needed. Therefore the spindle vibrations are measured via eddy current probes during the machining process too. Figure 5.17 shows the spindle vibrations during the cutting process where the time for one vibration event caused by one cuttermark is expanded along the time axis. The vibration magnitudes are extracted via a programming code within Matlab.

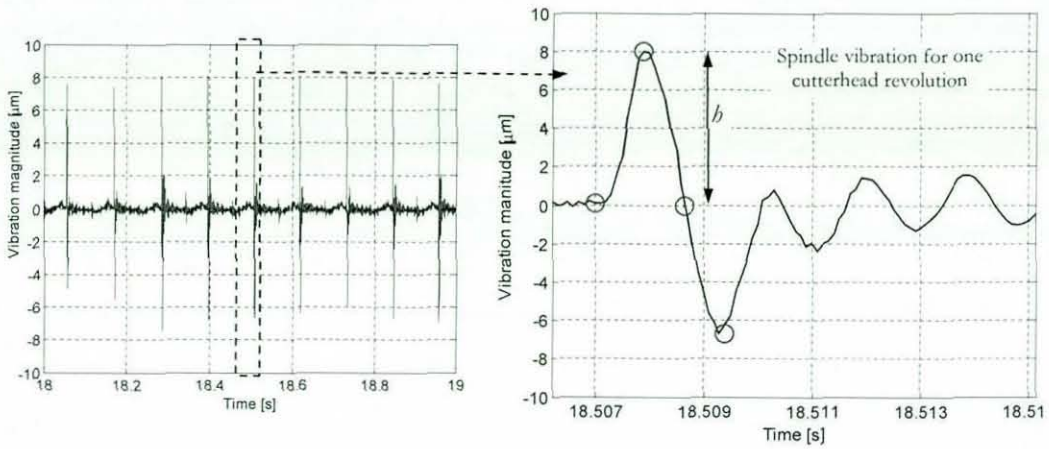

Figure 5.17 Spindle vibrations during the machining process

As it can bee seen from Figure 5.18, eddy current probes do not provide the vibrations at the tool tip, as they are located on the front bearing. Therefore these vibration magnitudes are estimated from the node of the measurement to the tool tip by considering the geometry as well as the dynamic characteristics of the spindle with an estimator, namely with the Kalman filter. If only the geometry of the spindle is considered for extrapolating the vibrations from the measurement point to the tool tip node, a simple extrapolation factor could be used. However, the FE model of the spindle revealed that the displacement of the tool tip and the node of measurement are roughly in the same direction for the first vibration mode (Figure 5.18). However, at higher frequencies where higher vibration modes become involved the extrapolation is more complicated. Especially, at the second vibration mode of the spindle system, the displacement of the measurement node and the tool tip node are in opposite directions (Figure 5.18). Therefore, a simple extrapolation with a factor is only reliable for the frequencies below the first vibration mode of the spindle. Considering the fact that vibrations caused during the machining operation can be arbitrarily and excite higher vibration modes, an estimator (Kalman filter) is designed to carry out the extrapolation during the machining operation, thus the introduced method is capable of providing reliable and accurate information about the surface profile over a wide range of frequencies. The estimator is described in more details in chapter 7.

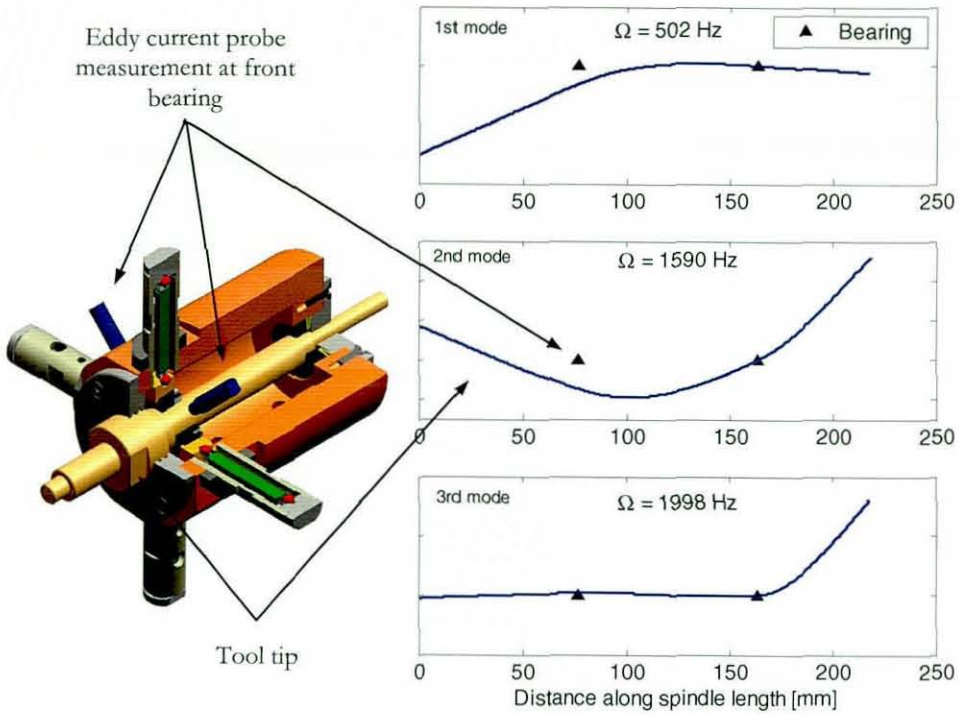

Figure 5.18 Mode shapes of the spindle system

The pitches are then calculated by rearranging the equation (4.2) and the obtained surface profile features (height and pitch) are shown in Figure 5.19.

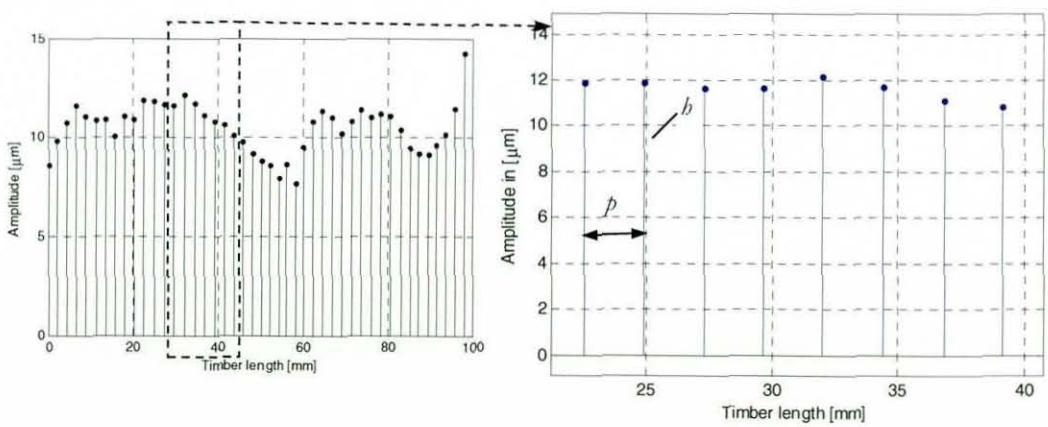

Figure 5.19 Surface profile recreation by using spindle vibrations

Table 5.2 shows that the re-created surface profile from spindle vibrations are in good agreement with both previous methods. The deviation from the measured mean pitch value is less than *3 %* with less than *2 μm* divergence from the mean surface heights. This relatively high accuracy and the straightforward instrumentation make the ISMS suitable for surface profile monitoring purposes within the planing operation.

Table 5.2 Comparison among the simulated, measured and re-created surface profiles

	Simulated ideal surface	measured surface with stylus	re-created surface from spindle speed	re-created surface from spindle vibration
p_{mean} [mm]	2.0	2.11	2.18	2.16
h_{mean} [μm]	8.33	11.66	9.89	10.11
R_w	1	0.72	0.79	0.75
R_h	1	0.63	0.70	0.66

Chapter 6 SYSTEM IDENTIFICATION OF THE TEST RIG

The aim of this chapter is to analyse the characteristics of the spindle system including the piezoelectric actuators in order to understand and identify the behaviour of the spindle system. Furthermore, the effect of piezoelectric actuators on the spindle is analysed. Analysis on the static and dynamic behaviour of the smart spindle system in terms of overall spindle stiffness has been carried out. Different methodologies have been applied to analyse the overall spindle system characteristics regarding vibration modes and stiffness characteristics of the system.

These tests are essential for two reasons. Firstly, the test rig characteristics (described in chapter 3) have only been investigated to certain extend by Hynek (2006). Therefore, further investigations are necessary to identify the limitations and capabilities of the test rig. Secondly, the system identification of the test rig is essential for the modal control approach. Thus, modelling spindle and actuator characteristics are vital for a reliable closed loop modal control system design (described in chapter 7). Therefore, theoretical modelling as well as experimental work have been carried out on the test rig.

6.1 Introduction to Piezoelectric Actuator

The Piezoelectric actuators are electromechanical transducers, which convert electrical energy into mechanical energy. They are widely used in different kinds of applications ranging from static and dynamic micro positioning, optics, smart structures, precision machining and active vibration control.

They are capable of providing large displacements in micrometer range and generating large forces with typical frequency bandwidth up to *30 kHz*. The maximum force delivered by the piezoelectric actuator is usually in the range from *0.2 kN* up to *10 kN* depending on its stiffness.

The maximum displacement of the piezoelectric actuators is in the range from *2 μm* for single layer actuators and up to *200 μm* for multi layered large stacks (Hynek 2004).

6.2 Piezoelectric Actuator Types

Piezoelectric actuators are manufactured from piezoelectric ceramic which becomes electrically polarized if it underlay mechanical stress. This characteristic of the piezoelectric ceramic is termed as direct piezoelectric effect and it is widely used to manufacture sensors such as accelerometers and load cells. Conversely, if the electric field is applied to piezoelectric ceramic, it expands in direction of the polarisation. This is known as inverse piezoelectric effect on which the piezoelectric actuators are based. There are several different types of piezoelectric actuators. The three main types are:

- Flexure element

The flexure element is produced from thin piezoelectric ceramic strips which are combined into a bimorph. The operation of this element is based on the simultaneous contraction of one strip with the expansion of the other, which results in bending (Figure 6.1).

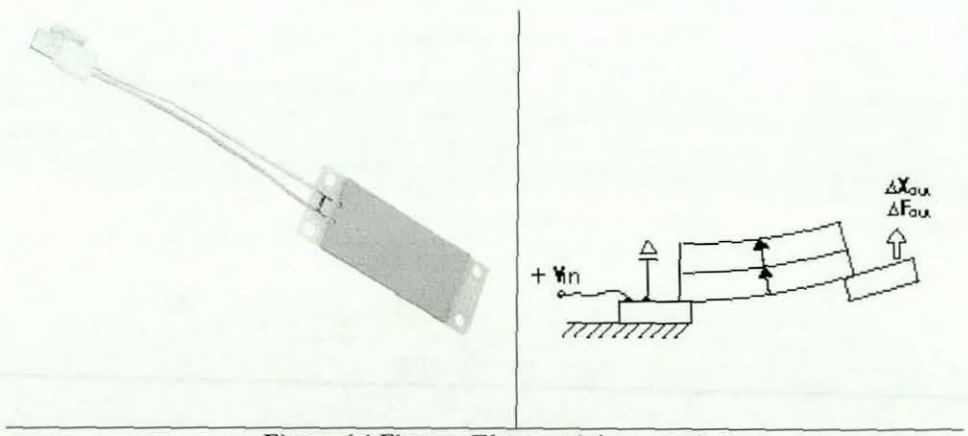

Figure 6.1 Flexure Element (piezo.com)

This type of actuator is capable of providing high displacements (i.e. up to few millimetres) with the drawback that the generated force is relatively low (i.e. up to *1N*) (piezo.com).

- Tube actuator

These types of piezoelectric ceramic tubes are monolithic actuators which contract laterally and longitudinally when a voltage is applied between the inner and outer electrodes (Figure 6.2). This type of actuator is widely used for positioning of scanning microscopes (physikinstrumente.com).

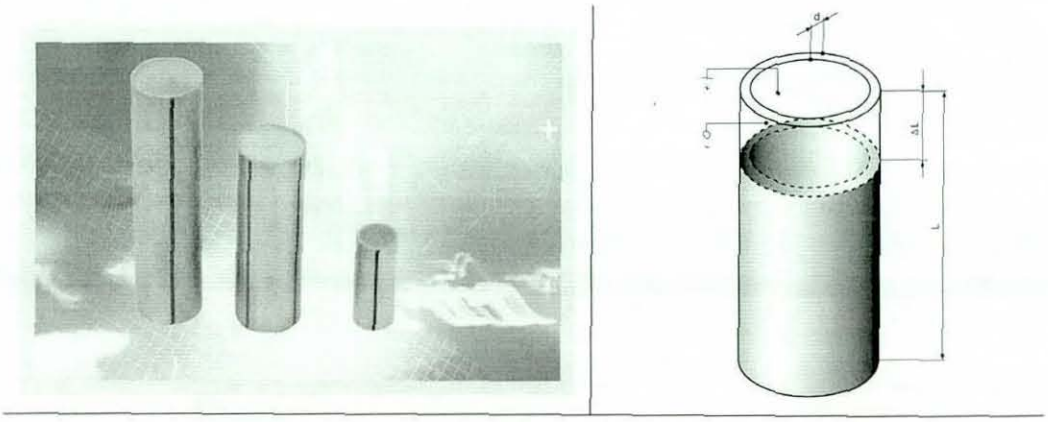

Figure 6.2 Tube piezoelectric actuators (physikinstrumente.com)

- Stack type actuator

Stack type actuator is constructed as a stack of thin piezoelectric ceramic layers. The stack expands if voltage is applied to its electrodes (Figure 6.3). This type of actuator is able to deliver relatively large displacements (i.e. *<200 μm*) and very high force (i.e. *< 30 kN*) (physikinstrumente.com).

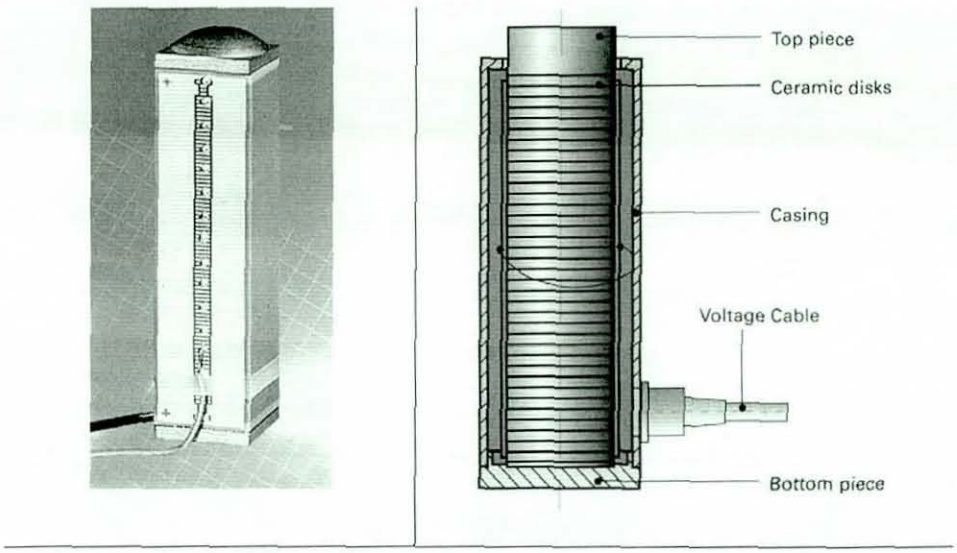

Figure 6.3 Stack type piezoelectric actuator (physikinstrumente.com)

Due to their desirable characteristics (i.e. delivering relatively large displacement and high force), the stack type piezoelectric actuators are widely used for precision machining, vibration cancellation (i.e. chatter suppression) and dynamic positioning of structures and parts.

6.3 Modelling Stack Type Piezoelectric Actuators

The characteristics of the piezoelectric actuator and its deployment for spindle systems can be classified into three sub models. The first model describes the mathematical properties of the actuators. The second model describes an equivalent mechanical model of the piezoelectric actuators, whereas the third model outlines the electrical characteristics.

6.3.1 Mathematical Model of the Piezoelectric Actuators

The piezoelectric stack type actuator, depicted in Figure 6.4, is constructed of n layers of piezoelectric elements, which are connected mechanically in series but electrically in parallel.

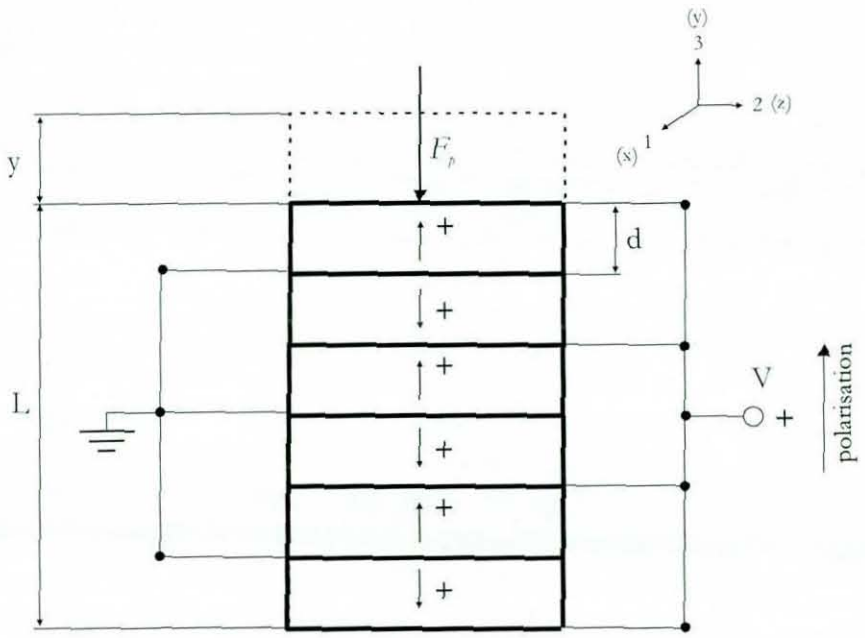

Figure 6.4 Principal of piezoelectric stack type actuator

Each layer has a thickness d and the overall length of the actuator is $L = nd$. The piezoelectric ceramic has anisotropic properties. Three axes are used to determine directions in a piezoelectric element. These axes are termed 1, 2, and 3 by convention and they are analogous to X, Y, Z of the classical right-hand orthogonal axis set. The direction 3 is taken parallel to the direction of polarization. It can be assumed the only stress component in the piezoelectric stack type actuator is in the direction of polarization. The constitutive equations of the actuator in direction 3 are expressed as follows

$$\begin{aligned} e_3 &= S_{33}^{E}\sigma_3 + d_{33}E_3 \\ D_3 &= d_{33}\sigma_3 + K_3^{\sigma}\varepsilon_0 E_3 \end{aligned} \tag{6.1}$$

where e_3 is the mechanical strain, σ_3 is the mechanical stress, E_3 is the electric field ε_0 is the vacuum permittivity and D_3 is the electrical displacement. The piezoelectric material constants are relative dielectric constant at constant mechanical stress K^{σ}_{3}, mechanical compliance S^{E}_{33} at constant electric field and d_{33} is the strain constant relating the mechanical strain to the applied electric field. The subscript "33" in equation (6.1) indicates that the electric field and the mechanical stress are both along the direction 3.

The piezoelectric material constants depend on the applied voltage and on the mechanical strain developed in the actuator, which results in a non-linear behaviour of the actuator. The piezoelectric material is manufactured from Lead Zirconate Titanate (PZT), which is the most common material used for piezoelectric sensors. Typical values of the piezoelectric material properties are stated in Table 6.1.

Table 6.1 Typical piezoelectric material properties (PZT)

Property	Symbol	Value range	Units
Strain constant	d_{33}	230 - 700	10^{-12} m/V
Relative dielectric constant	K	1300 - 2400	-
Compliance	S_{33}	13 - 20	10^{-12} 1/Pa

The stress in the piezoelectric actuator shown in Figure 6.4 can be considered uniformly distributed, if the actuator operates below its natural frequency. The stress and strain are then expressed as follows

$$\sigma_3 = \frac{F_p}{A} \tag{6.2}$$

$$e_3 = \frac{y}{L} \tag{6.3}$$

where F_p is the actuator load and A is the actuator cross-sectional area. The thickness of a single layer is very small (e.g. *0.1 – 0.3 mm*) in comparison with the cross-sectional dimensions. Thus, the electric field and the electric displacement can be expressed as follows

$$D_3 = \frac{q}{nA} \tag{6.4}$$

$$E_3 = \frac{V}{d} \tag{6.5}$$

where V is the applied voltage and q is the charge stored in the actuator. Inserting equations (6.2), (6.3), (6.4) and (6.5) into (6.1) results in

$$\begin{aligned} y &= \frac{S_{33}^E L}{A} F_p + n d_{33} V \\ q &= n d_{33} F_p + n \frac{A K_3^\sigma \varepsilon_0}{d} V \end{aligned} \tag{6.6}$$

The capacitance of the piezoelectric actuator and the actuator stack stiffness are defined as

$$C_p = n \frac{A K_3^\sigma \varepsilon_0}{d} \tag{6.7}$$

$$k_p = \frac{A}{S_{33}^E L} \tag{6.8}$$

Taking the capacitance and the stiffness of the actuator into consideration, the equation (6.6) can be rewritten as follows

$$y = \frac{1}{k_p} F_p + nd_{33} V$$
$$q = nd_{33} F_p + C_p V \tag{6.9}$$

6.3.2 Mechanical Model of the Piezoelectric Actuators

The capabilities (i.e. maximum force, maximum displacement) of the piezoelectric actuators are determined by the material properties of the piezoceramic and by the actuator design (i.e. number of layers, layer thickness, layer cross sectional area). This usually constitutes a large set of parameters. Therefore, for simplicity, the actuator capabilities are usually specified in datasheet by two parameters, namely zero load displacement y_0 and blocked force F_{p0} (Figure 6.5).

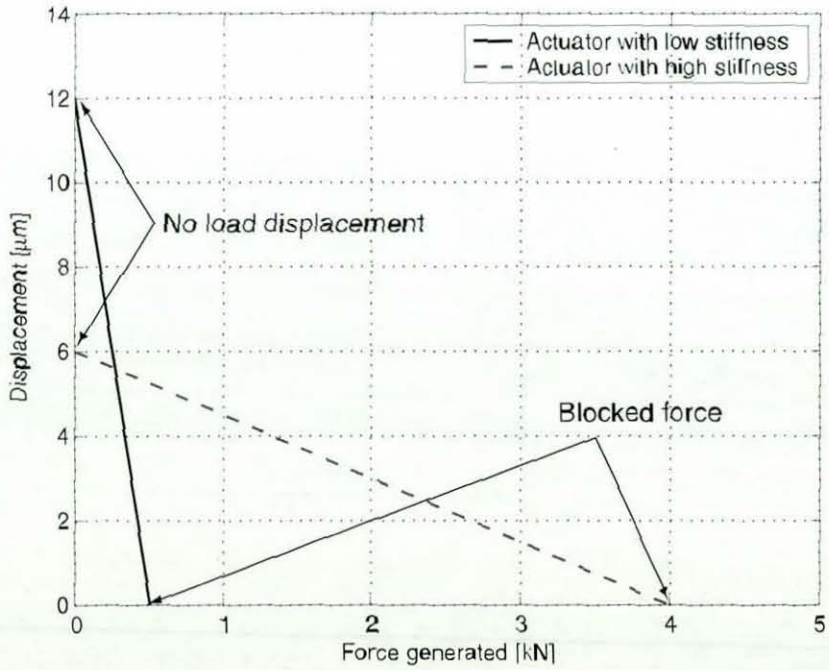

Figure 6.5 Force-displacement characteristic at constant voltage (Hynek 2004)

For example, piezoelectric actuator generates maximum force when its displacement is prevented. Conversely, maximum displacement is achieved only with an unloaded actuator. This characteristic is depicted in Figure 6.5.

The maximum displacement of a free actuator at nominal voltage (i.e. $150V$) is achieved when the load is equal to zero. The maximum displacement can be derived from equation (6.9) by setting F_p to zero which yields equation (6.10).

$$y_0 = nd_{33}V \tag{6.10}$$

The maximum actuator force (blocked force) is achieved when the displacement is prevented. Again, it can be derived from equation (6.9) by setting the displacement y to zero. This is described by the equation (6.11).

$$F_{p0} = -k_p nd_{33}V \tag{6.11}$$

Equation (6.9) reveals that the displacement y of a piezoelectric actuator depends on the voltage V applied to the actuator as well as on the actuator load F_p.

An equivalent mechanical model that describes this behaviour is an infinitely stiff pusher connected in series with a spring, where the displacement of the infinitely stiff pusher is proportional to the applied voltage (i.e. $nd_{33}V$ term in equation (6.9)) and the spring stiffness is equal to the actuator stack stiffness k_p (Palazzolo et al. 1993, Barret and Palazzolo 1995).

Figure 6.6 shows the simplified equivalent mechanical model of two piezoelectric actuators on a cutterhead mass. This model is based on the push-pull configuration.

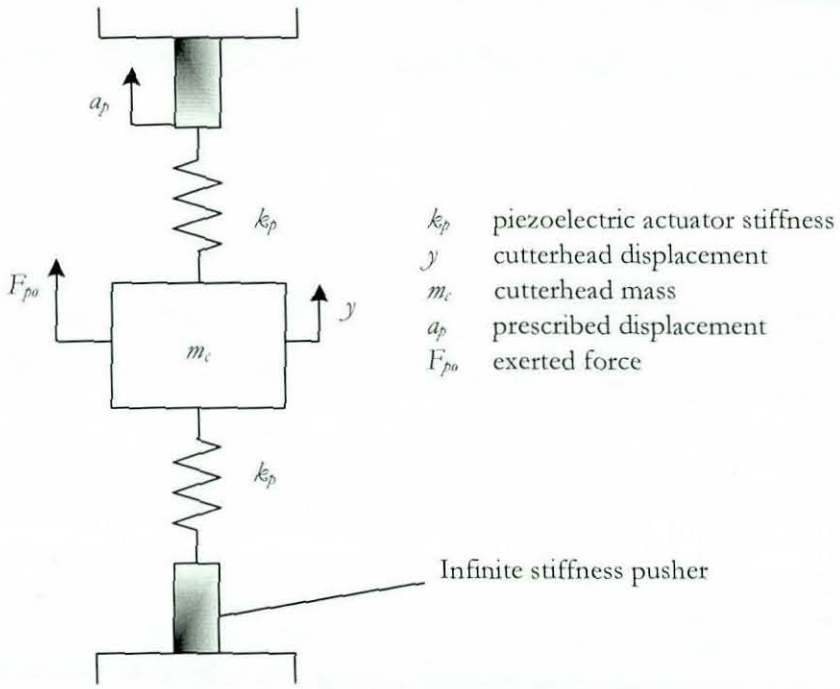

Figure 6.6 Simplified piezoelectric actuator model as infinite stiffness pusher

The motion y of the mass m_c is controlled by the prescribed displacement a_p of the piezoelectric actuators which are represented as infinitely stiff pushers. Two piezoelectric actuators are considered for the push-pull operation, because they are very susceptible to tensile force. The negative and positive values of the prescribed displacement a_p are controlled by the bottom and top actuators respectively.

The movement of the infinitely stiff pusher is proportional to the applied voltage. This relationship is described by the equation (6.10). Considering equation (6.9), the force exerted by the actuator on the mass m_c can be expressed as follows

$$F_{po} = k_p\left(a_p - y\right) \tag{6.12}$$

It should be noticed $F_{pa} \neq F_{p0}$, since the latter one represents the blocked force. In fact, equation (6.12) is derived with the assumption that the piezoelectric actuators behave linearly, which is not the case in reality. The limitations of the piezoelectric actuators (i.e. hysteresis) are described in more details in section 6.7.

6.3.3 Electrical Model of the Piezoelectric Actuators

Models described in section 6.3.1 and 6.3.2 represent the mathematical and mechanical behaviour of the piezoelectric actuator respectively. The electrical model of the piezoelectric actuator presented in Figure 6.7. It consists of a piezoelectric actuator modelled as a capacitor with a driving amplifier comprising of an output impedance R_o.

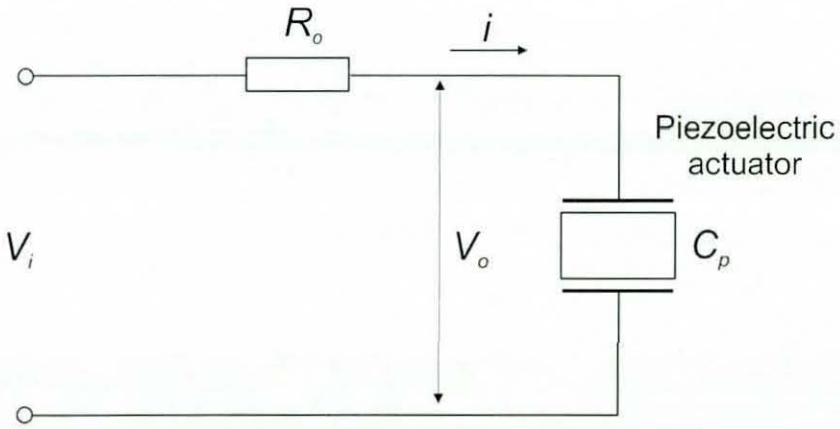

Figure 6.7 Electrical model of the piezoelectric actuator

The circuit diagram depicted in Figure 6.9 can be calculated as follows

$$V_i = R_o i + V_o \tag{6.13}$$

where V_i is the amplifier input voltage, V_o is the output voltage from the amplifier applied to the actuator and i is the driving current in the circuit.

The driving current can be calculated as rate of change of the charge q stored in the actuator as

$$i = \frac{dq}{dt} \tag{6.14}$$

whereas the current i can also be expressed from the governing equation (6.9) by taking equation (6.14) into consideration as follows

$$i = k_p n d_{33} \frac{dy}{dt} - k_p n^2 d_{33}^2 \frac{dV_o}{dt} + C_p \frac{dV_o}{dt} \tag{6.15}$$

whereas the applied voltage V is replaced by the amplifier output voltage V_o. Equation (6.15) shows the current flowing through the capacitor C_p, hence through the piezoelectric actuator. The product nd_{33} (i.e. number of actuator layers n and strain constant d_{33}), which appears in equation (6.15) describes basically the relation between the actuator displacement y and the applied voltage V_o for a free actuator (i.e. no load case).

In the data sheets of the stack type piezoelectric actuator, the number of layers and strain constants are not always available. Therefore, it is convenient to introduce the following constant which can be estimated from the actuator specifications.

$$\eta_p = n d_{33} \tag{6.16}$$

Inserting equation (6.15) into equation (6.13) results in a first order differential equation for the amplifier output voltage V_o.

$$\frac{dV_o}{dt} = \frac{1}{R_o\left(C_p - k_p \eta_p^2\right)}\left(V_i - V_o - R_o k_p \eta_p \frac{dy}{dt}\right) \tag{6.17}$$

The force F_{po} that actuator exerts onto the attached structure is then expressed according to the governing equation (6.9) as follows

$$F_{po} = -k_p\left(y - \eta_p V_o\right) \tag{6.18}$$

It should be mentioned that the force F_{po} is taken as negative, because the force F_p that appears in equation (6.9) is force acting on the actuator while F_{po} is the force acting on the attached structure (i.e. cutterhead). From the equations (6.13), (6.17) and (6.18) a state space model can be expressed as follows

$$\begin{bmatrix} \frac{dV_o}{dt} \end{bmatrix} = \begin{bmatrix} -\frac{1}{R_o C_1} \end{bmatrix} \begin{bmatrix} V_o \end{bmatrix} + \begin{bmatrix} 0 & -\frac{C_2}{C_1} & \frac{1}{R_o C_1} \end{bmatrix} \begin{bmatrix} y \\ \frac{dy}{dt} \\ V_i \end{bmatrix}$$

$$\begin{bmatrix} F_{po} \\ V_o \\ i \end{bmatrix} = \begin{bmatrix} C_2 \\ 1 \\ -\frac{1}{R_o} \end{bmatrix} \begin{bmatrix} V_o \end{bmatrix} + \begin{bmatrix} -k_p & 0 & 0 \\ 0 & 0 & 0 \\ 0 & 0 & \frac{1}{R_o} \end{bmatrix} \begin{bmatrix} y \\ \frac{dy}{dt} \\ V_i \end{bmatrix} \tag{6.19a}$$

$$C_1 = C_p - k_p \eta_p^2$$

$$C_2 = k_p \eta_p$$

Whereas the structure displacement y, the velocity dy/dt and the driving amplifier input voltage V_i can be defined as input variables. The outputs of the model are the generated force F_{po} from the actuator, the driving amplifier output voltage V_o and current flowing in the circuit i.

Considering equation (6.19a) and the actuator specifications shown in Table 3.1, a state space model of the actuator can be obtained as follows

$$\begin{aligned} \dot{x} &= Ax + Bu \\ y &= Cx + Du \end{aligned} \tag{6.19b}$$

where k_p=14 $N/\mu m$; C_p=2.3 μF; η_p=0.23 $\mu m/V$; R_o=65Ω;

$$u=\begin{bmatrix} y \\ \frac{dy}{dt} \\ Vi \end{bmatrix}; \qquad x=\begin{bmatrix} V_o \end{bmatrix}; \qquad y=\begin{bmatrix} F_{po} \\ V_o \\ i \end{bmatrix}$$

$$A=\begin{bmatrix} -\frac{1}{R_o \cdot C_1} \end{bmatrix}=\begin{bmatrix} -9.8657 \end{bmatrix}; B=\begin{bmatrix} 0 & -\frac{C_2}{C_1} & \frac{1}{R_o \cdot C_1} \end{bmatrix}=\begin{bmatrix} 0 & -2.0649 \cdot 10^6 & 9.8657 \end{bmatrix}$$

$$C=\begin{bmatrix} C_2 \\ 1 \\ -\frac{1}{R_o \cdot C_1} \end{bmatrix}=\begin{bmatrix} 3.22 \\ 1 \\ -0.0154 \end{bmatrix}; D=\begin{bmatrix} -k_p & 0 & 0 \\ 0 & 0 & 0 \\ 0 & 0 & \frac{1}{R_o} \end{bmatrix}=\begin{bmatrix} -14 \cdot 10^6 & 0 & 0 \\ 0 & 0 & 0 \\ 0 & 0 & 0.0154 \end{bmatrix}$$

The resultant state space model has the following inputs:

y structure displacement (i.e. spindle displacement at actuator location)

dy/dt velocity of the structure (i.e. spindle velocity at actuator location)

V_i driving amplifier input voltage

The output of the state space model is as follows:

F_{po} force generated by the actuator

V_o output voltage of the driving amplifier

i amplifier output current

The state space actuator model can then be combined with the state space model of the structure (i.e. spindle system). This enables to describe the overall system characteristics (described in chapter 7 in more details).

6.4 Piezoelectric Actuators' Operation

The push-pull arrangement of the piezoelectric actuators can be analysed by the model depicted in Figure 6.8.

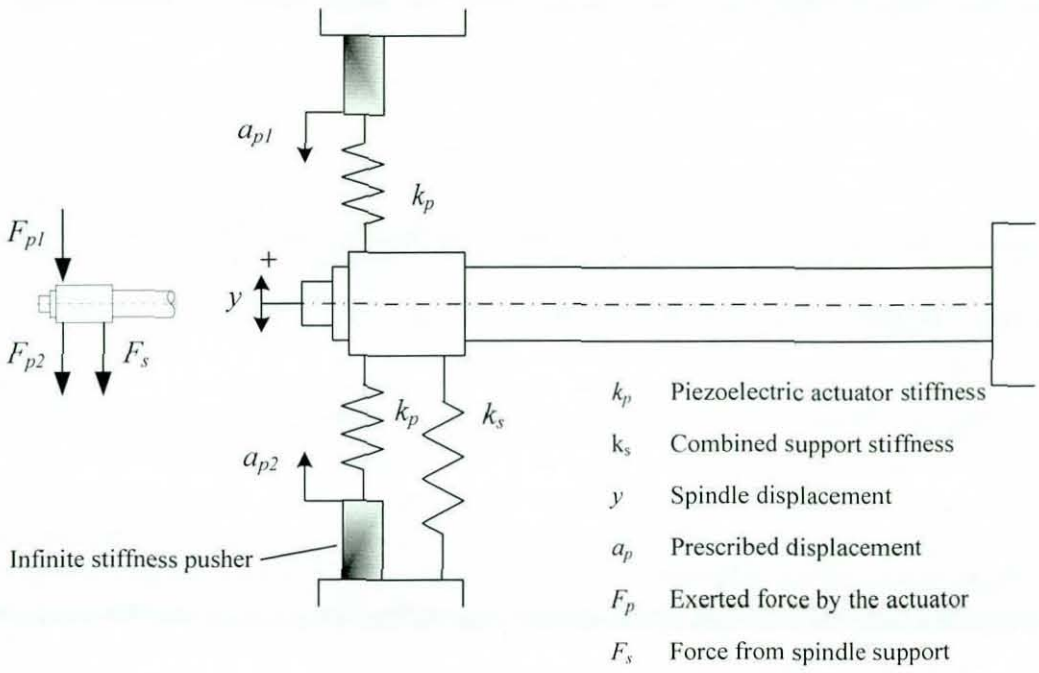

Figure 6.8 Piezoelectric actuator operation

The model consists of two opposing piezoelectric actuators modelled as infinite stiffness pusher and a spring in series. The spindle system has a support stiffness contributed by the integral components (i.e. spindle housing) which is connected in parallel. For the static case, forces acting on the spindle system can be described as follows

$$-F_s - F_{p1} - F_{p2} = 0 \tag{6.20}$$

Spindle displacement is then expressed with the following equation as

$$y = \frac{k_p}{k_s + 2k_p}\left(a_{p1} + a_{p2}\right) \tag{6.21}$$

Equation (6.21) reveals that the maximum control range of the spindle displacement is primarily determined by the stiffness characteristics of the system (k_s and k_p) as well as by the prescribed displacement (a_p) of the stack type actuator. The relationship between the applied voltage V and the prescribed displacement a_p is defined in the governing equation (6.9). Hence, by introducing a ratio between the support stiffness k_s and the piezoelectric actuator stiffness k_p,

$$\gamma = \frac{k_s}{k_p} \tag{6.22}$$

equation (6.21) can be formed into a voltage-displacement characteristic as

$$y = \frac{1}{2+\gamma} n d_{33} \left(-V_1 + V_2\right) \tag{6.23}$$

As previously mentioned, piezoelectric actuators are able to perform only in one direction because they are very susceptible to tensile stress, thus they cannot pull the load. In order to avoid actuator damage through any tensile stress, they need to be protected. A common method used in commercially available piezoelectric actuators is to employ a preload spring. This prevention method has however a remarkable disadvantage. It reduces the effective range of the actuator displacement (i.e. if the stiffness of the preload spring is equal to the actuator stiffness, actuator displacement is reduced by factor of two). By arranging the actuators in the push-pull configuration as depicted in Figure 6.8, the voltage of the top actuator appears in equation (6.23) as negative. In other words, by applying voltage to the top actuator, the spindle system displacement becomes negative. Two opposing actuators are capable of higher effective displacement range than one preloaded actuator as it can be seen from equation (6.23).

For example, consider two actuator arranged in push-pull configuration as shown in Figure 6.8; if the zero load displacement for each actuator is *40 μm* at *150 V*, the maximum displacement is then ± *20 μm* (for γ=0, assuming that the support stiffness k_s is much smaller than the actuator stiffness k_p) as depicted in Figure 6.9 and indicated in blue colour. Generally, one preloaded actuator with the length equal to the combined length of the two actuators would provide the same effective displacement range. However, longer actuator has lower stiffness and higher capacitance, which would decrease the dynamic performance and require higher driving voltages. The actuator arrangement used for the test rig is based on the push-pull configuration for both *x* and *y* directions. From the control point of view, a large spindle displacement range is desirable.

The spindle housing provides additional support stiffness k_s for the spindle system. However, it reduces the effective displacement of the actuators. The amount of influence depends on the ratio γ as can be seen in Figure 6.9, where the ratio value is set to γ =*0.5* with the corresponding actuator operation range indicated in dashed green line. Therefore, it is desirable to keep the support stiffness low (i.e. low γ values). The effective displacement of the actuator on the test rig is at approximately *±18.7 μm*. The support stiffness k_s of the test rig is at approximately *2 N/μm*. This value is determined by measuring the maximum spindle displacement and using the equation (6.23).

Furthermore, Figure 6.9 reveals that preloading actuator (i.e. energizing actuator with a certain voltage) does not change the static stiffness value of the spindle system, because the behaviour of the preloaded actuator (dashed blue lines in Figure 6.9) is parallel to the actuator operation (solid blue line in Figure 6.9) without preload. In other words, preloading one actuator does not change the stiffness value of the spindle system.

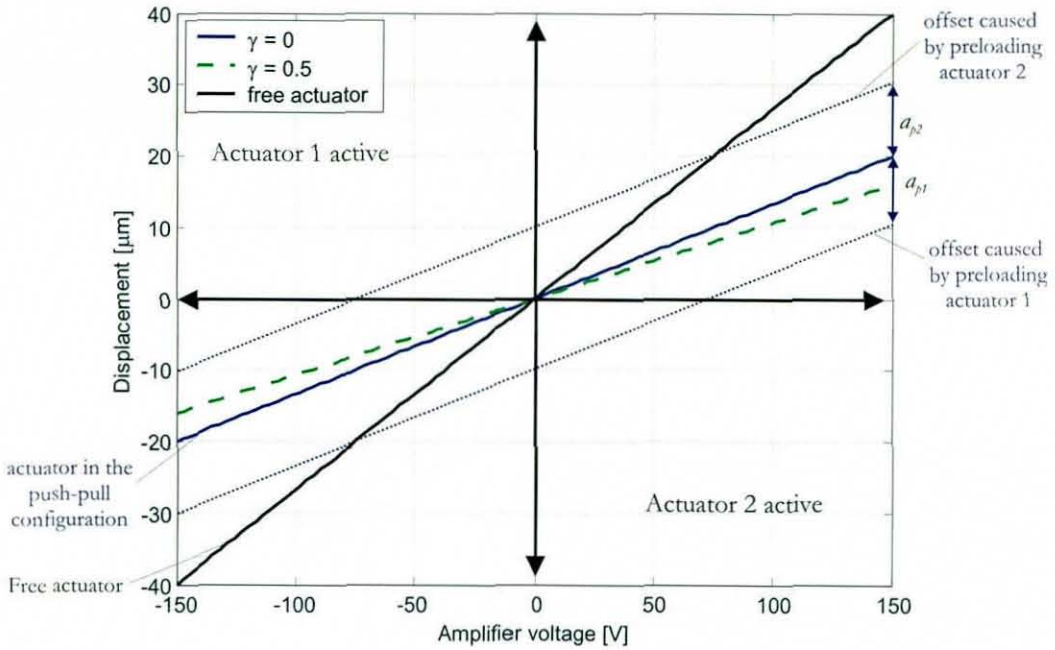

Figure 6.9 Principal of actuator operation in push-pull configuration

Moreover, it has been assumed that piezoelectric actuators have linear voltage to displacement characteristic, which is not the case in reality, because they possess non-linear behaviour (i.e. hysteresis). The non-linear behaviour of the actuators is not considered within the theory presented. Therefore, spindle characteristics in terms of force to displacement as well as voltage to displacement characteristics are experimentally analysed in the next section.

6.5 Static Stiffness Characteristics of the Spindle System

As has been described in section 2.3, the stiffness of a system plays an important role in the vibration analysis. Vibration can simply be defined as a response to other conditions in a dynamic system. It is a ratio of the forces acting on the system which has a specific stiffness characteristic. A change in force and/or in stiffness behaviour can be considered as the root causes of vibration occurring in a dynamic plant. A change of unbalance is an example of force alterations.

Considering vibration as a ratio of the force to stiffness, any change in vibration level (i.e. increasing decreasing vibration level) can generally be referred to either stiffness or force alteration. In order to implement active vibration control, the dynamic characteristics of the plant (i.e. test rig) has to be analysed prior to controller design. Therefore, various methods have been used to experimentally analyse the behaviour of the test rig. Moreover, if the stiffness of a dynamic system can be changed, the natural frequency and even higher vibration modes (i.e. higher resonant frequencies) could be damped according to the particular application.

The small scale planer consists of 4 piezoelectric actuators and their operation in push-pull configuration has been investigated theoretically in section 6.4. In this section, the test rig stiffness characteristics and the corresponding natural frequencies are investigated for various actuator operations (i.e. actuator on/off, preloaded actuator). Hereby, three different experiments have been performed to analyse the spindle system behaviour. In the first experimental work, a platform with a load cell has been used to identify the static spindle stiffness behaviour. With the second experiment, piezoelectric actuators were energized to apply a force against the spindle and the corresponding deflection is measured. The objective of this experimental work is to reveal the effect of piezoelectric actuator under various load conditions on the overall spindle stiffness behaviour. The third experiment is based on the impact hammer method with the aim to analyse the dynamic system response with and without energized actuator. The latter experiment provides the overall dynamic system behaviour under various load conditions.

6.5.1 Static Stiffness Measurement of the Spindle Unit

In this section the static stiffness behaviour of the spindle system is experimentally investigated in order to confirm the theory presented in section 6.4. Figure 6.10 shows the experimental set up comprising of a platform and a load cell.

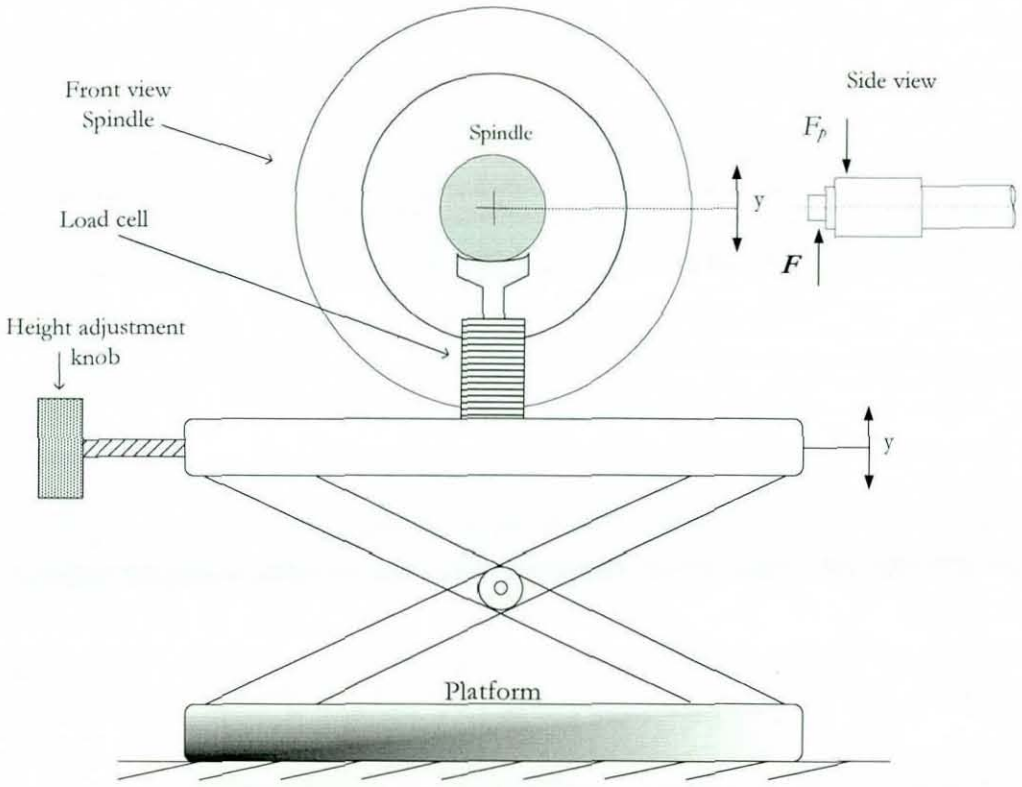

Figure 6.10 Static stiffness measurement of the spindle system with a platform

The load cell is attached to the spindle shaft and placed on a platform. By increasing the height of the platform, a force is applied against the spindle which is measured with a force indicator. The corresponding deflection is measured with a high precision dial indicator with $\pm 0.1\ \mu m$ accuracy. It should be noted that the stiffness value is identified at the tool holder (node 4 in Figure 7.1) on the shaft where the force F is applied. Furthermore, the stiffness of the platform is considered as infinite when compared to the stiffness of the spindle system. The experimental set up on the test rig is depicted in Figure 6.11.

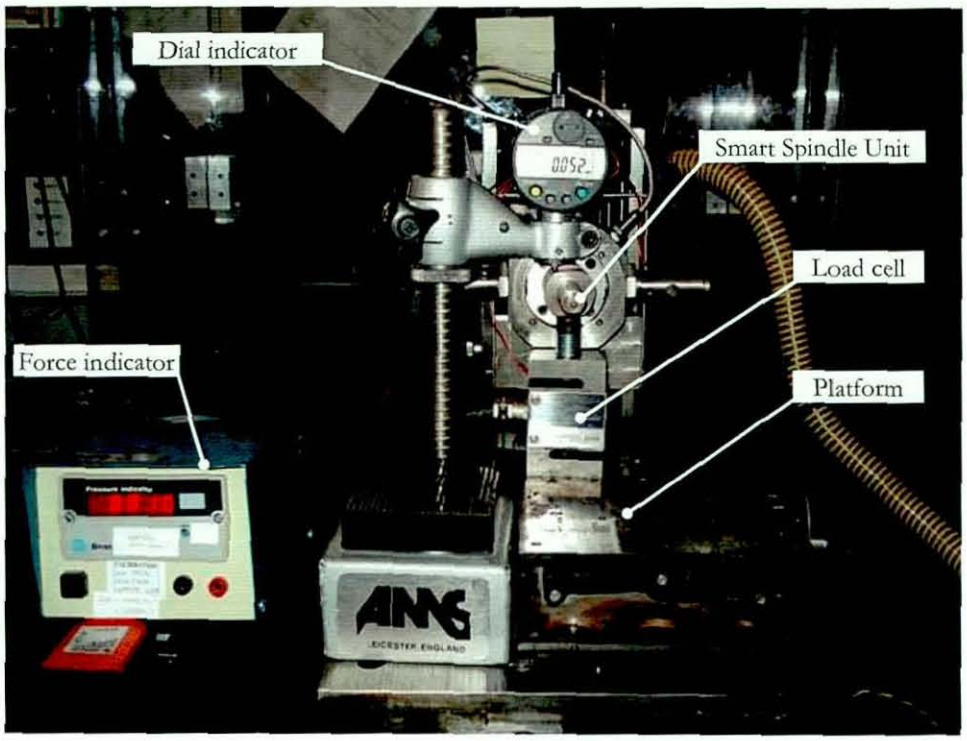

Figure 6.11 Experimental set up for spindle stiffness measurement

Firstly, the stiffness measurement was carried out for inactive actuators (i.e. actuator driving amplifiers off) and the displacement is measured against the applied force F exerted through the platform. In the second instance, the piezoelectric actuators were switched on but only the voltage for the actuator B was gradually increased from *0* to *120 V* in order to apply a counter force F_{pB} generated by the actuator B against the spindle. This measurement set up is illustrated in Figure 6.12. The full range of the actuator displacement was not demonstrated (i.e. U_{pB}= *150V*) in order to avoid actuator damage due to compression forces acting in bidirectional vertical way (i.e. force F generated by the platform against the force F_{pB} generated by the piezoelectric actuator). The objective of increasing the voltage, thus the force generated by the actuator acting on the spindle, was to investigate the effect of active piezoelectric actuator on the stiffness characteristics of the spindle system.

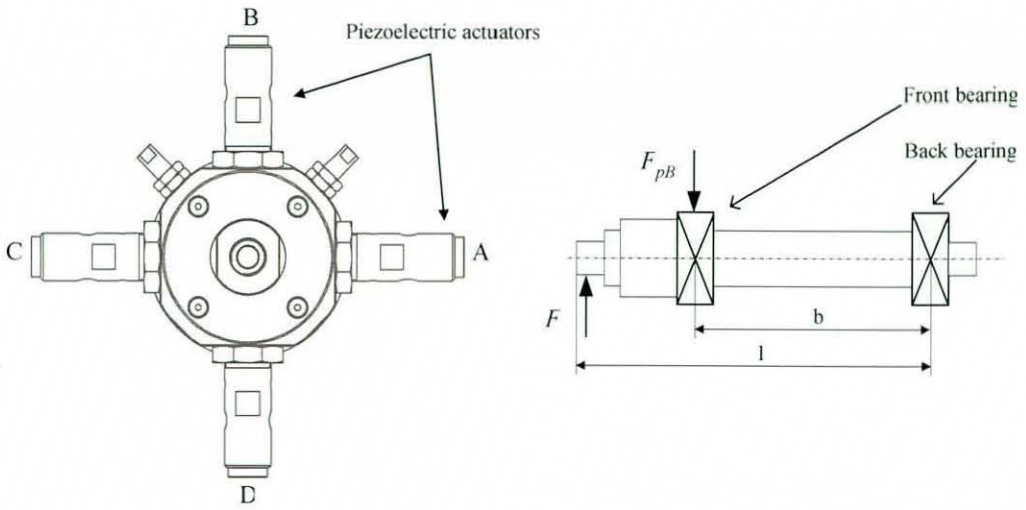

Figure 6.12 Spindle stiffness behaviour with active and inactive piezoelectric actuators

Figure 6.13 shows the measurement results. They show that increasing the voltage of the actuator B shift the curve alongside the x-axis and the preload increases.

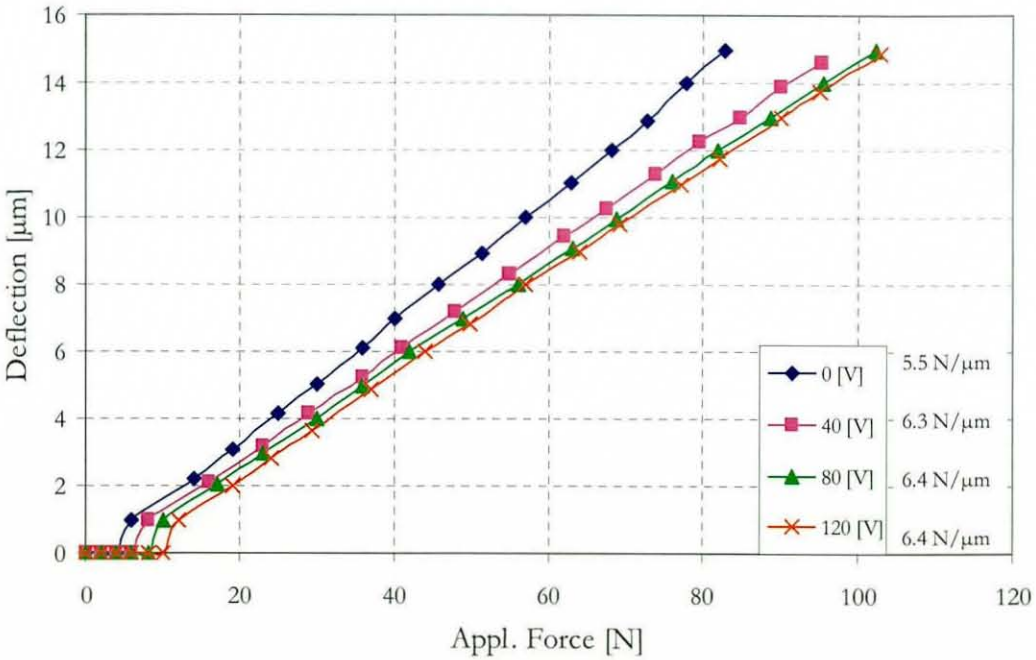

Figure 6.13 Static stiffness behaviour of the spindle system from experimental work

The measurements also reveal that the active piezoelectric actuator does not significantly change the stiffness characteristics of the spindle system (i.e. for active actuators $U_{pB}=40V$ and $U_{pB}=120V$ the difference between stiffness values is less than 2%). For the case when the actuators are not energized (i.e. inactive actuator $U_{pB}=0V$) the spindle stiffness is lower than the stiffness values of the active actuators. This mainly suggests some clearance between the actuators and the spindle. Theoretically, the dependency between the applied force and the resultant deflection is expected to exhibit linear behaviour, because the stiffness of the free actuator provided in the data sheet is a constant which is primarily determined by the actuator design (i.e. material properties and number of layers used to form the stacks). Therefore, this linearity should also be reflected in form of parallel lines with respect to the preloaded actuator. For example, Figure 6.13 shows that the stiffness curve obtained with the preloaded actuator ($U_{pB} = 80V$) is parallel to the one obtained with a higher preload ($U_{pB} = 120V$). Thus, the slope of the stiffness curves is the same. In other words, the static behaviour of the spindle system described by the theory in section 6.4 is supported by the experimental work. Preloading actuator does not change the static stiffness characteristics of the spindle system. Furthermore, depending on the preload (i.e. U_{pB}) the deadband (i.e. force applied by the platform but no deflection observable) is present up to ca. 10 N as can be seen in Figure 6.13. In the next section a further experiment has been carried out to determine the effects of the push-pull configuration of the piezoelectric actuators on the spindle stiffness characteristics.

6.5.2 Static Stiffness Characteristics in Push-Pull Configuration

This section aims to show the effects of the push-pull configuration on the overall static stiffness behaviour of the spindle system. Figure 6.14 shows an overview of the experimental set up. Firstly, the driving voltage for the actuator B is set to zero and at the same time the driving voltage of the opposing actuator D is gradually increased from $0 - 100\ V$ to create the spindle deflection.

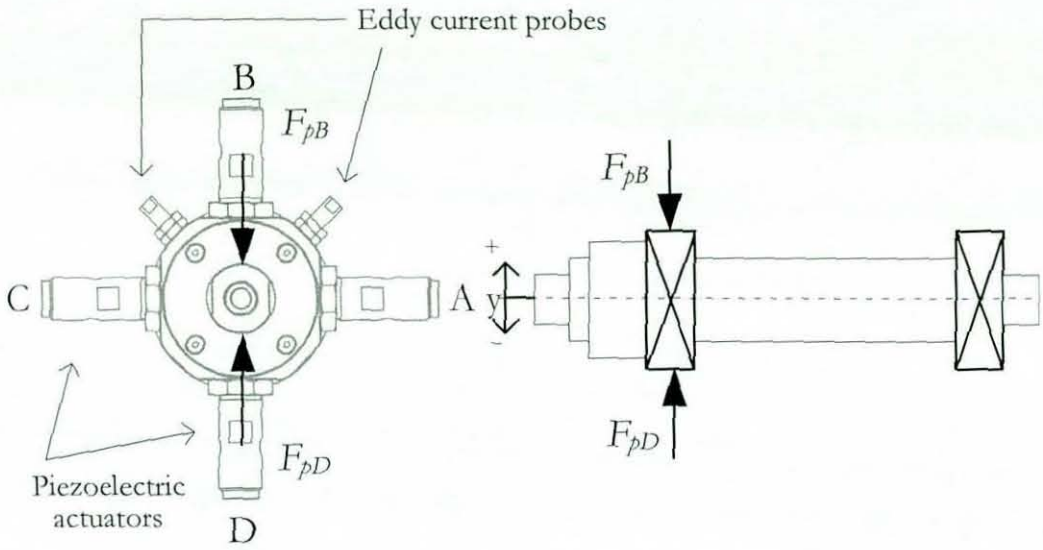

Figure 6.14 Experimental set up to identify the effects of push-pull arrangement

In the second instance, the voltage of the actuator B is set to a constant value (i.e. U_{pB} = *40 V*) and the voltage of the opposing actuator D is again gradually increased in same manner as in the first instance. The resultant deflection is measured with the contactless eddy current probes. As aforementioned, the aim of these experiments is to support the theory of push-pull configuration and to investigate the effect on the static stiffness behaviour of the spindle unit presented in section 6.4.

Measured spindle deflection against the voltage in Figure 6.15 exhibits a linear relationship between these parameters. It can also be observed that with increasing the preload (i.e. U_{pB} from *0* to *100 V*) the linearity is shifted with respect to preloaded actuator voltage, but it does not change its linear characteristics. In Figure 6.15 this relationship can also be observed from the parallel distribution of the curves. Applying a mathematical linear trend line on the curves shows that for preloaded actuator (i.e. $U_{pB} > 0V$), the slope of the curves remains almost constant with ca. 2.5 % deviation. The measurement results confirm that the slope of the curves does not change thus the static stiffness value of the spindle system is not affected by the actuator preload.

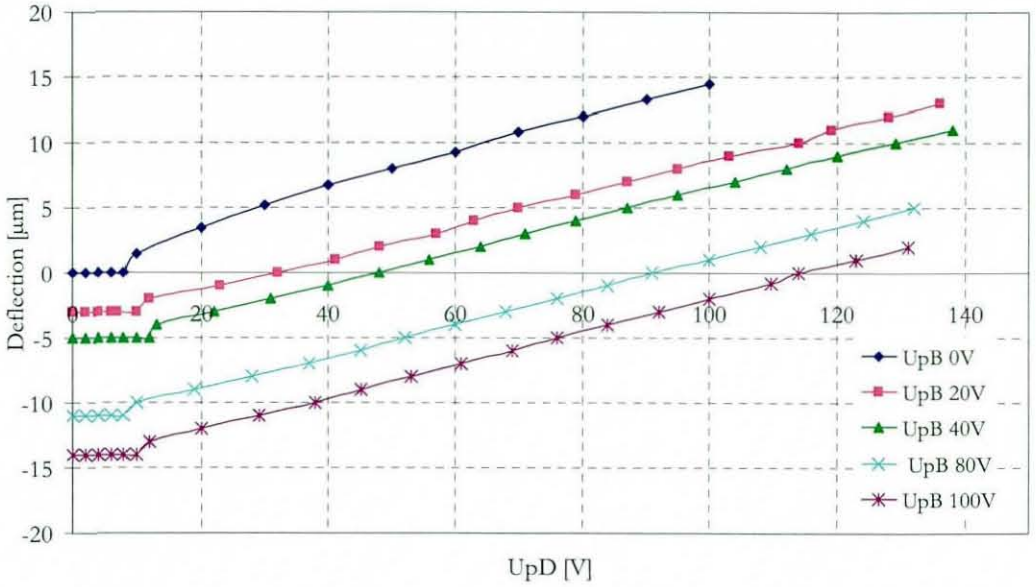

Figure 6.15 Static stiffness behaviour in push-pull configuration

6.5.3 Summary of the Static Stiffness Measurements

In the first experimental work, an external force is applied to the spindle system in order to identify its static behaviour (Figure 6.10). The experimental results are in good agreement with the theory presented in section 6.4. The experimental results showed that the static stiffness characteristics do not change with preloaded actuator. Preloading actuator causes basically a shift in the operation range which can be perceived as an initial offset but it does not change the slope of the force to displacement curves. Therefore, it can be concluded that the static stiffness behaviour of the spindle system is not affected by the actuator preload. In the second experimental work, the effect of the push-pull configuration on the spindle system is analysed. Herein the voltage of the actuator B is set to zero and the voltage of the opposing actuator D is gradually increased. In the second instance, the actuator B was activated to produce a counter force against spindle whereas the voltage of the opposing actuator is again gradually increased to obtain a spindle deflection.

With the push-pull arrangement, the effective displacement of the actuator is reduced by half (equation 6.23), because the opposing actuator has the same stiffness value. In other words, if the full displacement range of the free actuator is at $40\mu m$ at nominal voltage (i.e. typically 150 V for stack type piezoelectric actuators), when arranged in push-pull configuration the maximum effective displacement for $\gamma = 0$ decreases to $20\mu m$. This value is even further reduced through the support stiffness k_s (equation 6.23). The disadvantage of using two opposing actuator is that two driving amplifiers are required for each axis. On the other hand the advantage of this arrangement is that the load is split between both actuators. Furthermore, the push-pull configuration provides the double static stiffness ($2*k_p + k_s$) than one actuator. However, the static stiffness value of the spindle system is not affected by energizing the actuator at different voltage levels as has been shown in Figure 6.15. It only causes a preload. The preload can be considered as an initial displacement of the infinite stiffness pusher as depicted in Figure 6.8. Taking the arrangement of the two piezoelectric actuators into consideration, the spindle displacement can be described as follows

$$y = \frac{1}{2+\gamma}\left(nd_{33}\left(-V_1 + V_2\right) + \left(-a_{pre1} + a_{pre2}\right)\right) \tag{6.24}$$

where V_1 is the driving voltage of the actuator B and V_2 is the driving voltage of the actuator D with preload displacements a_{pre1} and a_{pre2} respectively. As has been described by equation (6.24), the preload causes a spindle offset which could also be observed from the experimental work depicted in Figure 6.15. Due to the parallel distribution of the obtained curves from the experimental work (Figure 6.15), it can be concluded that the slope of the curves remains constant, thus the static stiffness behaviour of the spindle system is not affected by actuator preload. In the next section the dynamic stiffness characteristics of the spindle system is analysed.

6.6 Dynamic Characteristics of the Spindle System

In this section, the effect of the piezoelectric actuators on the dynamic characteristics of the spindle system is investigated. The impact excitation method was performed to carry out the experiments. The most common excitation method used for modal analysis is the hammer excitation technique. Considering the spindle system as a "black box", input and output characteristics are used to determine its frequency response function FRF. This system identification method is also used in chapter 7 to compare the behaviour of the spindle system with the numerical model obtained through FEM analysis. Unlike the system identification described in Chapter 7 which is primarily performed to tune the numerical model, the experiments in this subsection focus on the dynamic effects of preloaded actuators on the system response. Figure 6.16 shows the principal diagram of the experimental set up. The impact hammer tip consists of a piezoelectric force transducer for measuring the impact force. It allows compressive force measurements up to *1000 N*.

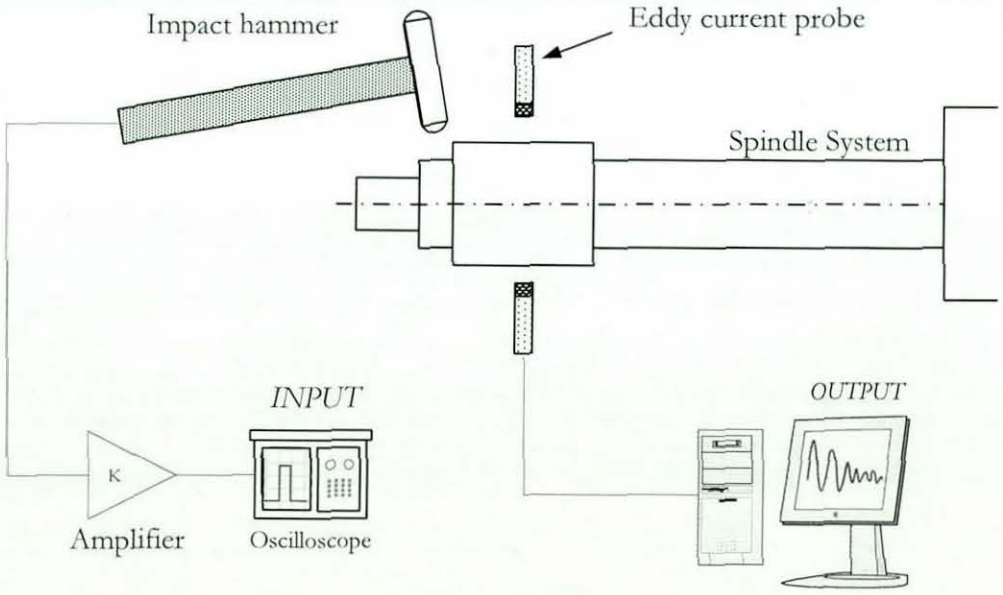

Figure 6.16 Experimental set up to identify the dynamic behaviour of the spindle system

The sensitivity of the impact hammer is at *22.8 mV/N*. A charge amplifier is used for a better signal resolution.

The charge amplifier is connected to an oscilloscope to measure the impact force. The resultant vibration of the spindle system is measured via two eddy current probes. The duration, thus the shape of the spectrum of an impact is primarily determined by the mass and the stiffness of the "black box". In the first experiment, the driving voltages of the piezoelectric actuators are switched off and the impact test was performed. In the second instance, the actuator D was preloaded with different voltage levels to analyse the effects of the preload on the natural frequency of the spindle system. The intention behind the preloading actuator D was to create a counter force on the spindle whilst the impact through the hammer takes place. In the third instance, all for actuators were preloaded and their effects on the dynamic characteristics of the spindle system were analysed. Figure 6.17 shows the input (impact force) and the resultant output (spindle vibration) in the time domain. In order to analyse the spindle system characteristics, these values are first transferred into the frequency domain within Matlab through Fourier transformation.

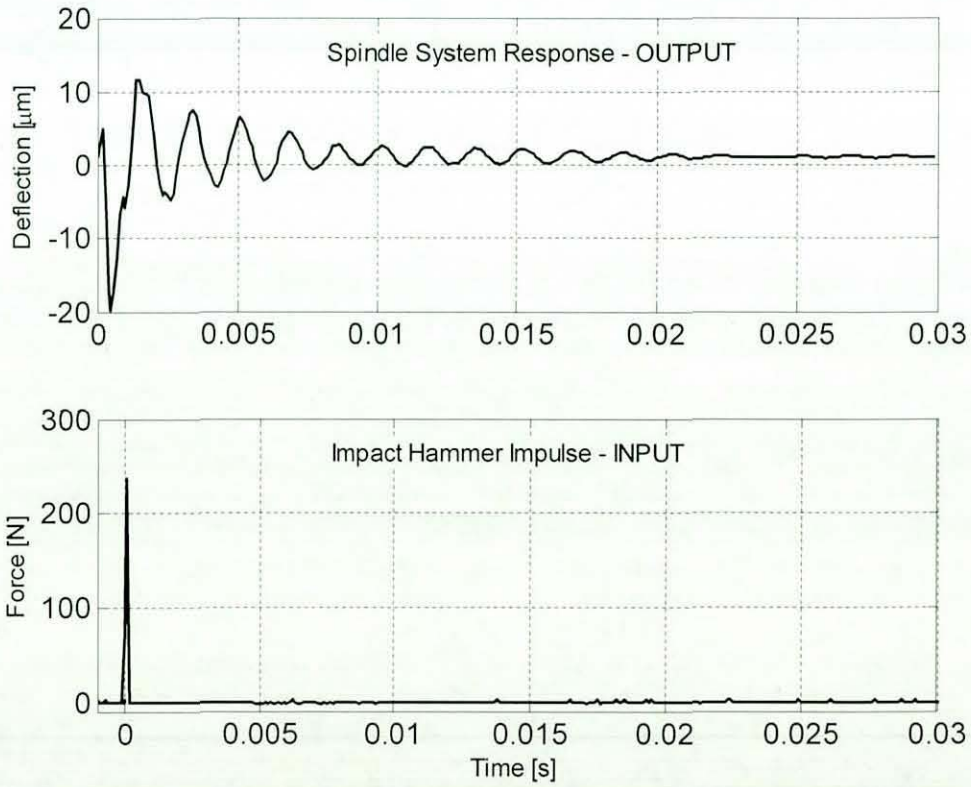

Figure 6.17 Input and output characteristics of the spindle system within the time domain

The frequency response function FRF is then obtained as follows

$$H(\omega) = \frac{Output(\omega)}{Input(\omega)} \tag{6.25}$$

This relationship is also termed as the compliance of a system when the input and output corresponds to force and displacement respectively. Figure 6.18 shows the FRF of the spindle system for inactive piezoelectric actuator (i.e. driving amplifiers switched off). The spindle response characteristics are almost linear up to the natural frequency which is at *596 Hz*.

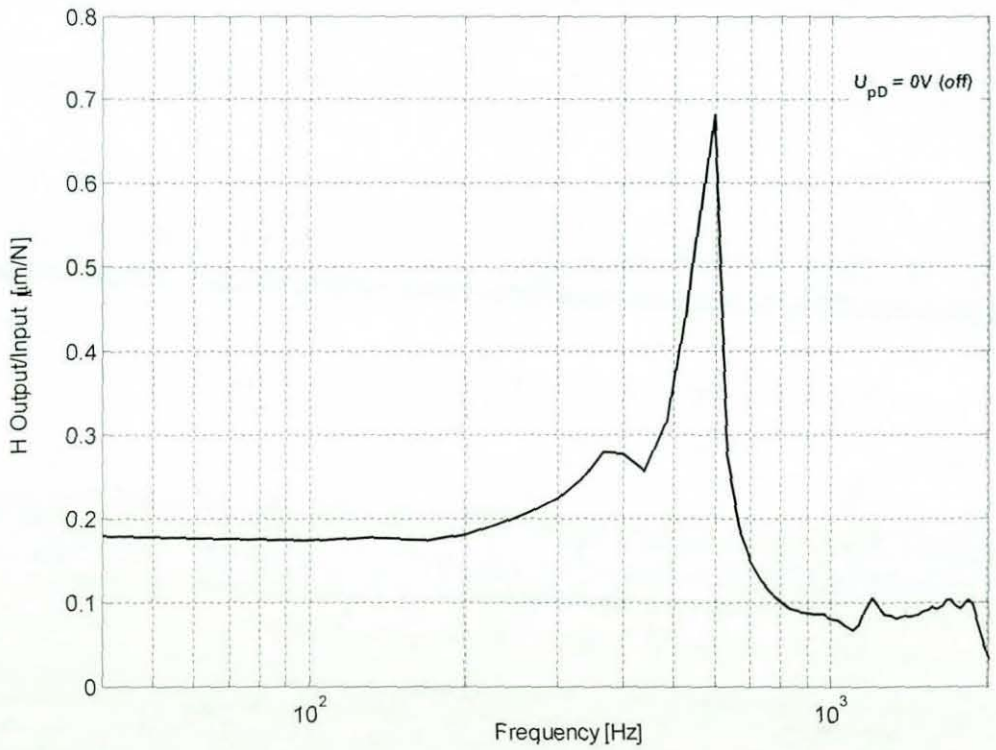

Figure 6.18 Frequency response of the spindle system for inactive actuators

In the next experiment it is to find out whether actuator preload changes the dynamic characteristics of the spindle system. Therefore, the actuator D (as indicated in Figure 6.12) is preloaded with different voltage levels ($U_{pD}=80V$ and $U_{pD}=120V$) and the impact test is carried out.

The reason for preloading the actuator D is to produce a counter force against the spindle whilst the impact through the excitation hammer occurs. The results of the analysis reveal that the natural frequency of the spindle system increases at about *4.5%* from *596 Hz* for inactive actuator to *622 Hz* when the actuator is driven at *120 V* (Figure 6.19). Interestingly, it can also be seen from Figure 6.19 that once the piezoelectric actuators are activated, the natural frequency increases by less than *0.5%* from *620 Hz* to *622 Hz* for the actuator voltage increase from *80 V* to *120 V*.

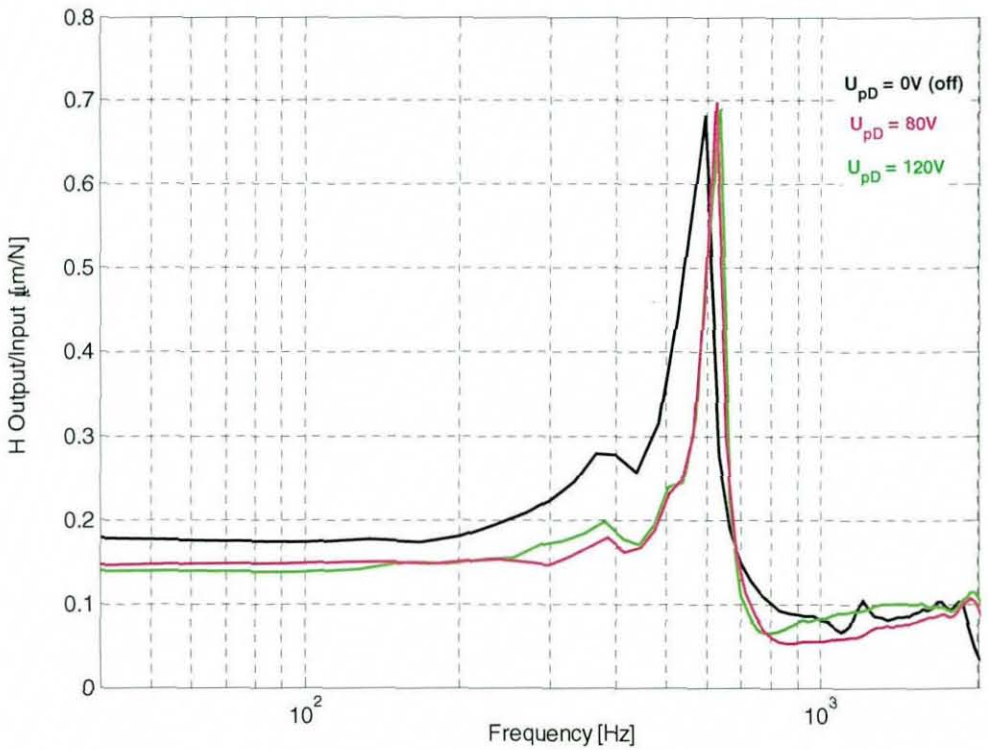

Figure 6.19 Frequency response of the spindle system for active actuators

The natural frequency of the spindle system remains almost constant when all four actuators are activated. Figure 6.20 shows the spindle system characteristics for inactive, one actuator active (i.e. U_{pD} = *80 V*) and for the case when all four actuators are driven at *80 V* (i.e. $U_{pA} = U_{pB} = U_{pC} = U_{pD}$ = *80 V*).

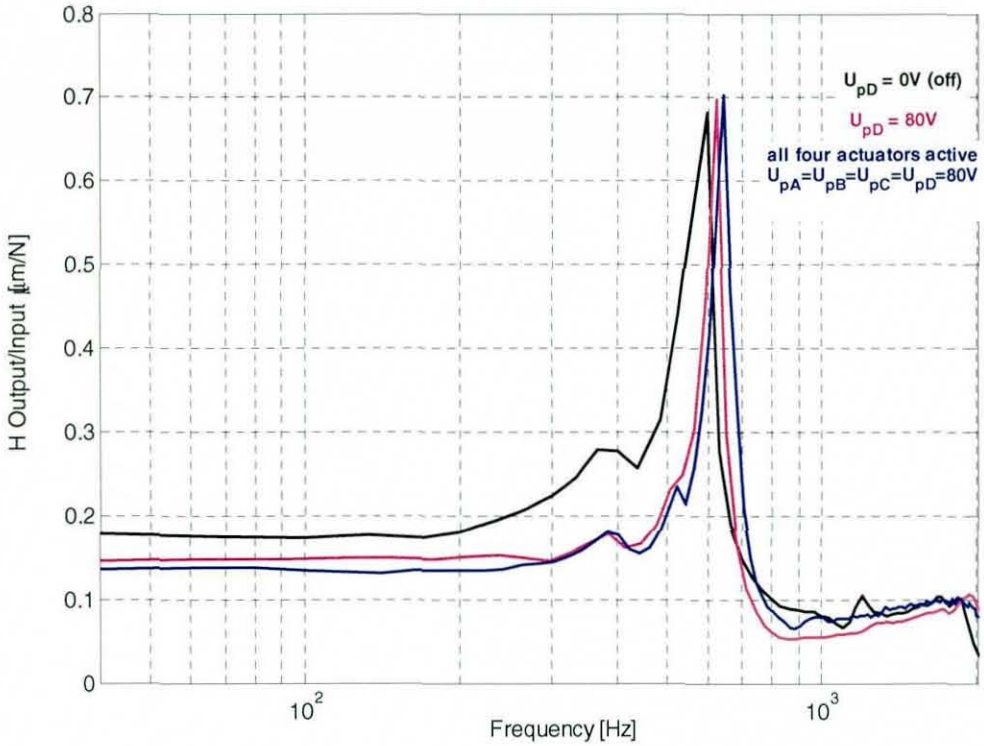

Figure 6.20 Spindle response for inactive, one active and all four active actuators

The natural frequency of the spindle system is negligibly increased from *622 Hz* for one active actuator to *627 Hz* when all four actuators are driven at *80 V*. It can be concluded that for the inactive actuators the dynamic stiffness characteristics with respect to the natural frequency of the system appear to be lower than for the case when the actuators are active. This suggests some degree of clearance in the structure of the actuator mounting, because the actuators are not physically bonded to the front bearing where the actuation takes place. The actuators are mounted on the front bearing with a ball tip as it depicted in Figure 3.2 in chapter 3. For active actuators, the natural frequency of the spindle system remains almost constant. Therefore, it can be concluded that preloading actuators do not significantly affect the natural frequency of the spindle system.

6.7 Limitations of the Piezoelectric Actuators

It should be pointed out that the theory presented in sections 6.3 and 6.4 are derived with the assumption that the piezoelectric actuator behaves linearly, which is not the case in reality. Equations presented in sections 6.3 and 6.4 show the relationship between the piezoelectric material properties, actuator design and actuator capabilities. However, the actual piezoelectric actuator possesses non-linear characteristics. The non-linear behaviour of the piezoelectric actuator is caused by the fact that the piezoelectric material constants listed in Table 6.1 depend on the applied voltage and the mechanical stress developed in the actuator. As a result, the piezoelectric actuator exhibits hysteresis, which is typically between *10 - 15%* for "soft" type piezoelectric material and at about *1 %* for "hard" type material. A typical hysteresis loop for a soft type piezoelectric material is shown in Figure 6.21.

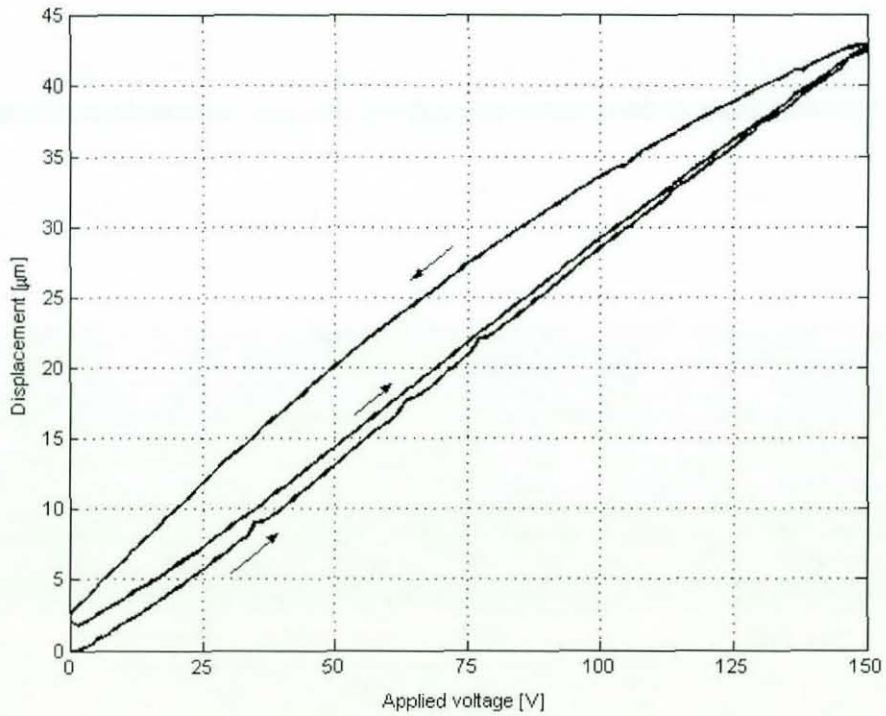

Figure 6.21 Hysteresis of a free actuator (Hynek 2004)

The hysteresis can be compensated for by introducing a closed loop control for positioning applications. The power requirements posed on the driving amplifier for positioning applications, where the actuator driving voltage changes slowly, are not usually critical. The required driving current is usually very low, because the piezoelectric actuator represents a capacitive load. It should be outlined that piezoelectric actuator does not require any power to hold the load in a steady state position. This is a significant advantage over actuators such as active magnetic bearing or voice coil, which consume power even when holding the load.

The hysteresis of the piezoelectric actuators measured on the test rig is depicted in Figure 6.22. The hysteresis of the actuator lies within ca. *12 %* which is typical for this type of actuators.

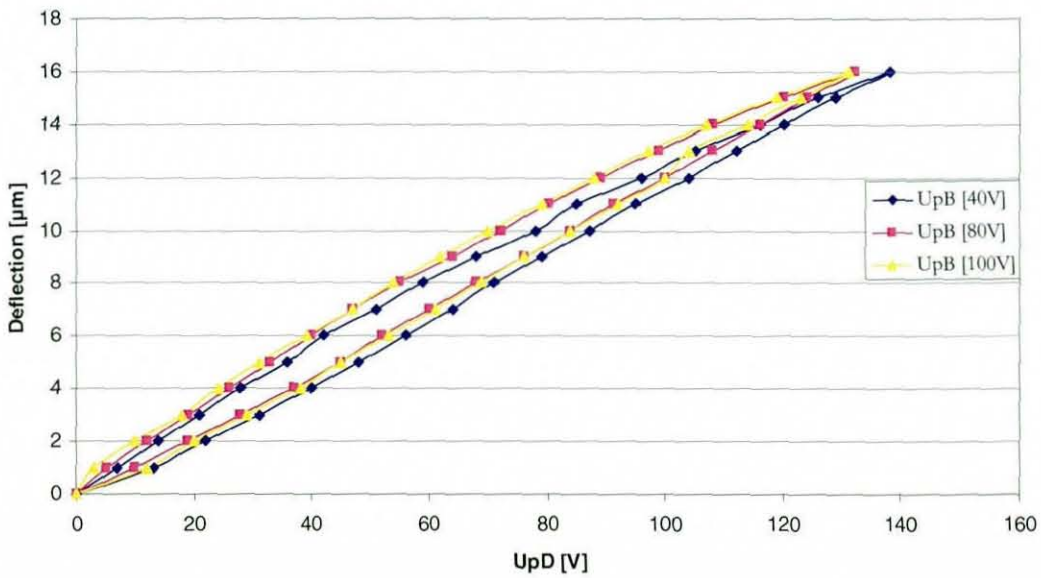

Figure 6.22 Hysteresis of the piezoelectric actuator

Chapter 7 CONTROLLER DESIGN

Active control is generally defined as applying a control force (i.e. by means of actuators such as active magnetic bearings or piezoelectric actuators) to a plant using external power for obtaining a desired response from a dynamic system. In contrast, passive control does not require external power and it relies on the dissipative and structural characteristics of the components integrated within the system (i.e. squeeze film dampers as reported by Chu and Holmes, 2000). The superiority of the active control methods over the passive control techniques is the degree of freedom to control a dynamic plant over a wide range of operating conditions. For example, the bandwidth and the damping of a dynamic system could be tuned to adapt the controller for various application environments. Furthermore, the active control approach is generally faster, more flexible and more efficient than the passive control methods (Chen et al. 2003). The purpose of the controller design is to achieve a closed loop operation so that the undesired vibrations during the cutting process are reduced. This in turn will yield an enhanced machining environment. In other words it will enable the performance of the machining environment to be improved by increasing its operational bandwidth. Considering the fact that on a planer, the number of cutting knives can be as high as 20, the knife passing frequency considerably increases, which, on the other hand, limits the machining operation range (e.g. lower cutting speed). From the machining point of view this means that if the knife passing frequency reaches the natural frequency of the spindle system it would cause excessive vibrations which may result in tool and machine damage. Therefore, the aim of the controller is to change the dynamic characteristics of the spindle system by increasing the damping in the critical frequencies close to the resonant frequencies of the spindle system. Control of the dynamic behaviour of systems can be obtained using modal control techniques as reported by Lalanne et al. (1983) and Inman (2001).

The controller implemented on the test rig is based on the modal control approach and requires a numerical model of the spindle system. The numerical model is obtained through the FEM (Finite Element Method) assisted by various experimental tests (i.e. system identification test) for the model tuning procedure.

The controller aims to reduce vibrations occurring in the vertical axis as they are considered to be more important than the vibrations occurring in the horizontal axis in terms of an enhanced machining environment (McKenzie 2001, Palmqvist 2003, Palmqvist et al. 2003). Therefore, the controller design described in the subsequent sections focuses on the vibration reduction in the vertical axis.

7.1 Spindle System Numerical Modelling and Simulation

The objective of this section is to develop a numerical model of the spindle system. A linear model of the spindle system comprising both electrical and mechanical parts is introduced. The finite element method was used by Hynek (2004) to model the mechanical part of the spindle system. The resultant model of the spindle system was a state space model with 38 states (Hynek et al. 2004). The authors used Matlab to develop software to obtain the FE model of the spindle unit. The overall spindle model consisted of 36 states and 2 states from the two actuators. However, this numerical model proved to be unstable in the closed loop operation. Further analysis of the numerical model obtained through FEM by Hynek et al. (2004) showed that it is neither observable nor controllable. Therefore, the FE model of the mechanical part has been tuned to achieve a controllable and observable numerical state space model. Herein, more nodes have been introduced into the FE model by using the software program developed within Matlab by Hynek et al. (2004).

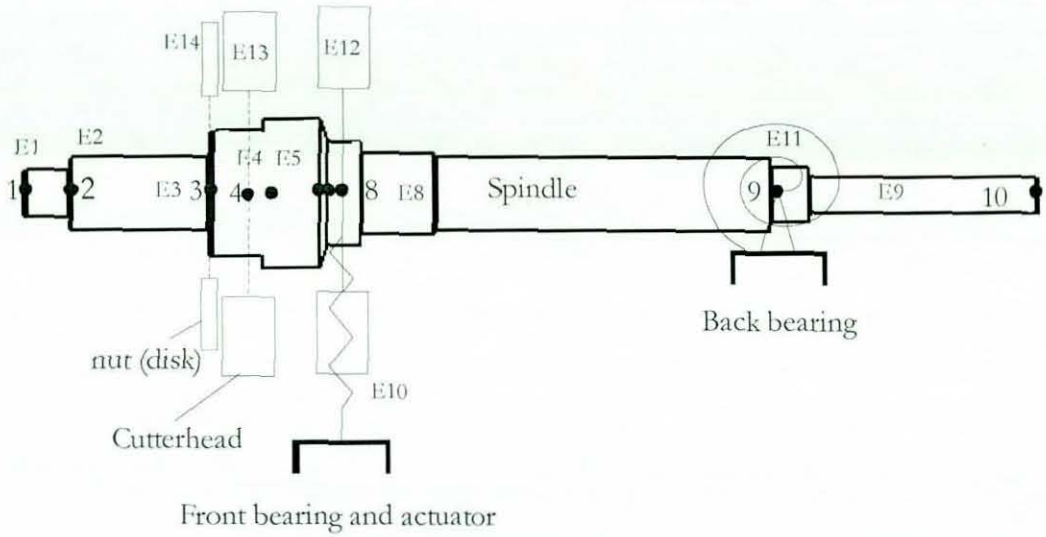

Figure 7.1 FE spindle system model

For example, the cutterhead (E13), cutterhead nut (E14) and the front disk (E12) have been added to the FE model. The FE model of the spindle with the actuators is shown in Figure 7.1. The FE spindle model consists of 10 nodes. The elements E1 to E10 characterize the spindle itself according to its geometrical dimensions. The front bearing and the front ring shown in chapter 3 (Figure 3.2) are represented by DISK elements (E10 and E12) and connected to node 8. The back bearing is connected to the spindle unit housing and represented in node 9 (E11). A more detailed description of the elements that can be modelled within the Matlab software to obtain an FE model of a spindle system is reported by Hynek et al. (2004).

The resultant FE model of the spindle system now has 78 states, of which 76 are related to the mechanical model; each of the other two states represents an actuator. The mechanical model is then combined with the model of the piezoelectric actuators, which is presented in section 6.3 as a state space model. Both these methods provide an overall numerical model of the spindle system (Figure 7.2).

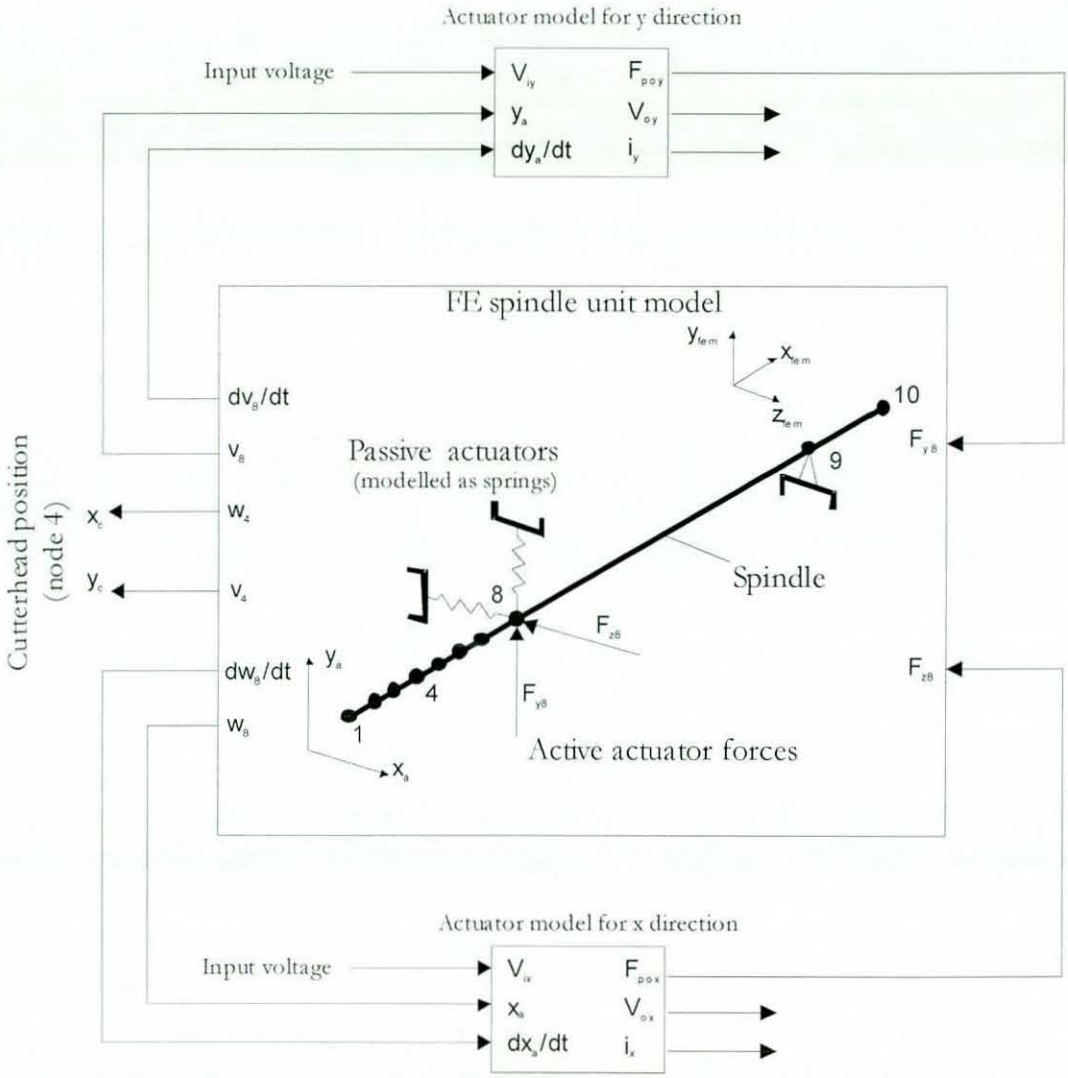

Figure 7.2 Overall spindle model

In the FE model depicted in Figure 7.1, the inputs of its state space representation are actuator forces acting in node 8. The outputs are displacement and velocity in node 8 (which are required as inputs for the actuator model) and displacement in node 4 where the cutterhead is attached.

The inputs and the outputs of the final model are summarized in Table 7.1.

Table 7.1 Overall spindle system model inputs/outputs

INPUTS		
Variable	**Unit**	**Description**
V_{ix}	V	Driving amplifier input voltage for x-axis
V_{iy}	V	Driving amplifier input voltage for y-axis
OUTPUTS		
x_a	m	Actuators displacement for x-axis (node 8)
y_a	m	Actuators displacement for y-axis (node 8)
x_c	m	Cutterhead displacement for x-axis (node 4)
y_c	m	Cutterhead displacement for y-axis (node 4)
F_x	N	Force generated by actuator in x-axis
V_{ox}	V	Driving amplifier output voltage
i_x	A	Driving amplifier output current
F_y	N	Force generated by actuator in y-axis
V_{oy}	V	Driving amplifier output voltage
i_y	A	Driving amplifier output current

Analysis on the overall numerical model (spindle + actuators) showed that the poles and zeros of the model are on the left half plane of the pole-zero-map, which indicates that the model is stable (Figure 7.3).

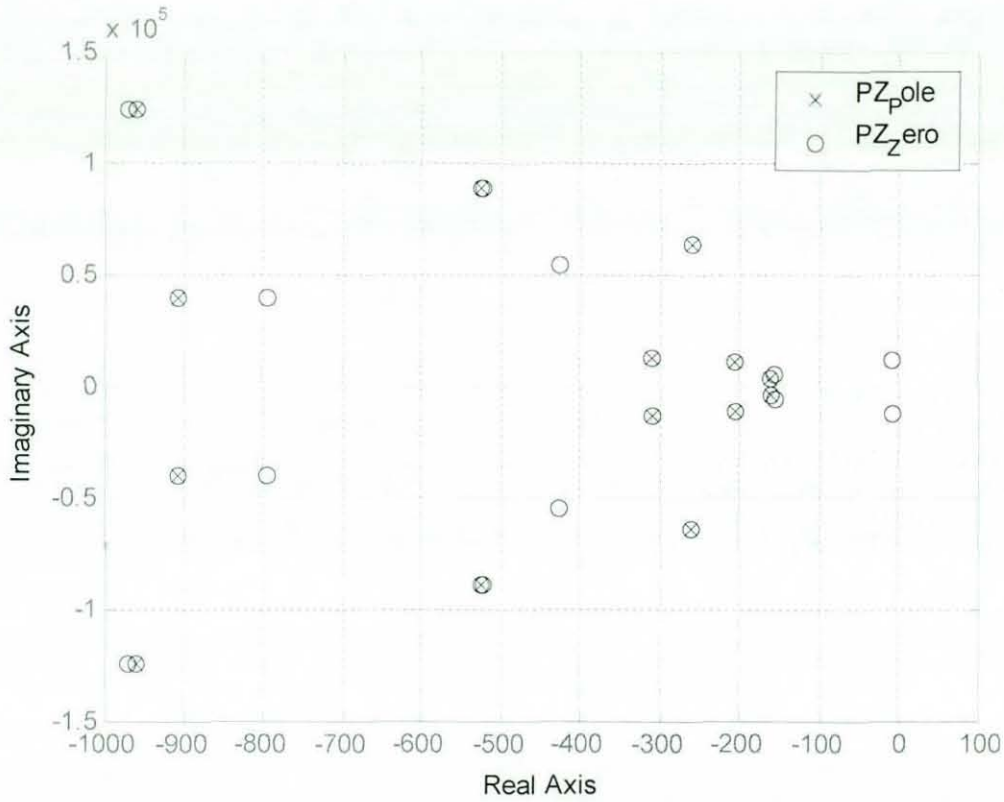

Figure 7.3 Pole-zero-map of the overall spindle model

The first three vibration modes (natural frequencies) and the corresponding damping ratios of the numerical spindle system model are shown in Table 7.2.

Table 7.2 Vibration modes and damping ratios of the overall numerical model

Modes	Frequency [Hz]	Damping ratios [%]
Mode#1	617	4.1
Mode#2	1779	1.8
Mode#3	2118	2.3

Table 7.2 shows that the first natural frequency of the numerical model of the spindle system is at *617 Hz* which varies only by ca. *1%* from *622 Hz*, the natural frequency of the spindle system determined experimentally with the excitation

hammer in section 6.6. The corresponding Bode diagram of the numerical model depicted in Figure 7.4 shows the first three vibration modes of the numerical model.

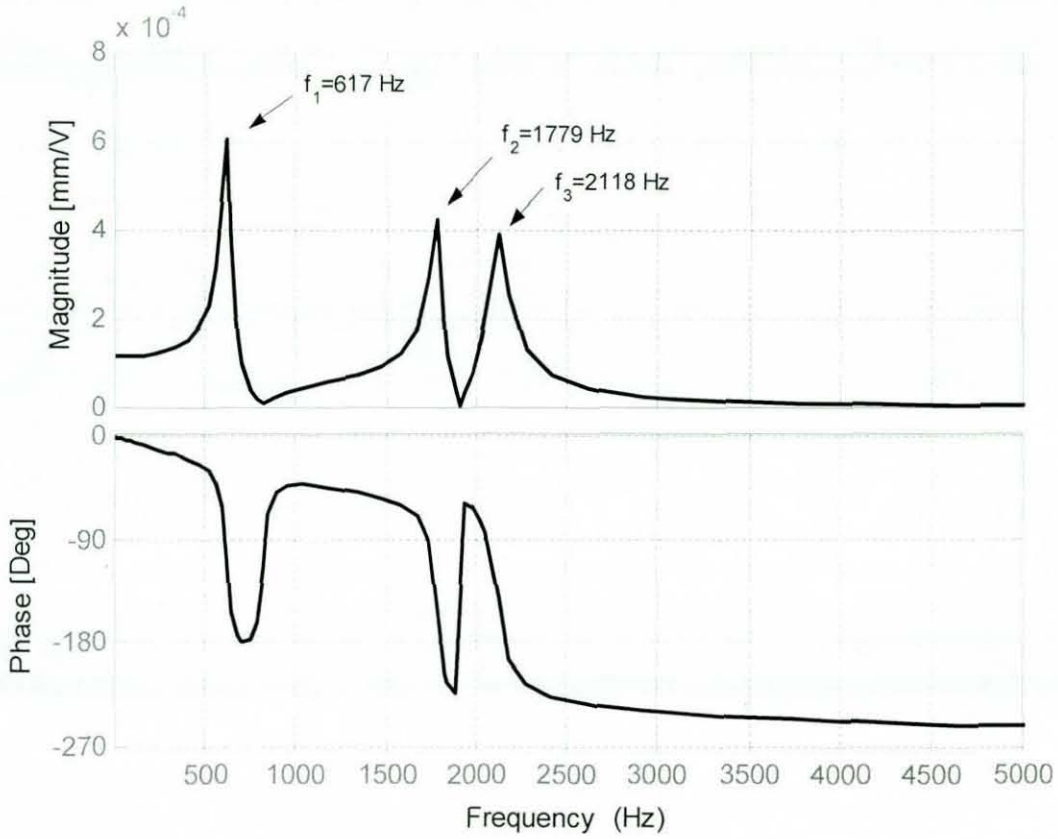

Figure 7.4 Bode diagram of the numerical model

7.2 Numerical Model Tuning

The overall model comprises of input parameters such as spindle dimensions, piezoelectric actuator capacitance, driving amplifier output impedance and bearing damping. Some of these parameters, such as spindle dimensions and actuator capacitance can be measured. However, it is difficult to experimentally determine the damping in the rolling bearings which support the spindle (Zeillinger et al. 1994), since the interaction and contribution of several damping sources (e.g. spindle material damping, front and back bearing) cannot be distinguished. In order to obtain a reliable numerical model, the actual plant (spindle + piezoelectric actuators) dynamics need to be analysed so that the numerical model can be adjusted accordingly. The tuning parameters are shown in Table 7.3.

Table 7.3 Numerical model tuning parameters

Tuning Parameters	Unit	Value	
		V22	V23
Damping of the element E10	Ns/m	10	9
Angular stiffness of element E10	Nm/rad	0	0
Angular damping of element E10	Nms/rad	0.3	0.2
Angular stiffness of element E11	Nm/rad	7e3	7e3
Angular damping of element E11	Nms/rad	0	0

The tuning parameters have been adjusted so that the frequency response function (FRF) of the numerical model shows similar behaviour as the actual spindle system. The FRF of the actual plant is analysed by two different approaches. The first approach involves the impact hammer tests as performed in chapter 6. The difference to the previous impact hammer tests is that the vibration is now measured with an accelerometer at the point of interest where the impact through the hammer takes place (Figure 7.5).

The second approach consists of FRF identification through piezoelectric actuators by using a sweep and an impulse function. In all experimental approaches the whole plant is considered as a "black box" and the input and output characteristics are analysed to determine the FRF.

7.2.1 Numerical Model Tuning through the Impact Hammer

The plant is excited with an impulse through the impact hammer and the output is measured with an accelerometer. This method is widely used for the FRF identification of a structure due to its convenience and well-known methodology (Roy and Ganesan 1995, McConnell 1995, Ahn et al. 2004). Figure 7.5 shows the experimental set up for measuring the dynamic characteristic of the spindle system. The impact hammer and the accelerometer outputs are measured with a multi IO analogue/digital card connected to the PC via a USB port.

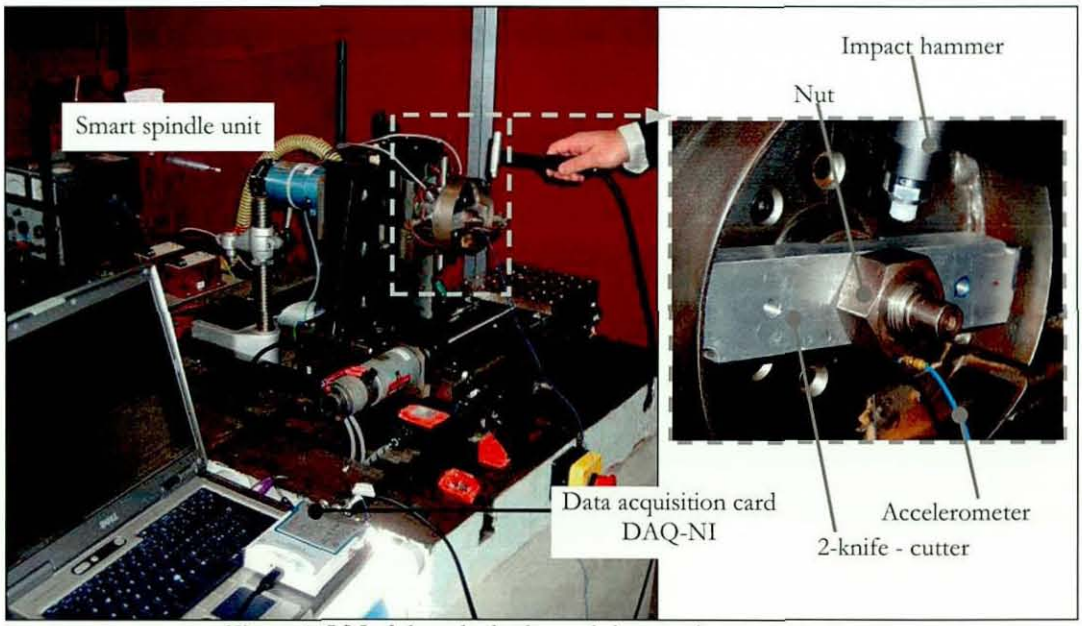

Figure 7.5 Modal analysis through impact hammer tests

The FRF of the spindle system is obtained and analysed within the software program CUTPro©. The impact hammer can be used with different tip types (i.e. steel, plastic,

rubber) which allow excitation over a wide range of frequencies. The experimental tests showed that the hammer tip made from rubber-teflon is mostly suitable for the impacts tests. This impact hammer tip type is capable of exciting frequencies up to *1000 Hz*. Although a steel hammer tip is capable of covering excitation frequencies up to *2000 Hz*, it was not suitable for the FRF identification on the test rig because it caused unavoidable double hits, which on the other hand, lead to incorrect FRF characteristics of the spindle system. Therefore, the rubber-teflon hammer tip was chosen to perform the impact tests. The drawback with this hammer tip is that it is not capable of exciting higher vibration modes of the spindle system beyond *1000 Hz*. Figure 7.6 shows the dynamic behaviour of the spindle system where the impact force and the corresponding deflection are used to identify the FRF. The legend "Y, on U_{pD}=20V" in Figure 7.6 indicates that the excitation through the impact hammer is performed on the cutterhead's nut (node 3 in Figure 7.1) and measured with the accelerometer at the point of impact (the cutterhead's nut) whilst the amplifiers are switched on and the opposing actuator's voltage is set to *20 V* (in order to generate a counter force against the spindle).

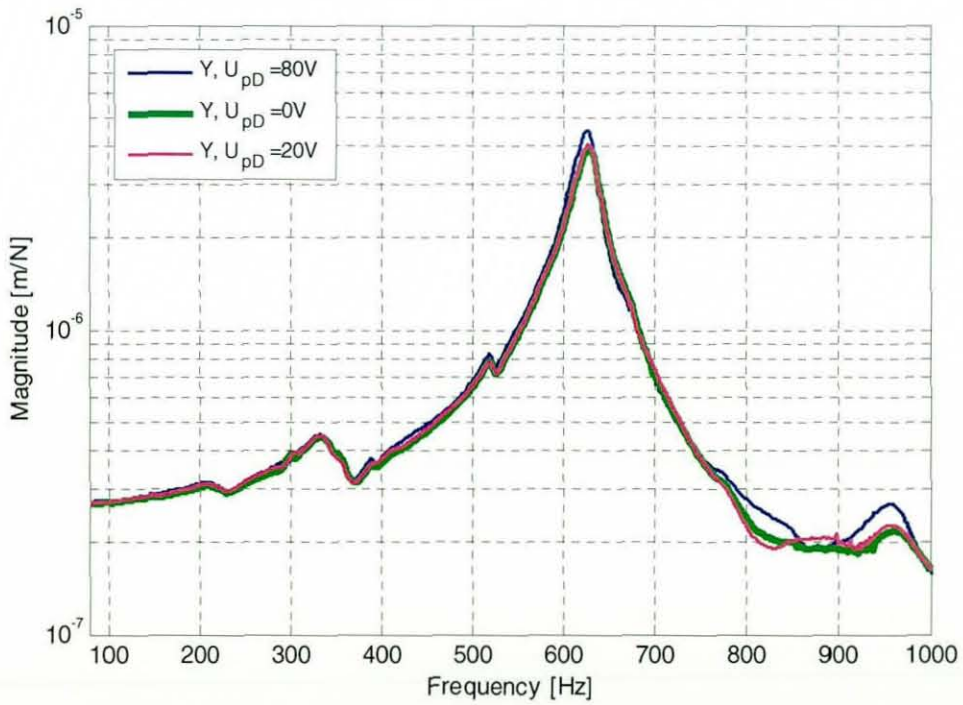

Figure 7.6 Frequency response function of the spindle system

The FRFs of the spindle system depicted in Figure 7.6 shows that the natural frequency of the spindle system is at *625 Hz*. Furthermore, it supports the results from section 6.6 that the preloaded actuator (i.e. actuator voltage at *20* or *80 V*) does not significantly change the dynamic behaviour of the spindle system. Based on the obtained FRF of the actual plant, the numerical model of the spindle system is tuned so that it shows similar dynamic characteristics. The tuning parameters in Table 7.3 are used to adjust the numerical model. Figure 7.7 shows the FRFs of the numerical model (indicated in black colour and in solid/dashed lines) and the actual plant behaviour (indicated in blue, magenta and green colours).

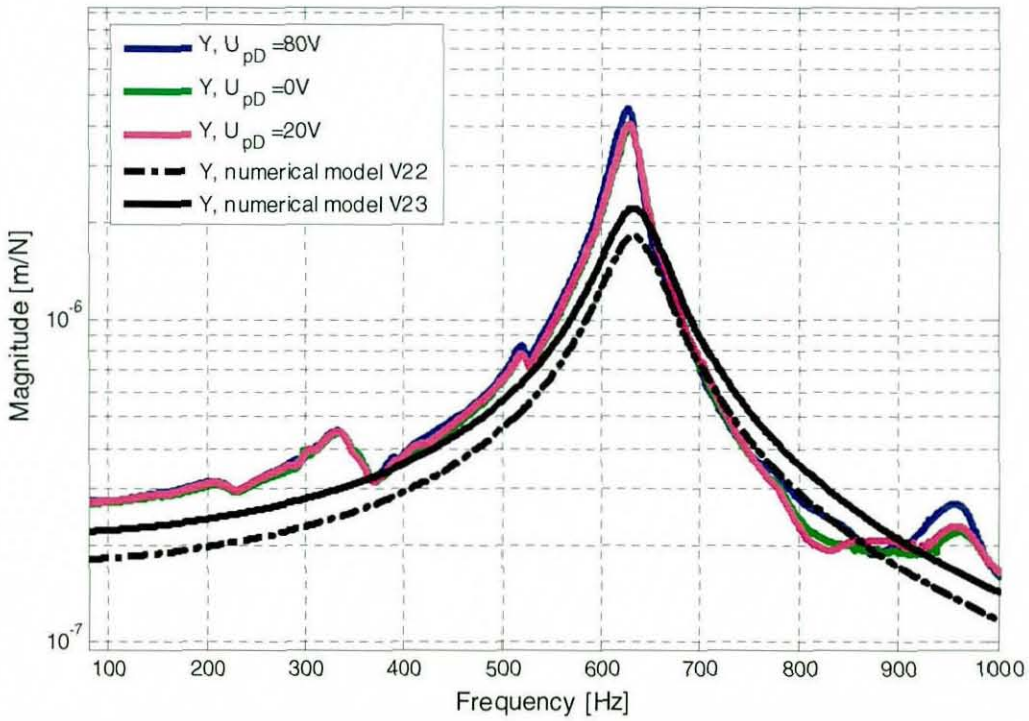

Figure 7.7 Frequency response functions of the numerical and the real plant

Although this experiment with the limited excitation bandwidth of the impact hammer tip could not excite all the vibration modes (i.e. second and third vibration modes as shown in Table 7.2) of the spindle system, it was useful when adjusting the first vibration mode of the numerical model.

7.2.2 Numerical Model Tuning with Piezoelectric Actuators

The tuning procedure is further refined by measuring the spindle response to a linear swept-frequency signal. In this approach the piezoelectric actuators are used to excite the spindle with a sweep frequency function with the aim of revealing other vibration modes of the spindle unit. The magnitude of the swept-frequency signal is *15 Vpp* to avoid excessive vibrations. Furthermore, the sweep range of the signal is *0 – 4 kHz* and the frequency change rate is at *0.8 kHz/sec* in order to limit the time spent in resonant peaks. Figure 7.8 shows the spindle response through a swept-frequency input measured with the eddy current probes.

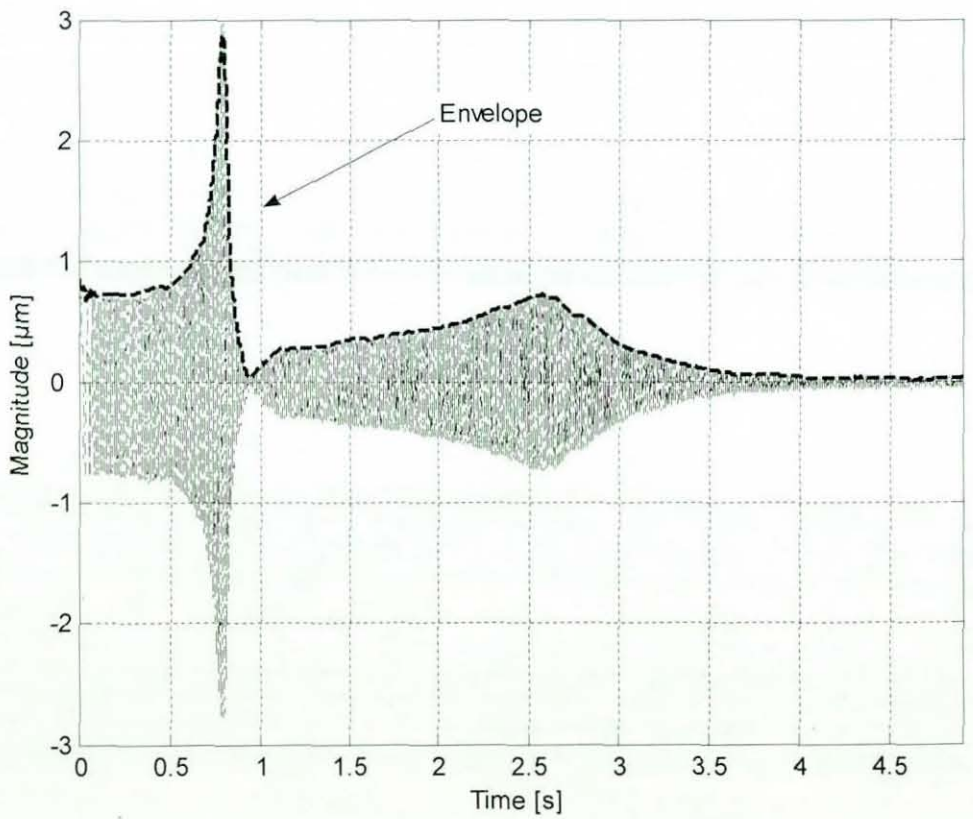

Figure 7.8 Frequency sweep on the test rig

A lower frequency rate might deliver a more accurate resonant peak amplitude because the sweep function will spend more time in this region and cause higher vibrations. However, in order to avoid actuator damage through excessive vibrations,

this value proved to be accurate enough. In fact, Hynek (2004) demonstrated through simulation that taking half of the frequency rate change (i.e. *0.4 kHz/sec*) will only deliver *4 %* more accuracy in the amplitude and less than *1 %* in resonant frequency. Therefore, the chosen swept-signal parameters are reasonable for the practical sweep tests performed on the test rig. The envelope of the spindle response is defined as output (i.e. system response) and the swept-frequency signal as the input source. From these two measures, the FRF of the spindle system is determined.

In order to verify the FRF obtained through the sweep function a further experiment has been carried out. An impulse generated by the piezoelectric actuators is taken as input and the output response is measured by the eddy current probes. The impulse consists of *45 V* in magnitude with a *0.3 ms* pulse width. The input pulse has been analysed with the FFT in order to identify its frequency range (Figure 7.9).

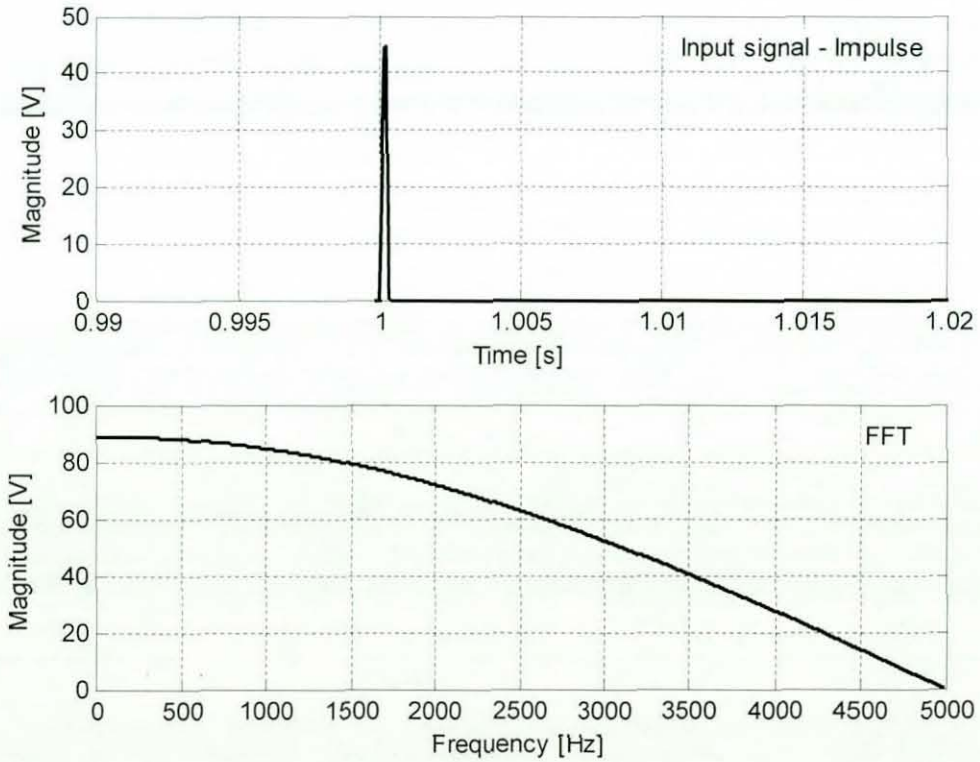

Figure 7.9 FFT of the input signal

Figure 7.10 shows both FRFs of the spindle system obtained by the swept-frequency signal and the impulse signal. Both methods show a very similar FRF for the spindle system. The first natural frequency of the spindle unit is at *625 Hz* in the FRF obtained through the sweep test and *627 Hz* with the impulse test (Figure 7.10). However, both methods could not reveal the second and the third modes of the spindle system which are present in the numerical model and given in Table 7.2. In fact, the FRFs from both experiments exhibit some indications of the second mode in the *2000 Hz* region shown in Figure 7.10.

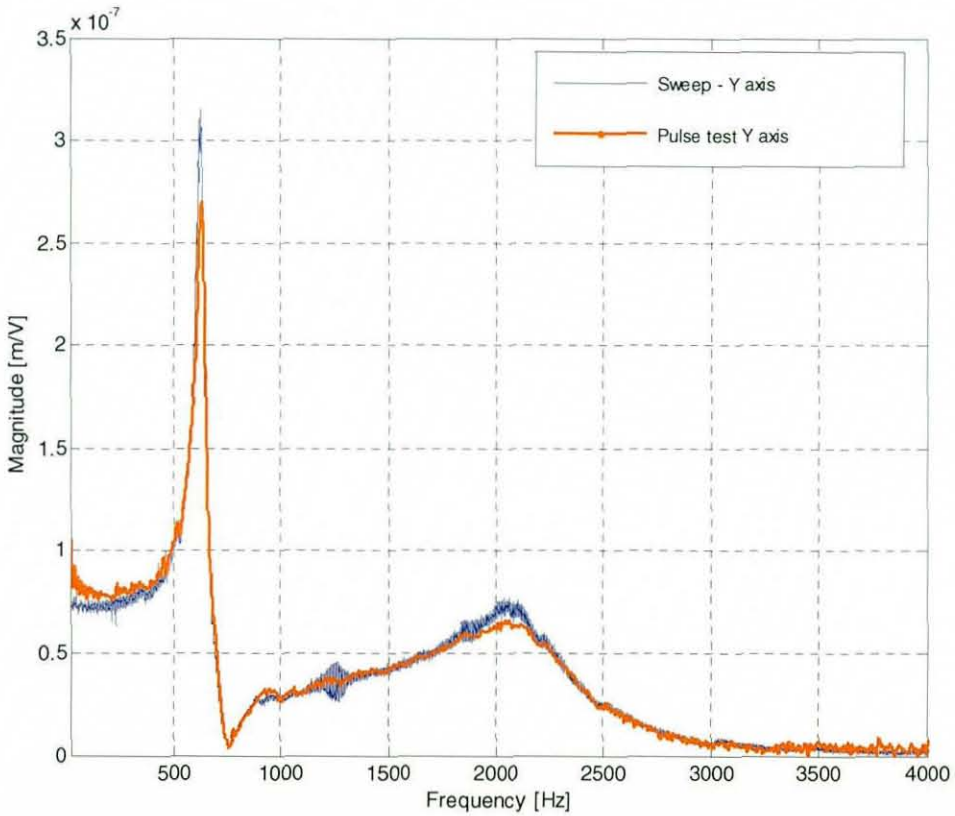

Figure 7.10 Frequency response function of the spindle system obtained through sweep and impulse tests

In order to analyse the behaviour of both FRFs in the higher frequency range (i.e. *f>1000 Hz*), the dynamic behaviour of the driving amplifier is investigated. For the system identification of the driving amplifier an input voltage in the form of an impulse with *2.5 V* of magnitude and *0.3 ms* pulse width is generated within

Matlab/Simulink and sent to the amplifier input. This input signal is amplified by the amplifier and sent to the piezoelectric actuator. The input and output of the amplifier are then measured with a multi-channel oscilloscope (Figure 7.11).

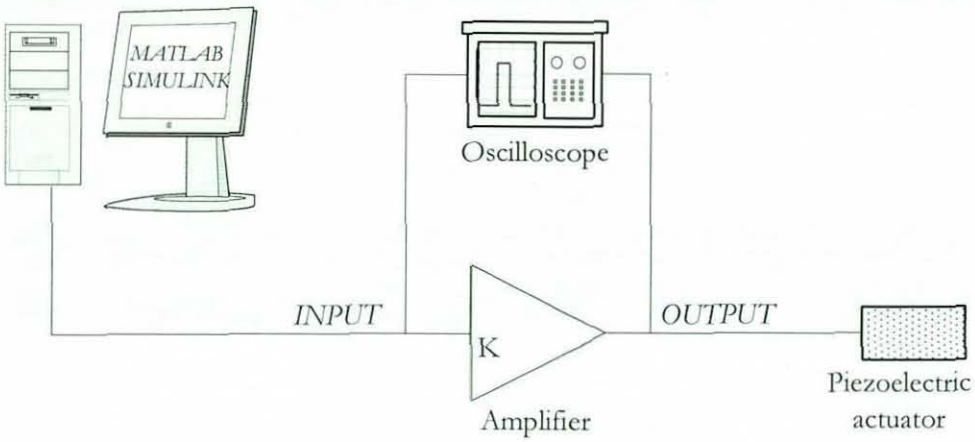

Figure 7.11 Schematic diagram to identify the dynamic characteristics of the amplifier

The input and output characteristics of the driving amplifier are shown in Figure 7.12.

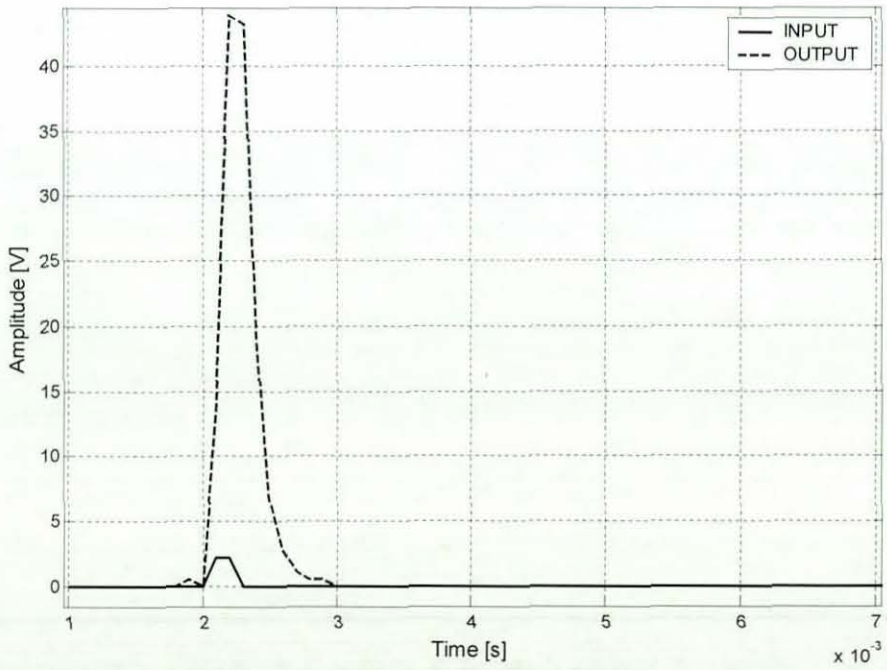

Figure 7.12 Input - output characteristics of the driving amplifier

The FRF of the amplifier shown in Figure 7.13 is identified from input and output characteristics. Figure 7.13 reveals that the bandwidth of the amplifier is at *1424 Hz* at *3 db*. This result leads to the conclusion that the second and third vibration modes of the spindle system stated in Table 7.2 cannot be effectively excited. Therefore, the piezoelectric actuator with the driving amplifier does not necessarily ensure that the dynamic properties of the spindle system at higher frequencies (i.e. *f>1424 Hz*) are captured.

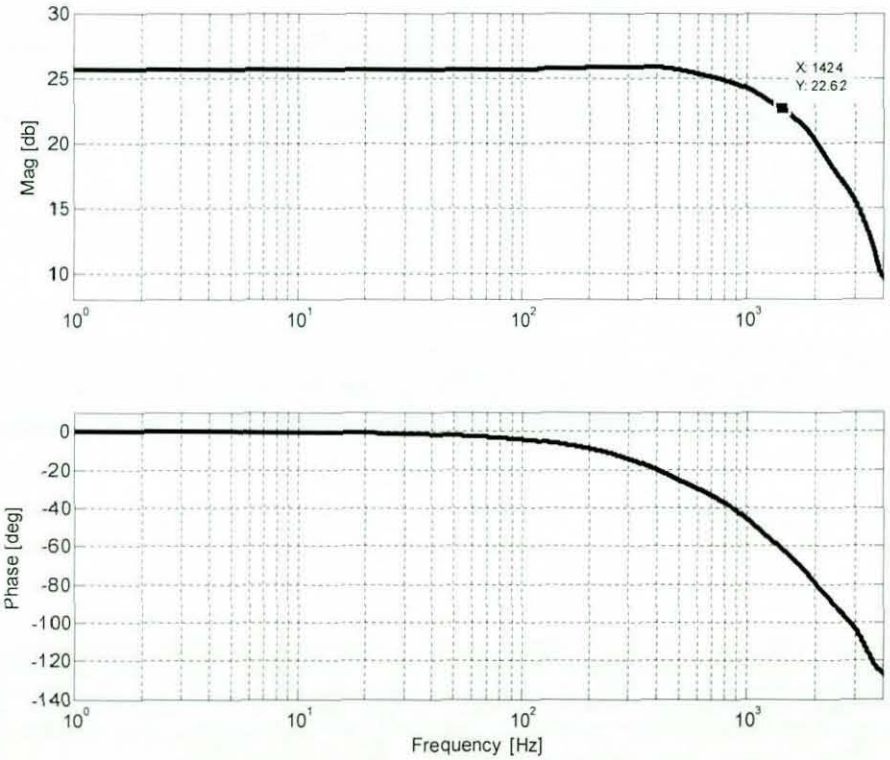

Figure 7.13 FRF of the driving amplifier

Furthermore, the real amplifier gain determined from Figure 7.13 is at *25.62 db* which corresponds to *19.1* amplification factor. This value varies by ca. 4 % from *20*, the gain factor given in the amplifier data sheet. Taking these results into consideration, the numerical model is further adjusted in order to match the dynamic behaviour of the spindle system determined through the experimental work.

Figure 7.14 shows the comparison between the dynamic characteristics of the spindle system identified through the experimental work and the numerical model. The FRF obtained with the swept-frequency signal (indicated in blue colour) and the FRF obtained with the impulse test (indicated in orange colour) are taken as reference and the FRF of the numerical model (indicated in black colour and in solid/dashed lines) is tuned by using the tuning parameters stated in Table 7.3. In addition to these tuning parameters, the driving amplifier gain, as well as its impedance, are also used as "knobs" to achieve an accurate numerical model.

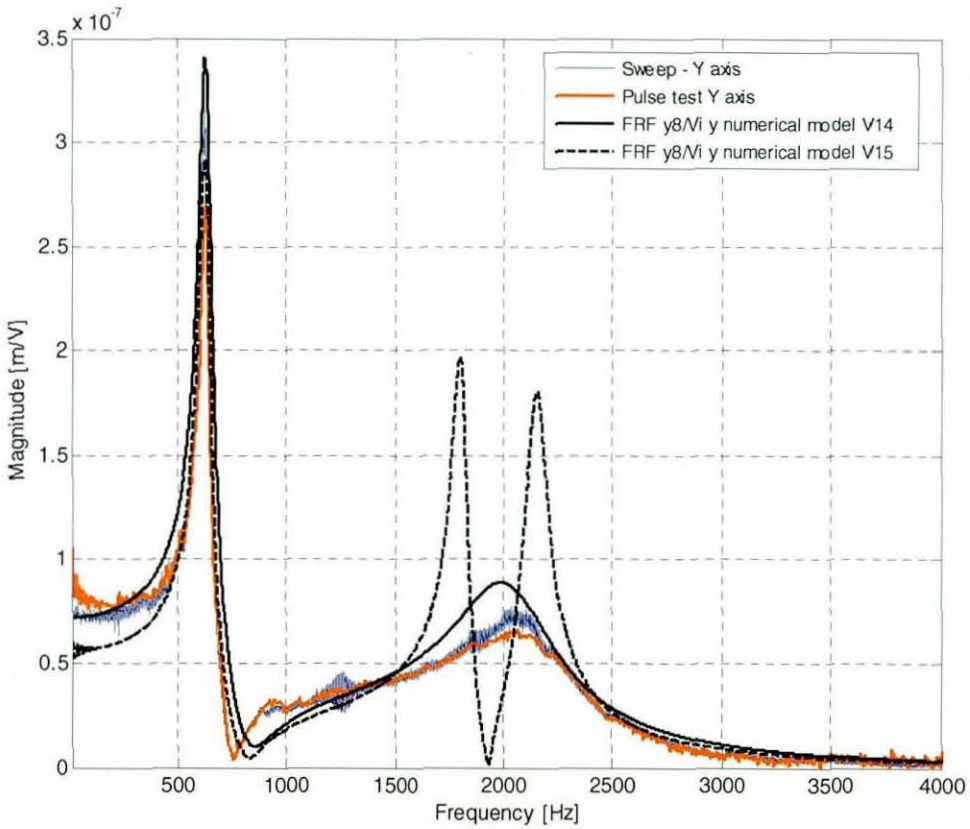

Figure 7.14 Dynamic characteristics of the spindle system in comparison with the numerical model

In a small number of iterations, the numerical model has been tuned so that important dynamic properties of the spindle system are covered.

The frequency response of the actual spindle in the near of the first natural frequency is zoomed from Figure 7.14 and shown in Figure 7.15. The FRF of the numerical model, indicated in solid black colour, is in good agreement with the spindle dynamics in the low frequency range as well as in the higher frequency area. However, it has a higher resonant peak than the actual spindle response. On the other hand the first resonant peak of the numerical model, indicated in dashed black colour, is in good agreement with the first resonant peak of the actual spindle system. Moreover, it shows some discrepancies in the low frequency range. Nevertheless this numerical model (indicated in dashed black line) shown in Figure 7.14 and Figure 7.15 covers the second and the third vibration modes of the spindle system. As aforementioned, the second and the third vibration modes of the actual spindle system could be excited neither with the impact hammer test from section 7.2.1 nor with the swept-frequency and the impulse tests. This does not necessarily mean that the second and the third vibration modes do not exist.

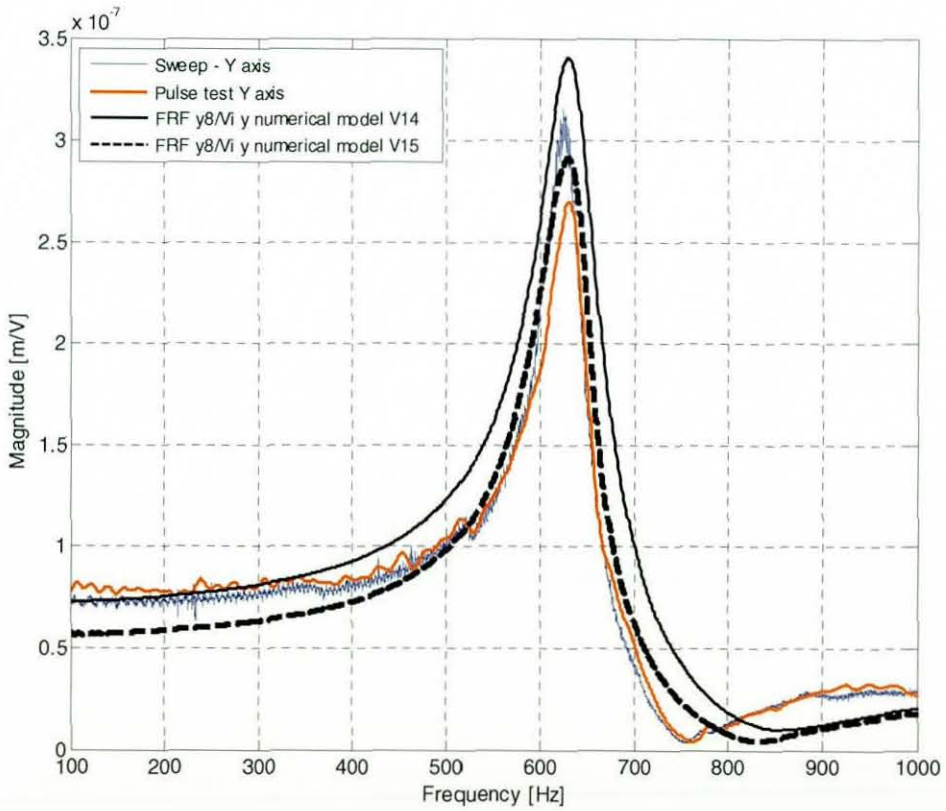

Figure 7.15 Comparison between the numerical model and the actual spindle dynamics

Therefore, the numerical model shown in dashed black with 6 states (3 vibration modes, namely at *626*, *1801* and *2152 Hz*) has been chosen for the proposed modal control approach. This has been achieved by using the Matlab command "balancmr" to reduce the 78 states of the numerical model to 6 states.

7.3 Optimal Control Technique

The motivation behind the optimal control technique used for the spindle system is two-fold. Firstly, a PID controller is not capable of delivering sufficient performance for higher-order systems (Astrom and Hagglund, 1995). Therefore, this conventional controller type is not suitable for implementation on the test rig, which has 6 states with three vibration modes. Secondly, for the PID controller, the performance of the control action cannot be controlled dynamically. This is a further drawback of the PID controller as there is a limited power supply with a certain bandwidth available for the actuator operation. Moreover, the modal control approach, especially the optimal control technique, has been mainly implemented for metalworking machinery as described in chapter 2. Apart from one application with woodworking machinery, namely, for the active vibration suppression of a circular saw by Wang and Sun (2001), there are no optimal-control-based applications reported for woodworking machinery. Therefore, the implementation of the optimal control method on the small scale planer is unique; hence this is the world's first actively controlled planer.

The design of the optimal control consists of an estimator and the state feedback gain. LQR/LQG (Linear Quadratic Regulator/Linear Quadratic Gaussian) is an optimal control technique used in modern control applications. The difference between LQR and LQG is that the latter includes the stochastic noise, the so-called Gaussian white noise, in the formulation of the optimal control method (Maybeck 1979, Bryson 2002). The optimal control approach requires two design steps. Firstly, the optimal control formulation is required to obtain the optimal state feedback gain

and secondly, an estimator is needed to predict the states of the system. Both these design steps are described in the subsequent sections.

7.3.1 Optimal Control Formulation

The closed loop controller overview without the estimator is shown in Figure 7.16

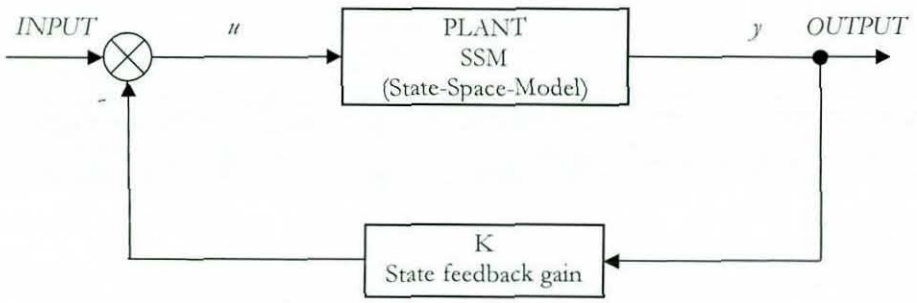

Figure 7.16 Controller overview

The dynamic characteristics of the plant (i.e. spindle system) are represented in the state space form as follows

$$\begin{aligned} \dot{x} &= A \cdot x + B \cdot u + H \cdot w_1 \\ y &= C \cdot x + w_2 \end{aligned} \tag{7.1}$$

where x: state vector $[x_1, x_2 \ldots x_n]$

u: control input vector $[u_1, u_2 \ldots u_r]$

y: output vector $[y_1, y_2 \ldots y_n]$

w_1: stochastic noise related to the states

w_2: stochastic noise related to the sensor measurement

A: system matrix

B: input gain matrix

C: measurement matrix

H: stochastic noise matrix

Given the system (plant) described in the state space form by equation (7.1), the optimal control formulation is defined as finding the control input u in equation (7.2) which minimizes the performance index given by equation (7.3).

$$u = K \cdot x \tag{7.2}$$

$$J = \frac{1}{2} \cdot \int_0^{\infty} \left(x^T \cdot Q \cdot x + u^T \cdot R \cdot u \right) dt \tag{7.3}$$

Where x^T: transposed state matrix

u^T: transposed input matrix

Q: weighting matrix related to the system response

R: weighting matrix related to the control effort

The performance index represented by equation (7.3) describes the integral performance measures which minimize the performance index J (also called the cost function). In other words, the performance index describes the trade off between the system response and the control effort (Dorf and Bishop 2005). The state feedback gain matrix K can then be formulated as follows

$$\begin{aligned} u = K \cdot x &= -R^{-1} \cdot B^T \cdot P \cdot x \\ K &= -R^{-1} \cdot B^T \cdot P \end{aligned} \tag{7.4}$$

Where matrix P is the solution of the Ricatti equation and obtained as follows

$$0 = A^T \cdot P + P \cdot A + Q - P \cdot B \cdot R^{-1} \cdot B^T \cdot P \tag{7.5}$$

An extensive numerical derivation of the equations (7.3), (7.4) and (7.5) is reported by Bay (1999). The equations are solved using Matlab.

The control input variables are determined by assuming that all the state variables are available, which is not the case in reality, therefore the feedback loop of the controller from Figure 7.16 has been supplemented by adding an estimator (i.e. a Kalman filter) to predict the state variables. This will ensure that all the state variables are available for the controller input matrix definition.

7.3.2 Estimator Design – Kalman Filter

Sensors usually do not provide perfect and complete data about a system. The measurement of the system variables is often corrupted to some extent by noise, biases and device inaccuracies. However, for the optimal control method all the states of the system have to be available (Bay 1999). In order to obtain all the states of a system, a state estimator is needed (also called an observer). A Kalman filter is an estimator used to predict the states of a linear dynamic system. It is generally defined as an optimal recursive (e.g. does not require all previous data to be kept in storage for estimation) data processing algorithm. An estimator that considers all the uncertainties to make the optimal estimation of the state is the Kalman filter. Even if the sensors were "perfect" (e.g. without noise and any distortion) the state variables could not be measured directly, because the sensors only provide the system output or input in the form of, for example, deflection or voltage respectively. From these measures, the state variables need to be derived accordingly. Therefore, for the modal control approach an estimator is necessary (Simoes et al. 2007).

One characteristic of the Kalman filter is that it incorporates all the information that can be provided to it. It processes all available measurements, regardless of their precision, to estimate the current value of the variables of interest. "All available measurements" can be understood as plant dynamics (e.g. a state space model of the plant), sensor properties (e.g. noise behaviour of the measurement device), system noise and the initial conditions of the variables of interest. The terminology "optimal" depends upon the criteria chosen to evaluate the performance. The

optimality of the Kalman filter is described in detail in various references (Maybeck 1979, Bay 1999, Grewal and Andrews 2001, Bryson 2002). Since the introduction of the Kalman filter in the 1960s, it has been used in many fields. It was also used by NASA for the Apollo project, the first manned moon mission, in 1969 (Grewal and Andrews 2001). Nowadays, the application of a Kalman filter encompasses many fields, such as GPS-assisted navigation systems (Geng and Wang 2008, Bian 2006), sensor calibration (Kramer et al. 2007), radar tracking (Kosuge et al. 1997), manufacturing efficiency improvement (Albrecht et al. 2005) and for active vibration control purposes (Simoes et al. 2007, Dohner et al. 2004, Wang et al. 2001) just to name a few application domains. As aforementioned, the motivation behind the estimator is the need for an estimated state that can be fed back to the input. According to the separation principle, the estimator and the controller can be designed separately and then combined together to control the plant (Bay 1999, Dorf and Bishop 2005). Due to the separation principle the control input u can be re-defined using the estimated state $\hat{x}$ instead of the state x as follows

$$u = K \cdot \hat{x} \tag{7.6}$$

The controller overview with the Kalman filter is shown in Figure 7.17.

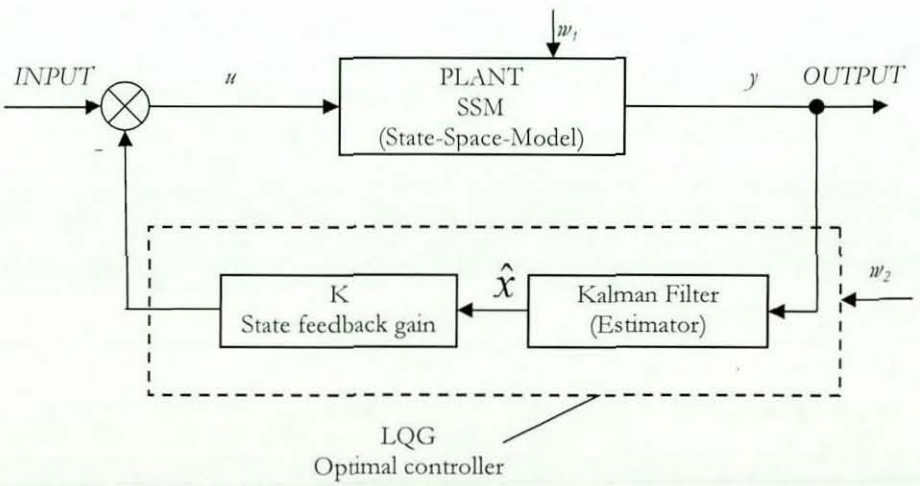

Figure 7.17 LQG controller

The goal of the Kalman filter is to provide an estimate $\hat{x}$ so that $\hat{x} \rightarrow x$ for $t \rightarrow \infty$. The state variables can be estimated using equation (7.7).

$$\begin{aligned} \dot{\hat{x}} &= A \cdot \hat{x} + B \cdot u + L_k\left(y - \hat{y}\right) \\ \hat{y} &= C \cdot \hat{x} + w_2 \\ \dot{\hat{x}} &= \left(A - L_k \cdot C\right) \cdot \hat{x} + L_k \cdot C.x + L_k \cdot w_2 + B \cdot u \end{aligned} \tag{7.7}$$

Where $\hat{y}$ is the estimate of y and L_k is the optimal Kalman gain matrix. The Kalman filter gain matrix is identified by minimizing the state estimation error covariance matrix $P_e = E[e\ e^T]$ where the error e is defined as $e = \hat{x} - x$. Based on the assumption that system and measurement noise are uncorrelated, zero-mean, white noise signals (i.e. Gaussian white noise) with covariance matrices $Q_e = E[w_1\ w_1^T] > 0$, $Re = E[w_2\ w_2^T] \geq 0$ and $E[w_1\ w_2] = 0$, the minimum state estimation error covariance matrix P_e can be evaluated by solving the Ricatti equation as follows

$$\dot{P}_e = A \cdot P_e + P_e \cdot A^T + H \cdot Q_e \cdot H^T - P_e \cdot C^T \cdot R_e^{-1} \cdot C \cdot P_e = 0 \tag{7.8}$$

The stochastic noise matrix H is generally determined by assuming that the state variables are effected by the system noise w_1, hence it is defined as $H = [0\ 1]^T$ (Albrecht et al. 2005).

The solution of equation (7.8) yields the optimal Kalman filter gain matrix as

$$L_k = P_e \cdot C^T \cdot R_e^{-1} \tag{7.9}$$

where, R_e is the measurement noise covariance matrix. It is determined by taking the RMS value of the displacement sensor (i.e. eddy current probes) readings when the

machine (i.e. small scale planer) is stationary. The system covariance matrix Q_e is then tuned to achieve a sufficient estimation of the system response. In other words, different values of R_e and Q_e result in a different Kalman filter gain L_k. The balance between Q_e and R_e can be interpreted as follows

- If R_e is very small in comparison to Q_e, the measurement noise w_2 is necessarily small, so the Kalman filter interprets a large deviation of $\hat{y}$ from y as an indication that $\hat{x}$ is a "bad" measurement and wants to correct it fast. Because the measurement noise has been set to a very small value, the Kalman filter "understands" that there is almost no measurement noise so, if there is a deviation, it reacts very fast to correct it. In practice, this leads to large values for the Kalman filter gain L_k, with the consequence of a fast response which can even make the system unstable.

- If R_e is very large when compared to Q_e, the measurement noise w_2 is very large, so the Kalman filter does not give too much "attention" to the measurements, hence the Kalman filter's response is much more conservative in case of a deviation. This in practice leads to low L_k values with the consequence of a slow response to correct the deviation. Therefore, the balance between the weighting parameters R_e and Q_e is usually determined by trial and error procedure (Bay 1999, Dorf and Bishop 2005).

The schematic overview of the overall controller is shown in Figure 7.18.

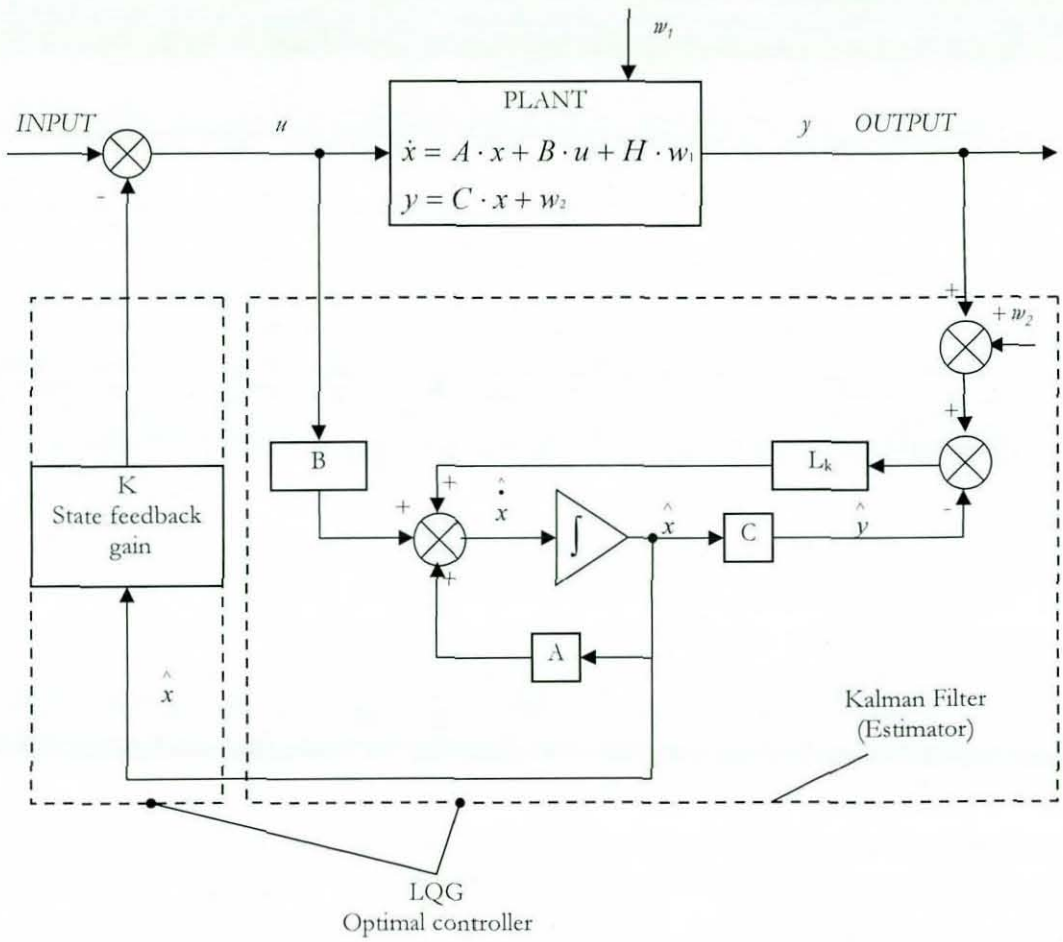

Figure 7.18 Schematic overview of the optimal control method

The state space matrix formulation of the control system is determined as follows

- State space form matrix

$$A = \begin{bmatrix} A_{11} & A_{12} & \cdots & A_{16} \\ A_{21} & \ddots & & \\ \vdots & & & \\ A_{61} & \cdots & & A_{66} \end{bmatrix}; \quad B = \begin{bmatrix} B_{11} \\ \vdots \\ B_{61} \end{bmatrix}; \quad C = \begin{bmatrix} C_{11} \\ \vdots \\ C_{61} \end{bmatrix}^T$$

- The optimal control weighting parameters' matrices

$$R = [R_{11}]; \quad Q = [Q_{11}]$$

- Kalman filter weighting parameters' matrices

$$R_e = [R_{e11}]; \; Q_e = \begin{bmatrix} Q_{e11} & Q_{e12} \\ Q_{e21} & Q_{e22} \end{bmatrix}$$

The numerical calculations are carried out within the software program Matlab.

7.4 **Controller Tuning**

The controller tuning parameters are on the one hand the weighting measures Q and R defining the optimal controller gain K and, on the other hand, the weighting measures Q_e and R_e for defining the Kalman filter gain L_k. Firstly, the Kalman filter weighting parameters are adjusted for the open loop operation, where the output response of the spindle system is matched to the output of the estimated response through the Kalman filter. A step input with *50 V* is sent to the spindle model and the output of the spindle model, termed as "y_{OL}" (spindle deflection in y-axis in open loop operation), is measured and compared to the estimated output y_{e_OL} (estimated spindle deflection in y-axis in open loop operation). The Matlab/Simulink model for adjusting the Kalman filter weighting parameters is shown in Figure 7.19, where the spindle system model (spindle + actuators) is now termed as the "plant".

Although the measurement covariance matrix R_e was determined from the RMS value of the measurement noise as an initial starting value, it is basically a balance between Q_e and R_e and usually determined by a trial and error procedure.

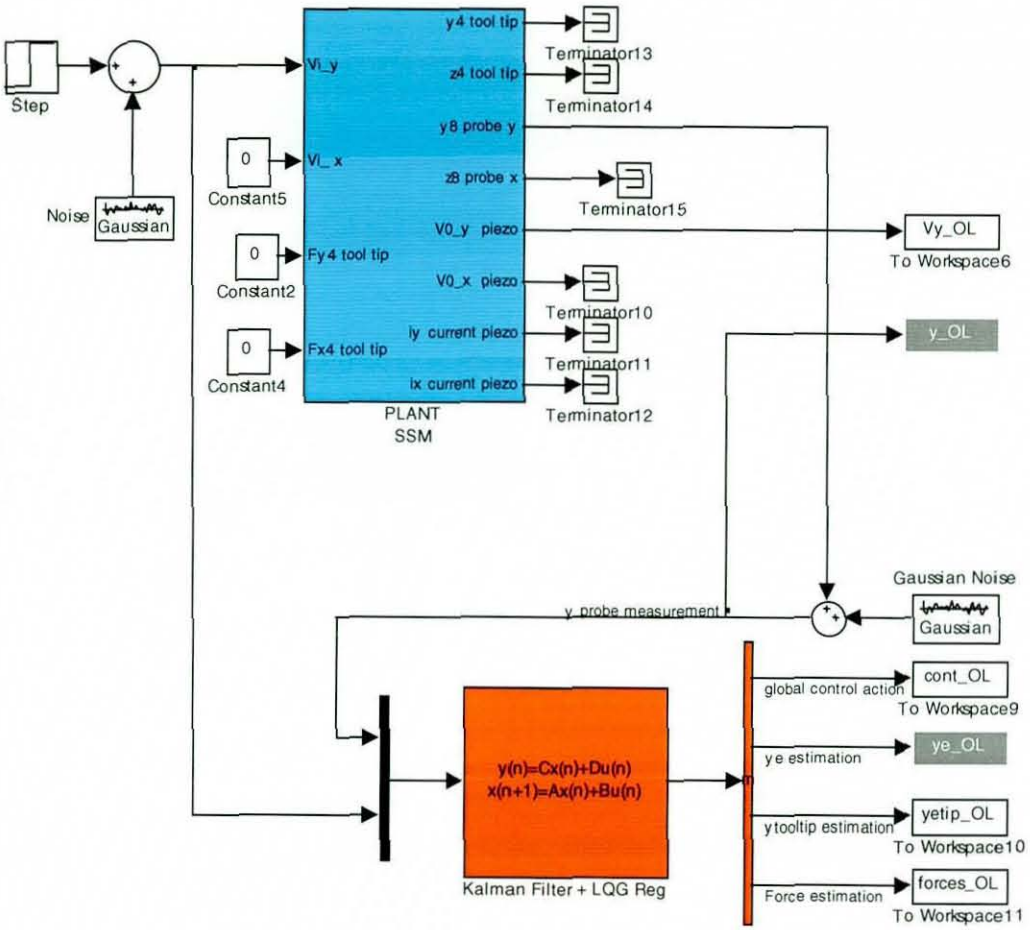

Figure 7.19 Matlab/Simulink model to adjust the Kalman filter

Figure 7.20 shows the comparison between the spindle deflection y and the estimation y_e to a step input. For tuning the Kalman filter weighting parameters, firstly, the parameter R_e is set to a constant value and the measurement noise matrix Q_e is varied. Secondly, the output estimation y_e can also be tuned so that it is close to the spindle deflection y, by setting Q_e to a constant value and varying R_e. The outcome of this procedure is also shown in Figure 7.21. The step function is also useful for tuning the estimated spindle response so that it matches the static response of the spindle system (i.e. after the dynamic part of the response has settled down) as shown in Figure 7.21.

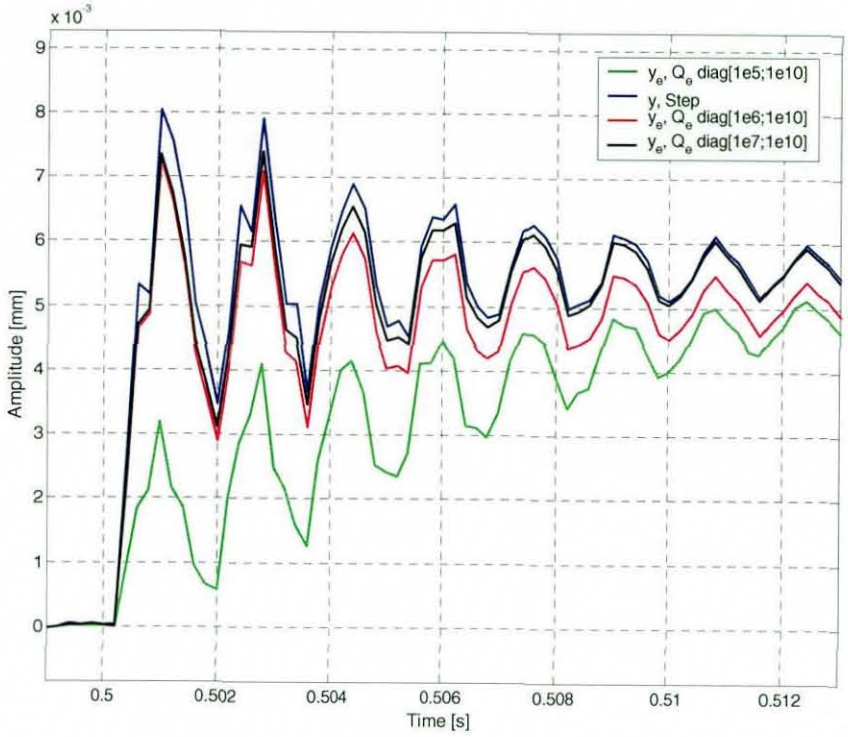

Figure 7.20 Kalman filter weighting parameters tuning; R_e=0.001 and Q_e varied

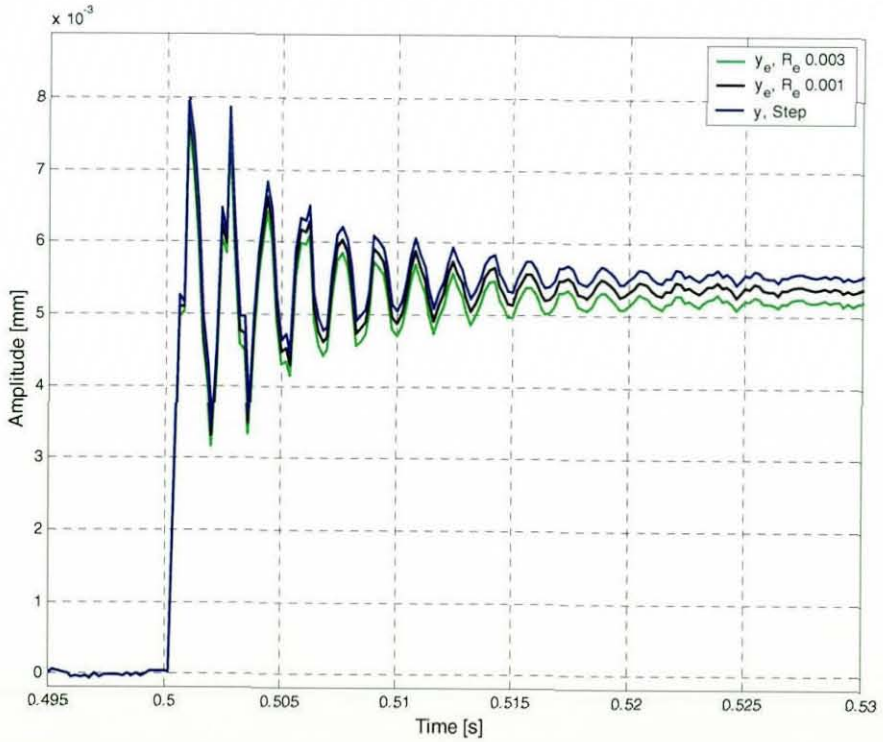

Figure 7.21 Kalman filter weighting parameters tuning; Q_e=diag[1e6;1e10] and R_e varied

Furthermore, the plant model is excited with an impulse function (with pulse magnitude of *20 V* and pulse width of *0.3 ms*). The estimated spindle deflection ye_{OL} through the Kalman filter and the plant response y_{OL} with the corresponding open loop control action are shown in Figure 7.22. From Figure 7.22 it can be observed that there are some discrepancies between the estimated response (indicated in dashed green colour) and the plant response (indicated in magenta colour).

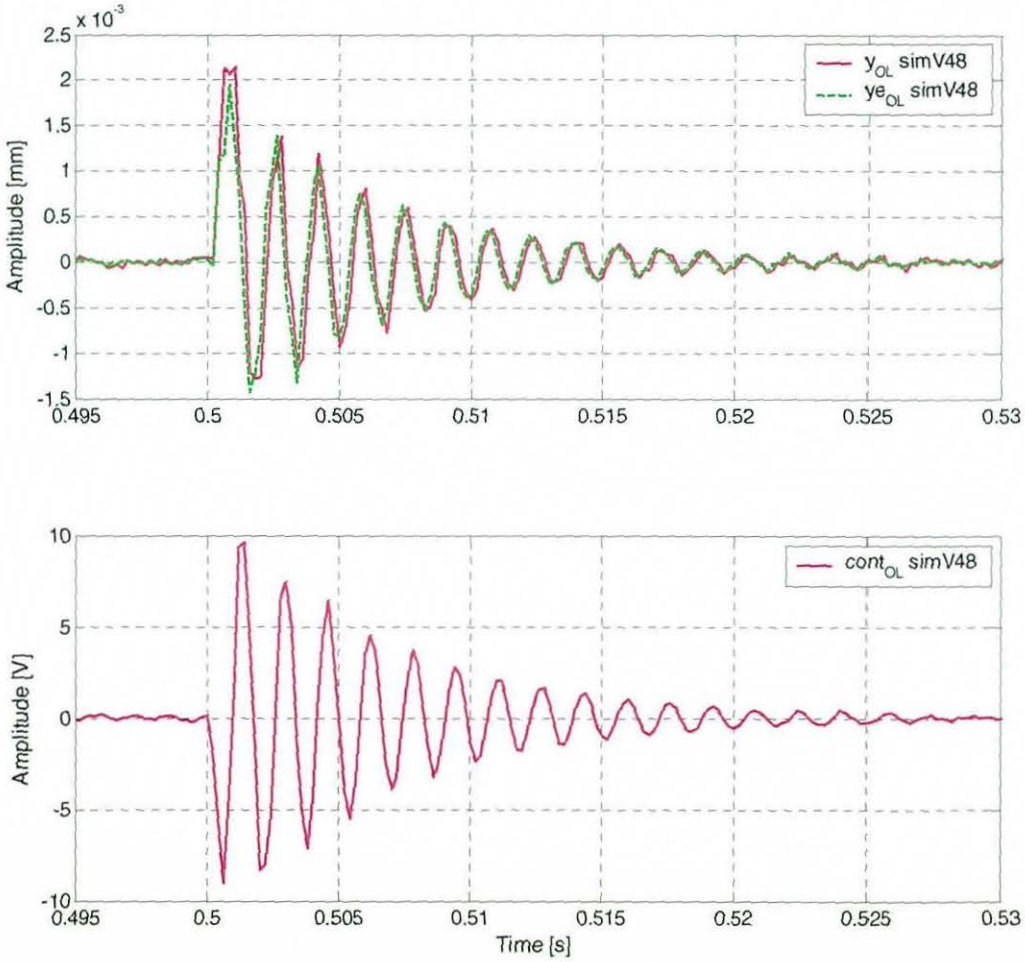

Figure 7.22 Comparison between the estimated response and the plant response with the corresponding open loop control action

The estimated response can be further tuned to achieve a behaviour very close to the plant response by adjusting the Kalman filter weighting parameters Q_e and R_e as shown in Figure 7.23 (model V48 parameters are Q_e=*diag[10;1e9]* and R_e=*0.1;* R=*0.0001* and Q=*1400;*)

This is achieved by setting one of the parameters to a constant value while increasing the other one (i.e. R_e varied, Q_e constant). This means that the estimation is very accurate and very fast (model V47 parameters are $Q_e=diag[10;1e9]$ and $R_e=0.001$; $R=0.0001$ and $Q=1400$). In fact, the Kalman filter becomes so accurate that it can even estimate the noise, as can be seen in Figure 7.23.

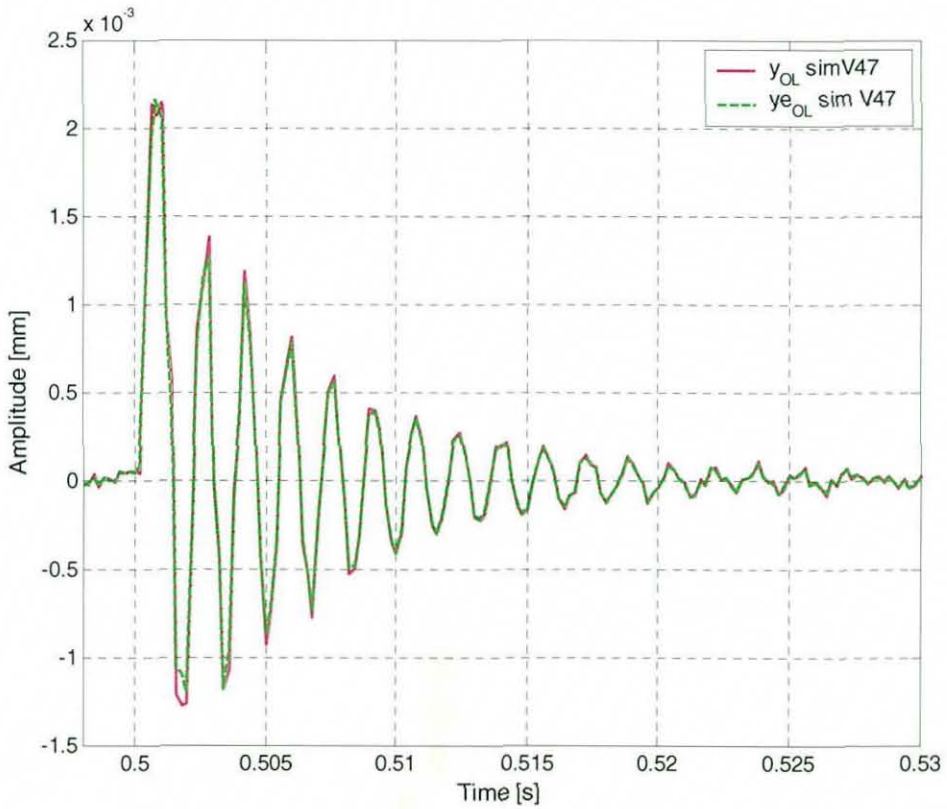

Figure 7.23 Comparison between estimated response and plant response

However, a very fast Kalman filter requires a very fast response from the driving amplifier whose bandwidth is limited. Therefore, high Kalman filter gain introduces more vibrations due to the very rapid control effort required. Figure 7.24 shows the effect of the fast Kalman filter on the closed loop operation. The upper graph in Figure 7.24 compares the open loop spindle response with the closed operation. It can be observed that in the closed loop operation, the spindle response contains more vibrations than the response in the open loop operation. The bottom graph in Figure 7.24 shows the noisy and high frequency control signal sent to the amplifier.

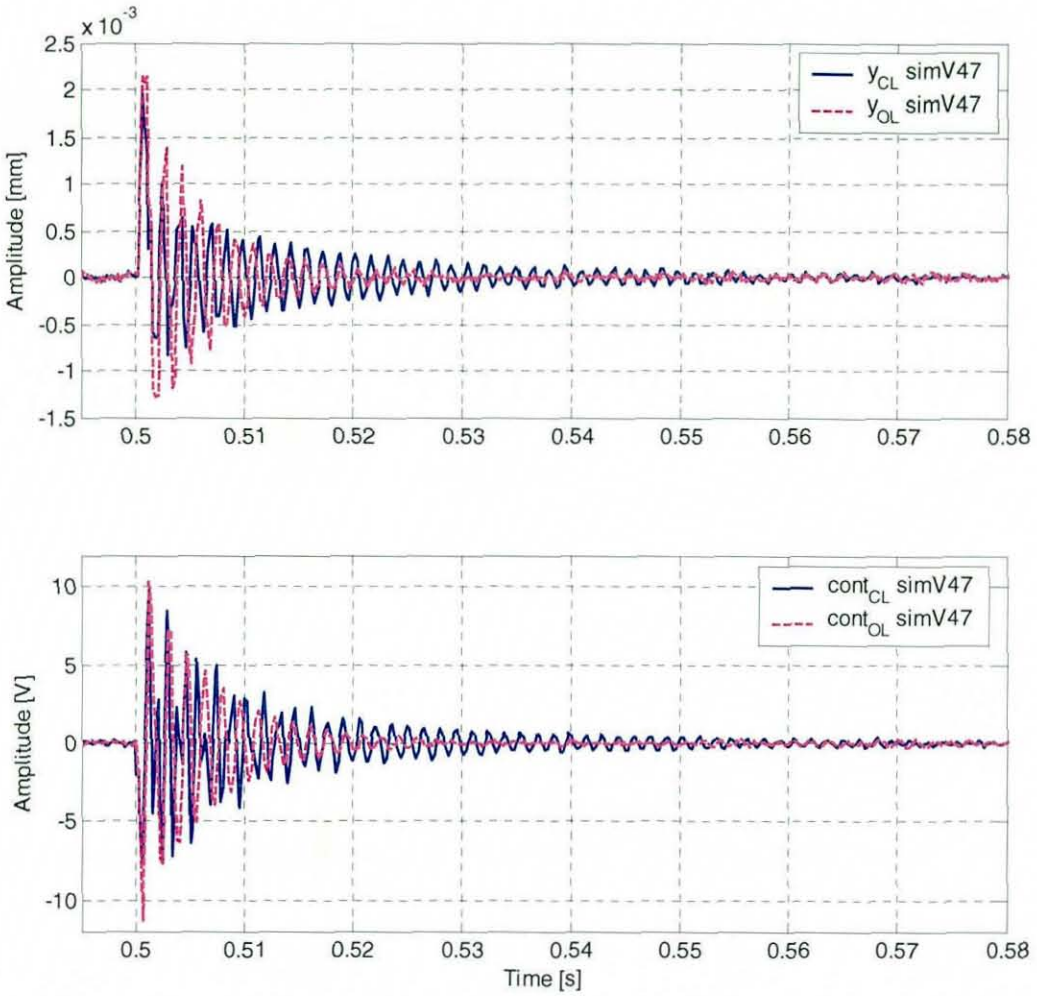

Figure 7.24 Effects of a fast Kalman filter on the spindle response with the corresponding control effort

Therefore, a trade off has to be made between the control effort and the spindle response. The Kalman filter weighting parameters (R_e and Q_e) and the state feedback weighting parameters (R and Q) have to be set with the focus on obtaining a close estimation on the one hand and an appropriate control effort on the other. The tuning parameters Q and R can be adjusted according to the Bryson rule, however, it often provides just the starting point for a trial and error procedure (Bryson 2002). After a number of iterations, an appropriate balance between the control effort and the system response can be achieved. The simulation and experimental results are both presented in the subsequent section.

7.5 Simulation and Experiment Results

This section presents the results obtained through the simulation model as well as the results obtained through experiments performed on the test rig. The spindle response for open and closed loop operations are compared and analysed.

7.5.1 Simulation Results

The plant model is excited with an impulse of *20 V* in magnitude with *0.3 ms* of pulse width. The resultant spindle responses of the closed and open loop operations are compared in Figure 7.25. The simulation results show that the controller in the closed loop operation can significantly reduce spindle vibrations.

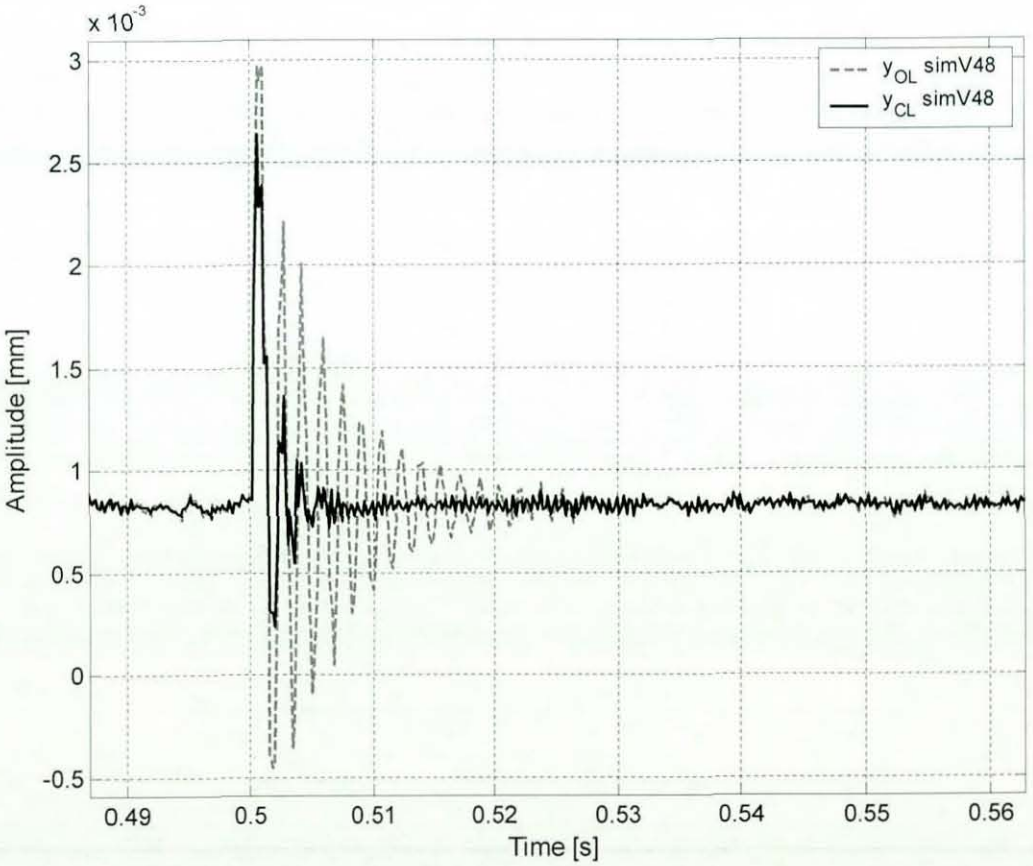

Figure 7.25 Simulation of closed loop vs. open loop

Furthermore, the control signal of both closed and open loop operations are compared in Figure 7.26 (the legend "$cont_{CL}$ simV48" means; simulation of control action in closed loop operation whereas "$cont_{OL}$" indicates the open loop operation). The simulation results show that in the closed loop operation, the decay of the control signal is higher than the control signal decay of the open loop operation. This comparison suggests that the control is stable in the closed loop operation (the control action is further analysed in the next subsection).

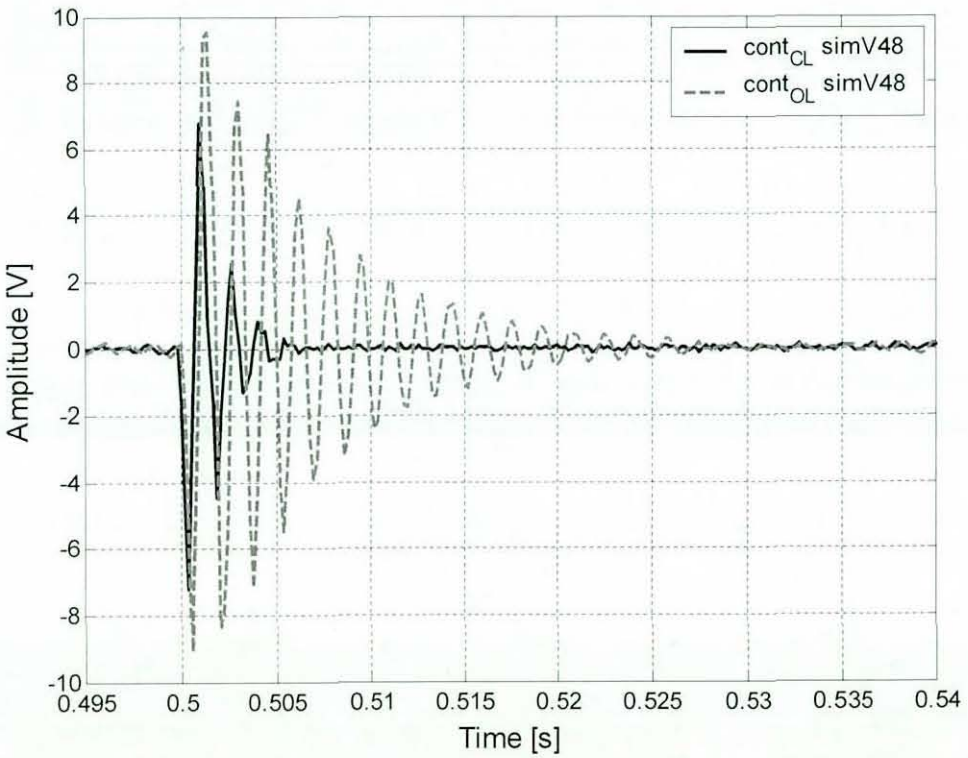

Figure 7.26 Control signal of closed and open loop operations in comparison

7.5.2 Experiment Results

The controller is converted into a digital form with a *5 kHz* sampling frequency using Matlab. For the implementation of the controller on the test rig, the Matlab xPC- Target prototyping environment is used to carry out the real-time control application. The Matlab xPC-Target prototyping environment consists of a host computer and a target computer. The controller is first designed within the Matlab/Simulink environment on the host PC and, after compiling, the executable code is uploaded via an Ethernet link to the target PC which runs the executable in real-time. The controller is further tuned on the test rig. Figure 7.27 shows the effect of a fast Kalman filter on the actual plant response (the legend "y_{CL} expV32" means; spindle deflection is measured experimentally in the closed loop operation with controller version 32). In the closed loop operation, the system response contains more vibrations than in the open loop operation.

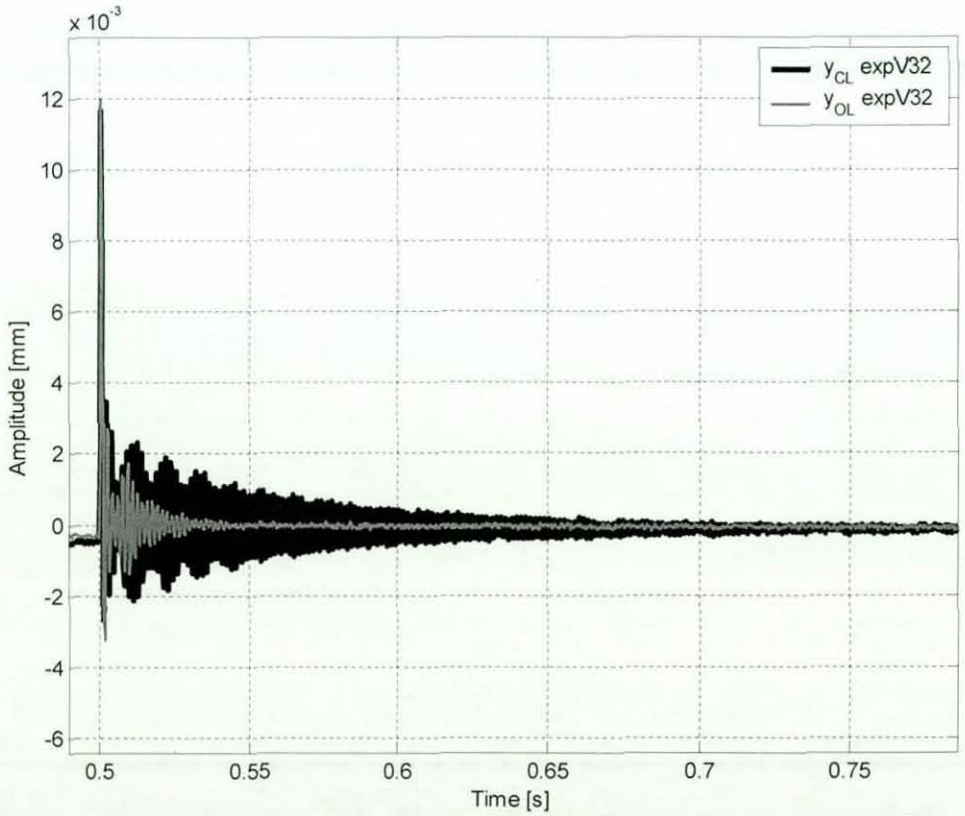

Figure 7.27 Effect of fast Kalman filter on the system response - open loop vs. closed loop

In some cases where the balance between the system response and the control effort is not appropriately set (i.e. Kalman filter gain values very high), the control action can become unstable, thus the controller causes excessive vibrations. Figure 7.28 shows the unstable control action for the closed loop operation. This behaviour of the control action can cause excessive spindle vibrations which can lead to tool and actuator damage.

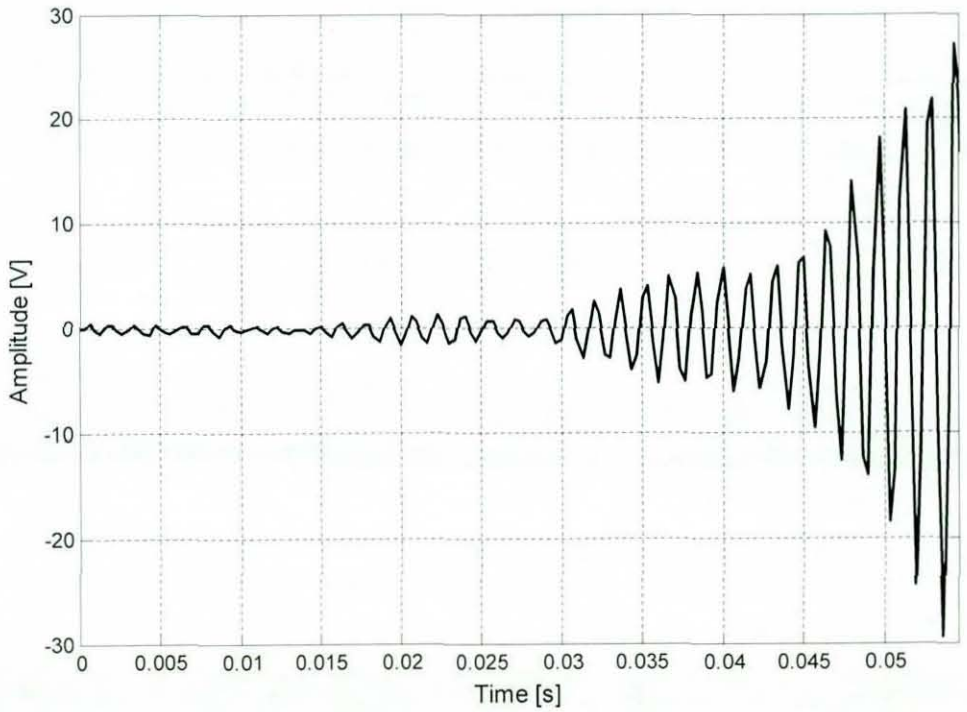

Figure 7.28 Unstable control action in the closed loop operation

Therefore, the Kalman filter is tuned so that it shows behaviour close to the actual plant response without causing instabilities. This again is achieved by trial and error procedure (Figure 7.29).

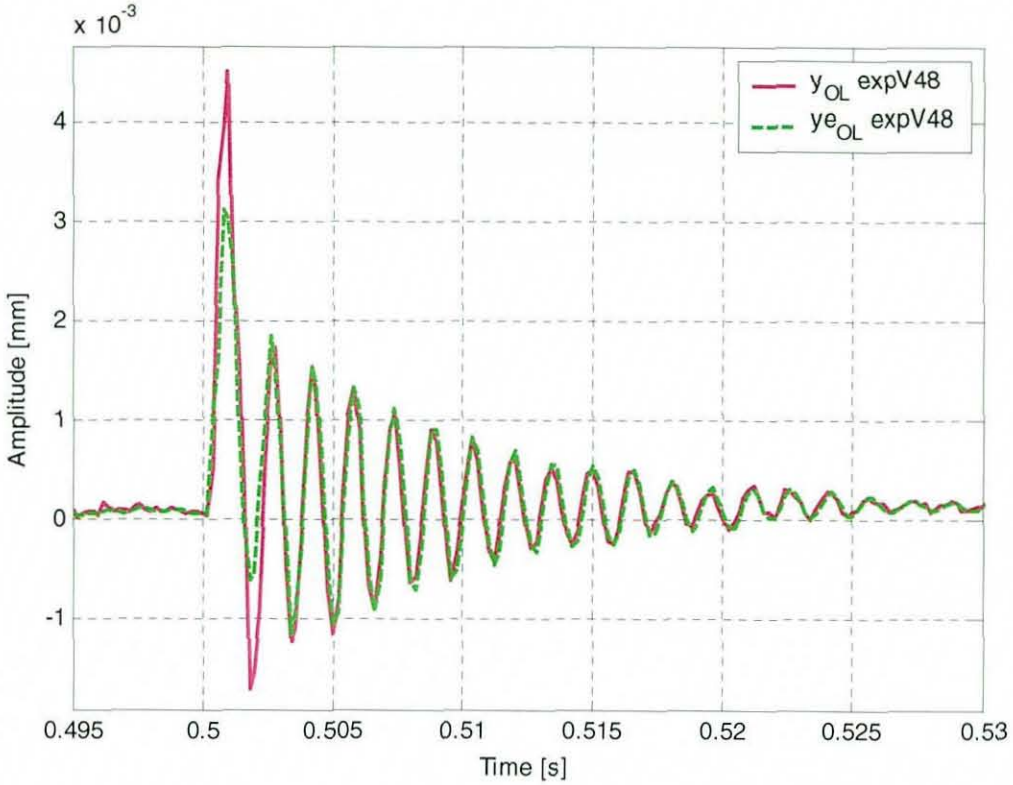

Figure 7.29 Actual plant response vs. estimation through Kalman filter - open loop

After the Kalman filter was tuned in the open loop operation, the controller was performed in the closed loop operation. Figure 7.30 compares the open and the closed loop responses of the actual plant to the same impulse input. From Figure 7.30, it can be observed that in the closed loop operation, vibrations are suppressed significantly. The corresponding control actions for the open and closed loop operations exhibit stable behaviour (Figure 7.31).

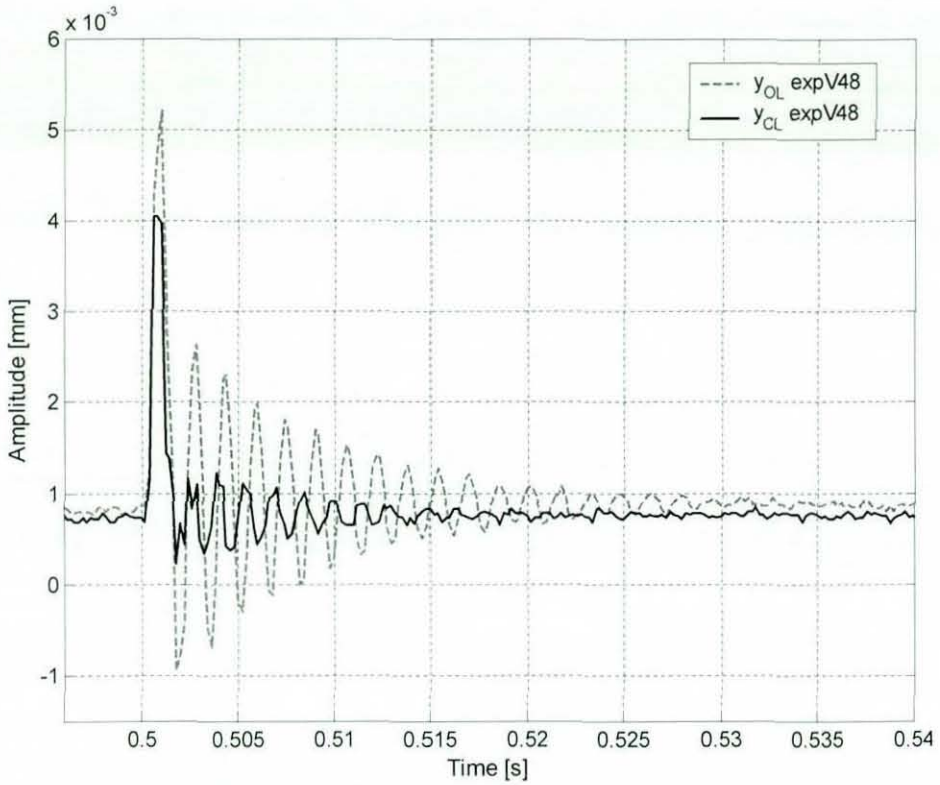

Figure 7.30 Actual plant response - open loop vs. closed loop

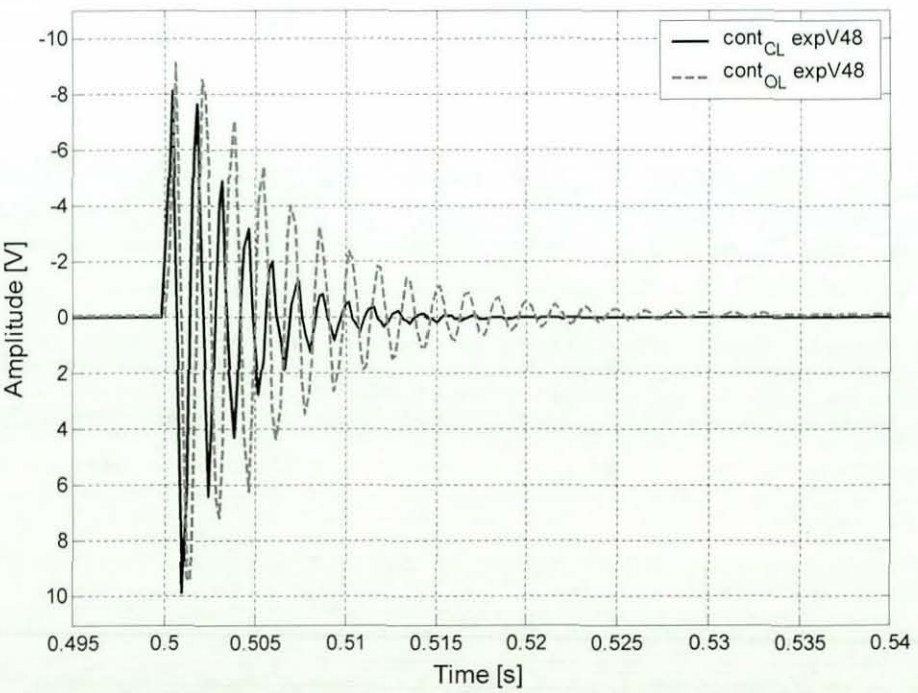

Figure 7.31 Control action - open loop vs. closed loop

Figure 7.30 shows that in the closed loop operation the controller is capable of reducing vibrations significantly in the time domain. In order to analyse the dynamic characteristics of the actual plant, the FRF of the open loop and the closed loop responses are investigated. The FRFs of the open and closed loop operations are shown in Figure 7.32.

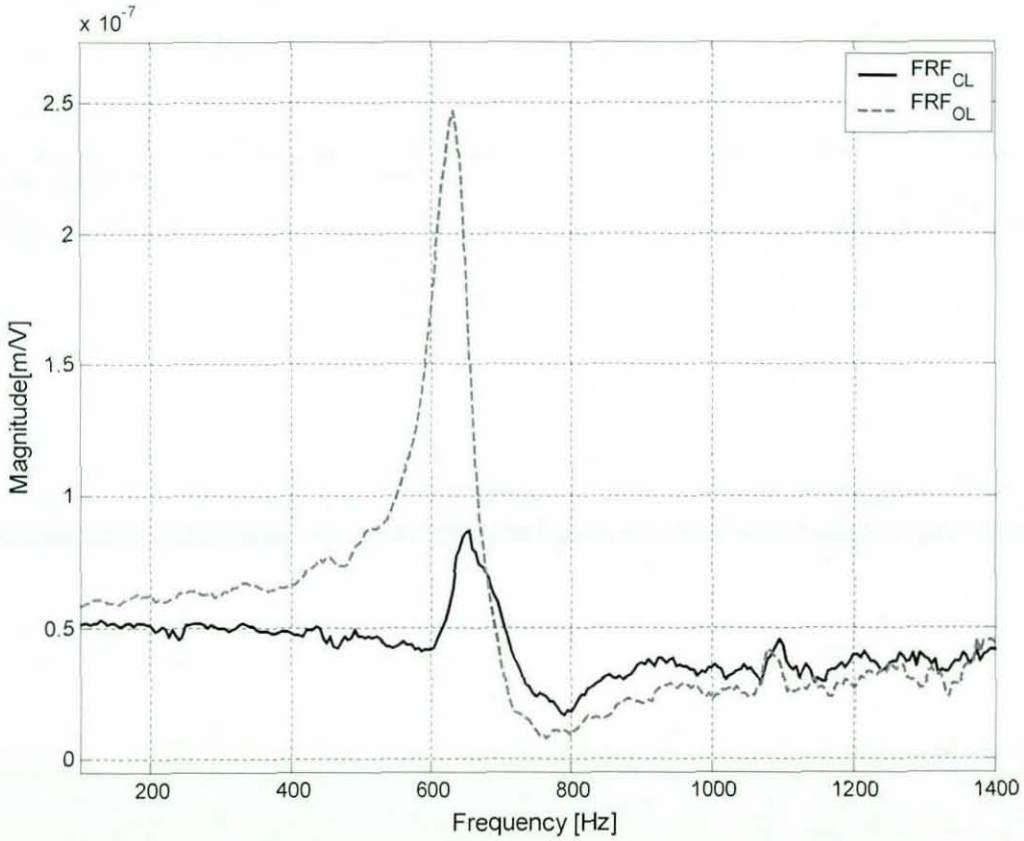

Figure 7.32 Frequency response functions - open loop vs. closed loop

From Figure 7.32 it can be observed that in the closed loop operation, the vibration peak of the natural frequency of the spindle system is reduced by ca. 68%. This indicates a significant improvement of the plant dynamics when compared to the dynamic characteristics of the plant in the open loop operation. From the machining point of view, this means that the operation bandwidth is no longer limited to the natural frequency of the plant.

For example, considering a planer with a cutterhead comprising of *20* cutting knives and the natural frequency at *625 Hz*, the maximum safe operation bandwidth would be around *500 Hz*. This value sets the maximum knife passing frequency of the planer, thus the maximum operation speed (i.e. knife passing frequency = *500 Hz*). The planer with this configuration can run at a maximum speed of *1500 rpm* (i.e. *500 Hz / 20 = 25 Hz =1500 rpm*). Assuming that the driving motor of the planer can run up to *5000 rpm*, the planer would not be operated at its maximum speed, hence the performance of the planer would be reduced by 70%. Generally, in the woodworking domain, high speed machining is a desirable operation. As has been discussed in chapter 4 and described by equation (4.1), the higher the machining speed the better the pitch. Therefore a planer with implemented optimal control is capable of higher operation ranges, even beyond its natural frequency, hence the desired surface quality can be machined independent of the operation bandwidth. As aforementioned, vibrations in the range of the natural frequency are significantly reduced, which enables the knife passing frequency to pass beyond the natural frequency and reach higher operation ranges. This substantial improvement of the dynamic characteristics of the spindle system enables high performance machining; hence it is termed as an "Advanced Machining Process" (AMP). The benefits of the AMP for the woodworking industry can be summarized as follows

- Higher degree of freedom in terms of machining operation (machining speed can be set independent of operation bandwidth, hence higher throughput rates can be achieved)
- Desired product quality can be achieved with one machining operation, this again reduces production costs and manufacturing space
- Complex and costly design improvement methods for high performance machining operation can, to a certain extent, be limited
- Additional machining operations, such as sanding, can become obsolete; hence enabling an efficient and healthy machining environment (no dust from the sanding operation, cost-effective production)

Chapter 8 DISCUSSION

Figure 8.1 is similar to Figure 1.5 and gives an overview of the research work with the corresponding chapters which are the subject of discussion.

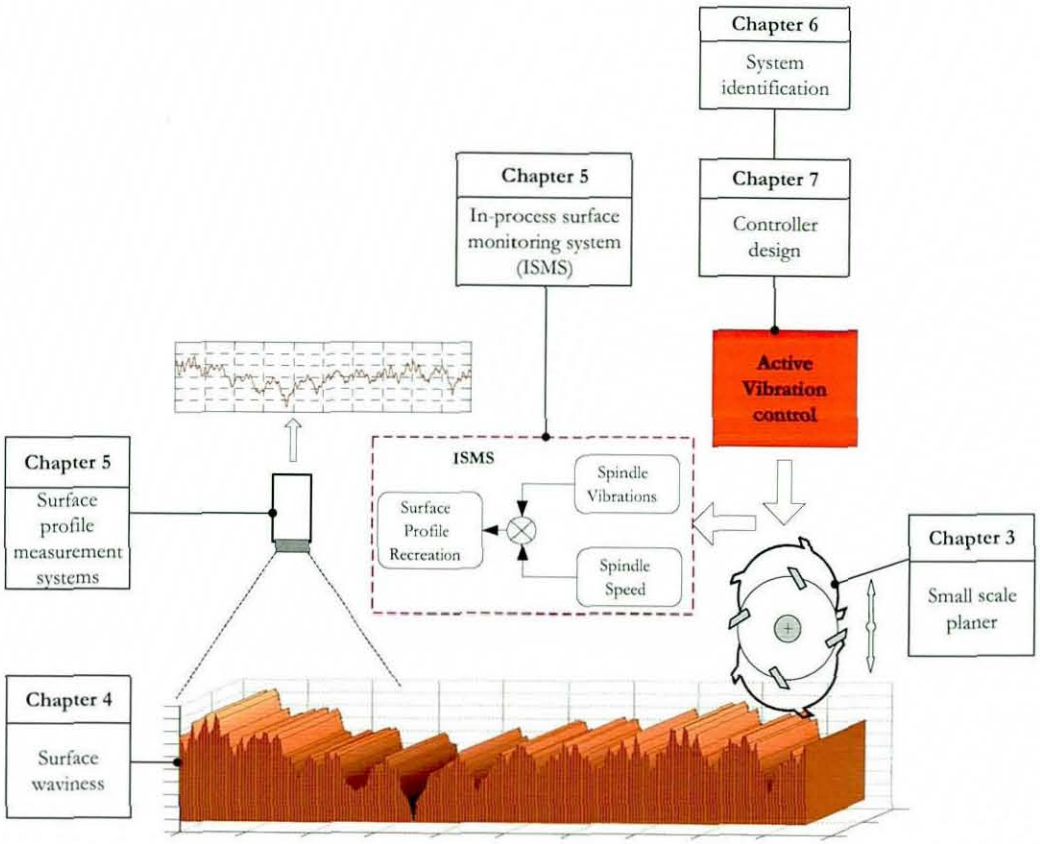

Figure 8.1 General overview of the project

8.1 Previous Work

Firstly, the small scale planer which was built by Hynek (2004) as a part of his PhD project was introduced in chapter 3. The objective of his work was to improve the surface profile by adjusting the vertical trajectory of the cutterhead in real-time. As a result of this approach, a smoother surface with shallower cuttermarks was achieved by shaping the cuttermarks on the surface.

Referring to the equation (4.2), the shallower cuttermarks are due to the virtual increase of the cutterhead radius R. The principal behind this approach is that when a cutting knife is at the start of the cutting path, the cutterhead moves upwards until it reaches the maximum predefined displacement. After reaching the maximum displacement, the cutterhead moves downwards. The control action takes place in a time window Δt, which is basically the time required to machine one cuttermark as described by the equation (3.1). If a surface profile of high quality is required (i.e. *1 mm* pitch), as specified in the Table 4.1, the time window becomes very narrow. The consequence of a narrow time window is that the cutterhead has to move upwards and downwards within the given short time period. This set some limitations on this control approach, because the acceleration forces (i.e. up to *63 kN* as described in section 3.5) required to carry out the vertical cutterhead movement are outside of the performance regime of the piezoelectric actuators. Therefore, the surface profile improvement through vertical cutterhead movement is more suitable for lower cutting parameters (i.e. ω*=600 rpm*, v_f*= 20mm/s*). This approach can be classified under the category "rotary machining process modification" as shown in the overview of the rotary machining process improvement in Figure 2.4.

Unlike the previous approach, the main focus of this thesis work can be classified under the category "active vibration control" as shown in Figure 2.4.

8.2 Waviness on Machined Surface

In the rotary machining process, moulding and planing have played an important role within the woodworking industry. Due to the kinematics of these processes, the resultant wave shapes are considered as unavoidable. For a given quality requirement, the machining variations and disturbances need to be minimized. Especially, spindle vibrations and cutting tool inaccuracy have a great impact on the resultant surface quality. These effects have been first investigated theoretically and further analysed through simulation as well as experimental work.

The motivation behind this investigation was to demonstrate the effect of specific disturbances (i.e. spindle vibrations and tooling inaccuracies) on the machined surface. Firstly, the effects of tooling inaccuracies on the surface quality have been discussed and demonstrated through experimental work which was assisted by the simulation. The experimental work has been performed with the small scale planer (described in chapter 3). The combination of the surface simulation and the defect generation with the small scale planer, termed as defect generation tool (DGT), allows analyses of the effect of machining variations on the resultant surface profile. It has been shown that tooling inaccuracies can lead to lower surface quality and reduce the performance of the machining operation. Secondly, the effect of the *1/rev* spindle vibration on the resultant surface is first simulated within the software program Matlab/Simulink environment and then generated on a sample using the small scale planer. FFT analysis of machined timber surface traces indicates good correlation between the simulated and the actual surface wave lengths. To date, it has not been possible to control the wood machining process so that these disturbances can be machined to order. The DGT contributes to the broader understanding of the machine variations and the associated drawbacks on the surface profile. The advantages of the DGT can be summarized as follows

- Combination of surface simulation and defect generation forms a powerful tool for analysis of machine system variations
- Surface defects can be made to order for quality perception tests
- The simulation allows the identification of waviness defects (i.e. FFT analysis)
- DGT helps to understand the relationship between spindle vibrations and resultant surface form
- DGT can be used for calibration standards, especially for optical measurement devices (i.e. generating specific defects and measuring with optical devices)

8.3 Surface Profile Measurement Systems

In order to ensure the surface quality requirements a measurement system is needed. Therefore, various surface profile measurement systems which can measure the surface profile of machined timber have been introduced and evaluated. The measurement methods can be classified under two categories; contact based method and non-contact method. The contact based method is usually associated with the mechanical profilometer in form of a stylus tracer. The main advantage of this technique is its simplicity and measurement resolution which is mainly used for laboratory conditions. However, this technique has two major drawbacks. Firstly, this method is not suitable for in-process surface profile measurement, due to the high throughput rates employed within the woodworking process. The stylus tip tends to jump at higher measurement speeds, hence the measurement is not always reliable. Secondly, the stylus tip causes deformation on the measured surface, hence reduces the surface quality and provides incorrect data.

The non-contact measurement systems evaluated in this work are based on optical methods. The optical profilometer, Talysurf CLI, has been used as reference due to its high measurement resolution within the micrometer range as well as its traceable calibration to UKAS standards. The major advantage of this system is the high measurement resolution and the capabilities of scanning the surfaces in 3 D. The main drawbacks of this technique are the measurement speed and relatively high device costs (ca. 80000£). The optical profilometer is therefore not suitable for in-process inspection of machined surfaces.

The light sectioning method is also not suitable for in-process surface profile measurement purposes. This technique was not capable of measuring surface profiles of higher quality, because the scattering effect of the laser beam increases for lower pitches (i.e. *pitch<1.5 mm*). The measurement reliability drops immensely if the surface of the specimen is either black or white (i.e. white or black plastic samples).

Furthermore, extensive filtering was required to extract the surface information from the images.

The WSMS was the fastest among the tested measurement systems in terms of measurement speed. It took approximately one minute to extract the surface profile data from the images. The time required to extract the surface profile was mainly due to the surface profile extraction algorithm implemented on the WSMS. The surface waviness lengths could be measured satisfactorily. However, the WSMS is not capable of delivering the absolute waviness heights. Furthermore, the WSMS is too bulky to fit near cutterhead. Unlike other measurement systems, the WSMS captures an area of the machined surface, thus providing an averaged profile of the overall machined surface.

8.4 In-Process Surface Monitoring System (ISMS)

Most of the surface profile in-process monitoring systems are either too expensive, bulky or too slow to monitor the surface profile in real-time. A novel in-process surface profile monitoring system (ISMS) comprising of two steps has been introduced. The ISMS can potentially be employed for planing operation where continuous real-time inspection of the surface profile is needed. The first step is the re-creation of the surface profile by analysing the spindle speed of the small scale planer. This technique (i.e. surface profile re-creation with the spindle speed) shows relatively accurate surface profile information, however it is not capable of classifying surface defects caused by the spindle vibrations.

Therefore, a second complementary step has been introduced which considers the dynamic behaviour of the spindle system during the machining operation. Vibrations caused during the machining operation are captured and the surface profile is re-created. The combination of both steps allows classification of the surface profile relatively accurate when compared with the surfaces traced by the mechanical stylus.

As it can be seen from Figure 5.18, the eddy current probes do not provide the vibrations at the tool tip as they are located at the front bearing, thus delivering the spindle vibrations at the node 8 where the front bearing is located (Figure 7.1). However, for the surface profile re-creation, the vibrations at the tool tip are needed (node4 in Figure 7.1). Therefore, node 4 in Figure 7.1 indicating the tool tip location has also been identified as an output parameter in the state space model of the spindle system. Since the vibrations at the tool tip could not be measured physically (i.e. no displacement sensors at the tool tip), these are predicted with an estimator (Kalman filter). The estimation through Kalman filter takes also the dynamic characteristics of the spindle system into consideration. Figure 8.2 shows the comparison between the spindle vibrations at the front bearing measured with the eddy current probes (indicated in solid line and termed in the legend as "y expV48") and the estimated tool tip vibrations (indicated in dashed line and termed as ye_{tip} expV48"). From Figure 8.2 It can be observed that the estimated tool tip vibrations are higher than the spindle vibrations measured with the eddy current probes.

With ISMS, the surface profile information can be obtained with only two sensors (i.e. eddy current probes and incremental encoder) and an estimator which makes this approach cost effective and easy to implement. The main advantage of this new method is the capability of monitoring the surface profile in real-time. The disadvantage of this technique is the implementation of an estimator to predict the tool tip vibrations which requires a model of the spindle system.

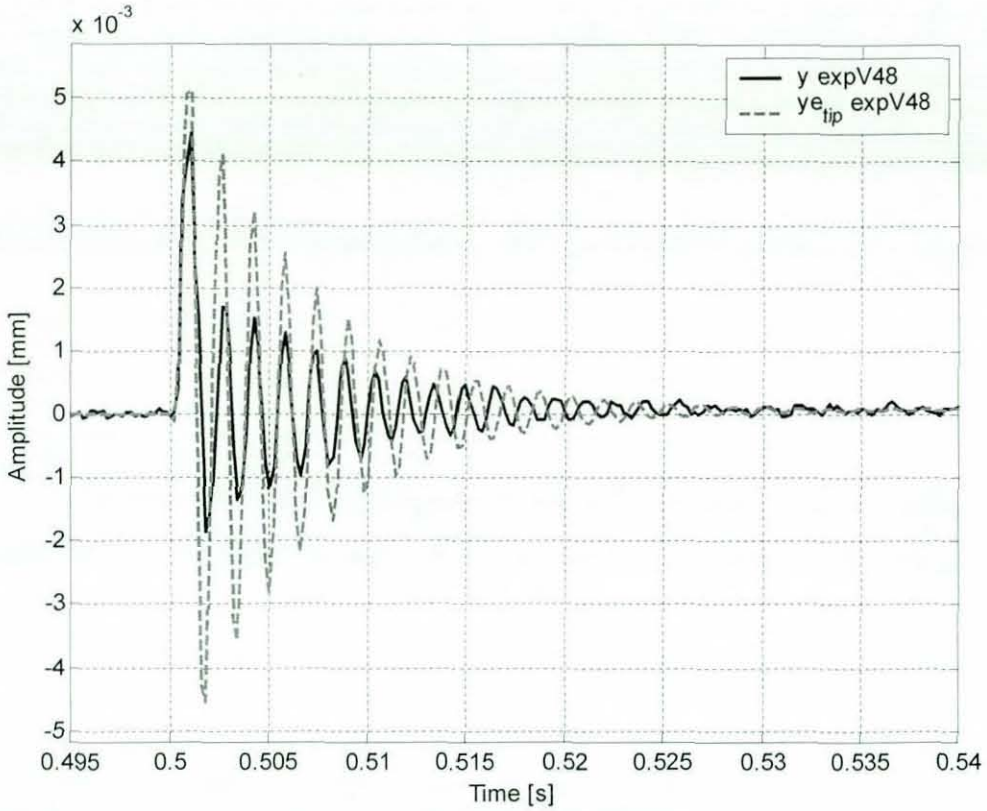

Figure 8.2 Spindle vibrations at the front bearing vs. estimated tool tip vibrations

Furthermore, if the Kalman filter is not configured appropriately (i.e. slow/fast Kalman filter) the surface profile information might be inaccurate, therefore setting the estimator to an adequate speed is essential (Kalman filter settings are discussed in section 7.4). Another drawback of the ISMS is that if the controller is performed in the closed loop operation, the dynamic behaviour of the spindle system changes, hence vibrations occurring at the tool tip are suppressed and their correlation to the surface profile is difficult. Although in the closed loop operation, the surface profile features can still be extracted from the spindle speed, however if there are spindle vibrations causing surface defects (i.e. *1/rev* spindle vibration) which generally do not affect the spindle speed, the extracted surface profile information from the spindle speed would not be reliable. Clearly, on the one hand the closed loop operation suppresses the spindle vibrations (hence changes the dynamic behaviour of the spindle system) and on the other hand the spindle vibrations are used to re-create the

surface profile. Therefore, the extracted surface profile features would be corrupted to a certain degree (i.e. depending on the vibration suppression level). A solution to this problem could be to develop an algorithm which takes the amount of vibration suppression into consideration. This requires further investigation and could be subject of future work.

8.5 System Identification and Test Rig Modelling

The modelling and the system identification of the test rig have been investigated for two reasons. Firstly, the spindle system behaviour was only investigated to a certain extent by Hynek, (2005). Therefore, further investigations were necessary to identify the dynamic behaviour and the capabilities of the test rig. Secondly, for the modal control approach, system identification, spindle system modelling was necessary. Therefore, a comprehensive model of the spindle and the piezoelectric actuators has been created (chapter 6). The mechanical part of the spindle system has been created with use of finite element method (Chapter 7). The finite element model is combined with the electrical model of the piezoelectric actuators to obtain an overall model of the spindle system. The resultant spindle model has been tuned so that it matches the dynamic characteristics of the actual spindle system. In order to reveal the dynamic characteristics of the actual spindle system, various experiments have been carried out.

Although, initially the system identification tool (SIT) available within Matlab was used to create a model of the spindle system, this attempt could not provide satisfactory results. This approach is formulated as a curve-fitting problem where input and output characteristics obtained from the experimental work are used to obtain a numerical model of the spindle system. This approach has also been implemented and reported by some researchers (i.e. Chen et al. 2003). However, the model obtained with this technique did not provide satisfactory results, therefore the FEM software developed by Hynek et al. (2004) was used to model the mechanical

part of the spindle system. The spindle system model shows good agreement with the characteristics of the actual spindle system. However, there are some discrepancies between the actual spindle system behaviour and the spindle system model. Figure 8.3 shows the actual spindle response in open and closed loop operation in comparison to the model response to same impulse input signal (legend "y_{OL} simV48" indicates the simulation model in the open loop operation whereas "y_{CL} expV48" indicates the actual spindle response in the closed loop operation). The simulation as well as the experimental results show that in the closed loop operation the spindle vibrations could be reduced significantly.

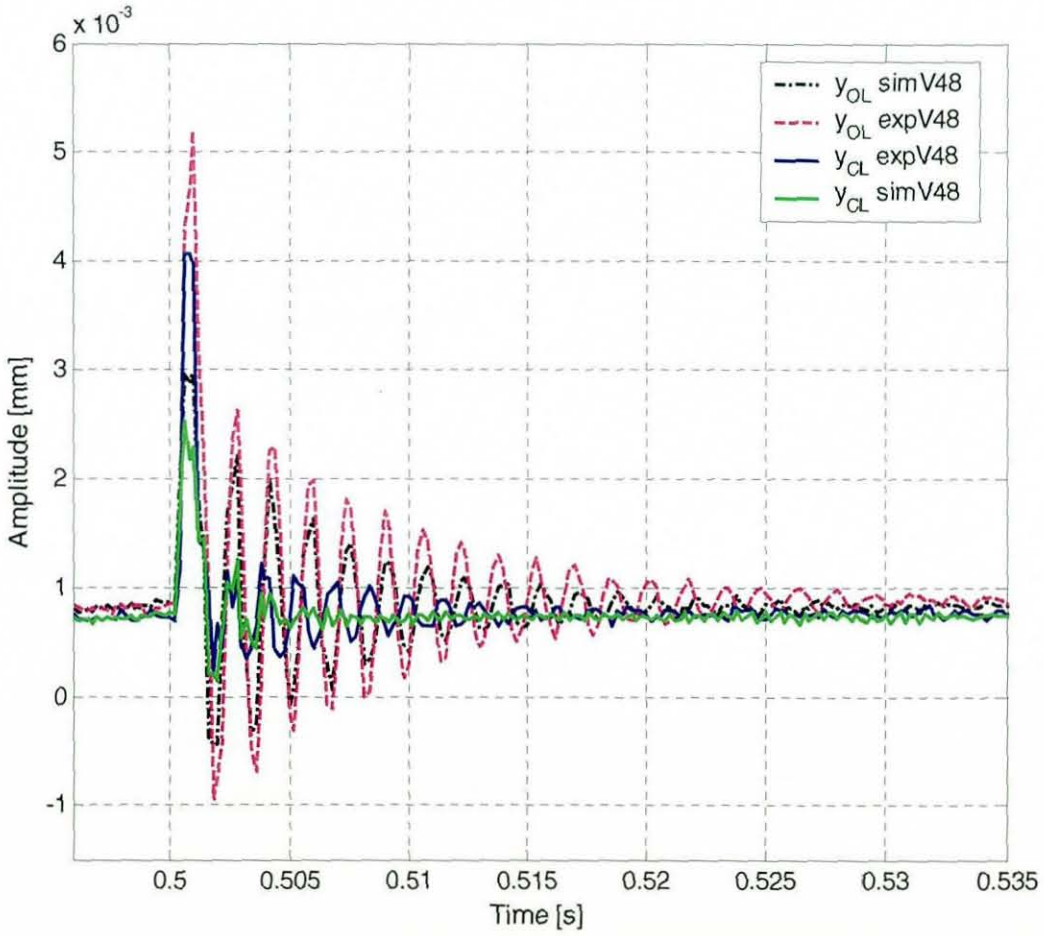

Figure 8.3 Model response vs actual spindle system response

However, the peak vibration value of the actual spindle is slightly higher than the peak vibration value of the model. The reason for the discrepancy is two fold. Firstly, the FRF of the model shown in Figure 7.14 appears to be slightly stiffer than the actual model in the low frequency range. Secondly, the model is linear therefore it does not take the non-linearities of the spindle system such as the hysteresis of the piezoelectric actuators into consideration. Nevertheless, the model covers the important dynamic characteristics of the spindle system satisfactorily, hence the spindle vibrations could be suppressed significantly (Figure 8.3).

8.6 Improving Dynamics of the Spindle System

The spindle unit is capable of controlling the spindle movement in the plane perpendicular to spindle's axis. As a part of his PhD studies, Hynek (2004) used this capability for reducing surface waviness heights. The small scale planer can also be used to implement active vibration control in order to improve the dynamic characteristics of the spindle system for an advanced machining environment. The investigations reported in this thesis work focuses mainly but not only on the implementation of active vibration control on the small scale planer.

It is suggested that with active vibration control, the dynamic characteristics of a plant can be improved. The methodology of implementing active vibration control can be different for specific applications, however the objective is similar in that sense that using external power for obtaining a desired response. Unlike the passive control which can reduce the operation bandwidth by introducing additional modes as discussed in section 2.3.1, the active vibration control could adapt the system dynamics for various applications. With the use of active vibration control, the operation bandwidth of the machining environment could be improved by introducing damping in the system. The controller implemented on the test rig to achieve this goal is based on the optimal control method. The design of the optimal control technique requires an estimator (i.e. Kalman filter).

This is mainly due to the controller requirement which is based on the assumption that all the state variables are available. However, in the real machining environment, sensors usually do not provide complete data about a system. Therefore, Kalman filter is used to provide the controller input matrix with the estimation of the state variables. The main drawback of the optimal control technique is that it requires a relatively accurate model of the plant (i.e. spindle model + actuator model). Furthermore, the controller weighting parameters are usually set by trial and error procedures, which means that the control action can become unstable and lead to actuator damage if the weighting parameters are not set appropriately. Therefore, the weighting parameters for the control action as well as for the Kalman filter need to be set very carefully.

The advantages of the optimal control method are firstly, the capability of adjusting the performance index according to the particular application. In other words, a trade off between the system response and the control effort can be set according to the specific application. This is useful where the control effort is an issue. For example, for a given maximum power supply, the controller would try to achieve the best system response or if a specific response is required, the controller would try to perform with a minimum control effort. Secondly, once the controller weighting parameters are set appropriately, the system operation is stable.

The major achievement of the implemented controller is the ability to substantially improve the dynamic characteristics of the system. The dynamic behaviour of a mechanical system sets limitations on the operation range, hence limits the machining bandwidth. With the implementation of active vibration control on the small scale planer, this bandwidth has been increased, hence enabling a higher degree of freedom in the machining process. In other words, active vibration control enables operating ranges beyond the mechanical limitations of the system. For example, when the FRFs of the open and closed loop operations are compared, the peak amplitude value of the natural frequency was reduced by ca. 68% in the closed loop operation (Figure 7.32).

This substantial improvement of the dynamic characteristics of the spindle system allows machining operations beyond the natural frequency of the spindle system. This advanced machining process (AMP) has many benefits for the woodworking industry. As has been mentioned in section 7.5.2, the desired product quality can be machined at higher throughput rates irrespective of machine's operation bandwidth. As a result of this freedom in the machining operation, AMP enables high performance machining, which is a desirable characteristics from the economic point of view. Furthermore, surface finish quality can be enhanced by increasing the operation bandwidth (i.e. increasing spindle speed) as described by the equation (4.1). This in turn can make additional machining processes such as sanding obsolete.

Chapter 9 CONCLUSION AND FURTHER WORK

9.1 Conclusion

In this thesis work, improvements and investigations on a small scale planer have been proposed. Hereby three major novelties have been achieved.

Firstly, it was shown through simulation as well as experimental work that machine system variations have great impact on the resultant surface quality. Especially, the effects of spindle vibrations and tooling inaccuracies can significantly reduce the surface waviness quality. To date, it has not been possible to demonstrate the effect of specific disturbances on the machined surface profile. Although the theory reported by Jackson et al. (2007) provides unique insight into the wood machining dynamics, it was not possible to address and demonstrate the cause of disturbances. The defect generation tool (DGT) presented in this thesis, allows the generation of a specific to generate the effect of a specific disturbance to order. This in turn contributes to the broader understanding of the machine system variations and its effects on the resultant surface quality. The revelation of the effects of the specific disturbance could be further used to take specific measures against the particular disturbance.

Secondly, in order to monitor the surface quality, a surface profile measurement system is needed. Various surface profile measurement systems have been evaluated and their real-time capabilities have been analysed. Most of these measurement systems lack the measurement speed or bulky and expensive to implement for real-time surface profile measurement. Therefore, a novel in-process surface profile monitoring system (ISMS) has been introduced. This method requires only two sensors and an estimator to monitor the surface profile in real-time. Experimental results showed that this novel method is capable of providing the surface profile features accurate enough for real-time monitoring purposes.

Thirdly, active vibration control has been implemented on the small scale planer, hence it is the world's first actively controlled planer. A relatively comprehensive model of the spindle system has been obtained and optimal control method has been implemented successfully. Experimental results showed that with the implemented control method, the dynamics of the spindle system have been improved significantly. The machining operation is no longer limited by the mechanical properties, hence a higher degree of freedom in the machining environment was achieved.

9.2 Recommendation for Further Work

For an enhanced machining environment further improvements on the small scale planer could be pursued. With the active vibration control, the dynamic characteristics of the spindle system have been improved, which means that higher operation ranges beyond the natural frequency of the spindle system are possible. However, forces acting on the mechanical parts of the spindle system need to be taken into consideration. In order to monitor the forces during the machining operation, a method reported by Park and Altintas (2004), and Albrecht et al. (2005) for a metal milling machine using Kalman filter, has also been implemented for the small scale planer. The results are not reported in this thesis work as they have not been verified experimentally. The evaluation could be carried out with a dynamometer during the cutting process. This will enable smart machining operations at the physical limits of the spindle system.

Furthermore, two lightweight cutterheads, with each comprising of 4 cutting knives, have been designed. The specially designed weight units can be attached to these cutterheads in order to investigate the effect of the imbalance on the resultant surface.

The proposed design of the actuation system could prevent its industrial deployment due to the relatively costly driving amplifiers. Further investigations could be carried out on the amplifier. Moreover, for the implementation of the active vibration control two PCs are necessary. This could be implemented with microcontroller for an embedded design environment. On the other hand one could argue that the PCs are becoming more affordable and compact, therefore the cost factor may not be decisive.

REFERENCES

Abduljabbar, Z., ElMadany, M. M. and AlAbdulwahab, A. A. (1996). Active Vibration Control of a Flexible Rotor. *Computers and Structures* 58(3), pp: 499-511.

Aenis, M., Knopf, E. and Nordmann, R. (2002). Active Magnetic Bearings for the Identification and Fault Diagnosis in Turbomachinery. *Mechatronics* 12(8), pp: 1011-1021.

Ahn, S. J., Jeong, W. B. and Yoo, W. S. (2004). Unbiased Expression of Frf with Exponential Window Function in Impact Hammer Testing. *Journal of Sound and Vibration* 277(4-5), pp: 931-941.

Albrecht, A., Park, S. S., Altintas, Y. and Pritschow, G. (2005). High Frequency Bandwidth Cutting Force Measurement in Milling Using Capacitance Displacement Sensors. *International Journal of Machine Tools and Manufacture* 45(9), pp: 993-1008.

Al-Regib, E., Ni, J. and Lee, S.-H. (2003). Programming Spindle Speed Variation for Machine Tool Chatter Suppression. *International Journal of Machine Tools and Manufacture* 43(12), pp: 1229-1240.

Andren, L., Hakansson, L. and Claesson, I. (2003). Active Control of Machine Tool Vibrations in External Turning Operations. *Proceedings of the Institution of Mechanical Engineers, Part B: Journal of Engineering Manufacture* 217(6), pp: 869-872.

Astrom, K. J. and Hagglund, T. (1995). *Pid Controllers: Theory, Design and Tuning.* ed. Noth Carolina: Instrument Society of America.

Atkins, A. G. (2005). Toughness and Cutting: A New Way of Simultaneously Determining Ductile Fracture Toughness and Strength. *Engineering Fracture Mechanics* 72(6 SPEC ISS), pp: 849-860.

Baker, J. R. and Rouch, K. E. (2002). Use of Finite Element Structural Models in Analyzing Machine Tool Chatter. *Finite Elements in Analysis and Design* 38(11), pp: 1029-1046.

Barrett, T. S., Palazzolo, A. B. and Kascak, A. F. (1995). Active Vibration Control of Rotating Machinery Using Piezoelectric Actuators Incorporating Flexible Casing Effects. *Journal of Engineering for Gas Turbines and Power, Transactions of the ASME* 117(1), pp: 176-187.

Bay, J. S. (1999). *Fundamentals of Linear State Space Systems.* ed. Boston: WCB/McGraw-Hill.

Bennett, J. M. (1992). Recent Developments in Surface Roughness Characterization. *Measurement Science & Technology* 3(12), pp: 1119-1127.

Benning, R. D., Hodgins, M. G. and Zipfel, G. G., Jr. (1997). Active Control of Mechanical Vibrations. *Bell Labs Technical Journal* 2(2), pp: 246-257.

Bian, H., Jin, Z. and Tian, W. (2006). Iae-Adaptive Kalman Filter for Ins/Gps Integrated Navigation System. *Journal of Systems Engineering and Electronics* 17(3), pp: 502-508.

Bleuler, H. (1992). Survey of Magnetic Levitation and Magnetic Bearing Types. *JSME International Journal, Series 3: Vibration, Control Engineering, Engineering for Industry* 35(3), pp: 335-342.

Bleuler, H., Vischer, D., Schweitzer, G., Traxler, A. and Zlatnik, D. (1994). New Concepts for Cost-Effective Magnetic Bearing Control. *Automatica* 30(5), pp: 871-876.

Brandon, J. A. and Al-Shareef, K. J. H. (1992). Optimization Strategies for Machine Tool Spindle-Bearing Systems: A Critical Review. *Journal of Engineering for Industry, Transactions of the ASME* 114(2), pp: 244-253.

Brown, N., Parkin, R. M. and Jackson, M. R. (2002). Simulation of a Modified Rotary Timber Machining Process to Improve Surface Form. *Mechatronics* 12(3), pp: 489-502.

Bryson, E. A. (2002). *Applied Linear Optimal Control.* ed. Cambridge: Cambridge University Press.

Chen, C. H., Wang, K. W. and Shin, Y. C. (1994). Integrated Approach toward the Dynamic Analysis of High-Speed Spindles, Part I: System Model. *Journal of Vibration and Acoustics, Transactions of the ASME* 116(4), pp: 506-513.

Chen, Y., Wang, X. G., Sun, C., Devine, F. and De Silva, C. W. (2003). Active Vibration Control with State Feedback in Woodcutting. *JVC/Journal of Vibration and Control* 9(6), pp: 645-664.

Chiu, W. M., Lam, F. W. and Gao, D. (2002). An Overhung Boring Bar Servo System for on-Line Correction of Machining Errors. *Journal of Materials Processing Technology* 122(2-3), pp: 286-292.

Chu, F. and Holmes, R. (2000). Damping Capacity of the Squeeze Film Damper in Suppressing Vibration of a Rotating Assembly. *Tribology International* 33(2), pp: 81-97.

Costes, J.-P., Pak, L. K., Ji, T., Deces-Petit, C. and Altintas, Y. (2004). Orthogonal Cutting Mechanics of Maple: Modeling a Solid Wood-Cutting Process. *Journal of Wood Science* 50(1), pp: 28-34.

De Silva Clarence W. (2007). *Vibration Fundamentals and Practice.* ed. Boca Raton: Taylor & Francis Group.

Dietzsch, M., Gröger, S., Gerlach, M. and Krystek, M. (2007). Extraction of the Mechanical Surface in Measurement of Nano Structures. *CIRP Annals - Manufacturing Technology* 56(1), pp: 537-540.

Dohner, J. L., Hinnerichs, T. D., Lauffer, J. P., Kwan, C. M., Regelbrugge, M. E. and Shankar, N. (1997). Active Chatter Control in a Milling Machine. San Diego, CA, USA. Society of Photo-Optical Instrumentation Engineers, Bellingham, WA, USA. pp: 281-294.

Dohner, J. L., Lauffer, J. P., Hinnerichs, T. D., Shankar, N., Regelbrugge, M., Kwan, C.-M., Xu, R., Winterbauer, B. and Bridger, K. (2004). Mitigation of Chatter Instabilities in Milling by Active Structural Control. *Journal of Sound and Vibration* 269(1-2), pp: 197-211.

Dorf, C. R. and Bishop, H. R. (2005). *Modern Control Systems.* ed. New Jersey: Pearson Prentice Hall.

Ellis, R. W. and Mote, C. D., Jr. (1979). Feedback Vibration Controller for Circular Saws. *Journal of Dynamic Systems, Measurement and Control, Transactions of the ASME*(1), pp: 44-49.

Elmas, S., Jackson, M. R. and Parkin, R. M. (2007). Planing Timber with an Active Machining System. *Proceedings of the 18th Wood machining Seminar,* Vnacouver, Canada. pp: 107-115.

Eyma, F., Meausoone, P.-J. and Martin, P. (2004). Strains and Cutting Forces Involved in the Solid Wood Rotating Cutting Process. *Journal of Materials Processing Technology* 148(2), pp: 220-225.

Fannin, C. A., Saunders, W.R. (1997 a). Analog Adaptive Piezoelectric Sensoriactuator Design for Collocated Rate Feedback. *Proceedings - National Conference on Noise Control Engineering* 2, pp: 357-366.

Fannin, C. A. and Saunders, W. R. (1997). Analog Adaptive Piezoelectric Sensoriactuator Design. Kissimmee, FL, USA. AIAA, New York, NY, USA. pp: 1728-1737.

Faust, T. D. (1987). Real Time Measurement of Veneer Surface Roughness by Image Analysis. *Forest Products Journal* 37(6), pp: 34-40.

Fawcett, S. C. (1990). Small Amplitude Vibration Compensation for Precision Diamond Turning. *Precision Engineering* 12(2), pp: 91-96.

Gallina, P., Scuor, N. and Mosetti, G. (2005). Delayed-Reference Control (Drc) Applied to Machining Operations. *International Journal of Machine Tools and Manufacture* 45(12-13), pp: 1386-1392.

Ganguli, A., Deraemaeker, A., Horodinca, M. and Preumont, A. (2005). Active Damping of Chatter in Machine Tools - Demonstration with a 'Hardware-in-the-Loop' Simulator. *Proceedings of the Institution of Mechanical Engineers. Part I: Journal of Systems and Control Engineering* 219(5), pp: 359-369.

Gao, D., Yao, Y. X., Chiu, W. M. and Lam, F. W. (2002). Accuracy Enhancement of a Small Overhung Boring Bar Servo System by Real-Time Error Compensation. *Precision Engineering* 26(4), pp: 456-459.

Garratt, J. D. and Nettleton, D. J. (1992). A Stylus Instrument for Roughness and Profile Measurement of Ultra-Fine Surfaces. *International Journal of Machine Tools and Manufacture* 32(1-2), pp: 233-238.

Geng, Y. and Wang, J. (2008). Adaptive Estimation of Multiple Fading Factors in Kalman Filter for Navigation Applications. *GPS Solutions* 12(4), pp: 273-279.

Grewal, S. M. and Andrews, P. A. (2001). *Kalman Filtering: Theory and Practice.* ed. New York: Wiley.

Groeger, S., Dietzsch, M., Gerlach, M. and Jess, S. (2005). Real Mechanical Profile - the New Approach for Nano-Measurements. *Journal of Physics* 13, pp: 13-19.

Hakansson, L., Claesson, I. and Lago, T. (1999). Active Control of Machine Tool Chatter. Kissimmee, FL, USA. SEM, Bethel, CT, USA. pp: 1826-1831.

Hameed, R. A., Mannan, M. A. and Nee, A. Y. C. (2004). The Cutting Force Measurement in a Fixturing Setup with Instrumented Locators. *International Journal of Advanced Manufacturing Technology* 23(11-12), pp: 783-793.

Harris, F. J. (1978). One the Use of Windows for Harmonic Analysis with the Discrete Fourier Transform. *Proceedings of the IEEE* 66(1), pp: 51-83.

Hynek, P. (2004). *Wood Surface Form Improvement by Real Time Displacement of Tool Trajectory.* (PhD). Loughborough University, Loughborough, United Kingdom.

Hynek, P., Jackson, M. R., Parkin, R. M. and Brown, N. (2004). Modelling of a Smart Planing Unit. *3rd International Symposium on Multi-body Dynamics: Monitoring & Simulation Techniques*, Loughborough, United Kingdom.

Inamura, T. and Sata, T. (1974). Stability Analysis of Cutting under Varying Spindle Speed. *Annals of the CIRP* 23(1), pp: 119-120.

Inamura, T. and Sata, T. (1975). Stability Analysis of Cutting under Varying Spindle Speed. *Journal of the Faculty of Engineering, University of Tokyo, Series B* 33(1), pp: 13-29.

Inman, D. J. (2001). *Engineering Vibration.* ed. New Jersey: Prentice Hall.

Jackson, M. R., Hynek, P., Brown, N. and Parkin, R. M. (2003). Multi-Degree of Freedom Machining. Maribor, Slovenia. Institute of Electrical and Electronics Engineers Inc., Piscataway, NJ 08855-1331, United States. pp: 1225-1230.

Jackson, M. R., Hynek, P. and Parkin, R. M. (2007). On Planing Machine Engineering Characteristics and Machined Timber Surface Quality. *Proceedings of the Institution of Mechanical Engineers, Part E: Journal of Process Mechanical Engineering* 221(1), pp: 17-32.

Jackson, M. R., Parkin, R. M. and Brown, N. (2002). Waves on Wood. *Proceedings of the Institution of Mechanical Engineers, Part B: Journal of Engineering Manufacture* 216(4), pp: 475-497.

Jemielniak, K. and Widota, A. (1984). Suppression of Self-Excited Vibration by the Spindle Speed Variation Method. *International Journal of Machine Tool Design & Research* 24(3), pp: 207-216.

Kim, J.-D. and Nam, S.-R. (1997). Development of a Micro-Depth Control System for an Ultra-Precision Lathe Using a Piezo-Electric Actuator. *International Journal of Machine Tools & Manufacture* 37(4), pp: 495-509.

Kim, T.-Y. and Kim, J. (1996). Adaptive Cutting Force Control for a Machining Center by Using Indirect Cutting Force Measurements. *International Journal of Machine Tools & Manufacture* 36(8), pp: 925-937.

Kim, T.-Y., Woo, J., Shin, D. and Kim, J. (1999). Indirect Cutting Force Measurement in Multi-Axis Simultaneous Nc Milling Processes. *International Journal of Machine Tools and Manufacture* 39(11), pp: 1717-1731.

Kiran, M. B., Ramamoorthy, B. and Radhakrishnan, V. (1998). Evaluation of Surface Roughness by Vision System. *International Journal of Machine Tools and Manufacture* 38(5-6), pp: 685-690.

Kosuge, Y., Kameda, H. and Mario, S. (1997). Kalman Filter and Α-Β Filters for Radar Tracking. *Electronics & Communications in Japan, Part I: Communications (English translation of Denshi Tsushin Gakkai Ronbunshi)* 80(3), pp: 67-77.

Kramer, K. A., Stubberud, S. C. and Geremia, J. A. (2007). Sensor Calibration Using the Neural Extended Kalman Filter in a Control Loop. Ostuni, Italy. Institute of Electrical and Electronics Engineers Computer Society, Piscataway, NJ 08855-1331, United States. pp: 19-24.

Lalanne, M., Berthier, P. and Hagopian, J. (1983). *Mechanical Vibrations for Engineers.* ed. Chichester: Wiley.

Laternser, R., Ganser, H.-P., Taenzer, L. and Hartmaier, A. (2003). Chip Formation in Cellular Materials. *Journal of Engineering Materials and Technology, Transactions of the ASME* 125(1), pp: 44-49.

Lauffer, J. P., Regelbrugge, M. E., Dohner, J. L., Hinnerichs, T. D., Kwan, C. M., Lin, Y. and Xu, R. (1998). Smart Spindle Unit for Active Chatter Suppression of a Milling Machine Part Ii: Dynamics and Control. San Diego, CA, United States. The International Society for Optical Engineering. pp: 167-173.

Lee, D.-S. and Choi, D.-H. (2000). Reduced Weight Design of a Flexible Rotor with Ball Bearing Stiffness Characteristics Varying with Rotational Speed and Load. *Journal of Vibration and Acoustics, Transactions of the ASME* 122(3), pp: 203-208.

Lewis (1992). *Applied Optimal Control and Filtering: Design and Implementation.* ed. Englewood Cliffs, New Jersey: Prentice-Hall.

Li, X., Djordjevich, A. and Venuvinod, P. K. (2000). Current-Sensor-Based Feed Cutting Force Intelligent Estimation and Tool Wear Condition Monitoring. *IEEE Transactions on Industrial Electronics* 47(3), pp: 697-702.

Lin, R. R., Palazzolo, A. B., Kascak, A. F. and Montague, G. T. (1993). Electromechanical Simulation and Testing of Actively Controlled Rotordynamic Systems with Piezoelectric Actuators. *Journal of Engineering for Gas Turbines and Power, Transactions of the ASME* 115(2), pp: 324-335.

Lin, R. R., Palazzolo, A. B., Kascak, A. F. and Montague, G. T. (1993). Electromechanical Simulation and Testing of Actively Controlled Rotordynamic Systems with Piezoelectric Actuators. *Journal of Engineering for Gas Turbines and Power ; Vol/Issue: 115:2*, pp: Pages: 324-335.

Liu, K. J. and Rouch, K. E. (1991). Optimal Passive Vibration Control of Cutting Process Stability in Milling. *Journal of Materials Processing Technology* 28(1-2), pp: 285-294.

Luo, G. Y., Osypiw, D. and Irle, M. (2003). Surface Quality Monitoring for Process Control by on-Line Vibration Analysis Using an Adaptive Spline Wavelet Algorithm. *Journal of Sound and Vibration* 263(1), pp: 85-111.

Matsubara, T., Yamamoto, H. and Mizumoto, H. (1989). Chatter Suppression by Using Piezoelectric Active Damper. Montreal, Que, Can. Publ by ASME, New York, NY, USA. pp: 79-83.

Maybeck, S. P. (1979). *Stochastic Models, Estimation and Control.* ed. New York: Academic Press.

McConnell, K. G. (1995). *Vibration Testing: Theory and Practice.* ed. New York: Wiley.

McKenzie, W. M., Ko, P., Cvitkovic, R. and Ringler, M. (2001). Towards a Model Predicting Cutting Forces and Surface Quality in Routing Layered Boards. *Wood Science and Technology* 35(6), pp: 563-569.

Merrit, H. E. (1965). Theory of Self-Excited Machine-Tool Chatter-Contribution to Machine Tool Chatter Research – 1. 87(4), pp: 447–454.

Min, B.-K., O'Neal, G., Koren, Y. and Pasek, Z. (2002). A Smart Boring Tool for Process Control. *Mechatronics* 12(9-10), pp: 1097-1114.

Nagaya, K., Yamazaki, H. and Kashimoto, H. (1997). Control of Micro-Vibrations of a Machine Head by Using Piezoelectric Actuators. *International Journal of Applied Electromagnetics and Mechanics* 8(4), pp: 315-328.

Nordmann, R. (2005). Use of Mechatronic Components in Rotating Machinery. *The Seventh International Conference on Vibration Problems ICOVP 2005*, Istanbul, Turkey. pp: 345-356.

Okazaki, Y. (1990). Micro-Positioning Tool Post Using a Piezoelectric Actuator for Diamond Turning Machines. *Precision Engineering* 12(3), pp: 151-156.

Palazzolo, A. B., Jagannathan, S., Kascak, A. F., Montague, G. T. and Kiraly, L. J. (1993). Hybrid Active Vibration Control of Rotorbearing Systems Using Piezoelectric Actuators. *Journal of Vibration, Acoustics, Stress, and Reliability in Design* 115(1), pp: 111-119.

Palmqvist, J. (2003). Parallel and Normal Cutting Forces in Peripheral Milling of Wood. *Holz als Roh - und Werkstoff* 61(6), pp: 409-415.

Palmqvist, J. and Gustafsson, S. I. (1999). Emission of Dust in Planing and Milling of Wood. *Holz als Roh - und Werkstoff* 57(3), pp: 164-170.

Palmqvist, J., Lenner, M. and Gustafsson, S.-I. (2003). Cutter Head Forces and Load Cell Scanning. *Wood Science and Technology* 37(3-4), pp: 199-211.

Park, S. S. and Altintas, Y. (2004). Dynamic Compensation of Spindle Integrated Force Sensors with Kalman Filter. *Journal of Dynamic Systems, Measurement and Control, Transactions of the ASME* 126(3), pp: 443-452.

Parkin, R. M. and Jackson, M. R. (1996). Mechatronic Approach for Analyzing Timber Surfaces. *Mathematics and Computers in Simulation* 41(5-6), pp: 445-450.

Physikinstrumente. Retrieved June 2008, from www.physikinstrumente.com/en/products/prspecs.php?sortnr=103100.

Piezo. Retrieved October 2006, from www.piezo.com/prodbm0nav.html

Pratt, J. and Nayfeh, A. H. (1998). Boring Bar Chatter Control. Santa Barbara, CA, USA. SEM, Bethel, CT, USA. pp: 215-223.

Pratt, J. R. and Nayfeh, A. H. (1999). Design and Modeling for Chatter Control. *Nonlinear Dynamics* 19(1), pp: 49-69.

Rashid, A. and Mihai Nicolescu, C. (2006). Active Vibration Control in Palletised Workholding System for Milling. *International Journal of Machine Tools and Manufacture* 46(12-13), pp: 1626-1636.

Ratnasingam, J. and Ioras, F. (2005). The Asian Furniture Industry: The Reality Behind the Statistics. *Holz als Roh - und Werkstoff* 63(1), pp: 64-67.

Ratnasingam, J., Ma, T. P. and Perkins, M. C. (1999). Productivity in Wood Machining Processes - a Question of Simple Economics ? *Holz als Roh- und Werkstoff* 57(1), pp: 51-56.

Ratnasingam, J. and Reid, H. F. (1996). Productivity Myth in Furniture Manufacturing. *Journal of the Institute of Wood Science* 14(2), pp: 102-105.

Regelbrugge, M. E., Lauffer, J. P., Dohner, J. L., Kwan, C. M. and Shankar, N. (2002). A Demonstration of Active Suppression of Milling-Tool Chatter. Denver, CO. American Inst. Aeronautics and Astronautics Inc. pp: 1209-1218.

Roy, P. K. and Ganesan, N. (1995). Transient Response of a Cantilever Beam Subjected to an Impulse Load. *Journal of Sound and Vibration* 183(5), pp: 873-890.

Sandak, J. and Tanaka, C. (2003). Evaluation of Surface Smoothness by Laser Displacement Sensor 1: Effect of Wood Species. *Journal of Wood Science* 49(4), pp: 305-311.

Sandak, J. and Tanaka, C. (2005). Evaluation of Surface Smoothness Using a Light-Sectioning Shadow Scanner. *Journal of Wood Science* 51(3), pp: 270-273.

Schweitzer G., B. H. a. T. A. (1994). *Active Magnetic Bearings*. ed. Zurich: VDF Hochschulverlag AG.

Sexton, J. S., Milne, R. D. and Stone, B. J. (1977). A Stability Analysis of Single-Point Machining with Varying Spindle Speed. *Applied Mathematical Modelling* 1(6), pp: 310-318.

Shamoto, E. and Moriwaki, T. (1997). Development of a 'Walking Drive' Ultraprecision Positioner. *Precision Engineering* 20(2), pp: 85-92.

Shankar, N., Bridger, K., Regelbrugge, M. and Winfough, W. R. (1998). A Smart Spindle Unit for Active Chatter Suppression of a Milling Machine Part I: Overview, Fabrication and Assembly. San Diego, CA, United States. The International Society for Optical Engineering. pp: 160-166.

Shinozaki, R., Sasaki, O. and Suzuki, T. (2004). Fast Scanning Method for One-Dimensional Surface Profile Measurement by Detecting Angular Deflection of a Laser Beam. *Applied Optics* 43(21), pp: 4157-4163.

Simoes, R. C., Steffen Jr, V., Der Hagopian, J. and Mahfoud, J. (2007). Modal Active Vibration Control of a Rotor Using Piezoelectric Stack Actuators. *JVC/Journal of Vibration and Control* 13(1), pp: 45-64.

Sims, N. D., Bayly, P. V. and Young, K. A. (2005). Piezoelectric Sensors and Actuators for Milling Tool Stability Lobes. *Journal of Sound and Vibration* 281(3-5), pp: 743-762.

Sims, W. L. (1985). *Two Hundred Years of History and Evolution of Woodworking Machinery.* Walders P.

Skricka, N. and Markert, R. (2002). Improvements in the Integration of Active Magnetic Bearings. *Control Engineering Practice* 10(8), pp: 917-922.

Skricka, N. and Markert, R. (2002). Improvements of the Integration of Active Magnetic Bearings. *Mechatronics* 12(8), pp: 1059-1068.

Steinschaden, N. and Springer, H. (1999). Some Nonlinear Effects of Magnetic Bearings. *Proceedings of the ASME Design Engineering Technical Conferences*, Las Vegas, Nevada, USA.

Takemura, T., Kitamura, T. and Hoshi, T. (1974). Active Suppression of Chatter by Programmed Variation of Spindle Speed. *Annals of the CIRP* 23(1), pp: 121-122.

Tanaka, H., Obata, F., Matsubara, T. and Mizumoto, H. (1994). Active Chatter Suppression of Slender Boring Bar Using Piezoelectric Actuators. *JSME International Journal, Series C* 37(3), pp: 601-606.

Tascioglu, Y. and Jackson, M. R. (2006). Mechatronic Design of a Novel Wood Moulder. *Proceedings of the Institution of Mechanical Engineers, Part B: Journal of Engineering Manufacture* 220(6), pp: 905-915.

Tewani, S. G., Switzer, T. C., Walcott, B. L. and Rouch, K. E. (1992). Active Vibration Control Using an Active Dynamic Absorber: Experimental Results. Anaheim, CA, USA. Publ by ASME, New York, NY, USA. pp: 133-140.

Tewani, S. G., Walcott, B. L. and Rouch, K. E. (1991). Active Optimal Vibration Control Using Dynamic Absorber. Sacramento, CA, USA. Publ by IEEE, Piscataway, NJ, USA. pp: 1182-1187.

Tlusty, J. P., M (1963). The Stability of Machine Tools against Self-Excited Vibrations in Machining. *Int. Res. Prod. Engng*, pp: 465–474.

Vipperman, J. S. a. C., R.L. (1997). Applications for the Adaptive Piezoelectric Sensoriactuator. *Proceedings National Conference on Noise Control Engineering* 2, pp: 347-356.

Wang, X. G. and Sun, J. C. (2001). Active Sensing and Control of Vibration of Circular Saws - a Comparison of Optimal and Variable Structure Control. Arlington, VA. Institute of Electrical and Electronics Engineers Inc. pp: 4294-4299.

Wang, X. P., Chen, X. J., Zhu, L. J. and Wang, W. (2001). Machine Tool Spindles and Active Magnetic Bearings. *Key Engineering Materials* 202-203, pp: 465-468.

Wong, B. W., Walcott, B. L. and Rouch, K. E. (1995). Active Vibration Control Via Electromagnetic Dynamic Absorbers. Albany, NY, USA. IEEE, Piscataway, NJ, USA. pp: 868-874.

Wong, P. L. and Li, K. Y. (1999). In-Process Roughness Measurement on Moving Surfaces. *Optics & Laser Technology* 31(8), pp: 543-548.

Woronko, A., Huang, J. and Altintas, Y. (2003). Piezoelectric Tool Actuator for Precision Machining on Conventional Cnc Turning Centers. *Precision Engineering* 27(4), pp: 335-345.

Yang, D. (2006). *Measurement of Cutter Marks on Planed Wood Surfaces with Machine Vision Methods.* (Ph.D.). Loughborough University, Loughborough, United Kingdom.

Yang, D., Jackson, M. R. and Parkin, R. M. (2005). Measuring Cutter Marks on Wood Surfaces with Machine Vision Techniques. *17th International Wood Machining Seminar*, Rosenheim, Germany.

Yang, D., Jackson, M. R. and Parkin, R. M. (2006). Inspection of Wood Surface Waviness Defects Using the Light Sectioning Method. *Proceedings of the Institution of Mechanical Engineers, Part I: Journal of Systems and Control Engineering* 220(7), pp: 617 - 626.

Yoo, S. M., Dornfeld, D. A. and Lemaster, R. L. (1990). Analysis and Modeling of Laser Measurement System Performance for Wood Surface. *Journal of Engineering for Industry, Transactions ASME* 112(1), pp: 69-77.

Zeillinger, R., Springer, H. and Kottritsch, H. (1994). Experimental Determination of Damping in Rolling Bearing Joints. Hague, Neth. Publ by ASME, New York, NY, USA. pp: 1-5.

Zhang, Y. and Sims, N. D. (2005). Milling Workpiece Chatter Avoidance Using Piezoelectric Active Damping: A Feasibility Study. *Smart Materials and Structures* 14(6), pp: 65-70.

APPENDIXES

Appendix A INSTRUMENTATION

MF614 Multifunction I/O Card

HUMUSOFT s.r.o.

e-mail: info@humusoft.com

WWW: http://www.humusoft.com

Specifications

A/D Converter

Resolution	12 bits
Number of channels	8 single ended
Conversion time	10 μs
Input ranges	±10V, ±5V, 0-10V, 0-5V, software selectable
Input protection	±16.5V
Input impedance	> 10 kS

D/A Converter

Resolution	12 bit
Number of channels	4
Settling time	max. 10 μs (1/2 LSB)
Slew Rate	10 V/μs
Output current	min. ±5 mA
Short circuit current	±30 mA
DC output impedance	0.1 S
Load capacitance	max. 500 pF
Differential nonlinearity	±1 LSB
Gain drift	typ. ±5 ppm/K
Zero drift	typ. ±5 ppmFSR/K

Digital Inputs

Number of bits	8
Input signal levels	TTL
Logic 0	0.8 V max.
Logic 1	2.0 V min.

Digital Outputs

Number of bits	8
Output signal levels	TTL
Logic 0	0.5 V max. @ 24 mA (sink)
Logic 1	2.0 V min. @ 15 mA (source)

Quadrature Encoder Inputs

Number of axes	4 independent
Resolution	24 bits
Counter modes	binary, BCD
Index input	programmable
Inputs	differential with Schmitt triggers
Input noise filter	digital, programmable (0.2 -50 μs)
Input frequency	max. 2 MHz
Quadrature modes	X1, X2, X4

Counters/Timers

Counter chip	CTS9513A
Number of channels	5, 4 of them available on I/O connector
Resolution	16 bits, cascadable up to 80 bits
Clock frequency	20 MHZ
Conter modes	up, down, binary, BCD
Triggering	software, external
Clock source	internal, prescalers, external
Inputs	TTL, Schmitt triggers
Outputs	TTL

VF-1500 Linear Amplifier

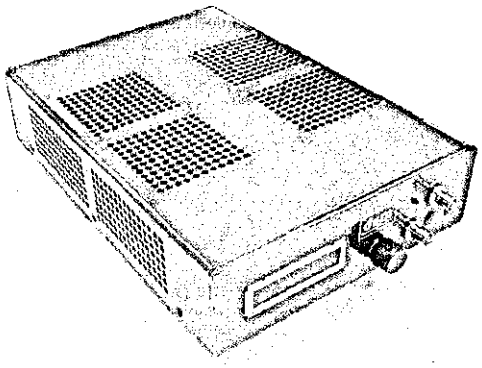

Dynamic Structures & Materials, LLC

Email: info@dynamic-structures.comVF-1500 SPECIFICATIONS

WWW: www.dynamics-structures.com

Specifications

Output Voltage	-30 to +150 V
Maximum Continuous Current	1000 mA
Maximum Peak Current	1500 mA
Maximum Output Power	180 W
Dimensions	2.75" x 8.25" x 12.0" (70 x 210 x 305 mm)
Gain	20
Input Control Voltage	-1.5 to +7.5 V
Small signal bandwidth	3 db Frequency > 700 Hz @ 180 Vpp, 3.5 μF load
Over-current and over-temperature protection	

MONITRAN

SENSORS FOR YOUR INDUSTRY

MTN/EP080

Industrial Eddy Probe

Applications

- Pump Monitors
- Turbines
- DC Gap Machine Tool
- Gauging

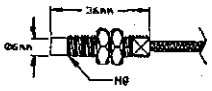

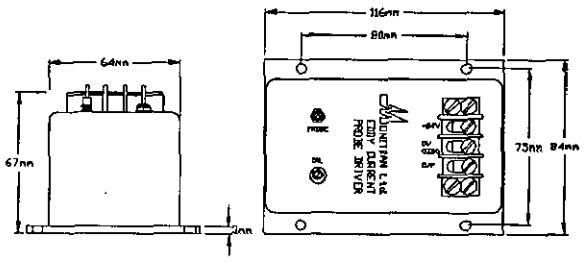

Technical Specification

Power Supply	-24 Volts DC @ 30mA
Sensitivity	8mV/μm nominal
Output Impedance	<50 Ohms
Linear Range	0 to 2mm
Linearity	1% nominal
Frequency Range	DC to 10 KHz
Operating Temperature	Probe: -30°C to +180°C Driver: -20°C to +80°C
Temperature Sensitivity	Probe: less than 5% at 150 Driver: less than 5% at 80
Tip Material	Peek encapsulated with potting
Case Material	Stainless Steel
Cable	RG179 PTFE insulated
Maximum Cable Length	9 Metres
Extension Cable	MTN/EXTOECP (Length to be Specified)
Options	4-20mA, Other Ranges, Submersible, Custom Design, Cable Length.

Supplied with Eddy Current Probe Driver MTN/ECPD

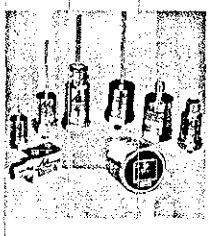

MONITRAN LTD MONITOR HOUSE HAZLEMERE RD PENN BUCKS UK HP10 8AD
TEL: +44 (0) 1494 816569 FAX: +44 (0) 1494 812256
EMAIL: INFO@MONITRAN.CO.UK WWW.MONITRAN.CO.UK

Appendix B SURFACE FORM MODELLING

The surface is often approximated by a series of circular arcs for simplicity. The typical machining parameters used within the woodworking industry for rotary machining processes make the approximation possible as can be seen from the following analysis.

Hynek (2004) established a measure which can describe the kinematical relationship of the rotary machining process regardless of actual cutting and feed speed. The ratio μ between cutting speed and feed speed is a suitable measure for describing the rotary machining process.

$$\mu = \frac{v_c}{v_f} \tag{A.1}$$

The ratio μ is typically in the range from 50 to 300. The length of the cuttermarks p is dependent on workpiece feed speed v_f, cutterhead rotational speed ω and the number of finishing cutting knives N. This relationship can be expressed by the following equation:

$$p = \frac{vf}{\omega \cdot N} \tag{A.2}$$

The length of the cuttermark p expressed by equation A.2 is effectively the length that the timber travels between two knives i.e. feed per knife (Figure A.1).

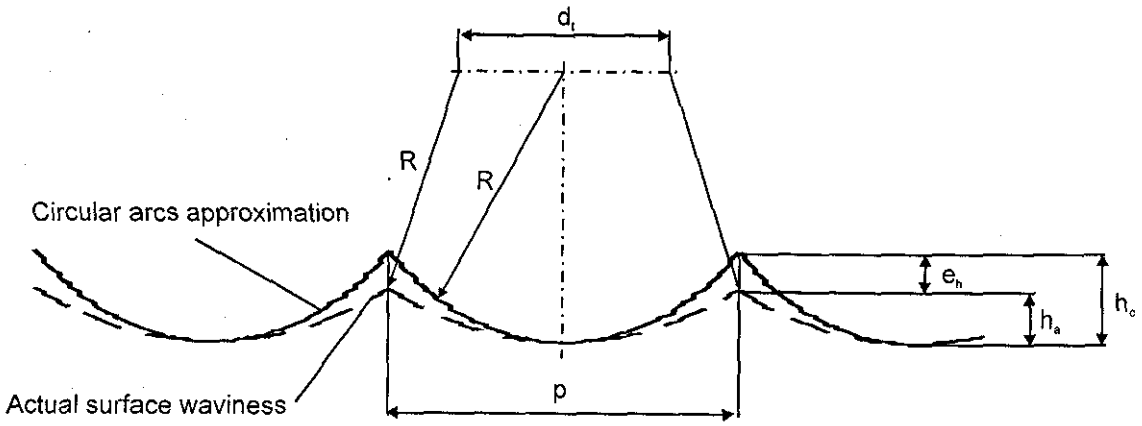

Figure A.1 Circular arcs approximation and cycloidal surface forms in comparison (Hynek 2004)

The waviness height h of the simplified surface can then be expressed by the following equation:

$$h_c = R - \sqrt{R^2 - \frac{p^2}{4}} \tag{A.3}$$

where as R is the cutterhead radius. The waviness height of the cycloidal surface is lower than the height of the simplified circular surface height and can be expressed as follows

$$h_a = R - \sqrt{R^2 - \frac{(p - d_t)^2}{4}} \tag{A.4}$$

where d_t is distance the cutterhead travels while the knife is cutting the length of cuttermark p. The distance d_t can be expressed as follows:

$$d_t = \int_0^p \frac{v_f}{v_{ox}(x)} dx \tag{A.5}$$

where v_{ox} is the horizontal component of the knife velocity v_o. The knife tip velocity relative to the work piece v_o is a vector sum of the cutting speed and the feed speed as depicted in Figure A.2.

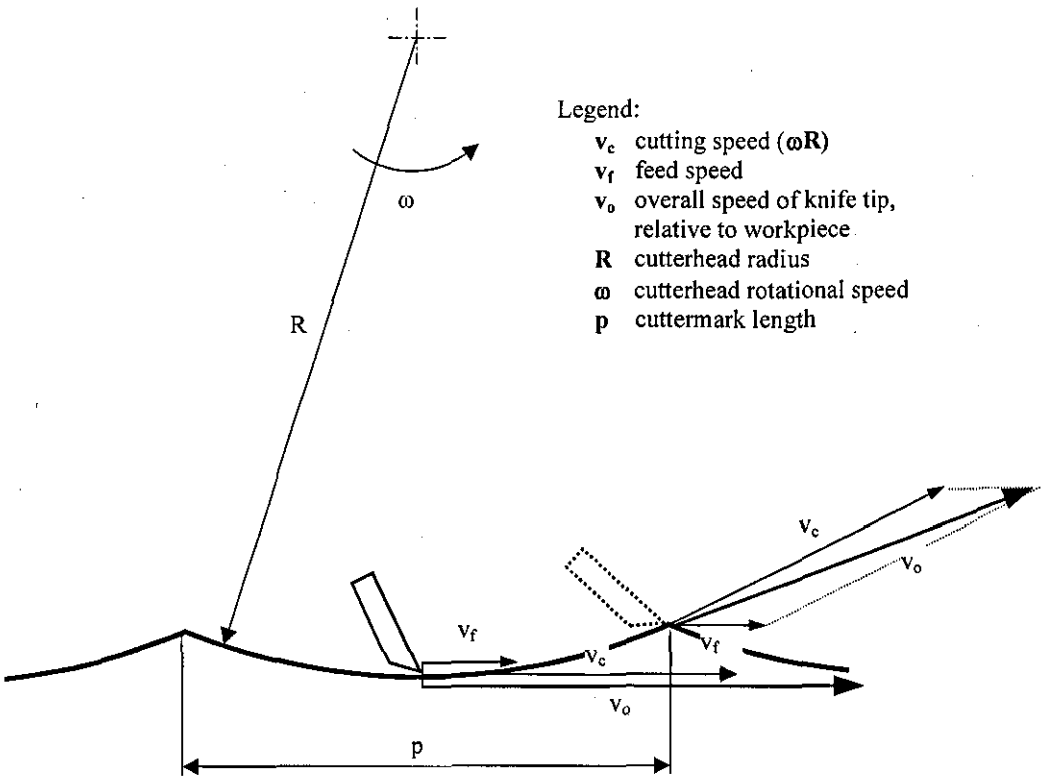

Figure A.2 Rotary machining process velocity relationships (Hynek 2004)

It is calculated as follows:

$$\vec{v}_o = \vec{v}_c + \vec{v}_f \tag{A.6}$$

The horizontal component of the knife tip velocity v_{ox} varies throughout the length of the cuttermark as can be seen from Figure A.2. However it can be taken as a constant throughout the length of the cuttermark p because the cutterhead angular displacement while the knife is machining one cuttermark is very small.

For instance, taking into account a typical cuttermark length (i.e.1.5 - 2,5 mm) and typical cutterhead radius R=60 mm, the angular displacement is approximately 0.7°. Thus the horizontal component of the knife tip velocity v_{ox} can be simplified as follows:

$$v_{ox} = v_f + v_c \tag{A.7}$$

Combining equations (A.1),(A.5) and (A.7) results in

$$d_t = \frac{p}{\mu + 1} \tag{A.8}$$

The time Δt_c that the cutterhead needs to travel a distance of d_t can be expressed as follows

$$\Delta t_c = \frac{d_t}{v_f} \tag{A.9}$$

Equation (A.9) can be rearranged into more practical form by inserting equations (A.8), (A.1) as follows:

$$\Delta t_c = \frac{p}{v_c + v_f} \tag{A.9}$$

The relative error between the cycloidal surface waviness height h_a and the circular waviness height of the surface h_c can be described as follows:

$$E_h = \frac{h_a - h_c}{h_a} \tag{A.9}$$

The dependence of the surface waviness height relative error on the ratio μ for N=4 is depicted in Figure A.3

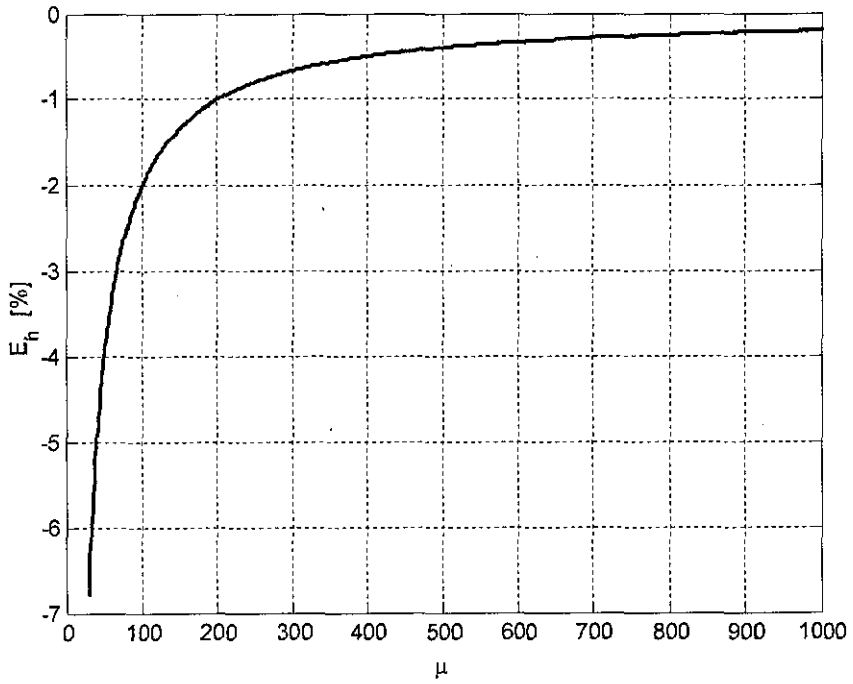

Figure A.3 Relative error between circular and cycloidal height (Hynek 2004)

The cycloidal surface waviness height described by equation (A.4) is always lower than the circular waviness height described by equation (A.3) as can be seen from Figure A.3. However, the error is very small (i.e. lower that 5%) for typical values of μ. This justifies the use of the surface waviness approximation by the circular arcs for the typical rotary machining process used within the woodworking industry as these equations are easier to deal with.

Appendix C PLANING TIMBER WITH AN ACTIVE MACHINING SYSTEM

Proceedings of the 18th Wood machining Seminar, Vancouver, Canada (2007).

Planing Timber with an Active Machining System

S. Elmas, M. R. Jackson, R. M. Parkin

Loughborough University, Wolfson School of Mechanical and Manufacturing Engineering, Mechatronics Research Centre, Holywell Way, LE11 3UZ Loughborough, United Kingdom

s.elmas@lboro.ac.uk

ABSTRACT

Planing and moulding are widely used within the wood working industry. According to the particular application, the surface of the machined timber is subject to a certain level of quality requirement. Undesired variations and disturbances within the machining process can often affect the consistency of surface quality. Especially, machining parameters, spindle vibrations and cutterhead inaccuracies have a great impact on the resultant surface waviness quality. In this paper some of these effects are demonstrated through simulation as well as through experimental work by a specially designed smart spindle unit which is controlled by four piezoelectric actuators. This spindle unit is used to produce surface waviness defects to order and thus improves understanding of the influence that cutter path inaccuracies have on machined surface quality.

Keywords—Active vibration control, piezoelectric actuator, surface finish, wood machining.

INTRODUCTION

Rotary machining has been an essential part of the woodworking industry for over two centuries and is applied to good effect in planing and moulding machinery. The principle of the rotary machining process is such that a timber is fed towards a rotating cutterhead containing a certain number of cutting knives. This process is illustrated in figure 1.

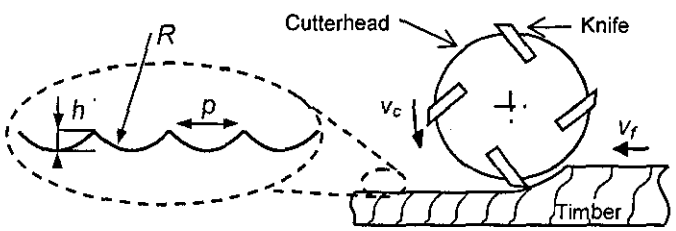

Fig. 1 Principle of rotary machining process

Rotary machined surfaces are not ideally smooth and flat. The machined surface has a series of waves due to the kinematics of the rotary machining process. The surface waves, also called cuttermarks, are generally accepted as unavoidable. The length of the cuttermark p, also called pitch, is usually taken as a measure of surface quality. A good surface finish should have a pitch p lower than 1.8 mm and surface waviness should follow a uniform pattern [1]. The length of the cuttermarks p is dependent on workpiece feed speed v_f, cutterhead rotational speed v_c and the number of finishing cutting knives N. This relationship can be expressed by the following equation:

$$p = \frac{v_f}{v_c \cdot N} \tag{1}$$

It is often assumed, for simplicity, that the shape of the cuttermarks is circular and that the surface can be considered as a series of intersecting circular arcs. The waviness height h of the simplified surface can then be expressed by the following equation:

$$h = R - \sqrt{R^2 - \frac{p^2}{4}} \tag{2}$$

Where as R is the cutterhead radius.

These equations (1) and (2) are well established and widely used [1]. Indeed, the shape of the cuttermarks is cycloid and the surface height is ca. 5% lower than the simplified height expressed by the equation (2) [2, 3]. This low error ratio justifies the use of surface waviness approximation by the circular arcs for rotary machining process used within the woodworking domain.

Although the modern planing machines provide a good surface quality, the undesired variations within the machining process do not guarantee a consistent surface quality. These variations can be divided into three major groups. Firstly, workpiece properties such as wood species and moisture content affect the surface quality. Secondly, machining parameters such as cutterhead speed, feed speed and number of cutting knives primarily determine the waviness form. Thirdly, undesired vibrations and inaccuracies within the machining process can reduce the surface quality severely. The subject of this paper is to demonstrate the effect of the latter factor on the machined surface.

REVIEW OF RELATED WORK

The presence of the vibrations during the machining process has an adverse effect on the surface quality. Vibrations mainly occur between the relative movements of the cutterhead and the workpiece. These vibrations can be suppressed by a passive or an active approach. The passive approach comprises tuned dampers and vibration absorbers. The active vibration control for the woodworking machinery is focused on controlling the

spindle vibrations. Some researchers developed design strategies for optimal spindle design in order to avoid the structural vibrations [4, 5]. Others [6, 7] used active vibration control methods to suppress the undesired vibrations in order to improve the overall performance. However, there is no significant record of research within the woodworking machinery regarding the effect of vibration factors such as cutterhead inaccuracies or spindle vibration on the machined surface [1].

Relatively small surface wave height values ranging from *2 – 20 μm* make the waviness highly susceptible to relative vibrations between cutting knives and the workpiece normal to the machined surface. This displacement can be caused by either structural vibration or by cutterhead inaccuracies. Two widely used techniques within woodworking domain, single-knife finish and multi-knife finish are presented and the effects of disturbances on the resultant surfaces are discussed [1].

Single knife finish exists where the surface wave form is determined by the cutter with the largest radius in the cutterhead. This results from the insufficient precision of the cutting knives due to the cutter sharpening machine tolerances and the relocation inaccuracies between grinding machine and planing machine spindles. The difference between the cutting knife with the largest radius and the cutting knife with the shortest radius is defined as the "total indicated run-out" (TIR). The difference among the cutting tool radii can reach up to 50 μm for knives set by hand in a cutterhead using a setting gauge. Cutters ground in the cutterhead and then relocated on the planing machine spindle using Hydrogrip tooling results in typically 5-10 μm TIR.

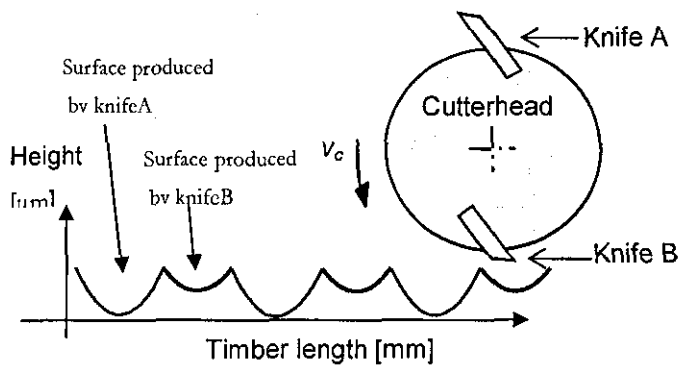

Fig. 2: The effect of inaccurate cutting knives on the surface finish

The hand set tooling leads to lower surface quality and reduces the performance of the machining operation (Fig. 2). For example, considering a cutterhead with two cutting edges and a TIR of *50 μm* located on a spindle rotating at *6000 rpm* with a timber feed of *12 m/min*. The resultant surface would have a pitch of *2 mm* which is in the low quality range, whereas with zero TIR, the ideal surface pitch would be *1 mm* which is a high quality finish (figure 3) because the number of finishing knives is now N=2.. This two knife case is actually the most exacting test of any tool grinder and planing machine because the two cutting edges are diametrically opposed and the slightest error (~ 1 μm) can create a noticeable waviness defect [1].

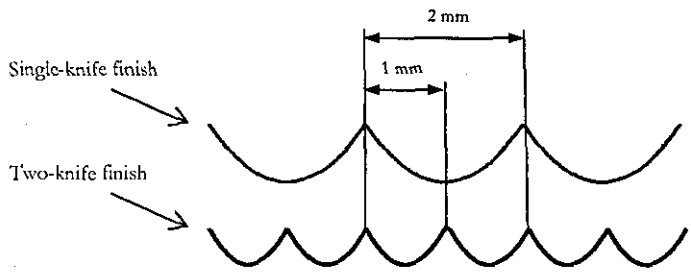

Fig. 3: The effect of single-knife finish and two-knife finish on the ideal surface form

Despite the deployment of high precision knives and the grinding of the knives in the cutterhead, the use of Hydrogrip tooling and super precision spindles the uniformity of the surface waviness with an acceptable surface quality for multi-knife finish, where all cutters leave an equal width surface wave, cannot be assured.

In high speed woodworking a machinery cutterhead can have up to 20 cutting knives. As it can be seen from equation (1), the greater the number of cutting knives the higher the timber feed speed for a given good quality (~1 mm) of wave pitch. The requirement for multi-knife finish is that all the cutting edges have the same radius. To realise this goal the jointing process is applied at the rotating cutterhead with the aim to true all the cutting edges to the same radius. The consequence of this jointing process is a cutter with zero back clearance angle that rubs the timber surface. All of the aforementioned precision improvement techniques have elevated the jointing process to a high level in order to reduce the rubbing effect, but it is still present. In addition the joint land width, determined by cutter tracking errors and also machine spindle/structural vibration, causes variations in normal cutting force (radial push off force) which produces cutter spindle deflection and hence variation in the cutter path. This presents a barrier to further surface finish improvements.

One particular case is where a four-knife cutterhead with cutters ground to the same radii is subject to a 1/rev displacement at the spindle rotational frequency [1]. Figure 4 shows that the cutting knives B and D are not affected by 1/rev vibration, whereas cutting knife A is pulled out of the workpiece and on the contrary cutting knife C is pushed into the workpiece by the vibration magnitude. This is shown for the case where the positive maximum of the vibration displacement aligns with cutter A. Variations in this particular case occur, depending on the phase relationship between the cutting knife rotational angle and the maximum or minimum point of the interfering with the 1/rev vibration cycle.

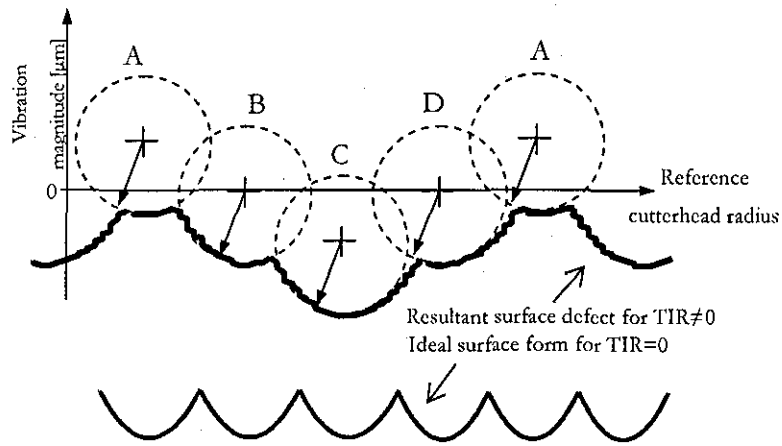

Fig.4: Effect of 1/rev spindle vibration on the surface

The resultant surface model in figure 4 is based on the circular arcs theory and represents a surface defect. Each cutting knife removes material from the surface with respect to their vibration magnitude. The resultant surface defect is superimposed by the adjacent circles in a plane representing the depth and length of the surface form. Figure 4 also demonstrates the greatest impact on the resultant surface, when the knife passing frequency coincides with the 1/rev vibration crest. It should be emphasized that the angular position of the cutterhead is not controlled on planing and moulding machines and so it is a lottery each time a cutterhead is placed on the machine spindle. When this surface defect is compared with the ideal surface form, the difference between the surface qualities is unacceptable. An alternative higher quality approach could actively vibrate the spindle centre in order to compensate for these vibrations and tooling inaccuracies. This needs a sophisticated control strategy to suppress and control the undesirable spindle vibrations as well as to remove the TIR values so that a consistent surface finish is achieved, with sharp cutters.

To date, it has not been possible to control the wood machining process so that the effect of specific disturbances such as cutterhead inaccuracies or cutterhead vibrations can be generated to confirm the theory presented. Although the systematic investigation reported [11] makes some attempt to understand some of the basic engineering influences on machine performance. The mechatronic control approach presented in this paper is capable of producing surface defects to order. Whilst this may seem at odds with reducing defects it is part of the wider understanding of how tool path inaccuracies cause surface waviness defects. A second benefit is to produce defective waviness surfaces so that human perception can be tested. A third benefit is for calibration standards for measurement equipment – especially optical sensing devices for surface assessment. This work builds on that previously reported [12].

MECHATRONICHS CONTROL APPROACH

The small scale planer consists of a base frame, on which the feed table and spindle system are mounted (Fig. 5) [12]. The smart spindle unit is the main part of the test rig. Four piezo electric actuators are mounted on the front bearing. Piezoelectric stack type actuators have been selected to control the movement of the front bearing, because they are able to provide high force, fast response and a controllable displacement in micrometer range. Two opposing actuators for each axis have been chosen in order to achieve a "push-pull" operation. This approach was also adopted by other researchers [8, 9]. Applying appropriate voltage levels to the piezoelectric actuators controls the movement of the spindle. The actuators are capable of moving the spindle by ±17 μm. Applying appropriate voltage levels to the piezo electric actuators controls the movement of the spindle in the plane perpendicular to the spindle's rotational axis.

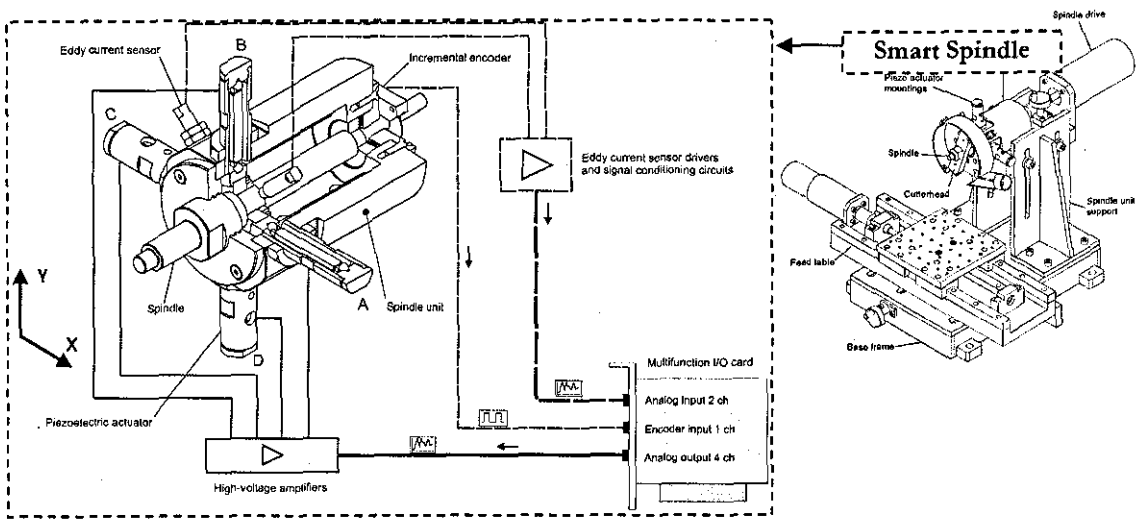

Fig. 5: Small scale planer comprising of a smart spindle unit

The smart spindle unit is a novel mechatronics control approach which comprises appropriate sensors, signal conditioning circuits, driving amplifiers and control computer in order to implement the controlled cutterhead movement. The system diagram of the test rig, shown in Fig. 5, shows all key components of the instrumentation along with the signal flow between the test rig and the control computer represented by the multifunction I/O card. The spindle unit is equipped with two non-contact eddy current sensors to measure the XY displacement of the spindle. The eddy current signals are then amplified with the eddy current driver in order to increase the resolution and minimize the influence of the noise. These signals are then converted into digital signals via the multifunction I/O card in the control PC. The smart spindle unit is also equipped with an incremental encoder in order to measure the angular position of the spindle. These two measures (XY displacement and the angular position of the spindle) are used as inputs to control software that determines the appropriate signal for the 150 Volt driver amplifiers that power the piezo electric actuators. The piezo actuators apply a force against the front spindle bearing mounted in flexural hinges to cause a controlled spindle radial

displacement. The Matlab xPC Target prototyping environment is used to carry out this real-time control application.

A vibration sweep test was carried out on the smart spindle unit fitted with a 0.65 kg cutterhead. Operating the spindle at speed close to one of the natural frequencies would result in excessive vibration and this must be avoided. It is often desirable to operate machine tools spindles below the natural frequency in order to avoid crossing any resonant regions during start up of the machine. Therefore, the natural frequency of the spindle experimentally determined which is at 885 Hz (Fig. 6)

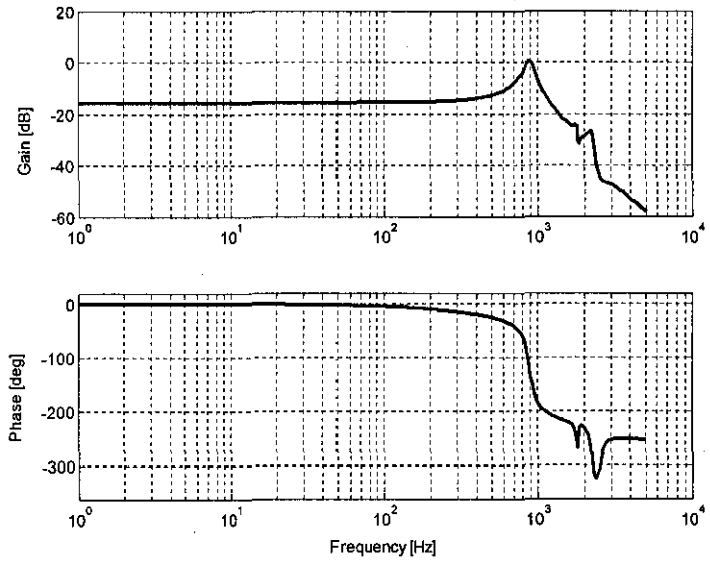

Fig. 6: Frequency response of the smart spindle unit

The test rig was designed to operate at spindle speeds below *5000 rpm (80 Hz)* and the experimental work was carried out at *600 rpm (10Hz)* which is well below the natural frequency of the spindle. Thus, any excessive vibration is avoided.

SIMULATION AND EXPERIMENTAL WORK

Simulation of the machined timber surface profiles has been carried out to assist in analysis of produced surface defects and to investigate the effects of disturbances independent of workpiece properties. Simulation is based on the principal of circular arc theory with an improved waviness height calculation algorithm that resembles the real height of the machined timber waviness. The smart spindle unit is used to generate machined timber samples to produce defects of a desired character.

Initial tests involved simply generating a single knife finish to compare the simulation of a perfect surface and that produced by the test rig with no radial displacement of the spindle centre. A cutterhead with two cutting knives is chosen with a TIR value of *70 μm* to ensure that only one cutter produces a finishing wave. The machined surface profile was measured by a contact based stylus tracer (Fig. 7).

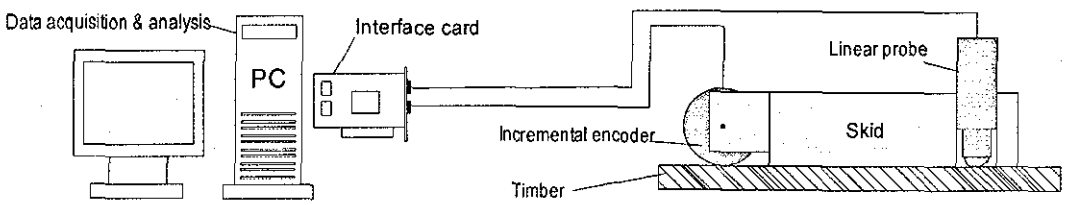

Fig. 7: Surface measurement system

With this surface measurement technique, the stylus tip contacts the machined surface and it is moved along the timber. The surface profile is recorded by the vertical movement of the stylus tip.

Figure 8 presents a reference simulated ideal surface produced by the knife with the larger cutting radius. Setting machining spindle speed to *400 rpm* with a feed speed of *30 mm/s* results according to the equations (1) and (2) in wave length *p* of *4.5 mm*. Analysis on the surface form with the Fast Fourier Transform (FFT) provides a better insight into the dominant wavelengths which form the resultant surface profile.

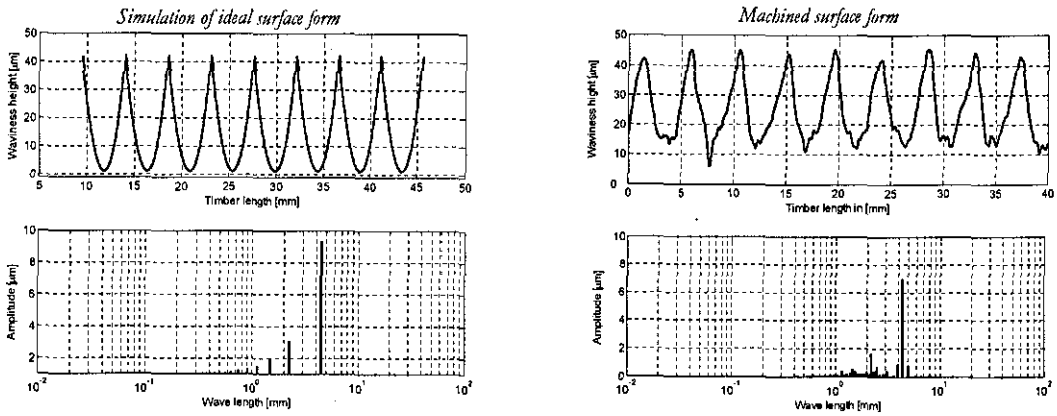

Fig. 8: Single-knife finish – simulated and machined surfaces in comparison

The simulated and machined surface forms are compared in Figure 8. Two graphs are shown to demonstrate the *single-knife finish*. Results from FFT analysis show that both simulated and machined surfaces have the dominant wavelength at *4.5 mm* which is the pitch of the resultant surface. It should be pointed out that the unit for the frequency is determined as *1/(unit length)* i.e. *1/mm,* which can be perceived as the number of cuttermarks per unit length.

Experimental work on surface defects has been performed with the small scale planer. These defects are successfully machined by a real time controlled displacement of the

cutterhead during the machining operation. The 1/rev case is reported here for a four knife cutterhead case. When the cutting knife first touches the surface of the workpiece, it starts to move vertically downwards with a defined pulse generated by the piezo electric actuators (Fig. 9). The height of the pulse correlates with the defined vibration amplitude. Only the upwards pulse is shown in figure 9.

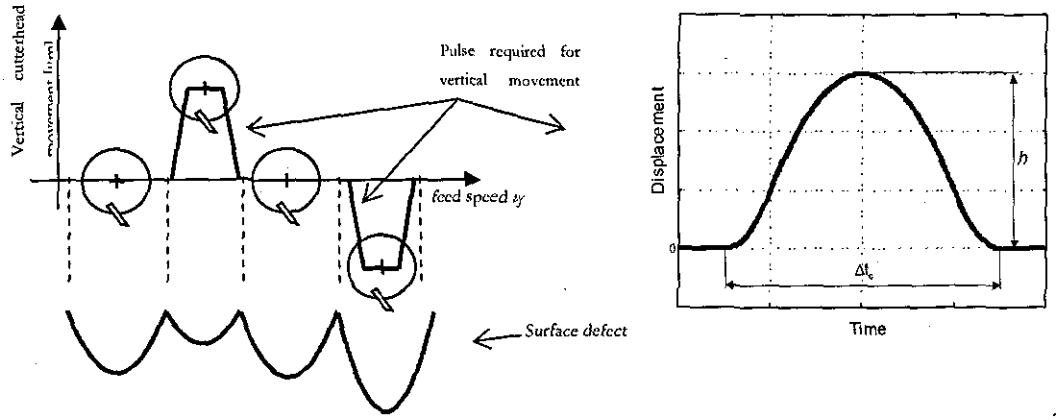

Fig. 9: Vertical cutterhead movement to produce surface defects

Figure 9 illustrates the vertical cutterhead movement, where the workpiece is stationary and the cutterhead travels along the workpiece. This modification is chosen for a better illustration of the cutterhead movement, since in the real machining operation, the cutterhead is fixed and the feed table moves towards the rotating cutterhead. For the experimental work, only one cutting knife is chosen to machine a specific surface defect. This allows generation of any type of interfering vibration and cutter inaccuracy profile via the software map generated in the control PC.

Figure 10 shows the surface defect caused by the 1/rev spindle vibration. Machining parameters are spindle speed v_c at *600 rpm* and feed speed at *20 mm/s.* The 1/rev spindle vibration frequency is set to the cutterhead speed with an amplitude of *3 μm* peak to peak. It can be observed that the surface profile does not consist of regular waves. For a normal machining operation (without spindle vibration) a wavelength of *2 mm* with *8.33 μm* of waviness height would be expected. For the additional spindle vibrations, the FFT analysis shows the dominant wavelength is at *2 mm* and also at *8 mm* which is four times larger than the expected value of wavelength under normal operating conditions. This is because knife C is pushed into the workpiece, hence cutting deeper while knife A is pushed upwards from the surface thus removing less material from the workpiece. This reflects the superimposed 1/rev spindle vibration introduced via the piezo-electric actuators. The resultant surface pitch is variable and does not have uniform pattern and is of reduced quality.

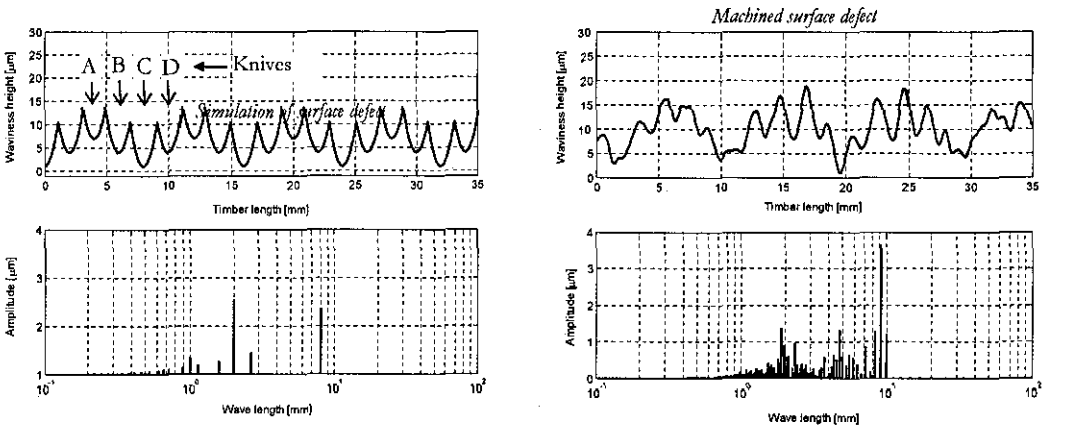

Fig. 11: Surface defect caused by 1/rev spindle vibration.

FFT analysis of the machined surface also shows that the surface waviness consists of more harmonic components than the simulated one this is due to the simulation which does not consider the inhomogeneous workpiece properties. Both simulated and machined surfaces shows that the effect of the undesirable spindle vibration on the resultant surface is evident.

CONCLUSIONS

The presence of the vibrations and cutting path inaccuracies during the machining process has a great impact on the resultant surface finish. Vibrations which mainly occur between the relative movements of the cutterhead and the workpiece can be caused by either structural vibrations or by cutterhead inaccuracies. The effect of the 1/rev spindle vibrations on the resultant surface is first simulated within the software program MATLAB/Simulink environment and then generated on a timber sample using a specially designed smart spindle unit. FFT analysis of machined timber surface traces indicates good correlation between simulated and actual surface frequency and amplitude characteristics. With this novel mechatronics control approach the effect of the spindle vibrations on the resultant surface can be made to order, thus aiding understanding of waviness generation mechanisms.

ACKNOWLEDGEMENTS

The authors would like to acknowledge the project funding body EPSRC - Innovative Manufacturing and Construction Research Centre at Loughborough University, UK.

REFERENCES

1. Jackson, M. R., Parkin, R. M., & Brown, N., "Waves on wood", Proceedings of the Institution of Mechanical Engineers, Part B: Journal of Engineering Manufacture, vol. 216, pp. 475-497, 2002.

2. Luo, G. Y., Osypiw, D., & Irle, M., "Surface quality monitoring for process control by on-line vibration analysis using an adaptive spline wavelet algorithm", Journal of Sound and Vibration, vol. 263, pp. 85-111, 2003.

3. Palmqvist, J., Lenner, M., & Gustafsson, S.-I., "Cutter head forces and load cell scanning", Wood Science and Technology, vol. 37, pp. 199-211, 2003.

4. Lee, D.-S. & Choi, D.-H., "Reduced weight design of a flexible rotor with ball bearing stiffness characteristics varying with rotational speed and load", Journal of Vibration and Acoustics, Transactions of the ASME, vol. 122, pp. 203-208, 2000.

5. Brandon, J. A. & Al-Shareef, K. J. H., "Optimization strategies for machine tool spindle-bearing systems: A critical review", Journal of Engineering for Industry, Transactions of the ASME, vol. 114, pp. 244-253, 1992.

6. Wang, X. G. & Sun, J. C., "Active sensing and control of vibration of circular saws - a comparison of optimal and variable structure control", Arlington, VA., pp 4294-4299, 2001.

7. Nagaya, K., Yamazaki, H., & Kashimoto, H., "Control of micro-vibrations of a machine head by using piezoelectric actuators", International Journal of Applied

   Electromagnetics and Mechanics, vol. 8, pp. 315-328, 1997.

8. Palazzolo, A.B., Lin, R.R., Alexander, R.M., Kascak, A.F., & Montague, J. "Test and theory for piezoelectric actuator-active vibration control of rotating machinery", Journal of Vibration, Acoustics, Stress, and Reliability in Design, 113, 167-175, 1991.

9. Dohner, J.L. , Lauffer, J.P., Hinnerichs, T.D., Shankar, N. , Regelbrugge, M., Kwan, C.-M., Xu, R., Winterbauer, B., & Bridger, K. "Mitigation of chatter instabilities in milling by active structural control". Journal of Sound and Vibration 269[1-2], 197-211. 2004.

10. Hynek, P., Jackson, M., R., Parkin, R., M., & Brown, N. "Improving wood surface form by modification of the rotary machining process". Proceedings of the Institution of Mechanical Engineers, Part B: Journal of Engineering Manufacture vo.213 No. 8, pp 875-887, 2004.

11. Jackson, M. R., Hynek, P. and Parkin, R. M., "On Planing Machine Engineering Characteristics and Machined Timber Surface Quality", Proc. IMechE Vol. 220 Part E: J. Process Mechanical Engineering, 16 pages, In Press 2006.

12. Hynek, P., Jackson, M., R., Parkin, R., M. and Brown, N., "Improvement of Rotary Machining Process", Proceedings IWMS17-2005, Rosenheim, Germany, Published by Retru-Verlag, pp 346-355, 2005.

Appendix D DEVELOPMENT OF A MONITORING SYSTEM FOR A SMART PLANING MACHINE FOR REAL-TIME OPERATION

Proceedings of the 11th Mechatronics Forum Biennial International Conference, Limerick, Ireland (2008).

Development of a Monitoring System for a Smart Planing Machine for Real-Time Operation

S. Elmas, M. R. Jackson[1], H. Wuerdemann, R. M. Parkin

Mechatronics Research Centre,
Wolfson School of Mechanical and Manufacturing Engineering,
Loughborough University
Loughborough, Leicestershire, LE11 3TU, United Kingdom

ABSTRACT

In planing and moulding which are commonly used within the woodworking industry, surface defects, torn and raised grain result in high production costs. In order to meet the requirements for a consistent surface quality and increased production efficiency, surface quality information is needed for enhanced process control. Whilst some techniques have been researched based on optical sensing these are too bulky to fit near to the machining process. Furthermore these optical sensing systems are costly and generally sophisticated image processing algorithms which require a considerable computation time are required to measure the surface profile. Therefore additional real-time surface feature extraction is desirable. The objective of this paper is to introduce a novel surface profile re-creation strategy which can potentially be employed for the real-time operation as feedback for a smart planing system. In this method spindle speed and spindle vibrations are measured in real-time to re-create the machined surface profile. Numerical analysis and experimental work have been carried out to demonstrate the capabilities of this technique.

1. INTRODUCTION

The dynamic behaviour of wood machining process has a negative impact on the surface quality of machined timber. The dynamic behaviour is due to the factors such as workpiece properties, cutting tool condition, engineering quality of the machine, cutterhead vibrations, spindle imbalance [1, 2]. Although modern planing machines are capable of providing good surface finish, they are highly susceptible to machine system variations. These variations are reflected to the machined surface, resulting in unacceptable quality levels. Therefore it is essential to deploy a feedback system in order to ensure the product quality and increase the efficiency by minimizing the variations during the machining process. Various surface profile measurement systems have been developed in recent years for an automated environment. The measurement techniques can be classified into two main groups; contact based and non-contact methods.

The nature of the wood machining process (i.e. high feed speed > 1m/sec, machined surface features < 5 μm, and high inherent surface texture of the timber > 20 μm), rules out tactile surface measurement techniques such as mechanical stylus. For this method, the stylus tip contacts the machined surface and it is driven along the workpiece and the surface profile is recorded by the vertical movement of the stylus tip. The two main drawbacks associated with this technique are the lack of measurement speed and the loading effect of the stylus tip which lead to deformation on the surface [3]. Moreover this method is not suitable for surface profile measurement of timber machined at high throughput rates, since the stylus tip tends to jump at high measuring speed (i.e. 1 – 2 m/sec). This "bouncing" effect occurs when the stylus tip loses contact with the machined

1 Corresponding author: Tel.: (+44) 1509-226571; Fax: (+44) 1509-226577; E-mail: m.r.jackson@lboro.ac.uk

surface which limits its in-process deployment. In order to monitor the quality of machined surfaces, various non-contact measurement techniques have been deployed over the years. Most of the methods used for non-contact measurements are optical method which include optical profilometers (mostly laser based), microscopes, image analyzers, imaging spectrographs, interferometers, fibre-optic transducers, white-light speckles, laser scattering, optical light sectioning systems [4, 5, 6, 7]. Most of these non-contact based methods are too expensive, bulky and lack the measurement speed due to the sophisticated image processing algorithms, thus they are not sufficient for applications where real-time control action is required. These drawbacks limit their application range for an automated process environment. Therefore an additional surface profile extraction is desirable to assist the optical methods which would enable real-time control action during the machining process. This paper introduces a new surface profile re-recreation method by considering the spindle speed and spindle vibration during the machining operation.

1.1 WOOD MACHINING PROCESS

Rotary machining has been an essential part of the woodworking industry for over two centuries and is applied to good effect in planing and moulding machinery. The principle of the rotary machining process is such that timber is fed towards a rotating cutterhead containing a number of cutting knives. This process is illustrated in figure 1.

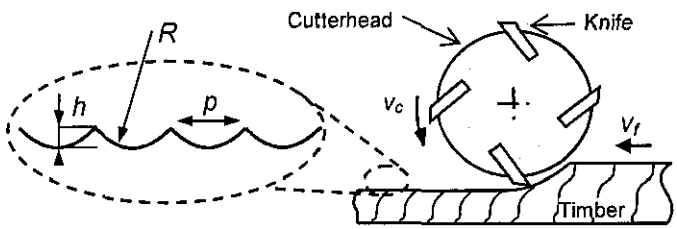

Fig. 1 Principle of rotary machining process

Rotary machined surfaces are not ideally smooth and flat. The machined surface has a series of waves due to the kinematics of the rotary machining process. The surface waves, also called cuttermarks, are generally accepted as unavoidable. The length of the cuttermark p, also called pitch, is usually taken as a measure of surface quality. A good surface finish should have a pitch p lower than 1.8 mm and surface waviness should follow a uniform pattern. The length of the cuttermarks p is dependent on workpiece feed speed v_f, cutterhead rotational speed v_c and the number of finishing cutting knives N. This relationship can be expressed by the following equation:

$$p = \frac{v_f}{v_c \cdot N} \tag{1}$$

It is often assumed, for simplicity, that the shape of the cuttermarks is circular and that the surface can be considered as a series of intersecting circular arcs. The waviness height h of the simplified surface can then be expressed by the following equation:

$$h = R - \sqrt{R^2 - \frac{p^2}{4}} \tag{2}$$

where R is the cutterhead radius. These equations (1) and (2) are well established and widely used [1, 2]. Indeed, the shape of the cuttermarks is cycloid and the surface height is ca. 5% lower than

the simplified height expressed by the equation (2) [8]. This low error ratio justifies the use of surface waviness approximation by the circular arcs for rotary machining process used within the woodworking domain [1].

1.2 SMART PLANING SYSTEM

A new surface profile re-creation method is intended to be used as a feedback loop for a smart planing system designed within the Mechatronics Research Centre at Loughborough University (Fig 2) [9]. The smart planing system consists of a base frame on which the feed table and spindle system are mounted. The smart spindle unit is the main part of the test rig. Four piezoelectric actuators are mounted on the front bearing. Two opposing actuators for each axis have been chosen in order to achieve a "push-pull" operation. Applying appropriate voltage levels to the piezoelectric actuators controls the movement of the spindle. The smart spindle unit is a based on mechatronics control approach which comprises appropriate sensors, signal conditioning circuits, driving amplifiers and control computer.

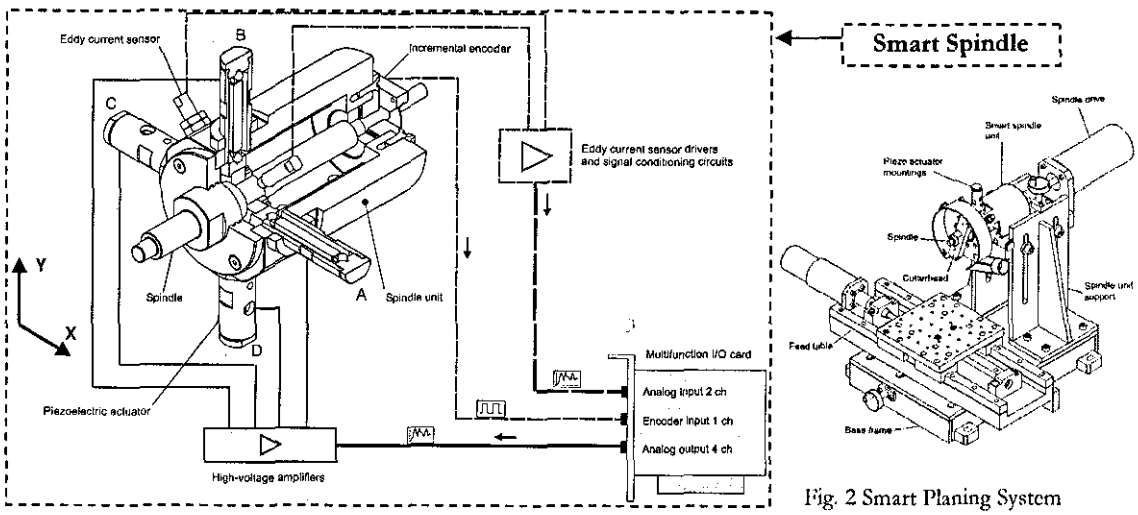

Fig. 2 Smart Planing System

The spindle unit is equipped with two non-contact eddy current sensors to measure the XY displacement of the spindle. These signals are then converted into digital signals via the multifunction I/O card in the control PC. The smart spindle unit is also equipped with an incremental encoder in order to measure the angular position of the spindle. These two measures (XY displacement and the angular position of the spindle) are used to asses the surface profile in real-time. The Matlab xPC Target prototyping environment is used to carry out this real-time control application. The proposed monitoring system will detect the spindle vibrations and spindle speed in-process and feed the control algorithm with information about the current surface quality. Thus, the new proposed smart planing system will be able to adapt the spindle displacement in real-time to the current surface waviness. As a result of this machining process, the disturbances and the machining variability will be reduced and a consistent and improved surface quality will be achieved.

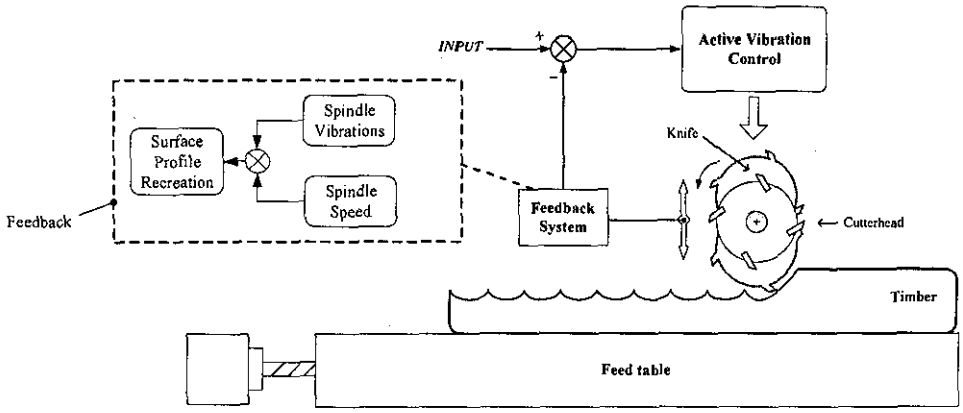

Fig. 3: Active vibration control strategy with a feedback system

2 NOVEL SURFACE PROFILE RE-CREATION TECHNIQUE

For any dynamic optimization of the machining process with the focus on an increased surface quality, characteristics of those vibration components can be used in a feedback loop so that the control system can compensate for it. The feedback system is mainly focused on cutterhead vibrations and cutterhead speed. Figure 3 shows the monitoring system integrated within the controller. Spindle vibrations are measured with the eddy current probes and the spindle speed is monitored via an incremental encoder. From these sensors output, surface profile of the machined timber is re-created and then compared with the input values. For example if the spindle speed is set to *600 rpm* and the feed speed to *20 mm/s* then according to the equation (1) and (2) the pitch is *2 mm* with *8.33 μm* of height. These values are taken as input parameters which are compared with the re-created surface pitch and height.

2.1 SURFACE PROFILE RE-CREATION BY USING SPINDLE SPEED

During the machining process, the spindle speed is monitored by an incremental encoder. The encoder is counting two thousand pulses for each revolution. The time that the cutterhead needs to perform one revolution is extracted from these readings. When the spindle speed is monitored over the whole machining cycle, from figure 4 it can be seen that the spindle speed is varying during the machining process.

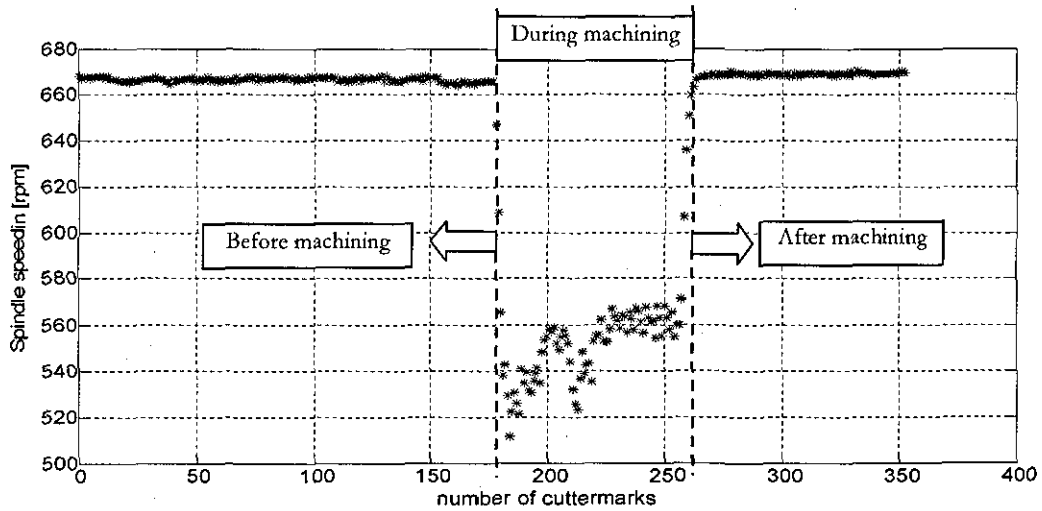

Fig. 4: Variation of the spindle speed during the machining process

Since the spindle speed is measured, the surface profile characteristics such as pitch and height can be calculated by the equations (1) and (2) respectively. The calculated pitch and corresponding heights are shown in figure 5.

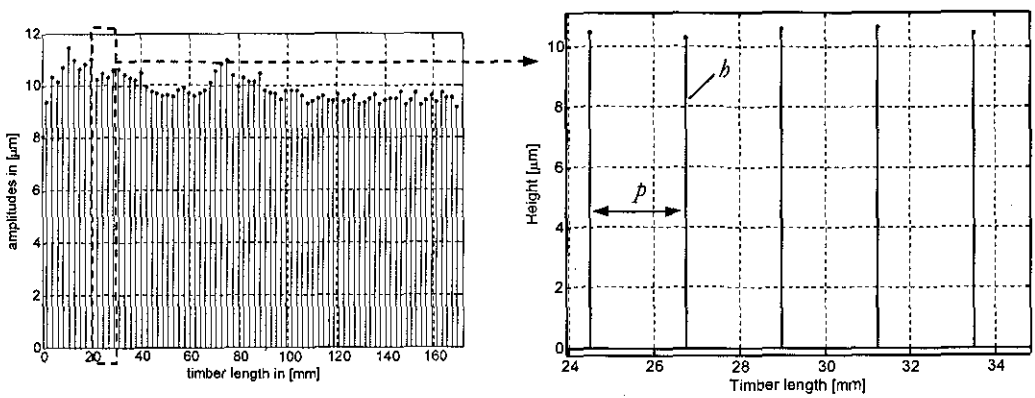

Fig. 5 Re-created surface profile by using spindle speed

In order to assess the performance of the introduced method, the same machined profile is also measured via a contact based stylus tracer for comparison reasons only, because during the machining operation the surface quality will solely be assessed by the feedback system.

As it is shown in table 1, the difference between the mean pitch values and the re-created and measured surface profile is at about 3 % which is in a good agreement, however the re-created surface profile does not take the work piece properties as well as the dynamic behaviour of the machining process (i.e. vibrations between workpiece and cutterhead) into account. Spindle vibrations can cause severe surface defects, hence reduce the surface quality immensely. The effect of spindle vibrations on the machined surface has extensively been studied in [2] and proved through simulation and experimental work in [1]. Therefore this method has been further improved by analysing and considering spindle vibrations which enables a more reliable monitoring system with accurate surface profile information.

2.2 SURFACE PROFILE RE-CREATION BY USING SPINDLE VIBATION

The spindle vibrations are measured via eddy current probes during the machining process. Figure 6 shows the spindle vibrations during the cutting process where the time for one vibration event caused by one cuttermark is expanded along the time axis.

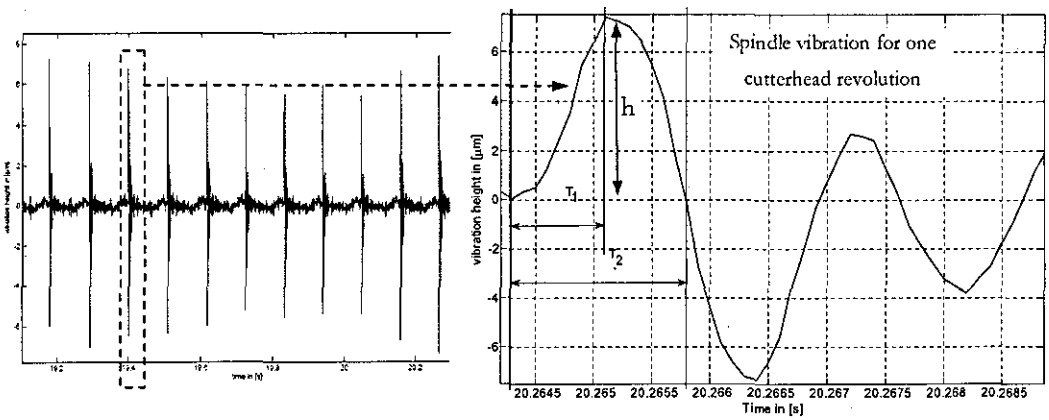

Fig 6: Spindle vibrations during the machining process

Spindle vibration magnitudes as well as spindle speed vary during the machining operation. The vibration magnitudes are extracted via programming code within Matlab. As it can bee seen from figure 2, eddy current probes do not provide the vibrations at the tool tip, as they are located on the front bearing. Therefore these vibration magnitudes are extrapolated from the node of the measurement to the tool tip by considering the geometry as well as the dynamic characteristics of the spindle through an FEM model. The FEM model of the spindle revealed that the displacement of the tool tip and the node of measurement are in the same direction for the first vibration mode. However at higher frequencies where higher vibration modes become involved the extrapolation is more complicated. Especially at the second vibration mode of the spindle system, the displacement of the measurement node and the tool tip node are in opposite directions. Therefore a simple extrapolation with a factor is only reliable for the frequencies below the first vibration mode of the spindle. Considering the fact that vibrations caused during the machining operation can be arbitrarily and contain higher vibration modes, an extrapolation through FEM is carried out, thus the introduced method is capable of providing reliable and accurate information about the surface profile over a wide range of frequencies. The pitches p are then calculated by rearranging the equation (2) and shown in figure 8. The re-created surface profile from spindle vibrations are in a good agreement with both previous methods. The deviation from the measured mean pitch value is less than 3 % with less than 2 µm divergence from the mean surface heights. This relatively high accuracy and the straightforward instrumentation make this method suitable for surface profile monitoring purposes within the planing operation.

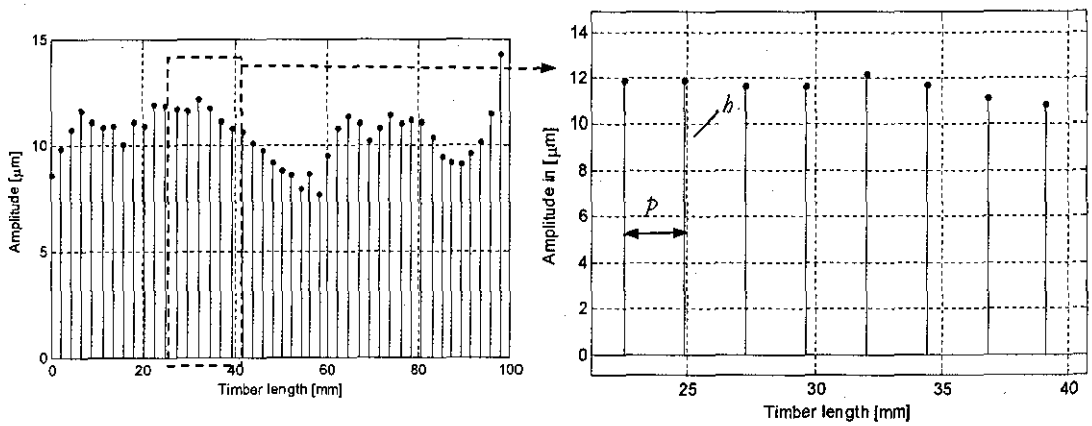

Fig 8: Surface profile recreation by using spindle vibrations

Table 1: Comparison among the simulated, measured and re-created surface profiles

	Simulated ideal surface	measured surface with stylus	re-created surface from spindle speed	re-created surface from spindle vibration
p_{mean} [mm]	2.0	2.11	2.18	2.16
h_{mean} [µm]	8.33	11.66	9.89	10.11

3. SUMMARY AND CONCLUSIONS

The dynamic behaviour of wood machining process has a negative impact on the surface quality. In order to meet the quality requirements, surface profile information is needed for enhanced process control. Most of the surface profile in-process monitoring systems are either too expensive, bulky or too slow to feed the control system with real-time information. A method comprising of two steps has been introduced which can potentially be employed for planing operation where real-time control action can be performed. The first step is the re-creation of the surface profile by analysing the spindle speed of the smart planing system. This method shows relatively accurate surface profile information, however it is not capable of classifying surface defects caused by the spindle vibrations. Therefore a second complementary step has been introduced which considers the dynamic behaviour of the spindle system during the machining operation. The vibrations caused during the machining operation are captured and the surface profile is re-created. These two steps allow a classification of the surface profile relatively accurately when compared with the surfaces traced by the mechanical stylus. With this method the surface profile information can be obtained with only two sensors (i.e. eddy current probes and incremental encoder) which make it cost effective and easy to implement. Furthermore it can provide surface profile information where real-time control action is required.

ACKNOWLEDGEMENTS

The authors would like to acknowledge the project funding body EPSRC - Innovative Manufacturing and Construction Research Centre at Loughborough University, UK.

REFERENCES

[1] *Elmas, S., M.R. Jackson, and R.M. Parkin. Planing timber with an active machining system. Proceedings of the 18th Wood Machining Seminar, pp 107-115, Vancouver, Canada, 2007.*

[2] *Jackson, M.R., R.M. Parkin, and N. Brown, Waves on wood. Proceedings of the Institution of Mechanical Engineers, Part B: Journal of Engineering Manufacture, 216(4): p. 475-497, 2002.*

[3] *Yang, D., M. Jackson, and R. Parkin, Inspection of wood surface waviness defects using the light sectioning method. Proceedings of the Institution of Mechanical Engineers, Part I: Journal of Systems and Control Engineering, 220(7): p. 617-626, 2006.*

[4] *Sandak, J. and C. Tanaka, Evaluation of surface smoothness by laser displacement sensor 1: Effect of wood species. Journal of Wood Science, 49(4): p. 305-311, 2003.*

[5] *Shinozaki, R., O. Sasaki, and T. Suzuki, Fast scanning method for one-dimensional surface profile measurement by detecting angular deflection of a laser beam. Applied Optics, 43(21): p. 4157-4163, 2004.*

[6] *Sandak, J. and C. Tanaka, Evaluation of surface smoothness using a light-sectioning shadow scanner. Journal of Wood Science, 51(3): p. 270-273, 2005.*

[7] *Yang, D., M. Jackson, and R. Parkin. Measuring cutter marks on wood surfaces with machine vision techniques. 17th International Wood Machining Seminar, Rosenheim, Germany 2005.*

[8] *Luo, G. Y., Osypiw, D., & Irle, M., "Surface quality monitoring for process control by on-line vibration analysis using an adaptive spline wavelet algorithm", Journal of Sound and Vibration, pp. 85-111, vol. 263, 2003.*

[9] *Hynek, P., Jackson, M., R., Parkin, R., M., & Brown, N. "Improving wood surface form by modification of the rotary machining process". Proceedings of the Institution of Mechanical Engineers, Part B: Journal of Engineering Manufacture vol.213 No. 8, pp 875-887*

Appendix E ANALYSIS OF PROFILE MEASUREMENT TECHNIQUES EMPLOYED TO SURFACES PLANED BY AN ACTIVE MACHINING SYSTEM

Proceedings of the Institution of Mechanical Engineers, Part E: Journal of Process Mechanical Engineering

This journal paper is currently under review.

Analysis of Profile Measurement Techniques Employed to Surfaces Planed by an Active Machining System

S Elmas, N Islam, M R Jackson, R M Parkin

Mechatronics Research Group, Loughborough University, Loughborough, UK

Abstract

The importance of a reliable and robust surface profile measurement system in the inspection of surface finish is beyond any doubt. For years, visual inspection has been employed in the industries to determine the quality of surface finish. Since, in most cases, it fails to ensure a consistent minimum standard of finish quality, mechanical stylus based measurement systems have successfully taken over from human inspection. However, in recent years, the trend is to explore other techniques for conducting the surface profile measurements. Non-contact optical methods have emerged as one of the leading candidates. One of most important aspect of using non-contact methods is avoiding damage to the machined surface for softer materials. In this paper, analysis of surfaces machined with an active mechatronic planar has been discussed. Mainly two kinds of materials have been used for the planing operation, one is made up of nylon and the other is hard wood. The surface profile of machined specimens is measured with the help of light-sectioning method, conventional mechanical stylus and a novel two-image photometric stereo method. An industry-standard Talysurf CLI system was used

to provide the benchmark, traceable to NPL standards, for the measurements. Suitability of different measurement techniques have been discussed based on the results obtained.

Keywords: active machining system, non-contact surface profile measurements, light sectioning method, mechanical stylus, two-image photometric stereo method, Talysurf.

1 Introduction

Wood machining is an essential part of the furniture and wooden product manufacturing industry. This speeds up the whole process as well as maintaining the quality of product finish [1]. Machining of wood consists of various processes such as sawing, rough planing, planing, moulding, sanding and so on. Among all these, two widely employed processes in wood machining industry are planing and moulding [2]. In order to carry out these machining operations, rotary machining technique has been used in industry for over two centuries [3]. It is a very well established fact that the rotary machining operation is able to provide the woodworking industry with the required surface finish of products coupled with the desired speed, lower labour cost and thus, cost-effectiveness. In the current ultra competitive business environment these are the required attributes for a manufacturing establishment to survive and prosper. During the process of planing, the cutter heads contain straight cutters on all the four faces [4]. The rotary wood machining process is similar in nature to the up-cut milling of metals

[5]. Although, the milling operation is similar to the one of metal working, there are some significant differences between the two processes. The primary one is the cutting speed. Whilst cutting speed for metal lies in the region of 0.5 to 1.5 m/s, the wood machining speed is in the region of 30 to 80 m/s. Also, the feed speed of the woodworking process is higher, at around 0.08 to 1.6 m/s [6]. Due to kinematics of the machining process, planed and moulded surfaces appear to have a series of waves whose peaks are perpendicular to the passage of the product through the machine [6]. However, these cutter-marks or waviness as termed in the woodworking industry are actually not defects, if the their heights and widths are small and uniform [7]. In order to ensure that this waviness is consistent and of acceptable patterns, a range of contact and non-contact accurate measurement techniques have been deployed over the years. Despite advances in other technologies, mechanical stylus based contact measurement remains the most widely used surface measurement system. This is essentially a slow and often destructive method of obtaining surface profile but has wide acceptability due to very well-established standards [8]. Advancements towards ever increasing levels of automation, higher speed of processes and the advent of various soft materials have caused this contact method to become inadequate in certain situations. As a result, non-contact methods are proving to be the way forward for measurement applications involving timber and similar softer materials. A brief literature review of the surface planing technique has been presented in this paper, along with some of the surface profile measurement techniques. In the latter part of the

paper, a comparative analysis of surface profile measurements is carried out using four different measurement techniques.

2 Timber Surface Forming

The dynamic behaviour of wood machining process has a negative impact on the surface quality of machined timber. The dynamic behaviour is due to the factors such as workpiece properties, cutting tool condition, engineering quality of the machine, cutterhead vibrations, spindle imbalance. These variations are reflected to the machined surface, which can reach unacceptable quality levels. In moulding and planing which are commonly used within the woodworking industry, surface defects, torn and raised grain result in high production costs [1]. This rotary machining process is similar to milling of metals in up-cutting mode. The principle of the rotary machining process is such that a timber is fed towards a rotating cutterhead containing a certain number of cutting knives. This process is illustrated in figure 1.

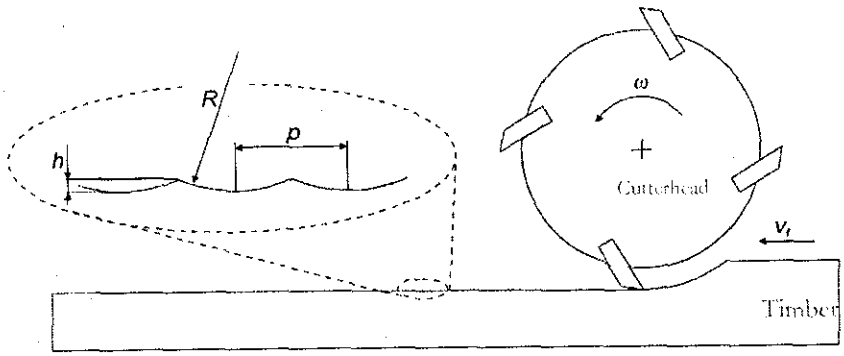

Figure 1 Rotary machining principle

The machined surface has a series of waves due to the kinematics of the rotary machining process. The surface waves, also called cuttermarks, are generally accepted as unavoidable, therefore machined surfaces are not ideally smooth and flat. The length of the cuttermark p, also called pitch, is usually taken as a measure of surface quality. A good surface finish should follow a uniform pattern. The length of the cuttermarks p is dependent on workpiece feed speed v_f, cutterhead rotational speed v_c and the number of finishing cutting knives N. This relationship can be expressed by the following equation:

$$p = \frac{v_f}{v_c \cdot N} \tag{1}$$

It is often assumed, for simplicity, that the shape of the cuttermarks is circular and that the surface can be considered as a series of intersecting circular arcs. The waviness height h of the simplified surface can then be expressed by the following equation:

$$h = R - \sqrt{R^2 - \frac{p^2}{4}} \tag{2}$$

where as R is the cutterhead radius. These equations (1) and (2) are well established and widely used. Although the modern planing machines provide a good surface quality, the undesired variations within the machining process do not guarantee a consistent surface quality. The presence of the vibrations during the machining process has an adverse effect on the surface quality. Vibrations mainly

occur between the relative movements of the cutterhead and the workpiece. Relatively small surface wave height values ranging from *2 – 20 μm* make the waviness highly susceptible to relative vibrations between cutting knives and the workpiece normal to the machined surface. This displacement can be caused by either structural vibration or by cutterhead inaccuracies. The effects of these disturbances are summarized in [3, 9].

In order to produce some specimens for the surface profile measurement systems a mechatronics approach based small scale planer is used (Fig 2). One of the advantages of the small scale planer is the ability to produce various surface qualities to order which means that the limitations as well as the quality of the measurement systems can be assessed and compared. Thus the reliability of the surface profile measurement systems can be compared more precisely.

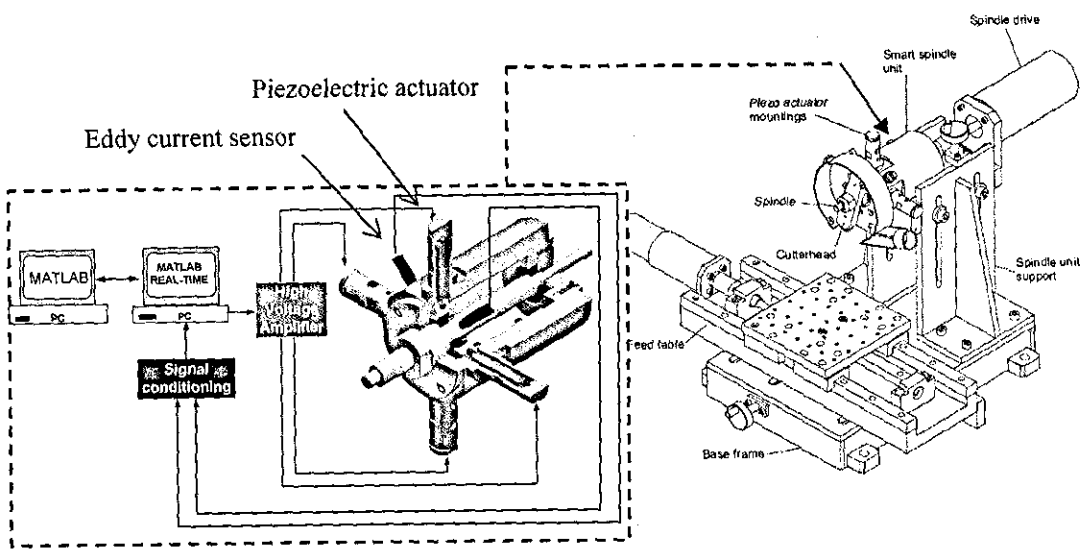

Figure 2 Smart planing system

The small scale planer consists of a base frame, on which the feed table and spindle system are mounted (Fig. 2) [10]. The smart spindle unit is the main part of the test rig. Four piezoelectric actuators are mounted on the front bearing. Piezoelectric stack type actuators have been selected to control the movement of the front bearing, because they are able to provide high force, fast response and a controllable displacement in micrometer range. Two opposing actuators for each axis have been chosen in order to achieve a "push-pull" operation. This approach was also adopted by other researchers [9, 11]. Applying appropriate voltage levels to the piezoelectric actuators controls the movement of the spindle in the plane perpendicular to the spindle's rotational axis. These capabilities of the smart spindle unit allow a higher degree of freedom in terms control over machining process. The smart spindle unit is a novel mechatronics control approach which comprises appropriate sensors, signal conditioning circuits, driving amplifiers and control computer in order to implement the controlled cutterhead movement. The system diagram of the test rig, shown in Fig. 2, shows all key components of the instrumentation.

Two widely used techniques within woodworking domain, single-knife finish and multi-knife finish are produced with the small scale planer to assess the measurement techniques whereas the latter one has been produced with a controlled generated disturbance the so called 1/rev vibration. A more detailed description of the various surface defects can be found in [3, 4]. The defect is machined on a black plastic sample in order to reduce the effect of workpiece

properties such as roughness. This defect as well as the single knife finish specimens are then measured with all four measurement devices for comparison. The measurement techniques are introduced in section 3.

3 Surface Profile Measurement Systems

The profile measurement systems currently being used in industry to obtain surface characteristics can be divided into two main groups – contact and non-contact methods.

3.1 Contact Method

The most common method of obtaining surface profile data is to pass a mechanical stylus probe across the surface and trace the movement of the probe to obtain surface profile information [12]. This is essentially a contact method for obtaining the surface data. These measurements are usually carried out in the micrometer range for most industrial applications. However, techniques to use mechanical profilometers in finer nanometre range have been explored in publications by Garratt and Nettleton [13], Whitehouse *et al* [14] and in a more recent research by Groeger *et al* [15]. The nanometre range measurements have found applications in wide ranging fields of manufacturing laser optics, electro optic devices, semi-conductors, computer memory devices etc. [15].

The contact based measurement system suffers from various drawbacks. One of the main drawbacks associated with this technique is the loading effect of the

stylus tip on the surface under test. This can lead to the deformation of the surface, especially for softer surfaces like wood, nylon etc. Also, the speed of measurement is somewhat slow, thus making this technique unsuitable for on-line measurements [7].

3.2 Non-contact Methods

Most of the methods used for non-contact measurements are optical method. These include optical profilometers (mostly laser based), microscopes, image analyzers, imaging spectrographs, interferometers, fibre-optic transducers, white-light speckles, laser scattering, optical light sectioning systems, etc. According to research published in [7], the optical methods can be classified into three categories according to their principle of operation –

- Triangulation sensing
- Shadow analysis
- Light sectioning

Equipment using triangulation sensors or auto-focusing sensors to measure surface quality is sometimes referred to as an optical profilometer. In fact, the optical profilometer is similar to the stylus profilometer in many aspects. The major difference is that the optical profilometer uses a non-contact 'optical stylus', while the stylus profilometer uses a contact stylus. A laser displacement sensor (LDS) based surface profile measurement system has been proposed in [16] as well as in [17] and [18]. This method uses the aforesaid triangulation

measurement approach. Laser light emitted by a semiconductor laser diode passes through a transmitter lens and is focused on the target surface. The reflected light is focused on a position-sensitive detector (PSD) after passing through a receiver lens. The detector uses the distribution of the entire beam spot entering the light-receiving element to determine the beam spot centre of gravity and identifies it as the target position. Of the LDS's distance to the measured surface changes, the position of the reflected spot on the detector changes proportionally. This process can be correlated to the smoothness of the measured surface.

Another method of evaluating the surface smoothness is the shadow sectioning method. Sandak and Tanaka [19] as well as Yang *et al* [20] have used this technique to evaluate machined wood surface. Light emitted with a fixed small angle to the surface plane by a projector is directed onto the measured surface. A curtain installed in the light path close to the surface creates a shadow on the measured surface. The shape of the border between bright and dark is a profile section of the surface. A camera installed over the surface captures an image of the border and a digital signal processor using image analysis techniques digitizes the profile section. In general, the shadow analysis method cannot measure surface heights.

Researchers in [21, 22] have proposed sensors based on light sectioning principle to measure the surface profile of fabric and width of steel plates respectively. In a more recent and relevant research [7], this light sectioning method has been used

to determine the surface profile of wood. This method requires oblique illumination and a laser light stripe is projected from the side of the sample on to the surface to produce light section. The light section is actually a wavy line produced by the projected light due to the waviness of the surface under test. Also, there is a triangular relationship between the height of the cutter mark wave H, and the height of its corresponding wave L in the light section. This can be given by equation (3).

$$H = L\tan\theta \tag{3}$$

where, θ is the angle of incidence of the projected light with respect to the surface. Thus, by measuring the wavy line, i.e. the light section, the widths and heights of cutter mark waves on the surface can be calculated.

A more robust extension of the light-sectioning concept is the two-image photometric stereo method. This has been discussed in detail in [23]. In this method, two suitable identical light sources are located opposite to each other and along the direction of the cutter-mark of the machined material. Two images using a high resolution camera are then taken, with only light source 1 turned on and only light source 2 turned on respectively. The radiance of the surfaces can be measured using the camera in the form of pixel intensities in the images. This pixel intensity can in turn be used to obtain the surface gradient of the machined surface. A novel algorithm is then used to obtain the surface shape in two-

dimension. The details of this technique are beyond the scope of this paper and will be reported in future publications.

4 Experimental work

This section of the paper gives a brief overview of the measurement setups and equipments used for the surface profile measurements. The following sub-sections look into the Talysurf measurement system from Taylor Hobson Ltd., mechanical stylus instrument, light-sectioning method and the photometric stereo method.

4.1 Talysurf CLI

The Talysurf (figure 3) is the most widely used surface metrology equipment in industry [24]. This equipment comes with various instruments including both contact and non-contact probes. However, the results produced in this paper are all obtained by the laser-based instrument mounted on the machine. The Talysurf system is calibrated with standardised artefacts and the calibrations can be traced back to the NPL standards (UKAS certificate number 29248). The system consists of a precision X-Y translation table to hold the sample underneath the probes and provide the scanning motion. The stand-off distance (Z-direction) of the Talysurf can be adjusted to achieve focusing of the probe. The Talymap software from Taylor Hobson is used for data acquisition and processing. A typical generated surface from Talymap is shown in figure 4.

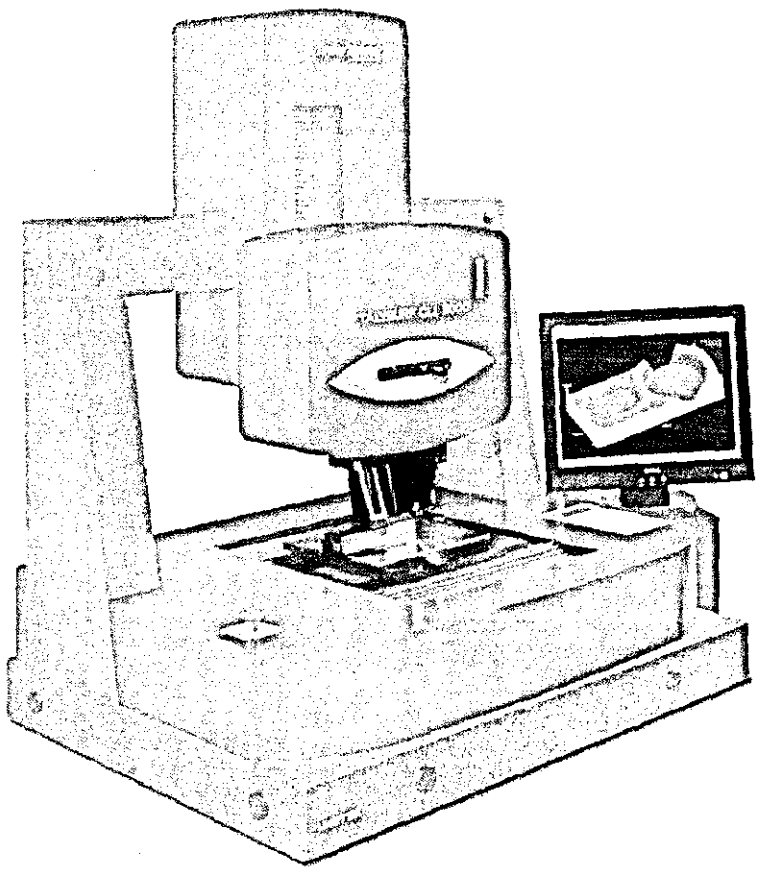

Figure 3Talysurf optical profilometer (Taylor Hobson 2007)

Figure 4 3D mapping of a measured surface generated by Talymap software

4.2 Light-sectioning Method

The measurement setup for light-sectioning method is shown in figure 5. A light source projects a light stripe on to the surface of the machined material from the side of the sample. This projected light creates a light section on the sample according to the shape of the surface. The light section is captured by the camera and then the image is processed off-line by MATLAB image processing toolbox. A light-sectioned image taken by the camera is also shown in figure 5.

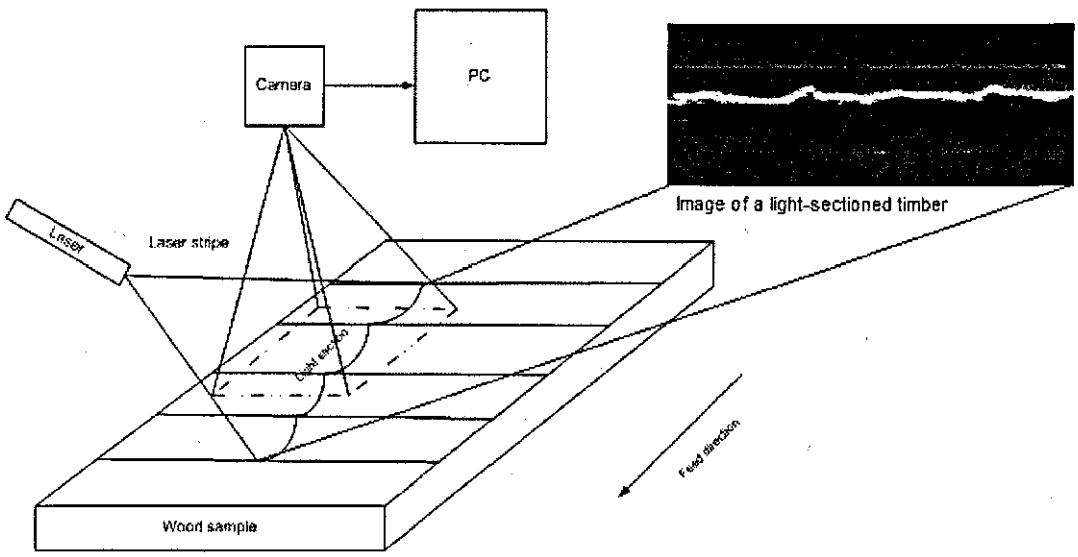

Figure 5 Measurement setup for light-sectioning method and the image obtained through the camera [7]

4.3 Two-image Photometric Stereo Method

This method was first proposed and demonstrated by Yang [23] as part of the Wood Surface Measurement System (WSMS). The experimental setup is illustrated in figure 6. The light sources consist of a laser, a collimator and a beam expander. A camera takes image of the timber surface with light source 1 turned

on. Then another image in taken by switching off the first light source and turning on light source 2.

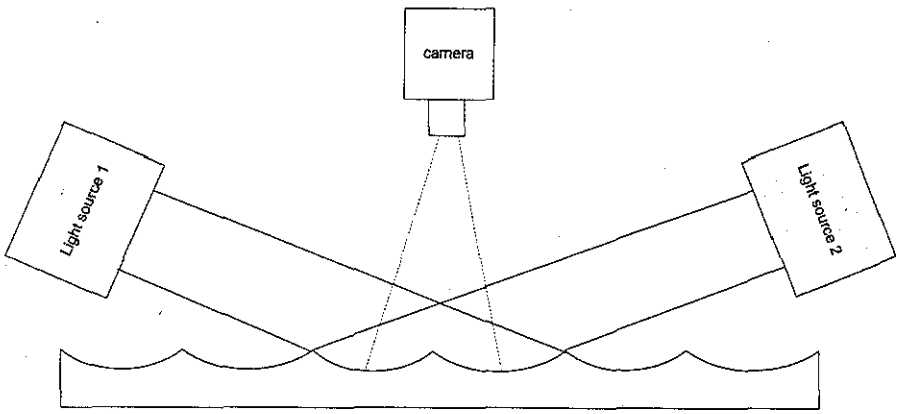

Figure 6 Experimental setup of the photometric stereo method [23]

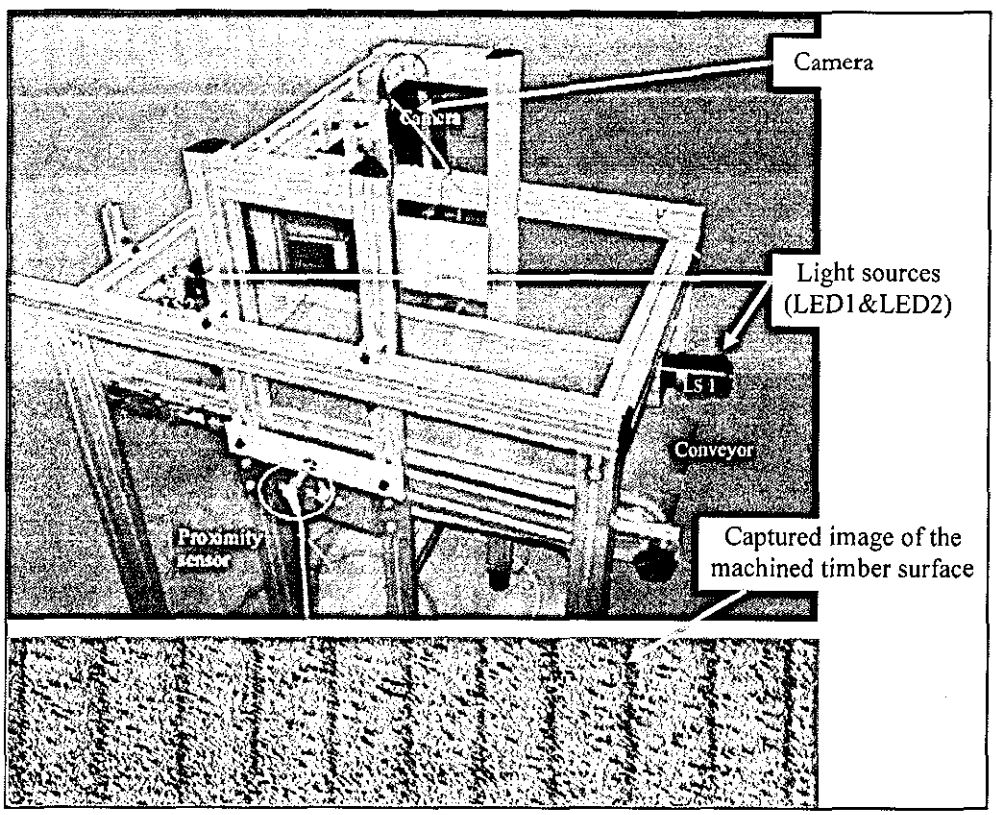

Figure 8 Test rig of the WSMS system

Surface profile of the machined timber is obtained by comparing and transforming the surface shape function to a 2-D profile. This two-image photometric stereo method will be referred to as WSMS in this paper. The actual test rig is shown in figure 7.

5 Results and Discussions

This section of the paper reports surface profile measurement results obtained by the four different methods. Two samples are used to make a comparative study of the aforesaid methods. The first sample is a machined timber of 2 mm pitch length, while the second one is a black nylon with surface defect.

5.1 Wood Sample with 2 mm Pitch Length

Surface profile of the machined timber with 2 mm pitch and the corresponding Fast Fourier Transform (FFT) results of the surface are shown in this sub-section. As discussed by Harris [25], the FFT analysis clearly reveals the wavelength components that make up a given waveform. It should be pointed out that the unit for the frequency is determined as *1/(unit length)* i.e. *1/mm,* which can be perceived as the number of cuttermarks per unit length. This is a very useful technique of determining the fundamental pitch length present in the measurement data.

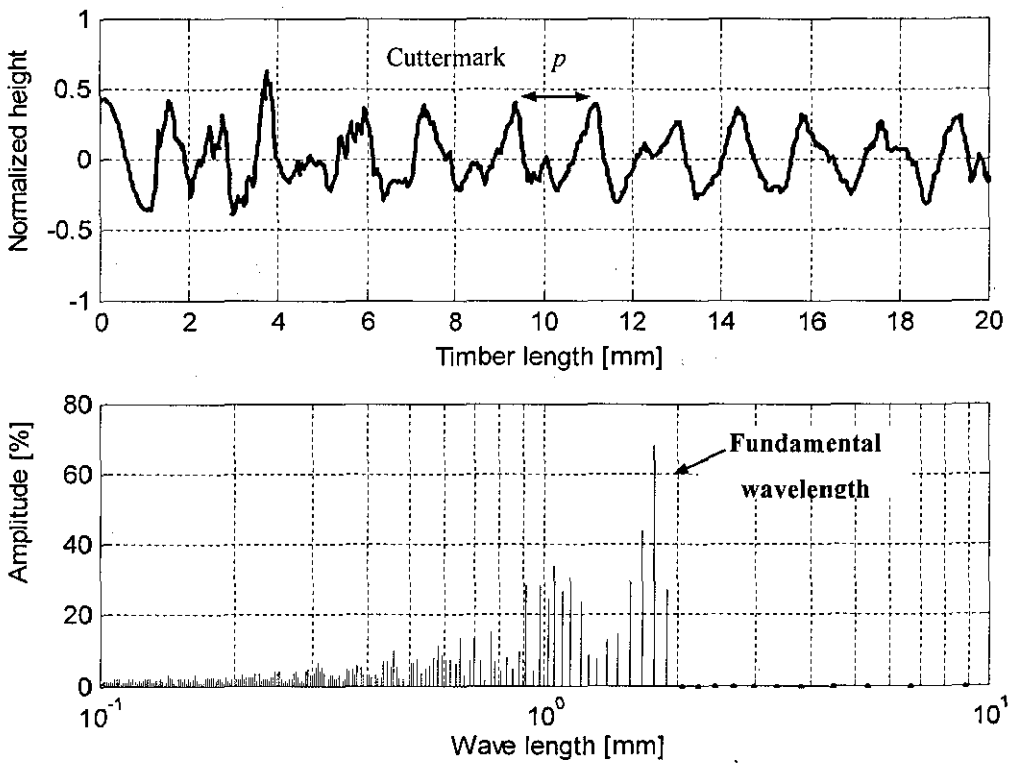

Figure 8 Surface profile and FFT analysis of machined timber obtained using light-sectioning method

Figure 8 depicts the surface profile obtained with the use of light-sectioning method. From the normalized profile measurement data it is evident that there are periodic cutter-marks on the timber surface. When the FFT analysis of the surface profile is carried out, it can be seen that the main wavelength component is 1.8 mm. This value is somewhat close to the fundamental wavelength of 2.0 mm in this specimen. Due to the scattering effects of the laser beams on the edges of the specimen, the measurement accuracy decreases which can also be observed in figure 8 at the beginning of the measurement (i.e. from 0 to 5 mm) where a more noisy behavior of the waviness is apparent. Since the machined surface is not ideally flat, the laser scattering would be present to a certain degree depending on

the tilting effect of the machined surface. This measurement technique also requires a precise setting of the laser beam by considering the incident angle for every measurement which also affects the overall scatter characteristics of the laser beam. For example if the incident angle is too low (i.e. <1°) then the scattering of the laser beam increases if it is >5° the measurement precision decreases. Furthermore the inspection area is limited to the laser beam length of up to 50mm. This measurement technique also needs to be performed under exclusion of the ambient light which can affect the measurement quality.

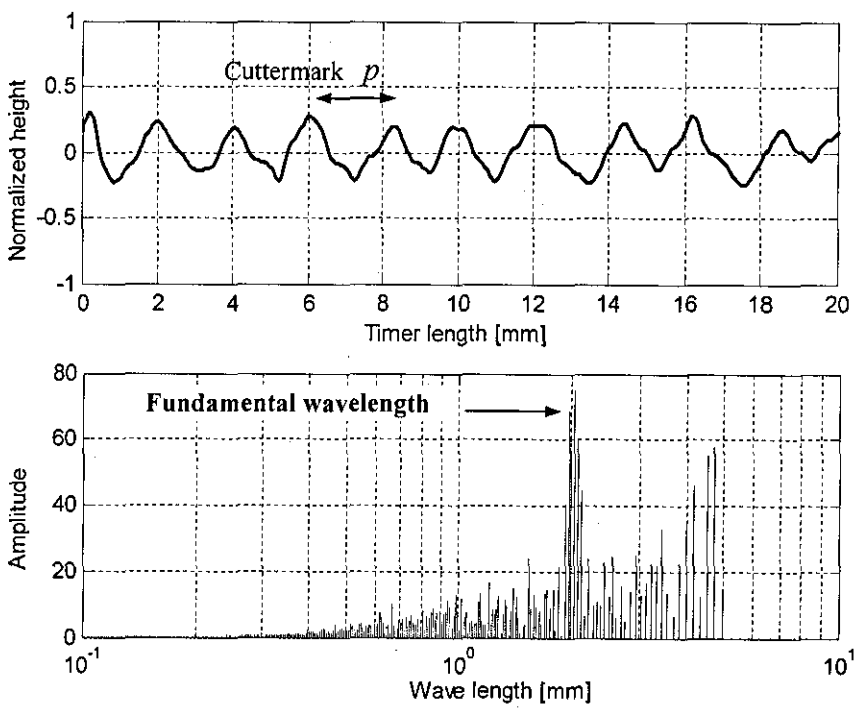

Figure 9 Surface profile and FFT analysis of machined timber obtained using mechanical stylus

Figure 9 shows the surface profile as traced by a mechanical stylus. It can be seen that the regular pitch marks of 2 mm are clearly visible from the surface trace of the stylus. From the FFT, it can be observed that the fundamental wavelength present in the surface profile is in fact 2 mm. Thus, the measurement closely corresponds to the actual surface. It should be pointed out the amount of surface roughness measured within the waviness depends on the stylus tip radius as this can show integrating behavior [3, 4].

Surface profile measurement data of the sample using Talysurf is shown in figure 10. This measurement serves as the benchmark for all the other systems as this measurement can be traced back to NPL standards.

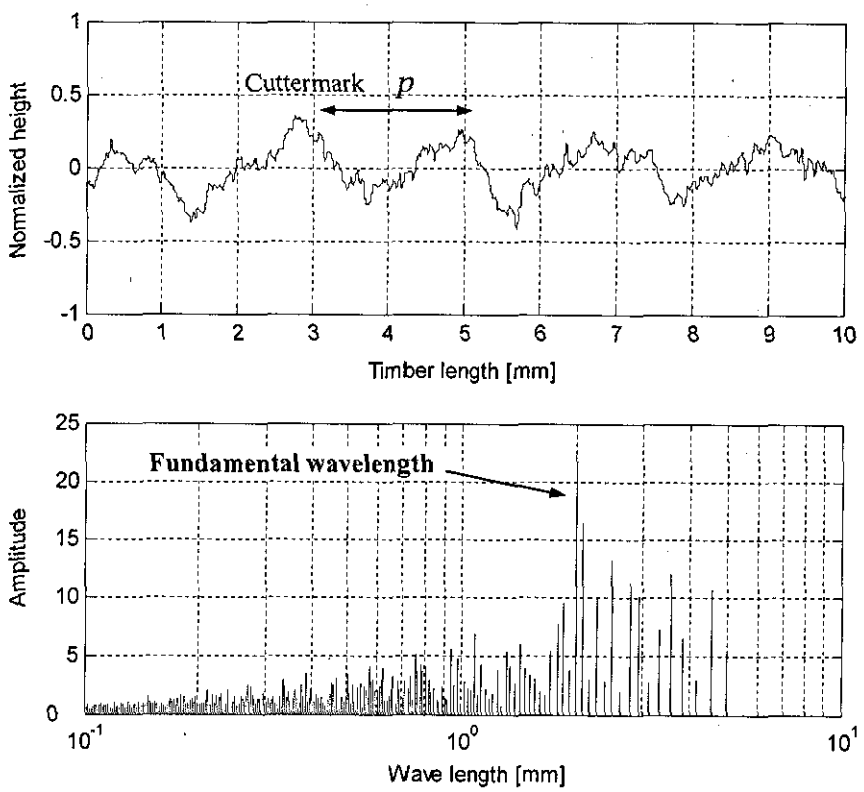

Figure 10 Surface profile and FFT analysis of timber measured using Talysurf

From the figure 10 it can be seen that the cuttermarks on the timber surface is evident with the periodic waveform. However, in contrast to other systems discussed in this paper, the surface appears to have very high frequency components on top of the machined waviness pattern. This fact can be clearly seen from the presence of harmonics within the lower wavelength components than other methods. Because of the fact that the Talysurf has a very high resolution of measurement (1 μm), apart from the waviness pattern on wood, it also measures the constituent grains of the timber. Thus, the measurement appears more 'noisy' due to the additionally measured roughness of the surface.

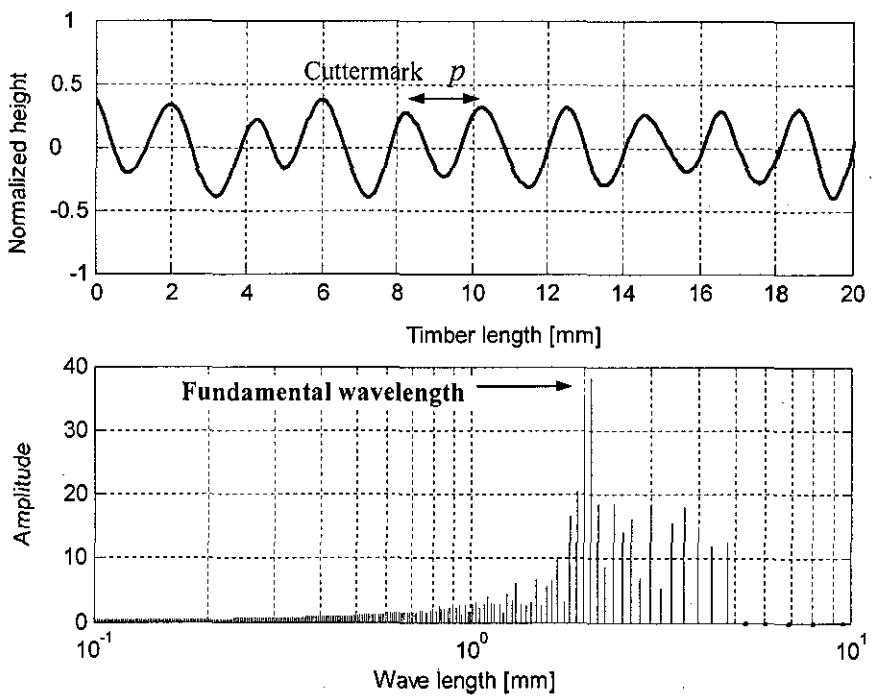

Figure 11 Surface profile and FFT analysis of machined timber obtained using WSMS

The surface profile of the machined timber as obtained by the use of WSMS is shown in figure 11. From the actual profile graph, it can be seen that the system is

able to detect the periodic nature of surface waviness. The FFT analysis reveals that the dominant wavelength present in the measured data is approximately 2 mm. Thus, the measurement obtained from the WSMS for a machined timber with 2 mm pitch length agrees very closely to the actual surface finish. As all four measurements candidates show the capability of measuring the surface profile of the machined timber at 2 mm pitch, the measurement diffuculty level has been raised by the next specimen. This is a special case of a multi - knife finish where all the cutting knives do not follow a common cutting path, hence producing a waviness defect. This type of defect with 6 μm peak to peak vibration amplitude is indeed difficult to generate on timber surfaces due to the inhomogeneous nature of timber, therefore a black plastic sample defect has been machined with the smart planing system [3]. For the non contact measurement systems is this type of defect indeed difficult to detect firstly due to the very low waviness heights variation and secondly due to the black color of the sample which absorb the light thus adding uncertainty in the accuracy of profile detection. In other words this defect is to show the limitations of the surface profile measurement candidates.

5.2 Nylon Sample with Defects

The surface profile of a black nylon sample with defects was measured using the aforesaid techniques. During the measurement exercises, it was found out that the light sectioning method was unable to detect the surface profile of the nylon sample. This was due to the fact that, the projected laser light was fully absorbed by the black-colored sample. Thus, no light pattern formed on the surface and as a

result, the camera wasn't able to capture any meaningful image. Therefore, in this sub-section only results obtained from the Talysurf, WSMS and mechanical stylus have been reported.

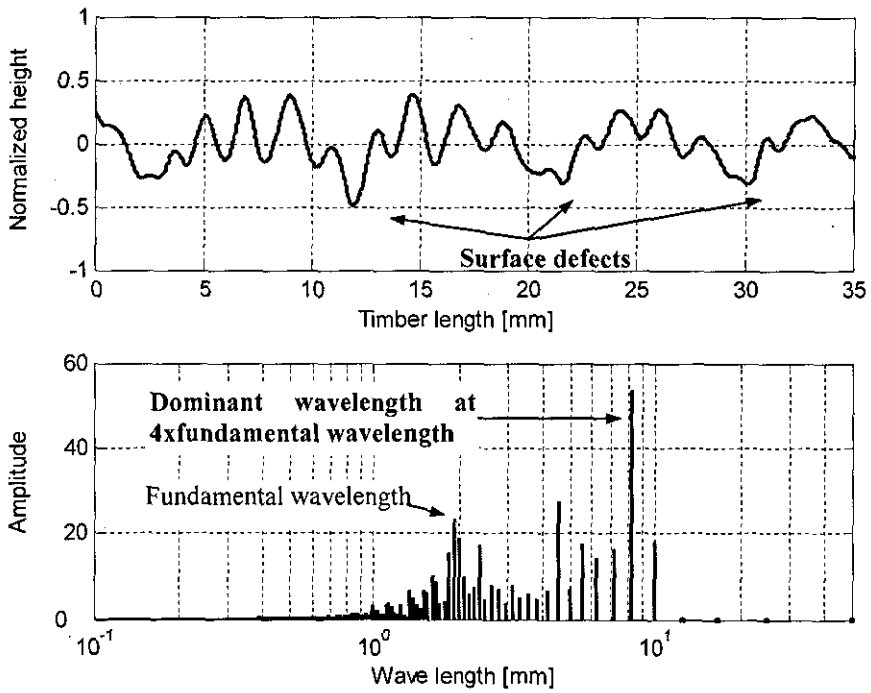

Figure 12 Surface profile and FFT analysis of defect using Talysurf

The surface defects can be observed from figure 12 and a detailed analysis of defect forming found in literature [3]. The FFT analysis clearly shows that the dominant wavelength can be observed at the approximately 8 mm, which is four times the fundamental wavelength of 2 mm. This is in perfect agreement with the defect analysis presented in the aforesaid paper [3].

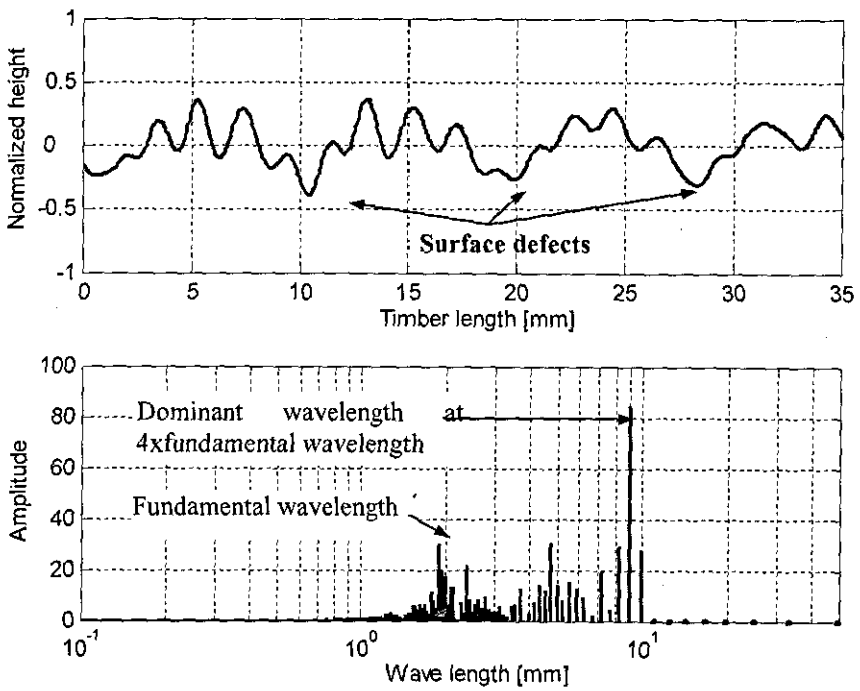

Figure 13 Surface profile and FFT analysis of defect using mechanical stylus [3]

A surface trace obtained by the use of a mechanical stylus has been reported in figure 13. The general shape of the curve is similar to the one reported in figure 12. The FFT analysis also reveals the trend of obtaining the dominant wavelength at 8 mm, four times the fundamental machined wavelength of 2 mm.

Surface profile measurement results obtained from the WSMS system is shown in figure 14. From the profile graph it can be easily seen that the shape of the plot corresponds very closely to the ones obtained through Talysurf and mechanical stylus.

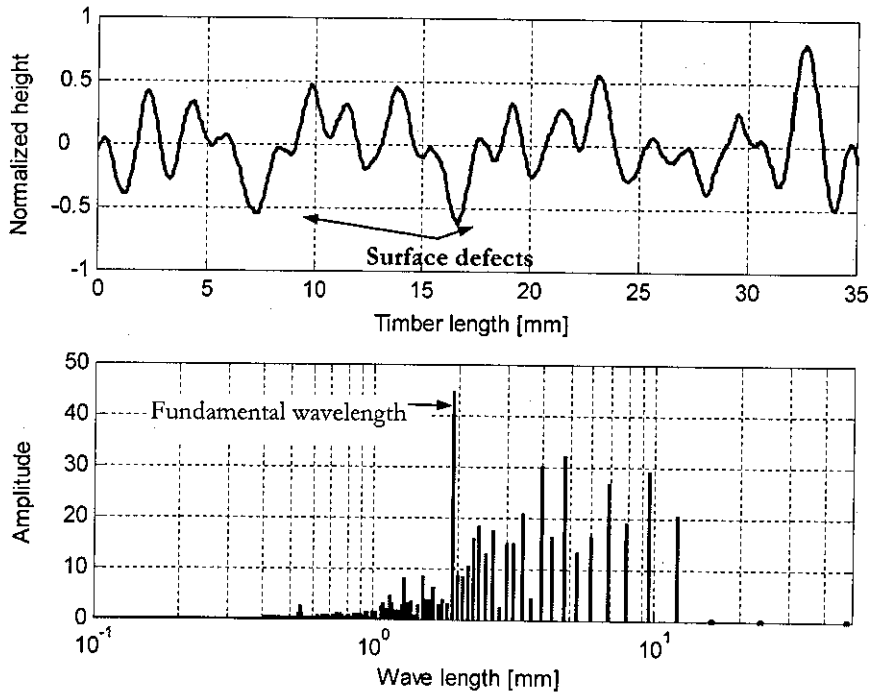

Figure 14 Surface profile and FFT analysis of defect using WSMS

The FFT analysis however is not conclusive in comparison to the first two methods. However the WSMS is still capable of measuring the shape of the surface defect. When figure 14 is compared with the 2 mm pitch in figure 11 it can clearly be seen that the surface profile of surface defect is very different.

5.3 Comparison of the Techniques

The previous sub-sections reported the surface profile measurement results obtained using four different profiling techniques. The Talysurf has been used in this paper as the benchmark for the samples, as its measurements are traceable to UKAS standards. It was found out that the fine measurements carried out by the Talysurf on timber surface not only picked up the waviness but also the surface

roughness. Thus, in order to recover the exact waviness pattern from the measurement data, some filtering is required. In order to carry out the measurements, around 20 minutes was required for each sample of 50 mm length. Thus, it is a very slow process and not suitable for online inspection of wood machining process where high throughput rates up to 40m/min are required.

The light sectioning method could not be used to measure the black nylon sample with defect. However, the 2 mm regular pitch length could be satisfactorily measured using this method. The main drawback of the system has been the tedious setup of the incident angle and the extensive filtering for surface profile extraction from the images. Nevertheless this technique can potentially be employed for offline surface analysis purposes; since it is relatively straight forward configuration allows a quick experimental set up of the components. Moreover for higher pitch values i.e. >2 mm the precision of the measurement increases significantly. However this method is not suitable to measure high quality surfaces where the pitch is lower than 1.5 mm [23].

The measurement results obtained through mechanical stylus instrument has closely resembled that of Talysurf. But this method is inherently slow and destructive for softer materials like wood and nylon. Also, the loading of the stylus tip affects the measurement data. Furthermore this technique is also not suitable for in-process inspection of timber surfaces where high throughput rates are required, since the stylus tip tends to jump at high measuring speed. This

effect also called "bouncing" where the stylus tip looses contact with the machined surface has been reported in various related publications [4, 26, 27].

The WSMS system has been successfully used to carry out both the regular machined surface as well as the surface with defect. Data acquisition with the system took only a few seconds and the analysis of the captured image to obtain the 2-D profile only about a minute. Thus, it was the fastest among the four methods of surface profile measurement. Also with the help of this system, a machined area of the sample was measured, thus providing an averaged profile of that area with a higher overall accuracy. Whereas all other measurement devices are capable of only measuring a line trace on the machined surface at a time. In order to obtain the true profile of the surface, multiple traces were taken in the area under investigation and an averaging was taken place. According to the detailed analysis in [23], this line tracing and subsequent averaging could give erroneous profile measurement, if not done properly. Thus, the method of taking the area measurement of WSMS is more suitable for such surface profile measurements. Furthermore this method is more promising in terms of in-process measurement application.

6 Conclusions

The research work presented in this paper compares and contrasts four different surface profile measurement systems. With the help of these systems two sample - one timber and a nylon one were traced. It is seen from the measurement data that

the Talysurf provided very good representation of the surfaces. Thus, this was used as the benchmark to compare the other systems.

Among the two optical non-contact methods, light-sectioning was not able to measure the surface profile of black nylon. However, it was able to provide satisfactory trace of the machined timber surface. The mechanical stylus was able to provide good surface profile measurement results with both nylon and timber. But the use of such an instrument is not recommended for surfaces such as wood and nylon due to the destructive nature of measurement.

The WSMS system was able to provide very fast measurements with highly satisfactory profile measurement results. The measurements very closely correspond to the ones obtained with Talysurf. From the results presented in this paper, it is evident that the WSMS is the most suitable system for measuring machined timber and nylon in terms of speed, non-destructiveness, accuracy and cost effectiveness.

7 Acknowledgement

The work reported here was supported by the EPSRC Innovative Manufacturing and Construction Centre (IMCRC) at Loughborough University.

8 References

1. Palmqvist, J., M. Lenner, and S.-I. Gustafsson, Cutter head forces and load cell scanning. Wood Science and Technology, 2003. 37(3): p. 199-211.

2. Parkin, R.M. and M.R. Jackson, A mechatronic approach for analysing timber surfaces. Mathematics and Computers in Simulation, 1996. 41(5-6): p. 445-450.

3. Elmas, S., M.R. Jackson, and R.M. Parkin. Planing timber with an active machining system. Proceedings of the 18th Wood Machining Seminar 2007, Vancouver, Canada, pp 107-115.

4. Jackson, M.R., R.M. Parkin, and N. Brown, Waves on wood. Proceedings of the Institution of Mechanical Engineers, Part B: Journal of Engineering Manufacture, 2002. 216(4): p. 475-497.

5. Palmqvist, J. and S.I. Gustafsson, Emission of dust in planing and milling of wood. Holz als Roh- und Werkstoff, 1999. 57(3): p. 164-170.

6. Brown, N. and R.M. Parkin, Improving wood surface form by modification of the rotary machining process-a mechatronic approach. Proceedings of the Institution of Mechanical Engineers, Part B: Journal of Engineering Manufacture 1999. 213(3): p. 247 - 260

7. Yang, D., M. Jackson, and R. Parkin, Inspection of wood surface waviness defects using the light sectioning method. Proceedings of the Institution of Mechanical Engineers, Part I: Journal of Systems and Control Engineering, 2006. 220(7): p. 617-626.

8. Jolic, K.I., C.R. Nagarajah, and W. Thompson, Non-contact, optically based measurement of surface roughness of ceramics. Measurement Science & Technology, 1994. 5(6): p. 671-684.

9. Palazzolo, A.B., Lin, R.R., Alexander, R.M., Kascak, A.F., & Montague, J. "Test and theory for piezoelectric actuator-active vibration control of rotating machinery", Journal of Vibration, Acoustics, Stress, and Reliability in Design, 113, 167-175, 1991.

10. Hynek, P., Jackson, M., R., Parkin, R., M. and Brown, N., "Improvement of Rotary Machining Process", Proceedings IWMS17-2005, Rosenheim, Germany, Published by Retru-Verlag, pp 346-355, 2005.

11. Dohner, J.L. , Lauffer, J.P., Hinnerichs, T.D., Shankar, N. , Regelbrugge, M., Kwan, C.-M., Xu, R., Winterbauer, B., & Bridger, K. "Mitigation of chatter instabilities in milling by active structural control". Journal of Sound and Vibration 269[1-2], 197-211. 2004.

12. Wong, P.L. and K.Y. Li, In-process roughness measurement on moving surfaces. Optics and Laser Technology, 1999. 31(8): p. 543-548.

13. Garratt, J.D. and D.J. Nettleton, Stylus instrument for roughness and profile measurement of ultra-fine surfaces. International Journal of Machine Tools & Manufacture, 1992. 32(1-2): p. 233-238.

14. Whitehouse, D.J., et al., Nano-calibration for stylus-based surface measurement. Journal of Physics E: Scientific Instruments, 1988. 21(1): p. 46-51.

15. Groeger, S., Dietzsch, M., Gerlach, M., Jess S., 'Real mechanical profile' - the new approach for nano-measurements. Journal of Physics: Conference Series, 2005. 13: p. 13-19.

16. Sandak, J. and C. Tanaka, Evaluation of surface smoothness by laser displacement sensor 1: Effect of wood species. Journal of Wood Science, 2003. 49(4): p. 305-311.

17. Shinozaki, R., O. Sasaki, and T. Suzuki, Fast scanning method for one-dimensional surface profile measurement by detecting angular deflection of a laser beam. Applied Optics, 2004. 43(21): p. 4157-4163.

18. Shinozaki, R., O. Sasaki, and T. Suzuki, In-process inspection of surface-profile properties by detecting laser beam deflection. Optical Engineering, 2006. 45(1): p. 013601.

19. Sandak, J. and C. Tanaka, Evaluation of surface smoothness using a light-sectioning shadow scanner. Journal of Wood Science, 2005. 51(3): p. 270-273.

20. Yang, D., M. Jackson, and R. Parkin. Measuring cutter marks on wood surfaces with machine vision techniques. 17th International Wood Machining Seminar. 2005. Rosenheim, Germany.

21. Tatsubo, H., T. Nakashima, and M. Sugiyama. Multifunction sensor that measures the width and surface profile of a steel plate. 2004. Providence, RI., United States: International Society for Optical Engineering, Bellingham, WA 98227-0010, United States.

22. Xu, B., D.F. Cuminato, and N.M. Keyes, Evaluating Fabric Smoothness Appearance with a Laser Profilometer. Textile Research Journal, 1998. 68(12): p. 900-906.

23. Yang, D., Measurement of cutter marks on planed wood surfaces with machine vision methods. Thesis (Ph.D.). 2006. Loughborough University, Leicestershire.

24. Bennett, J.M., Recent developments in surface roughness characterization. Measurement Science and Technology, 1992. 3(12): p. 1119-1127.

25. Harris, F.J., On the use of windows for harmonic analysis with the discrete Fourier transform. Proceedings of the IEEE, 1978. 66(1): p. 51-83

26. Yoo, S. M., Dornfeld, D. A., and Lemaster, R. L. Analysis and modelling of laser measurement system performance for wood surface, Journal of Engineering for Industry, Transactions ASME, 1990. (112): pp. 69-77

27. Faust, T. D. Real time measurement of veneer surface roughness by image analysis, Forest Products Journal, 987. (37): pp. 34-40